

DE GRUYTER

REFERENCE

Tharwat F. Tadros

HANDBOOK OF COLLOID AND INTERFACE SCIENCE

VOLUME 3: INDUSTRIAL APPLICATIONS

Copyright 2017. De Gruyter. All rights reserved. May not be reproduced in any form without permission from the publisher except fair uses permitted under U.S. or applicable copyright law.

Tharwat F. Tadros
Handbook of Colloid and Interface Science
De Gruyter Reference

Also of Interest



Handbook of Colloid and Interface Science.
Volume 1: Basic Principles of Interface Science and Colloid Stability
Tadros, 2017
ISBN 978-3-11-053990-5, e-ISBN 978-3-11-054089-5



Handbook of Colloid and Interface Science.
Volume 2: Basic Principles of Dispersions
Tadros, 2017
ISBN 978-3-11-053991-2, e-ISBN 978-3-11-054195-3



Polymeric Surfactants.
Dispersion Stability and Industrial Applications
Tadros, 2017
ISBN 978-3-11-048722-0, e-ISBN 978-3-11-048728-2



Suspension Concentrates.
Preparation, Stability and Industrial Applications
Tadros, 2017
ISBN 978-3-11-048678-0, e-ISBN 978-3-11-048687-2



Formulations.
In Cosmetic and Personal Care
Tadros, 2016
ISBN 978-3-11-045236-5, e-ISBN 978-3-11-045238-9



Emulsions.
Formation, Stability, Industrial Applications
Tadros, 2016
ISBN 978-3-11-045217-4, e-ISBN 978-3-11-045224-2

Tharwat F. Tadros

Handbook of Colloid and Interface Science



Volume 3:

Industrial Applications:

Pharmaceuticals, Cosmetics and Personal Care

DE GRUYTER

Author

Prof. Tharwat F. Tadros
89 Nash Grove Lane
Workingham RG40 4HE
Berkshire, UK
tharwattadros3@gmail.com

ISBN 978-3-11-055409-0
e-ISBN (PDF) 978-3-11-055525-7
e-ISBN (EPUB) 978-3-11-055490-8
Set-ISBN 978-3-11-055526-4

Library of Congress Cataloging-in-Publication Data

A CIP catalog record for this book has been applied for at the Library of Congress.

Bibliographic information published by the Deutsche Nationalbibliothek

The Deutsche Nationalbibliothek lists this publication in the Deutsche Nationalbibliografie; detailed bibliographic data are available on the Internet at <http://dnb.dnb.de>.

© 2018 Walter de Gruyter GmbH, Berlin/Boston
Cover image: satori13/iStock/Getty Images Plus
Typesetting: PTP-Berlin, Protago-TEX-Production GmbH, Berlin
Printing and binding: CPI Books GmbH, Leck
♻️ Printed on acid-free paper
Printed in Germany

www.degruyter.com

Preface

The field of colloid and interface science plays a major role in most industrial systems. This is particularly the case with most formulations consisting of disperse systems. In all formulations consisting of suspensions, emulsions, foams, gels, etc., the structure of the interfacial region determines their colloidal properties. The topics of colloid and interface science can be conveniently subdivided under two main headings, namely disperse systems and interfacial phenomena. This subdivision does not imply any separation for the following reasons. All disperse systems involve an interface. Many interfacial phenomena are precursors for formation of disperse systems, e.g. nucleation and growth, emulsification, etc. The main objectives of the present handbook, namely Volume 3, are to illustrate how the basic principles that are involved in interfacial phenomena (described in detail in Volumes 1 and 2) are applied in pharmaceuticals, cosmetics and personal care systems. Particular emphasis will be given to the formation of colloidal dispersions and their stabilisation. The colloid stability/instability of any disperse system is determined by the property of the interfacial region. In actual fact, colloid and interface science are one individual subject.

The field of colloid and interface science has no boundary since chemists, physicists, engineers, biologists, mathematicians can all be engaged in the field. For successful applications in industry, multidisciplinary teams are required. Understanding the basic principles of colloid and interface science will enable industry to develop many complex systems in shorter periods of time. Most colloidal systems used in industry are multiphase and complex formulations. They may contain more than one disperse phase, e.g. suspension/emulsion systems (suspoemulsions).

Two applications of colloid and interface science are given in this volume. The first application is in the field of pharmacy (Part I) which consists of five main topics. Chapter 1 describes the disperse systems with particular reference to the thermodynamics of their formation and the resulting kinetic stability. Particular reference is given to nanosuspensions and nanoemulsions which are used in many drug formulations. Chapter 2 deals with the surface activity and colloidal properties of drugs. Reference is also made to the naturally occurring micelle forming systems, such as the lipids. The biological implications of the presence of surfactant systems in pharmaceutical formulations is described. Chapter 3 describes the process of micellar solubilization and location of the drug molecules. The potential use of liposomes and vesicles in pharmacy is also described. Chapter 4 deals with solid lipid nanoparticles, microgels and capsules. Chapter 5 deals with application of biodegradable nanoparticles for drug delivery and drug targeting.

The second application (Part II) is in the field of cosmetics and personal care. Chapter 6 describes the surfactants that are used in cosmetic formulations and the requirement for the absence of any toxic effect. Chapter 7 deals with cosmetic emulsions, in particular hand creams and lotions and their formulation. The control of

<https://doi.org/10.1515/9783110555257-001>

consistency (rheology) of the formulation is described. Chapter 8 describes the use of nanoemulsions in cosmetics, highlighting their main advantages. The preparation of nanoemulsions by high and low energy methods is described. Chapter 9 deals with multiple emulsions and their advantages for controlled delivery of actives. The methods that can be applied for preparation of multiple emulsions and control of their stability are described. Chapter 10 describes the preparation of shampoos, gels and hair conditioners as well as control of their properties to achieve optimum interaction with hair. Chapter 11 deals with sunscreen dispersions for UV protection, with particular emphasis on the use of nanodispersions of titania that can be conveniently incorporated in emulsions for application. Chapter 12 describes the pigment dispersions that are used in colour cosmetics. Particular emphasis is given to the process of powder wetting and dispersion as well as control of their colloidal properties.

This text gives a number of examples illustrating the applications of colloid and interface science principles to pharmaceutical, cosmetics and personal care formulations. The handbook will be valuable for formulation scientists and chemical engineers involved in formulating the above mentioned industrial systems. It can also be valuable for research scientists and postgraduate students involved in these research areas.

Tharwat Tadros
April 2017

Contents

Preface — v

Part I: Colloid and interface science in pharmacy

- 1 Disperse systems — 3**
 - 1.1 Thermodynamic considerations — 3
 - 1.2 Stabilization of dispersions — 4
 - 1.3 Nanodispersions — 11

- 2 Surface activity and colloidal properties of drugs — 31**
 - 2.1 Introduction — 31
 - 2.2 Investigating the association behaviour of drugs — 31
 - 2.3 Naturally occurring micelle forming systems — 34
 - 2.4 Biological implications of the presence of surfactants in pharmaceutical formulations — 39

- 3 Solubilized systems, liposomes and vesicles in pharmacy — 43**
 - 3.1 Introduction — 43
 - 3.2 Analysis of solubilization — 44
 - 3.3 Experimental methods for studying solubilization — 45
 - 3.3.1 Maximum additive concentration — 45
 - 3.3.2 Micelle-water distribution equilibria — 46
 - 3.3.3 Determination of location of solubilize — 47
 - 3.4 Quantitative methods for obtaining the exact location of solubilize — 47
 - 3.4.1 X-ray diffraction — 47
 - 3.4.2 Absorption spectrometry — 48
 - 3.4.3 NMR methods — 48
 - 3.4.4 Fluorescence depolarization — 48
 - 3.4.5 Electron spin resonance (ESR) — 49
 - 3.5 Mobility of solubilize molecules — 49
 - 3.6 Factors affecting solubilization — 49
 - 3.6.1 Solubilize structure — 49
 - 3.6.2 Surfactant structure — 49
 - 3.6.3 Temperature — 50
 - 3.6.4 Addition of electrolytes and non-electrolytes — 50
 - 3.7 Liposomes and vesicles in pharmacy — 50
 - 3.7.1 Driving force for formation of vesicles — 53

- 3.7.2 Stabilization of liposomes by incorporation of block copolymers — 57
- 3.8 Liquid crystalline phases and microemulsions — 59

- 4 Solid lipid nanoparticles, polymer gels and capsules — 65**
 - 4.1 Solid lipid nanoparticles (SLN) — 65
 - 4.2 Polymer gels, microgels and capsules — 65
 - 4.3 Solid polymer nanoparticles — 70

- 5 Drug delivery and drug targeting — 73**
 - 5.1 Introduction — 73
 - 5.2 Polymeric nanoparticles — 73
 - 5.3 Biodegradable nanoparticles — 77

Part II: Colloid and interface science in cosmetics and personal care

- 6 Surfactants used in cosmetic and personal care formulations, their properties and surfactant–polymer interaction — 97**
 - 6.1 Surfactant classes — 97
 - 6.2 Physical properties of surfactant solutions and the process of micellization — 109
 - 6.3 Thermodynamics of micellization — 115
 - 6.4 Surfactant–polymer interaction — 122

- 7 Cosmetic emulsions — 133**
 - 7.1 Introduction — 133
 - 7.2 Thermodynamics of emulsion formation — 133
 - 7.3 Emulsion breakdown processes and their prevention — 135
 - 7.4 Selection of emulsifiers — 139
 - 7.4.1 The hydrophilic-lipophilic balance (HLB) concept — 139
 - 7.4.2 The phase inversion temperature (PIT) concept — 145
 - 7.5 Mechanism of emulsification — 147
 - 7.6 Rheological properties of cosmetic emulsions — 153

- 8 Nanoemulsions in cosmetics — 159**
 - 8.1 Introduction — 159
 - 8.2 Colloid stability of nanoemulsions — 160
 - 8.3 Preparation of nanoemulsions using high pressure homogenizers — 163
 - 8.4 Low-energy methods for preparing nanoemulsions — 171

- 8.4.1 Phase inversion composition (PIC) principle — 172
- 8.4.2 Phase inversion temperature (PIT) principle — 173
- 8.4.3 Preparation of nanoemulsions by dilution of microemulsions — 175
- 8.5 Preparation of nanoemulsions using the PIT technique — 176
- 8.6 Nanoemulsions based on polymeric surfactants — 185

9 Multiple emulsions in cosmetics — 193

- 9.1 Introduction — 193
- 9.2 Types of multiple emulsions — 194
- 9.3 Breakdown processes of multiple emulsions — 194
- 9.4 Preparation of multiple emulsions — 195
 - 9.4.1 The two-step process — 196
 - 9.4.2 The phase inversion method — 199
 - 9.4.3 Lamellar phase dispersion process — 200
 - 9.4.4 The oily isotropic dispersion process — 201
- 9.5 Main parameters that need to be controlled in the preparation of W/O/W multiple emulsions for cosmetic applications — 201
 - 9.5.1 Nature of the oil — 201
 - 9.5.2 Nature of the emulsifier — 201
 - 9.5.3 Gelling agents — 202
 - 9.5.4 Osmotic pressure control — 202
- 9.6 Examples of W/O/W multiple emulsions — 202
- 9.7 Characterization of multiple emulsions — 205
 - 9.7.1 Droplet size analysis — 205
 - 9.7.2 Dialysis — 206
 - 9.7.3 Rheological techniques — 206
- 9.8 Summary of the factors affecting stability of multiple emulsions and criteria for their stabilization — 210

10 Shampoos, gels and hair conditioners — 213

- 10.1 Introduction — 213
- 10.2 Surfactants for use in shampoo formulations — 214
 - 10.2.1 Anionic surfactants — 214
 - 10.2.2 Amphoteric surfactants — 215
 - 10.2.3 Nonionic surfactants — 215
- 10.3 Properties of a shampoo — 216
- 10.4 Components of a shampoo — 217
 - 10.4.1 Cleansing agents — 217
 - 10.4.2 Foam boosters — 218
 - 10.4.3 Thickening agents — 218
 - 10.4.4 Preservatives — 218
 - 10.4.5 Miscellaneous additives — 219

10.5	Role of the components —	219
10.5.1	Behaviour of mixed surfactant systems —	219
10.5.2	Cleansing function —	220
10.5.3	Foam boosters —	221
10.5.4	Thickeners and rheology modifiers —	222
10.5.5	Silicone oil emulsions in shampoos —	224
10.6	Use of associative thickeners as rheology modifiers in shampoos —	224
10.7	Morphology of hair —	228
10.8	Surface properties of hair —	230
10.8.1	Wettability investigations —	230
10.8.2	Electrokinetic studies —	234
10.9	Role of surfactants and polymers in hair conditioners —	234
11	Sunscreens for UV protection —	241
11.1	Introduction —	241
11.2	Mechanism of absorbance and scattering by TiO ₂ and ZnO —	242
11.3	Preparation of well-dispersed particles —	243
11.4	Experimental results for sterically stabilized TiO ₂ dispersions in nonaqueous media —	247
11.5	Competitive interactions in sunscreen formulations —	255
12	Colour cosmetics —	259
12.1	Introduction —	259
12.2	Fundamental principles for preparation of a stable colour cosmetic dispersion —	260
12.2.1	Powder wetting —	260
12.2.2	Powder dispersion and milling (comminution) —	264
12.2.3	Stabilization of the dispersion against aggregation —	265
12.3	Classes of dispersing agents —	270
12.4	Assessment of dispersants —	272
12.4.1	Adsorption isotherms —	272
12.4.2	Measurement of dispersion and particle size distribution —	273
12.4.3	Rheological measurements —	273
12.5	Application of the above fundamental principles to colour cosmetics —	275
12.6	Principles of preparation of colour cosmetics —	277
12.7	Competitive interactions in colour cosmetic formulations —	279

Index — 281

Part I: Colloid and interface science in pharmacy

1 Disperse systems

1.1 Thermodynamic considerations

Several types of disperse systems can be identified in pharmacy of which solid/liquid (suspensions), liquid/liquid (emulsions) and liquid/solid (gels) are perhaps the most important. All disperse systems are thermodynamically unstable [1]. This can be understood from the balance between the surface or interfacial energy and entropy of their formation. For example, the formation of suspensions from the bulk phase (with surface area A_1) to a large number of much smaller particles (with a total surface area A_2 that is much larger than A_1) results in an increase in the surface energy of $(A_2 - A_1)\sigma$ or $\Delta A\sigma$, where σ is the solid/liquid interfacial tension. This term is large and positive since σ is positive. Similarly, the formation of an emulsion with a large number of droplets from the bulk oil results in an increase in interfacial energy of $\Delta A\gamma$, where γ is the liquid/liquid interfacial tension. In the dispersion process, a large number of particles or droplets are produced and this is accompanied by an increase in entropy ΔS . According to the second law of thermodynamics, the free energy of formation of the system ΔG is given by the following two expressions for suspensions and emulsions,

$$\Delta G = \Delta A\gamma_{SL} - T\Delta S, \quad (1.1)$$

$$\Delta G = \Delta A\gamma_{OW} - T\Delta S. \quad (1.2)$$

In the above systems $\Delta A\sigma \gg T\Delta S$ and $\Delta A\gamma \gg T\Delta S$ and hence $\Delta G > 0$. This implies thermodynamic instability and the production of suspension or emulsions by the dispersion process is non-spontaneous, i.e. energy is required to produce the smaller particles or droplets from the larger ones. In the absence of any stabilization mechanism (that will be discussed below), the smaller particles or droplets tend to aggregate and/or coalesce to reduce the total interfacial area, hence reducing the total surface energy of the system. Prevention of aggregation and/or coalescence of suspensions or emulsions require a fundamental understanding of the various interaction forces between the particles or droplets and these will be discussed in subsequent sections.

As mentioned above, disperse systems lack thermodynamic stability and they tend to reduce their surface energy by aggregation and/or coalescence of the particles or droplets. The main driving force for the aggregation process is the universal van der Waals attraction. To overcome the aggregation and/or coalescence processes, one must overcome the van der Waals attraction by some repulsive mechanism and this will give the system kinetic stability with an adequate shelf life. Normally one requires a shelf life of 2–3 years under various storage conditions (e.g. temperature variation). Several stabilization mechanisms are encountered with disperse systems of which electrostatic and steric stabilization are the most common.

<https://doi.org/10.1515/9783110555257-002>

1.2 Stabilization of dispersions

Electrostatic stabilization can be achieved by the use of ionic surfactants that adsorb at the solid/liquid or liquid/liquid interfaces. In this case a repulsive energy is produced by formation of electrical double layers. This repulsive energy increases with increasing surface (or zeta) potential and decreasing electrolyte concentration. The repulsive energy counteracts the van der Waals attraction at intermediate distance of separation, thus producing an energy barrier that prevents flocculation of the dispersion. Van der Waals attraction, electrostatic repulsion and their combination form the basis of colloid stability.

For two particles or droplets with equal radius R , and surface-to-surface separation h , the van der Waals attractive energy, G_A , (when $h \ll R$) is given by [2],

$$G_A = -\frac{AR}{12h}, \quad (1.3)$$

where A is the effective Hamaker constant, which is given by,

$$A = (A_{11}^{1/2} - A_{22}^{1/2})^2, \quad (1.4)$$

where A_{11} is the Hamaker constant of the particles or droplets and A_{22} is the Hamaker constant of the medium.

The Hamaker constant of any material depends on the number of atoms per unit volume q and the London dispersion constant β ,

$$A = \pi q^2 \beta. \quad (1.5)$$

It can be seen that G_A increases very sharply with decreasing h when the latter reaches small values. In the absence of any repulsion between the particles or droplets, the latter will aggregate (flocculate) by simple diffusion through the medium. This leads to fast flocculation kinetics and the rate constant for the process, k_0 , has been calculated by Smoluchowski [3],

$$k_0 = \frac{4kT}{3\eta} = 5.5 \times 10^{-18} \text{ m}^3 \text{ s}^{-1}. \quad (1.6)$$

k is the Boltzmann constant, T is the absolute temperature and η is the viscosity of the medium.

As mentioned above, van der Waals attraction is counteracted by electrostatic repulsion. An electrical double layer can be created at the solid/liquid or liquid/liquid interface by charge separation due to the presence of ionogenic groups (e.g. $-\text{OH}$, $-\text{COOH}$) or by adsorption of ionic surfactants at the interface. A schematic representation of the double layer due to Gouy–Chapman–Stern [4] is shown in Fig. 1.1. The double layer is characterized by the following parameters [4]: Surface charge σ_0 , charge in the Stern Layer σ_s , charge of the diffuse layer σ_d (note that $\sigma_0 = \sigma_s + \sigma_d$), surface potential ψ_0 , Stern Potential ψ_d (\approx zeta potential). The double layer extension is determined by the electrolyte concentration and the valency of the counterions as given

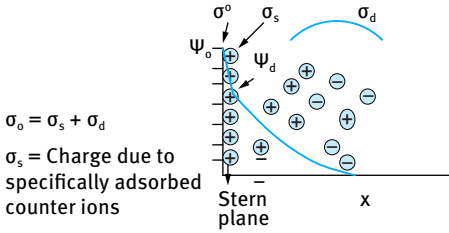


Fig. 1.1: Schematic representation of the electrical double layer.

by the reciprocal of the Debye–Huckel parameter ($1/\kappa$) – referred to as the thickness of the double layer,

$$\left(\frac{1}{\kappa}\right) = \left(\frac{\epsilon_r \epsilon_0 k T}{2 n_0 Z_i^2 e^2}\right), \tag{1.7}$$

where ϵ_r is the permittivity (dielectric constant) of the medium. ϵ_0 is the permittivity of free space, k is the Boltzmann constant and T is the absolute temperature, n_0 is the number of ions per unit volume of each type present in bulk solution, Z_i is the valency of the ions and e is the electronic charge. The double layer thickness increases with decreasing electrolyte concentration: $10^{-5} \text{ mol dm}^{-3} \text{ NaCl}$, $(1/\kappa) = 100 \text{ nm}$; $10^{-3} \text{ mol dm}^{-3} \text{ NaCl}$, $(1/\kappa) = 10 \text{ nm}$.

When two particles or droplets with double layers of the same sign approach to a distance of separation h that is smaller than twice the double layer thickness, double layer repulsion occurs, since the two double layers cannot be fully extended in the confined space, as illustrated in Fig. 1.2. This leads to repulsion energy G_{elec} that is given by the expression [5],

$$G_{\text{el}} = \frac{[4\pi\epsilon_r\epsilon_0 R^2 \psi_0^2 \exp(-\kappa h)]}{[2R + h]}. \tag{1.8}$$

Equation (1.8) shows that G_{elec} decreases exponentially with increasing h and the rate of this decrease depends on electrolyte concentration.

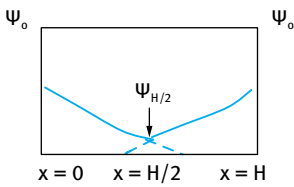


Fig. 1.2: Schematic representation of double layer overlap.

Combining G_A with G_{elec} at various values of h results in the total energy G_T –distance curve illustrated in Fig. 1.3. This presentation forms the basis of the theory of colloid stability due to Deryaguin–Landau–Verwey–Overbeek (DLVO Theory) [5, 6]. The G_T – h curve shows two minima and one maximum: A shallow minimum (of the order of few kT) units at large distances of separation. This may result in weak and reversible

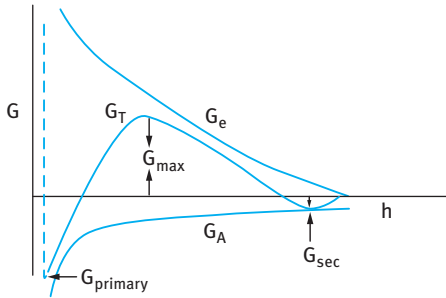


Fig. 1.3: Energy–distance curves according to DLVO theory [5, 6].

flocculation. A deep primary minimum (several $100kT$ units) exists at short distances of separation. This results in strong flocculation (coagulation). An energy maximum, G_{\max} , exists at intermediate distances which prevents flocculation into the primary minimum.

To ensure adequate colloid stability, G_{\max} has to be greater than $25kT$. The height of the maximum depends on the surface (or zeta) potential, electrolyte concentration, particle radius and Hamaker constant. When the zeta potential is higher than 40 mV and the electrolyte concentration is $< 10^{-2} \text{ mol dm}^{-3}$ for 1:1 electrolyte, $G_{\max} > 25kT$.

By increasing the electrolyte concentration, G_{\max} decreases until at a given concentration it vanishes and particle coagulation occurs. This is illustrated in Fig. 1.4 which shows the variation of G_T with h at various electrolyte concentrations.

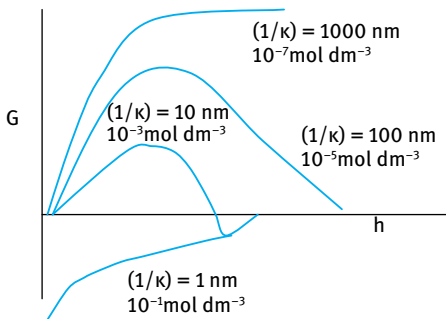


Fig. 1.4: Variation of G_T with h at various electrolyte concentrations.

In the presence of an energy barrier one can define a slow rate of flocculation k [7] which is related to the fast flocculation rate k_0 by the stability ratio W ,

$$W = \frac{k_0}{k}. \quad (1.9)$$

W is related to the energy maximum G_{\max} by [8]

$$W = \frac{1}{2} k_0 \exp\left(\frac{G_{\max}}{kT}\right). \quad (1.10)$$

To maintain colloid stability over a long period of time (i.e. 2–3 years), one needs to ensure the following conditions: High zeta potential by ensuring adequate coverage of the particles or droplets by ionic surfactant; low electrolyte concentration; low valency of the electrolyte (multivalent ions should be avoided).

Since approximate formulae are available for G_{elec} and G_A , quantitative expressions for $G_T(h)$ can also be formulated. These can be used to derive expressions for the coagulation concentration, which is the concentration that causes every encounter between two colloidal particles to lead to destabilization. Verwey and Overbeek [5] introduced the following criteria for transition between stability and instability,

$$G_T (= G_{\text{elec}} + G_A) = 0, \quad (1.11)$$

$$\frac{dG_T}{dh} = 0, \quad (1.12)$$

$$\frac{dG_{\text{elec}}}{dh} = -\frac{dG_A}{dh}. \quad (1.13)$$

Using the equations for G_{elec} and G_A , the critical coagulation concentration, CCC could be calculated as will be shown below. The theory predicts that the CCC is directly proportional to the surface potential ψ_0 and inversely proportional to the Hamaker constant A and the electrolyte valency Z . The CCC is inversely proportional to Z^6 at high surface potential and inversely proportional to Z^2 at low surface potential.

Another method to counteract van der Waals attraction is to use polymeric surfactants that adsorb strongly at the solid/liquid and liquid/liquid interfaces [9, 10]. Many polymeric surfactants are used for the preparation of disperse systems (suspensions and emulsions) in pharmaceutical formulations. Both homopolymers, such as polyvinylpyrrolidone, and block-copolymers, such as Poloxamers (A–B–A block copolymers of polyethylene oxide, A, and polypropylene oxide, B) are used for stabilizing pharmaceutical disperse systems. Their adsorption and conformation on a solid surface are schematically shown in Fig. 1.5.

On hydrophobic drug particles or oil droplets, the polymer adsorbs with the B hydrophobic chain (PPO) close to the surface, leaving the two hydrophilic A chains dangling in solution. These nonionic polymers provide stabilization against flocculation and/or coalescence by a mechanism that is usually referred to as steric stabilization [9]. In order to understand the principles of steric stabilization, one must first consider the adsorption and conformation of the polymer at the solid/liquid or liquid/liquid interface. The PPO chain adsorbs on the surface with many attachment points forming small “loops”, whereas the A chains (sometimes referred to as “tails”) extend to some distance (few nm) from the surface [10].

The adsorption of polymers at interfaces differs significantly from that of simple surfactant molecules. The adsorption isotherm is of the high affinity type, i.e. the first added molecules are virtually completely adsorbed and plateau adsorption is reached at low equilibrium concentration. Adsorption is practically “irreversible” because the molecule is attached with several segments to the surface.

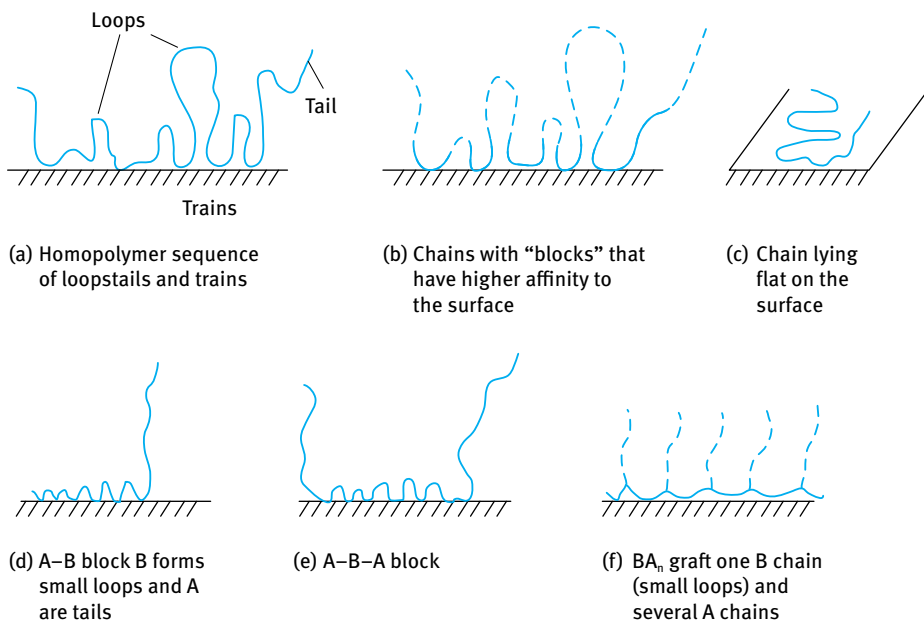


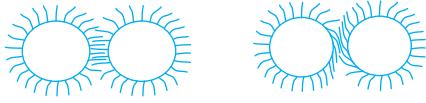
Fig. 1.5: Schematic representation of the adsorption and conformation of various polymers on a flat surface.

The adsorption isotherm depends on the structure, molecular weight and environment (temperature, electrolyte) of the chains. For fully characterizing polymer adsorption, one needs information on the following parameters: The amount of adsorption Γ ; the fraction of segments in "trains" and the adsorption energy per segment; the extension of the A chains in bulk solution, usually described as "segment density distribution", $\rho(z)$, or hydrodynamic thickness δ_h . It is essential to know how these parameters vary with the system parameters such as proportion of hydrophobic to hydrophilic chains, molecular weight, flexibility, temperature, addition of electrolyte.

The most important parameters for steric stabilization are the strong "anchoring" of the B chain to the surface and the extension of the A chains (adsorbed layer thickness, δ_h) and its solvation by the molecules of the medium.

When two particles or droplets each with a radius R and containing an adsorbed surfactant or polymer layer with a hydrodynamic thickness δ_h , approach each other to a surface-surface separation distance of separation h that is smaller than $2\delta_h$, the surfactant or polymer layers interact with each other resulting in two main conditions: the polymer chains may overlap with each other or the polymer layers may undergo compression. In both cases, there will be an increase in the local segment density of the chains in the interaction region. This is schematically illustrated in Fig. 1.6.

The real situation is perhaps in between the above two case, i.e. the polymer chains may undergo some interpenetration and some compression. Providing the



Interpenetration without compression

Compression without interpenetration

Fig. 1.6: Schematic representation of interaction of adsorbed layers.

dangling chains (A chains) are in good solvent (i.e. strongly solvated by the solvent molecules), this local increase in segment density will result in strong repulsion as a result of two main effects.

Two main repulsive energies can be defined:

- (i) Osmotic repulsion arising from the unfavourable mixing of the stabilizing A chains when these are in good solvent conditions. This is referred to as mixing interaction, G_{mix} .
- (ii) Entropic, volume restriction or elastic interaction resulting from the loss of configurational entropy of the chains on considerable overlap. This is referred to as elastic interaction, G_{el} .

As a result of the unfavourable mixing of the chains, when these are in good solvent conditions, an increase in the osmotic pressure in the interaction zone occurs, and G_{mix} is given by the following expression [9]:

$$\frac{G_{\text{mix}}}{kT} = \left(\frac{2V_2^2}{V_1} \right) v^2 \left(\frac{1}{2} - \chi \right) \left(\delta - \frac{h}{2} \right) \left(3R + 2\delta + \frac{h}{2} \right), \quad (1.14)$$

where k is the Boltzmann constant, T is the absolute temperature, V_2 is the molar volume of polymer, V_1 is the molar volume of solvent, v is the number of polymer chains per unit area, and χ is the Flory–Huggins interaction parameter.

The sign of G_{mix} depends on the value of the Flory–Huggins interaction parameter. When the chains are in good solvent conditions (strongly solvated by the molecules of the medium, $\chi < 1/2$ and G_{mix} is positive, i.e. the mixing interaction free energy is positive and this leads to strong repulsion as soon as $h < 2\delta$. Clearly, to maintain stability of a suspension or emulsion one must ensure that χ is less than $(1/2)$ under all conditions of storage (e.g. temperature variation, addition of electrolyte, etc.).

G_{el} may be given by the following simple expression (assuming the chains to be represented by simple rods that rotate in a circle with a radius δ),

$$\frac{G_{\text{el}}}{kT} = 2kTv^2 \ln \left[\frac{\Omega(h)}{\Omega(\infty)} \right], \quad (1.15)$$

where $\Omega(h)$ is the number of chain configurations after overlap ($h < \delta$), and $\Omega(\infty)$ is the number of chain configurations before overlap ($h > 2\delta$).

G_{el} is always positive and could play a major role in steric stabilization. The steric free energy of interaction G_s is given by the sum of G_{mix} and G_{el} , and when this is

added to the van der Waals attraction gives the total interaction energy G_T ,

$$G_T = G_S + G_A = G_{\text{mix}} + G_{\text{el}} + G_A. \quad (1.16)$$

A schematic representation of the variation of G_{mix} , G_{el} , G_A and G_T with h is given in Fig. 1.7. G_{mix} increases very sharply with decreasing h when $h < 2\delta$. G_{el} increases very sharply with decreasing h when $h < \delta$. G_T versus h shows a minimum, G_{min} , at separation distances comparable to 2δ and G_T shows a rapid increase with a further decrease in h [9]. Unlike the G_T - h predicted by DLVO theory (which shows two minima and one energy maximum), the G_T - h curve for systems that are sterically stabilized dispersions shows only one minimum, G_{min} , followed by a sharp increase in G_T when $h < 2\delta$. The depth of the minimum depends on the Hamaker constant A , particle radius R and adsorbed layer thickness. At a given A and R , G_{min} increases with decreasing δ . When δ is small (say less than 5 nm), G_{min} may reach sufficient depth (few kT units) for weak flocculation to occur. However, this flocculation is reversible and by gentle shaking of the container the suspension or emulsion can be easily redispersed.

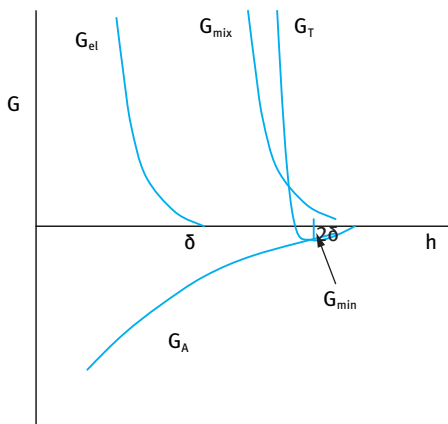


Fig. 1.7: Variation of G_{mix} , G_{el} , G_A and G_T with surface-surface distance between the particles.

When δ is sufficiently large (say > 10 nm), G_{min} may become so small that no flocculation will occur. In this case the suspension or emulsion approaches thermodynamic stability and no aggregation occurs over very long periods (more than two years). Clearly, the particle radius also plays a major role. The larger the particles, the deeper G_{min} becomes (at a given δ value).

Several criteria for effective steric stabilization can be defined:

- (i) The particles or droplets should be completely covered by the surfactant or polymer (the amount should correspond to the plateau value). Any bare patches may cause flocculation either by van der Waals attraction (between the bare patches) or by bridging flocculation (where a polymer molecule will become simultaneously adsorbed on two or more particles or droplets).

- (ii) The polymer should be strongly “anchored” to the particle’s or droplet’s surface to prevent any displacement during particle approach. This is particularly important for concentrated suspensions or emulsions. With an A–B–A block copolymer, the B chain is chosen to be highly insoluble in the medium and to have a strong affinity to the surface.
- (iii) The stabilizing chain(s) A should be highly soluble in the medium and strongly solvated by its molecules. In other words the Flory–Huggins interaction parameter for the A chains should always be less than (1/2). The most commonly used A chains are those based on PEO (e.g. with Poloxamers).
- (iv) The adsorbed layer thickness δ should be sufficiently large (> 5–10 nm) to prevent weak flocculation. This is particularly the case with concentrated suspensions and emulsions, since such flocculation may cause an increase in the viscosity of the system and make it difficult to redisperse on shaking.

1.3 Nanodispersions

Many water-insoluble drugs are formulated as nanodispersions, namely nanoemulsions and nanosuspensions. These systems enhance the bioavailability of insoluble drugs, since reducing the droplet or particle size to nanoscale dimensions increases the solubility of the drug. This can be clearly understood if one considers the effect of size on solubility as given by the Kelvin equation [11],

$$S(r) = S(\infty) \exp\left(\frac{2\gamma V_m}{rRT}\right), \quad (1.17)$$

where $S(r)$ is the solubility of a particle with radius r and $S(\infty)$ is the solubility of a particle with infinite radius (the bulk solubility), γ is the S/L interfacial tension, R is the gas constant and T is the absolute temperature. Equation (1.17) shows a significant increase in the solubility of a particle with the reduction of its radius, particularly when the latter becomes significantly smaller than 1 μm .

A schematic representation of the enhancement the solubility $c(r)/c(0)$ with decreasing particle or droplet size according to the Kelvin equation is shown in Fig. 1.8.

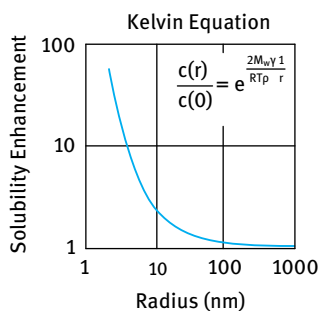


Fig. 1.8: Solubility enhancement with decreasing particle or droplet radius.

It can be seen from Fig. 1.8 that the solubility of nanodispersion particles or droplets increases very rapidly with decreasing radius, particularly when $r < 100$ nm. This means that a particle with a radius of say 4 nm will have about 10 times solubility enhancement compared say with a particle or droplet with 10 nm radius, which has a solubility enhancement of only 2 times.

Nanoemulsions are transparent or translucent systems mostly covering the size range 50–200 nm [12]. The long-term physical stability of nanoemulsions (with no apparent flocculation or coalescence) makes them unique and they are sometimes referred to as “approaching thermodynamic stability”. The inherently high colloid stability of nanoemulsions can be well understood from a consideration of their steric stabilization (when using nonionic surfactants and/or polymers) and how this is affected by the ratio of the adsorbed layer thickness to droplet radius as discussed above. Unless adequately prepared (to control the droplet size distribution) and stabilized against Ostwald ripening (that occurs when the oil has some finite solubility in the continuous medium), nanoemulsions may lose their transparency with time as a result of increasing droplet size.

Many lipophilic drugs are formulated as oil-in-water (O/W) nanoemulsions. The drug may be an oil with low viscosity which can be directly emulsified in water using a surfactant such as lecithin or castor oil ethoxylate. Viscous drug oils can be diluted with a low viscosity oil (hydrocarbon or vegetable oil) and the final mixture is then emulsified using the appropriate surfactant system. In some cases the lipophilic drug solid could be dissolved in an appropriate oil and the resulting oil solution is emulsified using the appropriate surfactant system.

The attraction of nanoemulsions for applications in pharmaceuticals is due to the following advantages [12]:

- (i) The very small droplet size causes a large reduction in gravity force and Brownian motion may be sufficient for overcoming gravity. This means that no creaming or sedimentation occurs on storage.
- (ii) The small droplet size also prevents any flocculation of the droplets. Weak flocculation is prevented and this enables the system to remain dispersed with no separation.
- (iii) The small droplets also prevent their coalescence, since these droplets are non-deformable and hence surface fluctuations are prevented. In addition, the significant surfactant film thickness (relative to droplet radius) prevents any thinning or disruption of the liquid film between the droplets.
- (iv) Nanoemulsions are suitable for efficient delivery of drugs.
- (v) The transparent nature of the system, its fluidity (at reasonable oil concentrations) as well as the absence of any thickeners make them easy to apply, e.g. in injectables.
- (vi) Nanoemulsions may be applied as a substitute for liposomes and vesicles (which are much less stable).

The most common method for preparing nanosuspensions is to use the top-down process where one starts with the bulk material (which may consist of aggregates and agglomerates) that is dispersed into single particles (using a wetting/dispersing agent) followed by subdivision of the large particles into smaller units that fall within the required nanosize [12]. This process requires the application of intense mechanical energy that can be achieved using bead milling, high pressure homogenization and/or application of ultrasonics. Finally, the resulting nanodispersion must remain colloidally stable under all conditions (such as temperature changes, vibration, etc.) with absence of any flocculation and/or crystal growth.

A schematic representation of the dispersion process is shown in Fig. 1.9. Most drugs are supplied as powders consisting of aggregates in which the particles are joined together with their “faces” (compact structures), or agglomerates in which the particles are connected at their corners (loose aggregates) as illustrated in Fig. 1.9. It is essential to wet both the external and internal surface (in the pores within the aggregate or agglomerate structures) and this requires the use of an effective wetting agent (surfactant) [13]. Wetting of a solid by a liquid (such as water) requires the replacement of the solid/vapour interfacial tension, γ_{SV} , by the solid/liquid interfacial tension, γ_{SL} .

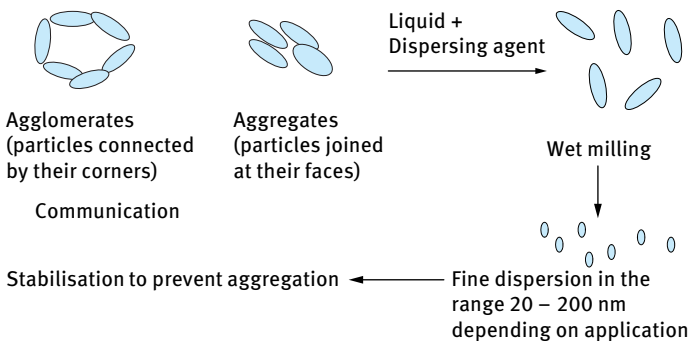


Fig. 1.9: Schematic representation of the dispersion process.

A useful parameter to describe wetting is the contact angle θ of a liquid drop on a solid substrate [14, 15]. If the liquid makes no contact with the solid, i.e. $\theta = 180^\circ$, the solid is referred to as non-wettable by the liquid in question. This may be the case for a perfectly hydrophobic surface with a polar liquid such as water. However, when $180^\circ > \theta > 90^\circ$, one may refer to a case of poor wetting. When $0^\circ < \theta < 90^\circ$, partial (incomplete) wetting is the case, whereas when $\theta = 0^\circ$ complete wetting occurs and the liquid spreads on the solid substrate forming a uniform liquid film.

Wetting and dispersion depends on: γ_{LV} , liquid surface tension; θ , contact angle between liquid and solid. The work of dispersion of a powder with surface area A , W_d ,

is given by [13],

$$W_d = A(\gamma_{SL} - \gamma_{SV}), \quad (1.18)$$

where γ_{SL} and γ_{SV} are the solid/liquid and solid/vapour interfacial tensions.

Using Young's equation,

$$\gamma_{SV} = \gamma_{SL} + \gamma_{LV} \cos \theta, \quad (1.19)$$

where γ_{LV} is the liquid/vapour interfacial tension and θ is the contact angle of the liquid drop at the wetting line.

$$W_d = -A\gamma_{LV} \cos \theta. \quad (1.20)$$

Equation (1.20) shows that W_d depends on γ_{LV} and θ , both of which are lowered by addition of surfactants (wetting agents). If $\theta < 90^\circ$, W_d is negative and dispersion is spontaneous.

Wetting of the internal surface requires penetration of the liquid into channels between and inside the agglomerates. The process is similar to forcing a liquid through fine capillaries. To force a liquid through a capillary with radius r , a pressure p is required that is given by,

$$p = -\frac{2\gamma_{LV} \cos \theta}{r} = \left[\frac{-2(\gamma_{SV} - \gamma_{SL})}{r\gamma_{LV}} \right]. \quad (1.21)$$

γ_{SL} has to be made as small as possible; rapid surfactant adsorption to the solid surface, low θ . When $\theta = 0$, $p \propto \gamma_{LV}$. Thus for penetration into pores one requires a high γ_{LV} . Thus, wetting of the external surface requires low contact angle θ and low surface tension γ_{LV} . Wetting of the internal surface (i.e. penetration through pores) requires low θ but high γ_{LV} . These two conditions are incompatible and a compromise has to be made: $\gamma_{SV} - \gamma_{SL}$ must be kept at a maximum and γ_{LV} should be kept as low as possible but not too low.

The above conclusions illustrate the problem of choosing the best dispersing agent for a particular powder. This requires measurement of the above parameters as well as testing the efficiency of the dispersion process.

The contact angle of liquids on solid powders can be measured by application of the Rideal–Washburn equation. For horizontal capillaries (gravity neglected), the depth of penetration l in time t is given by the Rideal–Washburn equation [16, 17],

$$l = \left[\frac{rt\gamma_{LV} \cos \theta}{2\eta} \right]^{1/2}. \quad (1.22)$$

To enhance the rate of penetration, γ_{LV} has to be made as high as possible, θ as low as possible and η as low as possible. For dispersion of powders into liquids one should use surfactants that lower θ while not reducing γ_{LV} too much. The viscosity of the liquid should also be kept at a minimum. Thickening agents (such as polymers) should

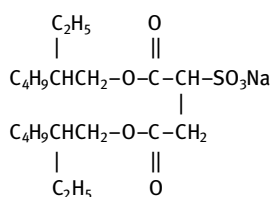
not be added during the dispersion process. It is also necessary to avoid foam formation during the dispersion process.

For a packed bed of particles, r may be replaced by K , which contains the effective radius of the bed and a tortuosity factor, which takes into account the complex path formed by the channels between the particles, i.e.,

$$l^2 = \frac{kt\gamma_{LV} \cos \theta}{2\eta}. \quad (1.23)$$

Thus a plot of l^2 versus t gives a straight line and from the slope of the line one can obtain θ . The Rideal–Washburn equation can be applied to obtain the contact angle of liquids (and surfactant solutions) in powder beds. K should first be obtained using a liquid that produces zero contact angle. A packed bed of powder is prepared say in a tube fitted with a sintered glass at the end (to retain the powder particles). It is essential to pack the powder uniformly in the tube (a plunger may be used in this case). The tube containing the bed is immersed in a liquid that gives spontaneous wetting (e.g. a lower alkane), i.e. the liquid gives a zero contact angle and $\cos \theta = 1$. By measuring the rate of penetration of the liquid (this can be carried out gravimetrically using for example a microbalance or a Kruss instrument) one can obtain K . The tube is then removed from the lower alkane liquid and left to stand for evaporation of the liquid. It is then immersed in the liquid in question and the rate of penetration is measured again as a function of time. Using equation (1.23), one can calculate $\cos \theta$ and hence θ .

For efficient wetting of hydrophobic solids in water, a surfactant is needed that lowers the surface tension of water very rapidly (within few ms) and quickly adsorbs at the solid/liquid interface [13]. To achieve rapid adsorption, the wetting agent should be either a branched chain with central hydrophilic group or a short hydrophobic chain with hydrophilic end group. The most commonly used wetting agent is Aerosol OT (diethylhexyl sulphosuccinate)



The above molecule has a low critical micelle concentration (cmc) of 0.7 g dm^{-3} and at and above the cmc the water surface tension is reduced to $\approx 25 \text{ mN m}^{-1}$ in less than 15 s.

Several nonionic surfactants such as the alcohol ethoxylates can also be used as wetting agents. These molecules consist of a short hydrophobic chain (mostly C_{10}) which is also branched. A medium chain polyethylene oxide (PEO) mostly consisting of 6 EO units or lower is used. These molecules also reduce the dynamic surface tension within a short time ($< 20 \text{ s}$) and they have reasonably low cmc.

In all cases, to avoid interference with the dispersant one should use the minimum amount of wetting agent necessary to maintain the colloid stability during dispersion and on storage.

Breaking of aggregates and agglomerates into individual units usually requires the application of mechanical energy. High speed mixers (which produce turbulent flow) of the rotor-stator type [13] are efficient in breaking up the aggregates and agglomerates, e.g. Silverson mixers, Ultra-Turrax. The mixing conditions have to be optimized: Heat generation at high stirring speeds must be avoided. This is particularly the case when the viscosity of the resulting dispersion increases during dispersion (note that the energy dissipation as heat is given by the product of the square of the shear rate and the viscosity of the suspension). One should avoid foam formation during dispersion; proper choice of the dispersing agent is essential and antifoams (silicones) may be applied during the dispersion process.

Rotor-stator mixers can be characterized as energy-intensive mixing devices. The main feature of these mixers is their ability to focus high energy/shear in a small volume of fluid. They consist of a high speed rotor enclosed in a stator, with the gap between them ranging from 100 to 3000 μm . Typically, the rotor speed is between 10 and 50 m s^{-1} , which, in combination with a small gap, generates very high shear rates. By operating at high speed, the rotor-stator mixers can significantly reduce processing time. In terms of energy consumption per unit mass of product, the rotor-stator mixers require high power input over a relatively short time. However, as the energy is uniformly delivered and dissipated in a relatively small volume, each element of the fluid is exposed to a similar intensity of processing. Frequently, the quality of the final product is strongly affected by its structure/morphology and it is essential that the key ingredients are uniformly distributed throughout the whole mixer volume.

There are a wide range of designs of rotor-stator mixers, of which the Ultra-Turrax (IKA Works, Germany) and Silverson (UK) are the most commonly used. They are broadly classified according to their mode of operation such as batch or in-line (continuous) mixers. In-line radial-discharge mixers are characterized by high throughput and good pumping capacity at low energy consumption. The disperse phase can be injected directly into the high shear/turbulent zone, where mixing is much faster than by injection into the pipe or into the holding tank. They are used for manufacturing very fine solid particles of relatively narrow dispersed size distribution. They are typically supplied with a range of interchangeable screens, making them reliable and versatile in different applications. Toothed devices are available as in-line as well as batch mixers. Due to their open structure they have a relatively good pumping capacity and they frequently do not need an additional impeller to induce bulk flow even in relatively large vessels.

The primary dispersion (sometimes referred to as the mill base) may then be subjected to a bead milling process to produce nanoparticles. Subdivision of the primary particles into much smaller units in the nanosize range (10–100 nm) requires application of intense energy. In some cases, high pressure homogenizers (such as the

Microfluidizer, USA) may be sufficient to produce nanoparticles. This is particularly the case with many drugs. In some cases, the high pressure homogenizer is combined with application of ultrasound to produce the nanoparticles [12]. It has been shown that high pressure homogenization is a simple technique, well established on large scale for the production of fine suspensions and already available in the pharmaceutical industry. High pressure homogenization is also an efficient technique that has been utilized to prepare stable nanosuspensions of several drugs such as carbazepin, bupravaquone, aphidicolin, cyclosporine, paclitaxel, prednisolone, etc. During homogenization, cavitation forces as well as collision and shear forces determine the breakdown of the drug particles down to the nanometre range. Process conditions lead to an average particle size that remains constant as a result of continuous fragmentation and reaggregation processes. These high energetic forces can also induce a change of crystal structure and/or partial or total amorphization of the sample, which further enhances the solubility. For long-term storage stability of the nanosuspension formulation, the crystal structure modification must be maintained over the storage time.

Microfluidization is a milling technique that results in minimal product contamination. Besides minimal contamination, this technique can be easily scaled up. In this method a sample dispersion containing large particles is made to pass through specially designed interaction chambers at high pressure. The specialized geometry of the chambers along with the high pressure causes the liquid stream to reach extremely high velocities and these streams then impinge against each other and against the walls of the chamber resulting in particle size reduction. The shear forces developed at high velocities due to attrition of particles against one another and against the chamber walls, as well as the cavitation fields generated inside the chamber are the main mechanisms of particle size reduction with this technique [12].

The process of microfluidization for the preparation of nanosuspensions varies in a complex way with the various critical processes and formulation parameters. Milling time, microfluidization pressure, stabilizer type, processing temperature and stabilizer concentration were identified as critical parameters affecting the formation of stable nanoparticles. Both ionic as well as steric stabilization were effective in stabilizing the nanosuspensions. Microfluidization and precipitation under sonication can also be used for nanosuspension preparation.

The extreme transient conditions generated in the vicinity and within the collapsing cavitation bubbles have been used for the reducing the size of the material to the nanoscale. Nanoparticles synthesis techniques include sonochemical processing and cavitation processing. In sonochemistry, an acoustic cavitation process can generate a transient localized hot zone with extremely high temperature gradient and pressure. Such sudden changes in temperature and pressure assist the destruction of the sonochemical precursor and the formation of nanoparticles [12].

An alternative method of size reduction to produce nanoparticles, which is commonly used in many industrial applications, is through wet milling [13]. Also referred

to as comminution (the generic term for size reduction), it is a complex process and there is little fundamental information on its mechanism. For the breakdown of single crystals or particles into smaller units, mechanical energy is required. This energy in a bead mill is supplied by impaction of the glass or ceramic beads with the particles. As a result, permanent deformation of the particles and crack initiation results. This will eventually lead to the fracture of the particles into smaller units. Since the milling conditions are random, some particles receive impacts far in excess of those required for fracture whereas others receive impacts that are insufficient for fracture. This makes the milling operation grossly inefficient and only a small fraction of the applied energy is used in comminution. The rest of the energy is dissipated as heat, vibration, sound, interparticulate friction, etc.

The role of surfactants and dispersants on the grinding efficiency is far from being understood. In most cases, the choice of surfactants and dispersant is made by trial and error until a system is found that gives the maximum grinding efficiency. Reh binder and his collaborators [18] investigated the role of surfactants in the grinding process. As a result of surfactant adsorption at the solid/liquid interface, the surface energy at the boundary is reduced and this facilitates the process of deformation or destruction. The adsorption of surfactants at the solid/liquid interface in cracks facilitates their propagation. This mechanism is referred to as the Reh binder effect.

Several factors affect the efficiency of dispersion and milling [10]:

- (i) The volume concentration of dispersed particles (i.e. the volume fraction).
- (ii) The nature of the wetting/dispersing agent.
- (iii) The concentration of wetter/dispersant (which determines the adsorption characteristics).

For optimizing the dispersion/milling process the above parameters need to be systematically investigated. From the wetting performance of a surfactant, that can be evaluated using contact angle measurements, one can establish the nature and concentration of the wetting agent. The nature and concentration of dispersing agent required is determined by adsorption isotherm and rheological measurements.

Once the concentration of wetting/dispersing agent is established, dispersions are prepared at various volume fractions keeping the ratio of wetting/dispersing agent to the solid content constant. Each system is then subjected to the dispersion/milling process keeping all parameters constant:

- (i) Speed of the stirrer (normally one starts at lower speed and gradually increases the speed in increments at fixed time).
- (ii) Volume and size of beads relative to the volume of the dispersion (an optimum value is required).
- (iii) Speed of the mill.

The change of average particle size with grinding time is established using for example the Mastersizer (Malvern, UK). Fig. 1.10 shows a schematic representation of the

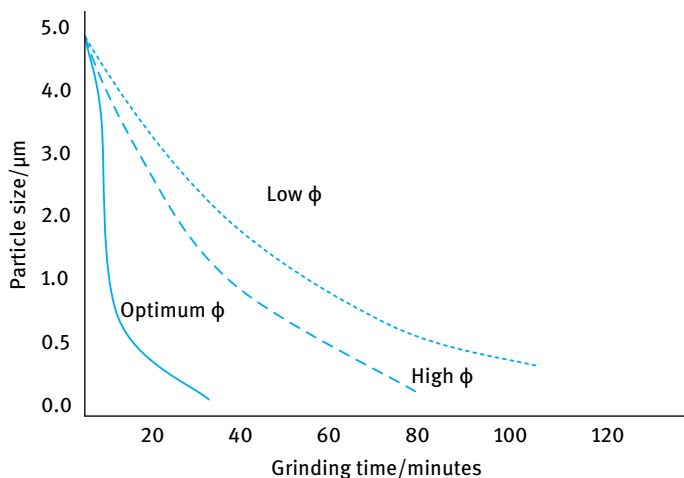


Fig. 1.10: Variation of particle size with grinding time in a typical bead mill.

reduction of particle size with grinding time in minutes using a typical bead mill (see below) at various volume fractions.

The presentation in Fig. 1.10 is only schematic and is not based on experimental data. It shows the expected trend. When the volume fraction ϕ is below the optimum (in this case the relative viscosity of the dispersion is low), a long time is required to achieve size reduction. In addition, the final particle size may be large and outside the nanorange. When ϕ is above the optimum value, the dispersion time is prolonged (due to the relatively high relative viscosity of the system) and the grinding time is also longer. In addition, the final particle size is larger than that obtained at the optimum ϕ . At the optimum volume fraction both the dispersion and grinding time are shorter and also the final particle size is smaller [12].

For preparing nanosuspensions, bead mills are most commonly used. The beads are mostly made of glass or ceramics (which are preferred due to minimum contamination). The operating principle is to pump the premixed, preferably predispersed (using a high speed mixer), millbase through a cylinder containing a specified volume of say ceramic beads (normally 0.5–1 mm diameter to achieve nanosize particles). The dispersion is agitated by a single or multidisc rotor. The disc may be flat or perforated. The mill base passing through the shear zone is then separated from the beads by a suitable screen located at the opposite end of the feedport [13].

Generally speaking, bead mills may be classified to two types:

- (i) vertical mills with open or closed top;
- (ii) horizontal mills with closed chambers.

The horizontal mills are more efficient and the most commonly used ones are: Netzsch (Germany) and Dyno Mill (Switzerland). These bead mills are available in various sizes

from 0.5 to 500 litres. The factors affecting the general dispersion efficiency are known reasonably well (from the manufacturer). The selection of the right diameter of the beads is important for maximum utilization. In general, the smaller the size of the beads and the higher their density, the more efficient the milling process [10].

To understand the principle of operation of the bead mill, one must consider the centrifugal force transmitted to the grinding beads at the tip of the rotating disc which increases considerably by its weight. This applies greater shear to the mill base. This explains why the more dense beads are more efficient in grinding. The speed transmitted to the individual chambers of the beads at the tip of the disc assumes that speed and force can be calculated [13].

The centrifugal force F is simply given by,

$$F = \frac{v^2}{rg}, \quad (1.24)$$

where v is the velocity, r is the radius of the disc and g is the acceleration due to gravity.

Several procedures can be applied for preparing nanoemulsions. Before describing the various methods, it is necessary to consider the process of emulsification, in particular the necessity of applying high energy to produce nanodroplets. As discussed before, the free energy of formation of drops from a bulk oil phase, ΔG , is positive and the process of emulsification is non-spontaneous and energy is necessary to produce the emulsion. The formation of large droplets (few μm), as is the case for macroemulsions, is fairly easy and hence high speed stirrers such as the Ultra-Turrax or Silverson mixers are sufficient to produce the emulsion. In contrast, the formation of small drops (submicron as is the case with nanoemulsions) is difficult and this requires a large amount of surfactant and/or energy [19, 20]. The high energy required for formation of nanoemulsions can be understood from a consideration of the Laplace pressure p (the difference in pressure between inside and outside the droplet,

$$p = \gamma \left(\frac{1}{R_1} + \frac{1}{R_2} \right), \quad (1.25)$$

where R_1 and R_2 are the principal radii of curvature of the drop.

For a spherical drop, $R_1 = R_2 = R$ and,

$$p = \frac{2\gamma}{R}. \quad (1.26)$$

To break up a drop into smaller ones, it must be strongly deformed and this deformation increases p . Consequently, the stress needed to deform the drop is higher for a smaller drop. Since the stress is generally transmitted by the surrounding liquid via agitation, higher stresses need more vigorous agitation, hence more energy is needed to produce smaller drops [11]. Surfactants play major roles in the formation of nanoemulsions: By lowering the interfacial tension, p is reduced and hence the stress needed to break up a drop is reduced. Surfactants prevent coalescence of newly formed drops.

Four methods may be applied for the preparation of nanoemulsions (covering the droplet radius size range 50–200 nm) [12]: Use of high pressure homogenizers (aided by appropriate choice of surfactants and cosurfactants); application of the phase inversion composition method; application of the phase inversion temperature (PIT) concept; dilution of a microemulsion.

As mentioned above, the production of small droplets (submicron) requires application of high energy. The process of emulsification is generally inefficient as simple calculations show that the mechanical energy required for emulsification exceeds the interfacial energy by several orders of magnitude. For example, to produce an emulsion at $\phi = 0.1$ with a Sauter diameter (volume/area) $d_{32} = 0.6 \mu\text{m}$, using a surfactant that gives an interfacial tension $\gamma = 10 \text{ mN m}^{-1}$, the net increase in surface free energy is $A\gamma = 6\phi\gamma/d_{32} = 10^4 \text{ J m}^{-3}$. The mechanical energy required in a homogenizer is 10^7 J m^{-3} , i.e. an efficiency of 0.1%. The rest of the energy (99.9%) is dissipated as heat [21].

The intensity of the process or the effectiveness in making small droplets is often governed by the net power density ($\varepsilon(t)$).

$$p = \varepsilon(t) dt, \quad (1.27)$$

where t is the time during which emulsification occurs.

Break-up of droplets will only occur at high ε values, which means that the energy dissipated at low ε levels is wasted. Batch processes are generally less efficient than continuous processes. This shows why with a stirrer in a large vessel, most of the energy applied at low intensity is dissipated as heat. In a homogenizer, p is simply equal to the homogenizer pressure.

Several procedures may be applied to enhance the efficiency of emulsification when producing nanoemulsions [12]: One should optimize the efficiency of agitation by increasing ε and decreasing dissipation time. The emulsion is preferably prepared at high volume fraction of the disperse phase and diluted afterwards. However, very high ϕ values may result in coalescence during emulsification. Add more surfactant, whereby creating a smaller γ_{eff} and possibly diminishing re-coalescence. Use surfactant mixture that shows more reduction in γ the individual components. If possible, dissolve the surfactant in the disperse phase rather than the continuous phase; this often leads to smaller droplets. It may be useful to emulsify in steps of increasing intensity, particularly with emulsions that have a highly viscous disperse phase.

The second method for preparing nanoemulsions is by application of the phase inversion composition (PIC) principle (low energy method) [12]. A study of the phase behaviour of water/oil/surfactant systems demonstrated that emulsification can be achieved by three different low energy emulsification methods, as schematically shown in Fig. 1.11.

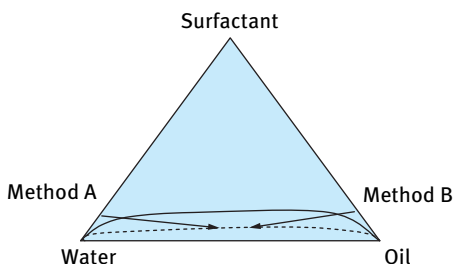


Fig. 1.11: Schematic representation of the experimental path in two emulsification methods: Method A, addition of decane to water/surfactant mixture; method B, addition of water to decane/Brij 30 solutions.

- (A) Stepwise addition of oil to a water surfactant mixture;
- (B) stepwise addition of water to a solution of the surfactant in oil;
- (C) mixing all the components in the final composition, pre-equilibrating the samples prior to emulsification.

In these studies, the system water/Brij 30 (polyoxyethylene lauryl ether with an average of 4 mol of ethylene oxide)/ decane was chosen as a model to obtain O/W emulsions. The results showed that nanoemulsions with droplet sizes of the order of 50 nm were formed only when water was added to mixtures of surfactant and oil (method B) whereby inversion from W/O emulsion to O/W nanoemulsion occurred.

The third method for preparing nanoemulsions is to apply the phase inversion temperature (PIT) principle. Phase inversion in emulsions can be one of two types: Transitional inversion induced by changing factors which affect the HLB of the system, e.g. temperature and/or electrolyte concentration; or catastrophic inversion which is induced by increasing the volume fraction of the disperse phase.

Transitional inversion can also be induced by changing the HLB number of the surfactant at constant temperature using surfactant mixtures. This is illustrated in Fig. 1.12 which shows the average droplet diameter and rate constant for attaining constant droplet size as a function of the HLB number. It can be seen that the diameter decreases and the rate constant increases as inversion is approached.

To apply the phase inversion principle one uses the transitional inversion method, which has been demonstrated by Shinoda and co-workers [22, 23] using nonionic sur-

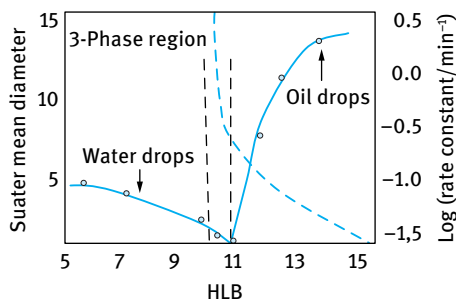


Fig. 1.12: Emulsion droplet diameters (circles) and rate constant for attaining steady size (squares) as function of HLB – cyclohexane/nonylphenol ethoxylate.

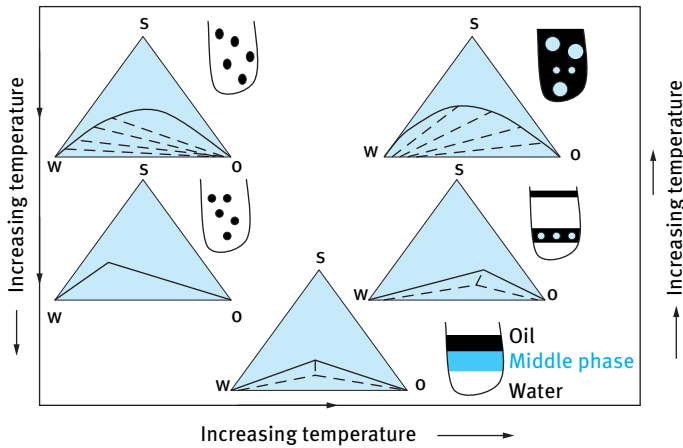


Fig. 1.13: The PIT concept.

factants of the ethoxylate type. These surfactants are highly dependent on temperature, becoming lipophilic with increasing temperature due to the dehydration of the polyethyleneoxide chain. When an O/W emulsion prepared using a nonionic surfactant of the ethoxylate type is heated, then at a critical temperature (the PIT), the emulsion inverts to a W/O emulsion. At the PIT the droplet size reaches a minimum and the interfacial tension also reaches a minimum. However, the small droplets are unstable and they coalesce very rapidly. By rapid cooling of an emulsion prepared at a temperature near the PIT, very stable and small emulsion droplets could be produced.

A clear demonstration of the phase inversion that occurs on heating an emulsion is illustrated from a study of the phase behaviour of emulsions as a function of temperature. This is illustrated in Fig. 1.13 which shows schematically what happens when the temperature is increased [12]. At low temperature, over the Winsor I region, O/W macroemulsions can be formed and are quite stable. On increasing the temperature, the O/W emulsion stability decreases and the macroemulsion finally resolves when the system reaches the Winsor III phase region (both O/W and W/O emulsions are unstable). At higher temperature, over the Winsor II region, W/O emulsions become stable.

Near the HLB temperature, the interfacial tension reaches a minimum. This is illustrated in Fig. 1.14. Thus, by preparing the emulsion at a temperature 2–4 °C below the PIT (near the minimum in γ) followed by rapid cooling of the system, nanoemulsions may be produced. The minimum in γ can be explained in terms of the change in curvature H of the interfacial region, as the system changes from O/W to W/O. For an O/W system and normal micelles, the monolayer curves towards the oil and H is given a positive value. For a W/O emulsion and inverse micelles, the monolayer curves towards the water and H is assigned a negative value. At the inversion point (HLB temperature) H becomes zero and γ reaches a minimum.

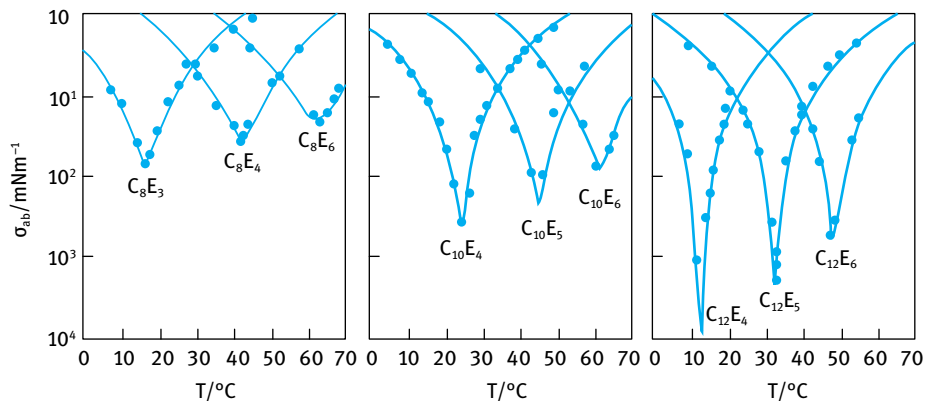


Fig. 1.14: Interfacial tensions of n-octane against water in the presence of various C_nE_m surfactants above the cmc as a function of temperature.

The fourth method for preparing nanoemulsions is by dilution of microemulsions, e.g. by self-emulsification by diluting an O/W microemulsion with water [12]. When diluting a microemulsion with water, part of the surfactant and/or cosurfactant diffuses to the aqueous phase. The droplets are no longer thermodynamically stable, since the surfactant concentration is not high enough to maintain the ultra-low interfacial tension ($<10^{-4} \text{ mN m}^{-1}$) for thermodynamic stability. The system becomes unstable and the droplets show a tendency to grow by coalescence and/or Ostwald ripening forming a nanoemulsion. This is illustrated in Fig. 1.15 which shows the phase diagram of the system water/SDS-Hexanol (ratio of 1 : 1.76)/dodecane.

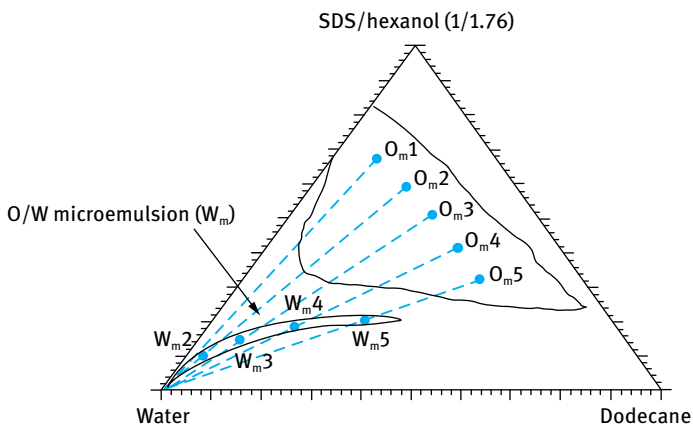


Fig. 1.15: Pseudoternary phase diagram of water/SDS/hexanol/dodecane with SDS : hexanol ratio of 1 : 1.76. Solid and dashed lines indicate the emulsification paths followed starting from both O/W (W_m) and W/O (O_m) microemulsion domains.

Nanoemulsions can be prepared starting from microemulsions located in the inverse microemulsion domain, O_m , and in the direct microemulsion domain, W_m , at different oil:surfactant ratios ranging from 12 : 88 to 40 : 60, and coincident for both types of microemulsions. The water concentration is fixed at 20 % for microemulsions in the O_m domain labelled as O_{m1} , O_{m2} , O_{m3} , O_{m4} , O_{m5} . The microemulsions in the W_m region are accordingly W_{m2} , W_{m3} , W_{m4} , W_{m5} and their water content decreases from W_{m2} to W_{m5} .

Several emulsification methods can be applied:

- (a) addition of microemulsion into water in one step;
- (b) addition of microemulsion into water stepwise;
- (c) addition of water into microemulsion in one step;
- (d) addition of water into microemulsion stepwise.

The final water content is kept constant at 98 wt%.

Starting emulsification from W_m microemulsions, low-polydispersed nanoemulsions with droplet sizes within the range 20–40 nm are obtained regardless of the emulsification method used. When starting from O_m microemulsions, nanoemulsion formation and properties depend on the emulsification method. From an O_{m1} microemulsion, a turbid emulsion with rapid creaming is obtained whatever method is used. In this case the direct microemulsion region W_m is not crossed. Starting from O_{m2} to O_{m5} and using emulsification method (d), in which water is gradually added to the microemulsion, the nanoemulsion droplet sizes coincide with those obtained starting from microemulsions in the W_m domain for the corresponding O : S ratio. Methods (a), (b) and (c) produce coarse emulsions.

To assess nanodispersion formation, one usually measures the particle or droplet size distribution using dynamic light scattering techniques (photon correlation spectroscopy, PCS). In this technique, one measures the intensity fluctuation of scattered light by the droplets as they undergo Brownian motion [12]. When a light beam passes through a nanodispersion, an oscillating dipole moment is induced in the particles or droplets, thereby reradiating the light. Due to the random position of the particles or droplets, the intensity of scattered light will, at any instant, appear as a random diffraction or “speckle” pattern. As the particles or droplets undergo Brownian motion, the random configuration of the pattern will, therefore, fluctuate such that the time taken for an intensity maximum to become a minimum, i.e. the coherence time, corresponds exactly to the time required for the droplet to move one wavelength. Using a photomultiplier of active area about the diffraction maximum, i.e. one coherence area, this intensity fluctuation can be measured. The analogue output is digitized using a digital correlator that measures the photocount (or intensity) correlation function of the scattered light. The photocount correlation function $G^{(2)}(\tau)$ is given by the equation,

$$G^{(2)}(\tau) = B(1 + \gamma^2 [g^{(1)}(\tau)]^2), \quad (1.28)$$

where τ is the correlation delay time. The correlator compares $G^{(2)}(\tau)$ for many values of τ . B is the background value to which $G^{(2)}(\tau)$ decays at long delay times. $g^{(1)}(\tau)$ is the normalized correlation function of the scattered electric field and γ is a constant (≈ 1).

For monodisperse noninteracting particles or droplets,

$$g^{(1)} = \exp(-\Gamma\tau), \quad (1.29)$$

where Γ is the decay rate or inverse coherence time, that is related to the translational diffusion coefficient D by the equation,

$$\Gamma = DK^2, \quad (1.30)$$

where K is the scattering vector,

$$K = \frac{4\pi n}{\lambda_0} \sin\left(\frac{\theta}{2}\right). \quad (1.31)$$

λ is the wavelength of light in vacuo, n is the refractive index of the solution and θ is the scattering angle.

The particle or droplet radius R can be calculated from D using the Stokes–Einstein equation,

$$D = \frac{kT}{6\pi\eta_0 R}. \quad (1.32)$$

η_0 is the viscosity of the medium.

The above analysis is valid for dilute monodisperse particles or droplets. With many nanodispersions, the particles or droplets are not perfectly monodisperse (usually with a narrow size distribution) and the light scattering results are analysed for polydispersity (the data are expressed as an average size and a polydispersity index that gives information on the deviation from the average size).

Since most nanoemulsions are prepared using nonionic and/or polymeric surfactants, it is necessary to consider the interaction forces between droplets containing adsorbed layers (steric stabilization). This was described in detail above. As shown in Fig. 1.7, the energy–distance curve for sterically stabilized dispersion shows a shallow minimum G_{\min} at separation distances h close to twice the adsorbed layer thickness 2δ . At a given droplet radius R and Hamaker constant A , G_{\min} decreases in magnitude and at sufficiently thick adsorbed layer δ it can become $< kT$. This is illustrated in Fig. 1.16 which shows the energy–distance curves as a function of increasing δ/R . It can be seen from Fig. 1.16 that the depth of the minimum decreases with increasing δ/R . This is the basis of the high kinetic stability of nanoemulsions. With nanoemulsions having a radius in the region of 50 nm and an adsorbed layer thickness of say 10 nm, the value of δ/R is 0.2. This high value (when compared with the situation with macroemulsions where δ/R is at least an order of magnitude lower) results in a very shallow minimum (which could be less than kT). This situation results in very high

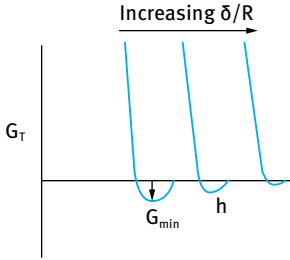


Fig. 1.16: Variation of G_T with h with increasing δ/R .

stability with no flocculation (weak or strong). In addition, the very small size of the droplets and the dense adsorbed layers ensure lack of deformation of the interface, lack of thinning and disruption of the liquid film between the droplets and hence coalescence is also prevented.

One of the main problems with nanoemulsions is Ostwald ripening which results from the difference in solubility between small and large droplets as shown above by the Kelvin equation [11].

For two droplets of radii r_1 and r_2 (where $r_1 < r_2$),

$$\left(\frac{RT}{V_m}\right) \ln \left[\frac{c(r_1)}{c(r_2)} \right] = 2\gamma \left(\frac{1}{r_1} - \frac{1}{r_2} \right). \quad (1.33)$$

Equation (1.33) shows that the larger the difference between r_1 and r_2 , the higher the rate of Ostwald ripening.

Ostwald ripening can be quantitatively assessed from plots of the cube of the radius versus time t (the Lifshitz–Slesov–Wagner, LSW, theory) [24, 25],

$$r^3 = \frac{8}{9} \left[\frac{c(\infty)\gamma V_m D}{\rho RT} \right] t, \quad (1.34)$$

where D is the diffusion coefficient of the disperse phase in the continuous phase and ρ is the density of the disperse phase.

Several methods may be applied to reduce Ostwald ripening [21]:

- (i) Addition of a second disperse phase component which is insoluble in the continuous phase (e.g. squalene). In this case significant partitioning between different droplets occurs, with the component having low solubility in the continuous phase expected to be concentrated in the smaller droplets. During Ostwald ripening in a two component disperse phase system, equilibrium is established when the difference in chemical potential between different size droplets (which results from curvature effects) is balanced by the difference in chemical potential resulting from partitioning of the two components. If the secondary component has zero solubility in the continuous phase, the size distribution will not deviate from the initial one (the growth rate is equal to zero). In the case of limited solubility of the secondary component, the distribution is the same as governed by equation (1.34), i.e. a mixture growth rate is obtained which is still lower than that of the more soluble component.

- (ii) Modification of the interfacial film at the O/W interface: According to equation (1.34), a reduction in γ results in a reduction of Ostwald ripening. However, this alone is not sufficient since one has to reduce γ by several orders of magnitude. It was suggested that by using surfactants which are strongly adsorbed at the O/W interface (i.e. polymeric surfactants) and which do not desorb during ripening, the rate could be significantly reduced. An increase in the surface dilational modulus and a decrease in γ would be observed for the shrinking drops. The difference in γ between the droplets would balance the difference in capillary pressure (i.e. curvature effects).

To achieve the above effect it is useful to use A–B–A block copolymers that are soluble in the oil phase and insoluble in the continuous phase. The polymeric surfactant should enhance the lowering of γ by the emulsifier. In other words, the emulsifier and the polymeric surfactant should show synergy in lowering γ .

References

- [1] Tadros T. *Formulation of Disperse Systems*. Weinheim: Wiley-VCH; 2014.
- [2] Hamaker HC. *Physica*. 1937;4:1058.
- [3] Smoluchowski MV. *Z Phys Chem*. 1927;92:129.
- [4] Kruyt HR. *Colloid Science Vol. I*. Amsterdam: Elsevier; 1952.
- [5] Verwey EJW, Overbeek JTG. *Theory of stability of lyophobic colloids*. Amsterdam: Elsevier; 1948.
- [6] Deryaguin BV, Landau L. *Acta Physicochem USSR*. 1941;14:633.
- [7] Fuchs N. *Z Physik*. 1936;89:736.
- [8] Reerink H, Overbeek JTG. *Discussion Faraday Soc*. 1954;18:74.
- [9] Napper DH. *Polymeric stabilisation of colloidal dispersions*. London: Academic Press; 1983.
- [10] Tadros TF. *Polymer Adsorption*. In: Buscall R, Corner T, Stageman JF, editors. *Polymer colloids*. London: Applied Sciences, Elsevier; 198., p. 105.
- [11] Thompson W (Lord Kelvin). *Phil Mag*. 1871;42:448.
- [12] Tadros T. *Nanodispersions*. Berlin: De Gruyter; 2016.
- [13] Tadros T. *Dispersions of powders in liquids and stabilisation of suspensions*. Weinheim: Wiley-VCH; 2012.
- [14] Young T. *Phil Trans Royal Soc (London)*. 1805;95:65.
- [15] Blake TB. *Wetting*. In: Tadros TF, editor. *Surfactants*. London: Academic Press; 1984.
- [16] Rideal EK. *Phil Mag*. 1922;44:1152.
- [17] Washburn ED. *Phys Rev*. 1921;17:273.
- [18] Reh binder PA. *Colloid J USSR*. 1958;20:493.
- [19] Tadros T, editor. *Emulsion science and technology*. Weinheim: Wiley-VCH; 2009.
- [20] Tadros T, editor. *Emulsion formation and stability*. Weinheim: Wiley-VCH; 2013.
- [21] Walstra P, Smolders PEA. In: Binks BP, editor. *Modern aspects of emulsions*. Cambridge: The Royal Society of Chemistry; 1998.
- [22] Shinoda K, Saito H. *J Colloid Interface Sci*. 1968;26:70.

- [23] Shinoda K, Saito H. The stability of O/W type emulsions as functions of temperature and the HLB of emulsifiers: The emulsification by PIT-method. *J Colloid Interface Sci.* 1969;30:258–263.
- [24] Lifshitz EM, Slesov VV. *Soviet Physics JETP.* 1959;35:331.
- [25] Wagner C. *Z Electrochem.* 1961;35:581.

2 Surface activity and colloidal properties of drugs

2.1 Introduction

A large number of drugs exhibit typical colloidal behaviour in aqueous solution in that they accumulate at interfaces, i.e. they are surface active. Thus, these molecules lower the surface tension of water and form aggregates at sufficiently high concentrations, resembling micelles that are produced with surfactants. Typical examples of drugs that produce such surface activity and association are the antihistamines, e.g. diphenylmethane derivatives (such as diphenhydramine), chlorcyclizine, chlorpromazine, and tricyclic antidepressants (such as amitriptyline) [1]. However, micellization of drugs represents only one pattern of association, since with many drug molecules rigid aromatic or heterocyclic chains replace the flexible hydrophobic chains present in most surfactant systems. This will have a pronounced effect on the mode of association, to an extent that the process may not be regarded as micellization. A self-association structure may be produced by hydrophobic interaction (charge repulsion plays an insignificant role in this case) and the process is generally continuous, i.e. with no abrupt change in the properties. It should be mentioned, however, that many drug molecules may contain aromatic groups with a high degree of flexibility. In this case, the association structures resemble surfactant micelles.

2.2 Investigating the association behaviour of drugs

The best technique to investigate the association behaviour of drugs is to measure light scattering as a function of drug concentration in solution. This is illustrated in Fig. 2.1 which shows the light scattering results for a number of diphenylmethane antihistamines [2].

The results of Fig. 2.1 clearly show distinct inflection points which may be identified with the critical micelle concentration (cmc). However, the aggregation numbers of these association units are much lower (in the region of 9–12) than those encountered with micellar surfactants (which show aggregation numbers of 50 or more depending on the alkyl chain length). This lower aggregation numbers cast some doubt on micelle formation and a continuous association process may be envisaged instead.

The light scattering results could be fitted by Attwood and Udeala [3] using the mass action model for micellization.

Considering the ionic micelle, M^{+p} to be formed by association of n drug ions, D^+ , and $(n - p)$ firmly bound counterions, X^- ,



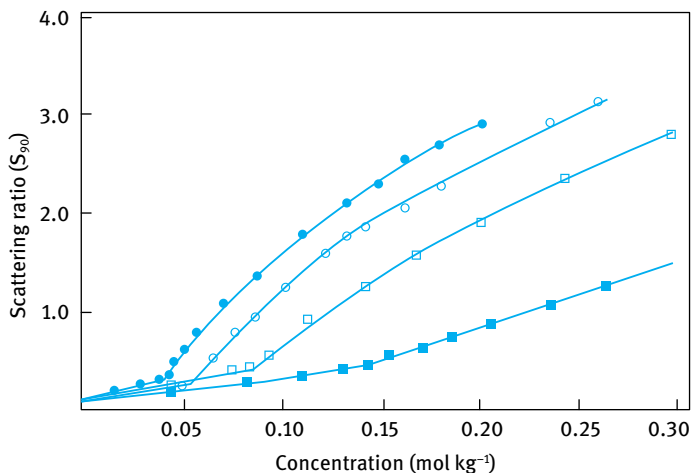


Fig. 2.1: Variation of the scattering ratio, S_{90} , with concentration for aqueous solutions of diphenylmethane antihistamines: ●, chlorocyclizine hydrochloride; ○, bromodiphenhydramine hydrochloride; □, diphenylpyraline hydrochloride; ■, diphenylhydramine hydrochloride; (—) calculated from mass action theory.

The equilibrium constant for micelle formation assuming ideality is given by the equation,

$$K_m = \frac{x_m}{[x_s]^n [x_x]^{n-p}}, \quad (2.2)$$

where x_x is the mole fraction of counterion.

The standard free energy of micellization per mole of monomeric drug is given by

$$\Delta G_m^0 = -\frac{RT}{n} \ln K_m = -\frac{RT}{n} \ln \frac{x_m}{[x_s]^n [x_x]^{n-p}} \quad (2.3)$$

which on rearrangement gives the following equation,

$$\log x_s = -\left(1 - \frac{p}{n}\right) \log x_x + \frac{\Delta G_m^0}{2.303RT} + \frac{1}{n} \log x_m. \quad (2.4)$$

Assuming the monomeric drug concentration x_s , in the presence of micelles, to be equal to the cmc, equation (2.4) may be written in a simple form,

$$\log \text{cmc} = -a \log x_x + b, \quad (2.5)$$

where a is equal to $(1 - p/n)$, i.e. $(1 - \alpha)$, where α is the degree of dissociation and b is equal to $(\Delta G_m^0/2.303RT) + (1/n) \log x_m$.

The solid line in Fig. 2.1 is based on calculations using equation (2.2). Addition of electrolyte to solutions of these diphenylmethane antihistamines produces an increase in the aggregation number and a decrease in the cmc, as commonly found with simple surfactants. Plots of $\log \text{cmc}$ versus counterion concentration are given in Fig. 2.2. These plots are linear as predicted from equation (2.4).

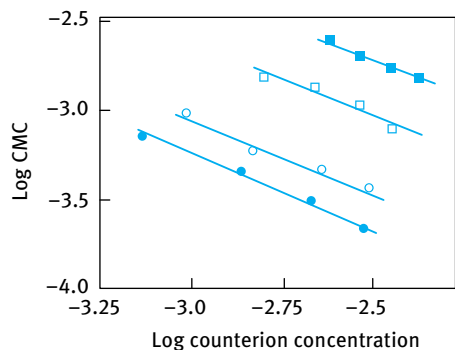


Fig. 2.2: log cmc against counterion concentration: ●, bromodiphenhydramine hydrochloride; ○, chlorocyclizine hydrochloride; □, diphenylpyraline hydrochloride; ■, diphenhydramine hydrochloride.

Values of the degree of dissociation α derived from the slopes of these lines are in agreement with those obtained from the light scattering data. In addition, the standard free energy of micellization, ΔG_m^0 , determined from the intercept of the lines is in reasonable agreement with the expected value derived from consideration of the free energy associated with the transfer of two phenyl rings from an aqueous to a nonaqueous environment. The micellar charge and hydration of the diphenylmethane antihistamines have been examined in detail by Attwood and Udeala [4].

The above results indicate that the diphenylmethane derivatives of histamines behave as normal surfactants with a clear cmc. However, this is not general since other derivatives such as mepyramine maleate (a pyridine derivative) did not show a clear breakpoint. This is illustrated in Fig. 2.3 which shows the light scattering results that indicate a continuous association process with no apparent cmc. The solid line in Fig. 2.3 was obtained using equation (2.2) with $n = 10$, $K_m = 10^{42}$ and $\alpha = 0.2$. Using such values, an inflection point is obtained that is not present in the experimental data. However, surface tension results showed in many cases a breakpoint in the γ - $\log C$ curves. Later studies on other drugs with nonmicellar association patterns showed that the apparent cmc detected by surface tension techniques arose because of the very limited change of monomer concentration with total solution concentration at high concentrations.

Both the surface activity and micellization have implications for the biological efficacy of many drugs. Surface active drugs tend to bind hydrophobically to proteins and other biological macromolecules. They also tend to associate with other amphipathic molecules such as other drugs, bile salts and of course with receptors. Guth and Spirtes [5] attributed the activity of phenothiazines to their interaction with membranes, which may be correlated with their surface activity. It is believed that these compounds act by altering the conformation and activity of enzymes and by altering membrane permeability and function.

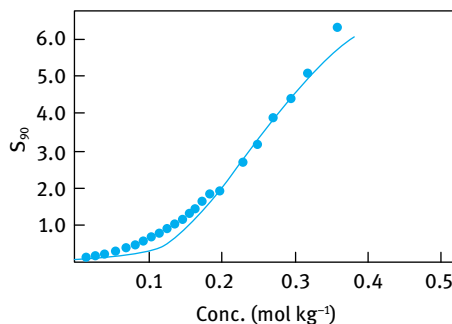


Fig. 2.3: Concentration dependence of the scattering ratio, S_{90} , for mepyramine maleate.

Several other examples may be quoted to illustrate the importance of surface activity of many drugs. Many drugs produce intralysosomal accumulation of phospholipids which are observable as multilamellar objects within the cell. The drugs which are implicated in phospholipidosis induction are often amphipathic compounds [6]. The interaction between the surfactant drug molecules and phospholipid render the phospholipid resistant to degradation by lysosomal enzymes resulting in their accumulation in cells.

Many local anaesthetics have significant surface activity and it is tempting to correlate their surface activity to their action. However, one should not forget other important factors such as partitioning of the drug into the nerve membrane (a factor that depends on the pK_a) and the distribution of hydrophobic and cationic groups which must be important for the appropriate disruption of nerve membrane function.

The biological relevance of micelle formation by drug molecules is not as clear as their surface activity, since the drug is usually applied at a concentration well below that at which micelles are formed. However, accumulation of drug molecules in certain sites may allow them to reach concentrations where micelles are produced. Such aggregate units may cause significant biological effects. For example, the concentration of monomeric species may increase only slowly or may decrease with increasing total concentration and the transport and colligative properties of the system are changed. In other words, the aggregation of the compounds will affect their thermodynamic activity and hence their biological efficacy *in vivo*.

2.3 Naturally occurring micelle forming systems

Several naturally occurring amphipathic molecules (in the body) exist, such as bile salts, phospholipids, cholesterol, and they play an important role in various biological processes. Their interactions with other solutes, such as drug molecules, and with membranes are also very important. A brief summary of some of these biological surfactants will be given below, illustrating their interactions.

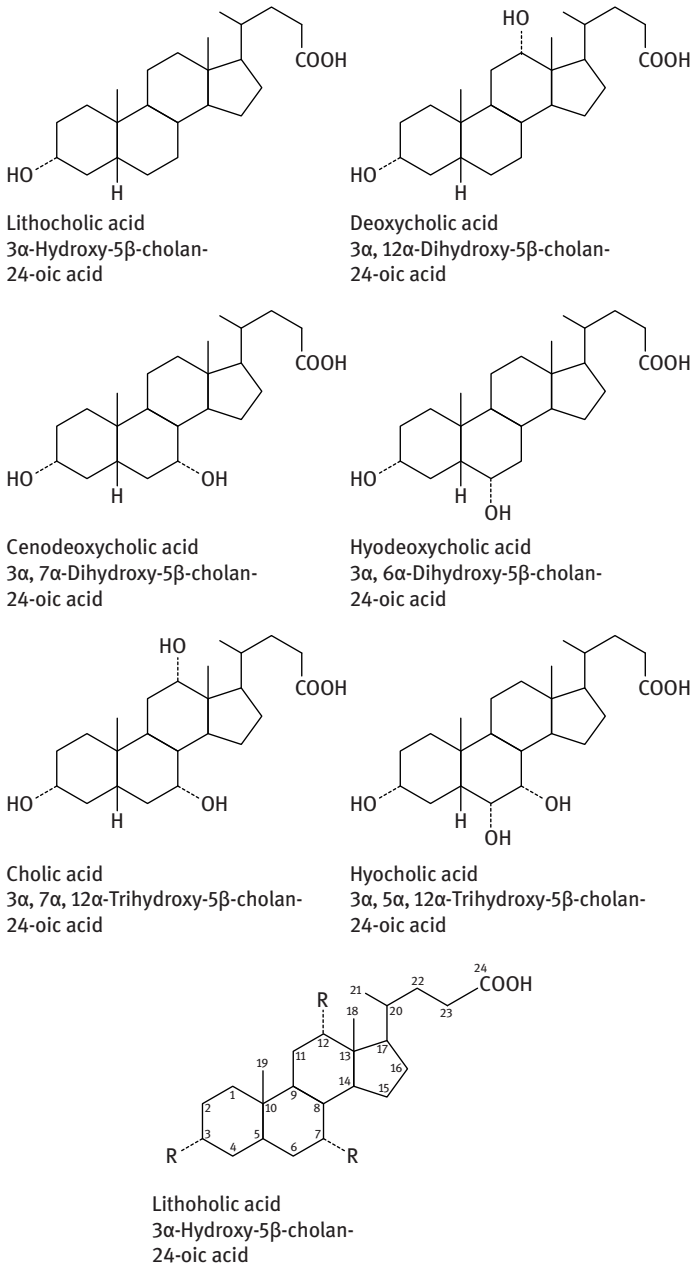


Fig. 2.4: Structures of commonly occurring bile salts.

Bile salts are synthesized in the liver and they consist of alicyclic compounds possessing hydroxyl and carboxyl groups. The structures of commonly occurring bile salts with the ring numbering system is given Fig. 2.4.

It is the positioning of the hydrophilic groups in relation to the hydrophobic steroidal nucleus that gives the bile salts their surface activity and determines their ability to aggregate.

Fig. 2.5 shows the possible orientation of cholic acid at the air-water interface; the hydrophilic groups being oriented towards the aqueous phase [7, 8]. The steroid portion of the molecule is shaped like a “saucer” as the A ring is *cis* with respect to the B ring. Small [9] suggested that small or primary aggregates with up to 10 monomers form above the cmc by hydrophobic interactions between the nonpolar side of the monomers. These primary aggregates form larger units by hydrogen bonding between the primary micelles. This is schematically illustrated in Fig. 2.6. Oakefull and Fisher [10] stressed the role of hydrogen bonding rather than hydrophobic bonding in the association of bile salts. However, Zana [11] regarded the association as a continuous process with hydrophobic interaction as the main driving force.

The cmc of bile salts is strongly influenced by its structure; the trihydroxy cholanic acids have higher cmc than the less hydrophilic dihydroxy derivatives. As expected, the pH of solutions of these carboxylic acid salts has an influence on micelle forma-

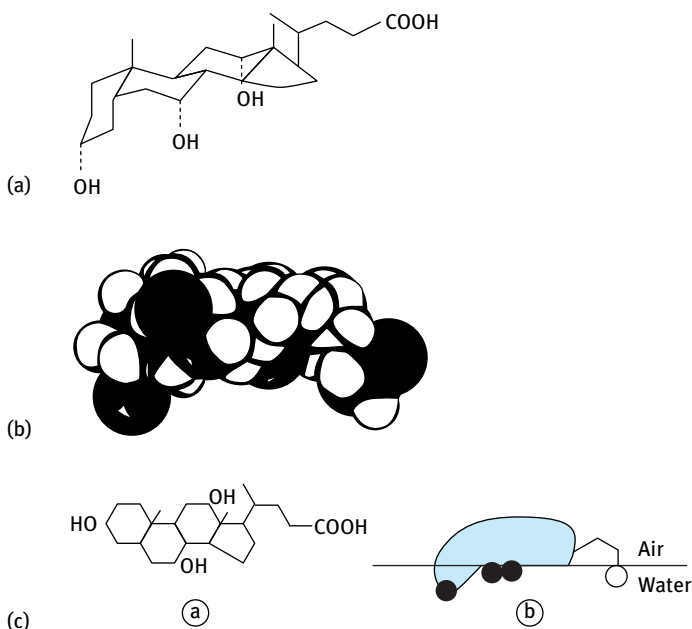


Fig. 2.5: (a) Structural formula of cholic acid showing the *cis* position of the A ring; (b) Courtauld space filling model of cholic acid; (c) orientation of cholic acid molecules at the air-water interface (hydroxyl groups represented by filled circles and carboxylic acid groups by open circles).

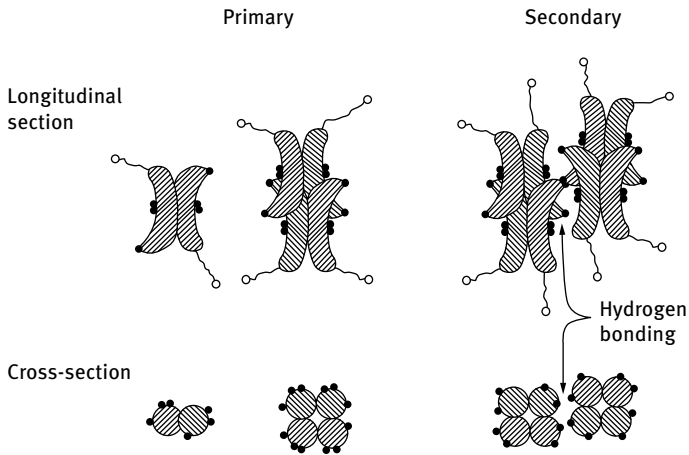


Fig. 2.6: Schematic representation of the structure of bile acid salt micelles.

tion. At sufficiently low pH, bile acids that are sparingly soluble will be precipitated from solution, initially being incorporated or solubilized in the existing micelles. The pH at which precipitation occurs, on saturation of the micellar system, is generally about one pH unit higher than the pK_a of the bile acid.

Bile salts play important roles in physiological functions and drug absorption. It is generally agreed that bile salts aid fat absorption. Mixed micelles of bile salts, fatty acids and monoglycerides can act as vehicles for fat transport. However, the role of bile salts in drug transport is not well understood. Several suggestions have been made to explain the role of bile salts in drug transport, such as facilitation of transport from liver to bile by direct effect on canicular membranes, stimulation of micelle formation inside the liver cells, binding of drug anions to micelles, etc. The enhanced absorption of medicinals on administration with deoxycholic acid may be due to a reduction in interfacial tension or micelle formation. The administration of quinine and other alkaloids in combination with bile salts has been claimed to enhance their parasiticidal action. Quinine, taken orally, is considered to be absorbed mainly from the intestine and a considerable amount of bile salts is required to maintain a colloidal dispersion of quinine. Bile salts may also influence drug absorption either by affecting membrane permeability or by altering normal gastric emptying rates. For example, sodium taurocholate increases the absorption of sulphaguanidine from the stomach, jejunum and ileum. This is due to increasing membrane permeability induced by calcium depletion and interference with the bonding between phospholipids in the membrane.

Another important naturally occurring class of surfactants which are widely found in biological membranes are the lipids, for example phosphatidylcholine (lecithin), lysolecithin, phosphatidylethanolamine and phosphatidylinositol. The structure of these lipids is given in Fig. 2.7. These lipids are also used as emulsifiers for intravenous fat emulsions, anaesthetic emulsions as well as for the production

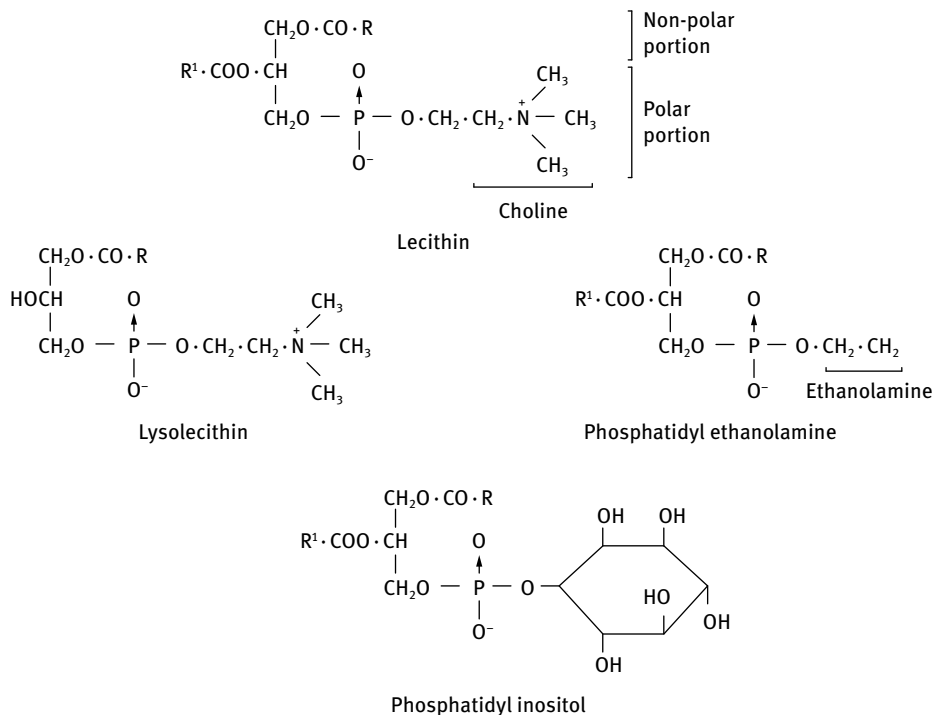


Fig. 2.7: Structure of lipids.

of liposomes or vesicles for drug delivery. The lipids form coarse turbid dispersions of large aggregates (liposomes) which on ultrasonic irradiation form smaller units or vesicles.

The liposomes are smectic mesophases of phospholipids organized into bilayers which assume a multilamellar or unilamellar structure (see Chapter 3). The multilamellar species are heterogeneous aggregates, most commonly prepared by dispersal of a thin film of phospholipid (alone or with cholesterol) into water. Sonication of the multilamellar units can produce the unilamellar liposomes, sometimes referred to as vesicles. The net charge of liposomes can be varied by incorporation of a long chain amine, such as stearyl amine (to give a positively charged vesicle) or dicetyl phosphate (giving negatively charged species). Both lipid-soluble and water-soluble drugs can be entrapped in liposomes. The liposoluble drugs are solubilized in the hydrocarbon interiors of the lipid bilayers, whereas the water-soluble drugs are intercalated in the aqueous layers. The use of liposomes as drug carriers has been reviewed by Fendler and Romero [12], to which the reader should refer for details. Liposomes, like micelles, may provide a special medium for reactions to occur between the molecules intercalated in the lipid bilayers or between the molecules entrapped in the vesicle and free solute molecules.

Phospholipids play an important role in lung functions. The surface active material to be found in the alveolar lining of the lung is a mixture of phospholipids, neutral lipids and proteins. The lowering of surface tension by the lung surfactant system and the surface elasticity of the surface layers assists alveolar expansion and contraction. Deficiency of lung surfactants in newborns leads to a respiratory distress syndrome and this led to the suggestion that instillation of phospholipid surfactants could cure the problem.

2.4 Biological implications of the presence of surfactants in pharmaceutical formulations

The use of surfactants as emulsifying agents, solubilizers, dispersants for suspensions and as wetting agents in formulations can lead to significant changes in the biological activity of the drug in the formulation. Surfactant molecules incorporated in the formulation can affect drug availability and its interaction with various sites in several ways. This is schematically illustrated in Fig. 2.8.

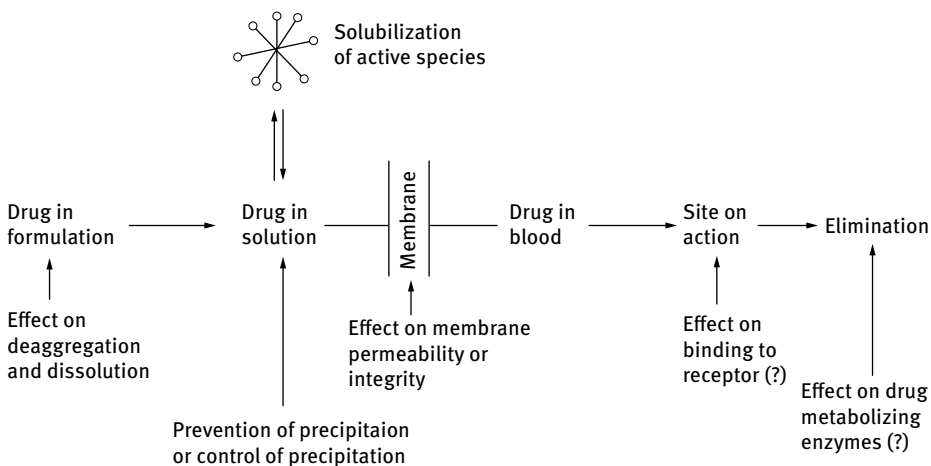


Fig. 2.8: Schematic representation of the effect of surfactants on drug absorption and its activity.

The surfactant may influence the desegregation and dissolution of solid dosage forms, by controlling the rate of precipitation of drugs administered in solution form, by increasing membrane permeability and affecting membrane integrity. Release of poorly soluble drugs from tablets and capsules for oral use may be increased by the presence of surfactants, which may decrease the aggregation of drug particles and, therefore, increase the area of the particles available for dissolution. The lowering of surface tension may also be a factor in aiding the penetration of water into the drug mass. This

wetting effect operates at low surfactant concentration. Above the cmc, the increase in saturation solubility of the drug substance by solubilization in the surfactant micelles can result in more rapid rates of drug dissolution. This will increase the rate of drug entry into the blood and may affect peak blood levels. However, very high concentrations of surfactant can decrease drug absorption by decreasing the chemical potential of the drug. This results when the surfactant concentration exceeds that required to solubilize the drug. Complex interactions between the surfactants and protein may take place and this will result in alteration of drug metabolizing enzyme activity. There have also been some suggestions that the surfactant may influence the binding of the drug to the receptor site. Some surfactants have direct physiological activity of their own and in the whole body these molecules can affect the physiological environment, e.g. by altering gastric residence time.

Numerous studies on the influence of surfactants on drug absorption have shown them to be capable of increasing, decreasing or exerting no effect on the transfer of drugs through membranes. As discussed above, the presence of surfactant affects the dissolution rate of the drug, although the effect is less than predicted by the Noyes–Whitney equation [13], which shows that the rate of dissolution dc/dt is related to the surface area A and the saturation solubility C_s .

$$\frac{dc}{dt} = kA(C_s - c). \quad (2.6)$$

Higuchi [14] assumed that an equilibrium exists between the solute and solution at the solid-liquid interface and that the rate of movement of the drug into the bulk is governed by the diffusion of free solute and solubilized drug across a stagnant diffusion layer. Drug solubilized in micelles will have a lower diffusion coefficient than the free solute molecules. This means that the effect of surfactant on the dissolution rate will be related to the dependence of dissolution rate on the diffusion coefficients of the species and not on their solubilities as suggested by equation (2.6). Thus, the rate of dissolution will be given by the expression,

$$\frac{dc}{dt} = \left[\frac{D_f c_f}{h} + \frac{D_m c_m}{h} \right], \quad (2.7)$$

where ‘f’ and ‘m’ refer to free and micellar drug and c_m is thus the increase in solubility due to the micellar phase; h is the thickness of the diffusion layer.

Predictions of dissolution rate may be made using diffusion coefficients of the solutes in their solubilized state by applying the Stokes–Einstein equation,

$$D = \frac{RT}{6\pi\eta N_A} \left(\frac{4\pi N_A}{3Mv} \right)^{1/3}, \quad (2.8)$$

where R is the gas constant, T is the absolute temperature, η is the viscosity of the solvent, N_A is the Avogadro constant, M is the micellar molecular weight and v is the partial specific volume of the micelles.

References

- [1] Attwood D, Florence AT. Surfactant systems, their chemistry, pharmacy and biology. New York: Chapman and Hall; 1983.
- [2] Attwood D, Udeala OK. *J Phys Chem.* 1975;79:889.
- [3] Attwood D, Udeala OK. *J Pharm Pharmacol.* 1975;27:395. Attwood D, Udeala OK. *J Pharm Pharmacol.* 1974;26:854.
- [4] Attwood D, Udeala OK. *J Pharm Pharmacol.* 1975;27:754.
- [5] Guth PS, Spirtes MA. *Int Rev Neurobiol.* 1964;7:231.
- [6] Blohm TR. *Pharmacol Rev.* 1979;30:593.
- [7] Barry BW, Gray GMT. *J Colloid Interface Sci.* 1975;52:314.
- [8] Oakenfull DG, Fisher LR. *J Phys Chem.* 1977;81:1838.
- [9] Small DM. *Advan Chem Ser.* 1968;84:31.
- [10] Oakenfull DG, Fisher LR. *J Phys Chem.* 1978;82:2443.
- [11] Zana R. *J Phys Chem.* 1978;82:2440.
- [12] Fendler JH, Romero A. *Life Sci.* 1977;20:1109.
- [13] Florence AT. In: Yalkowsky S, editor. *Techniques of solubilization of drugs.* New York: Marcel Dekker; 1982. Chapter 2.
- [14] Higuchi WI. *J Pharm Sci.* 1964;55:532.

3 Solubilized systems, liposomes and vesicles in pharmacy

3.1 Introduction

Solubilization is the process of preparing a thermodynamically stable isotropic solution of a substance (normally insoluble or sparingly soluble in a given solvent) by incorporation of an additional amphiphilic component(s) [1]. It is the incorporation of the compound (referred to as solubilizate or substrate) within micellar (L_1 phase) or reverse micellar (L_2 phase) system. Lipophilic (water-insoluble) substances become incorporated in the L_1 (normal micelle) phase. A schematic representation of the ternary phase diagram water/surfactant (sodium dodecyl sulphate)/cosurfactant (hexanol) is shown in Fig. 3.1.

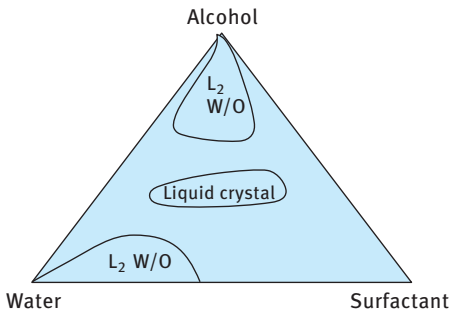


Fig. 3.1: Schematic representation of three-component phase diagram.

Hydrophilic (water-soluble) substances are incorporated in the L_2 phase. The site of incorporation of the solubilizate is closely related to its structure, as illustrated in Fig. 3.2: Nonpolar solubilizate is incorporated in the hydrocarbon core. Semi-polar or polar solubilizate is oriented within the micelle (short or deep) [2]. In aqueous systems, nonpolar solubilizates, e.g. aliphatic hydrocarbons, are dissolved in the hydrocarbon core of the micelle (Fig. 3.2(a)). Semi-polar substances, e.g. fatty acids and alkanols, may be oriented radically in the micelle with the polar group either buried (deep penetration) or near the micellar surface (short penetration). Adsorption on the micellar surface has been postulated for some solubilizates, e.g. dimethyl phthalate (Fig. 3.2(d)). It has been suggested that certain solubilizates, e.g. grisofulvin and chloroxylenol, may be incorporated in the polyethylene oxide exterior of nonionic surfactants of the polyoxyethylene (PEO) type (Fig. 3.2(c)). Although in many cases a particular location is preferred, the lifetime of a solubilizate within the micelle is long enough for a rapid exchange between different locations. The amount of solubilizate in the core and PEO region is assumed to be proportional to the number of

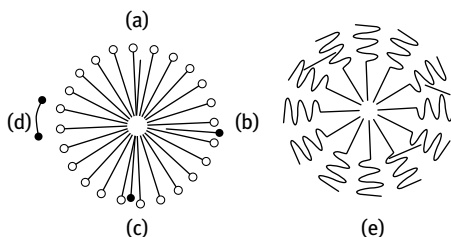


Fig. 3.2: Site of incorporation of solubilize: (a) in the hydrocarbon core; (b) short penetration; (c) deep penetration; (d) adsorption; (e) in the polyoxyethylene chain.

equivalents of alkyl chain moiety C_R and the number of equivalents of oxyethylene groups, C_{EO} , respectively. The total amount solubilized, S' , is then,

$$S' = aC_{EO} + bC_R, \quad (3.1)$$

or,

$$\frac{S'}{C_{EO}} = a + B \frac{C_R}{C_{EO}}. \quad (3.2)$$

Thus, a plot of S'/C_{EO} versus the inverse of the EO/R mole ratio of the surfactant should give a straight line with an intercept a representing solubilization in the PEO layer and a slope b representing solubilization in the core.

The presence of micelles and surfactant monomers in a drug formulation can have pronounced effects on its biological efficacy. As discussed in Chapter 2, the presence of surfactant micelles can affect the dissolution rate of the drug. The dissolution rate of the drug is given by,

$$\frac{dc}{dt} = \left[\frac{D_f C_f}{h} + \frac{D_m c_m}{h} \right], \quad (3.3)$$

where 'f' and 'm' refer to free and micellar drug and c_m is thus the increase in solubility due to the micellar phase; h is the thickness of the diffusion layer.

Surfactants (both micelles and monomers) can also influence the disintegration and dissolution of solid dosage forms by controlling the rate of precipitation (drug administration in solution), increasing membrane permeability and affecting membrane integrity. The release of poorly soluble drugs from tablets and capsules (oral use) may be increased in the presence of surfactants. The reduction of aggregation on disintegration of tablets and capsules increases the surface area. Lowering surface tension aids penetration of water into the drug mass. Above the cmc, an increase in flux by solubilization can lead to a rapid increase in the rate of dissolution.

3.2 Analysis of solubilization

The increase in flux by solubilization has been analysed by Noyes and Whitney [2]; the dissolution rate dC/dt depends on the surface area of the drug and its saturation solubility C_s . Higuchi [3, 4] assumed an equilibrium between solute and solu-

tion at the solid–solution interface. The rate of drug movement into the bulk is governed by the diffusion of the free solute (with a diffusion coefficient D_t) and the solubilized drug (with a diffusion coefficient D_m) across a stagnant diffusion layer of thickness h as discussed above. Prediction of dissolution rates may be made using the Stokes–Einstein equation for D discussed before. However, very high surfactant concentrations (above that required for solubilization) may decrease drug absorption by decreasing the chemical potential of the drug. The complex interaction between surfactant micelles, monomers and proteins may alter drug metabolizing activity. Surfactants may also alter the binding of the drug to its receptor site.

Block copolymers, particularly those of the PEO–PPO–PEO type (sold under the trade name Pluronics, or Poloxamers, BASF) have also shown significant ability to solubilize drugs. At low concentrations, approximating to those at which conventional nonionic surfactants form micelles, these block copolymer may produce monomolecular micelles by a change in configuration in solution. At higher surfactant concentrations, these monomolecular micelles aggregate to form aggregates of varying size which have the ability to solubilize drugs and to increase the stability of the solubilizing agent.

Hydrotropes, which increase the solubility of a solute without having any significant surface activity, are also added to increase solubilization. The mechanism of action of hydrotropes is complex and depends on different effects. Some hydrotropes act simply by complexation with the drug, e.g. piperazine, sodium salicylate, adenosine and diethanolamine that have been applied to solubilize theophylline. Apart from the possible prevention of unwanted physiological effects, hydrotropes can have a direct effect on efficacy. Complexation may occur by donor-acceptor interaction (hydrophobic and hydrogen bonding are thought to play a less important role). Several other hydrotropes have been suggested, e.g. p-toluene sulphonate and cumene sulphonate.

3.3 Experimental methods for studying solubilization

3.3.1 Maximum additive concentration

The concentration of solubilize that can be incorporated into a given system with the maintenance of a single isotropic solution (saturation concentration or maximum additive concentration, MAC) is obtained using the same procedures for measuring the solubility of any compound in a given solvent [5]. Since solubilization is temperature sensitive, adequate temperature control is essential.

If the refractive indices of the solubilizing system and the solubilize are sufficiently different, saturation is detected by the presence of supracolloidal aggregates with a concomitant increase in opacity. A long time may be required to reach equilibrium saturation, particularly with highly insoluble drugs. An excess of solubilize is shaken up with the surfactant solution until equilibrium is reached and the two

phases can be separated by centrifugation or using millipore filters. The data are best expressed as concentration of solubilize versus concentration of surfactant or as the ratio of solubilize dissolved per gram of surfactant versus surfactant concentration. It is also possible to express the results using a ternary phase diagram of solubilize–solvent–surfactant.

3.3.2 Micelle-water distribution equilibria

For solubilizes with significant water solubility, it is of interest to know both the distribution ratio of solubilize between micelles and water under saturation and unsaturation conditions. For measuring the distribution ratio under unsaturation conditions, a dialysis technique can be used using membranes that are permeable to solubilize but not to micelles. Ultrafiltration and gel filtration techniques can be applied to obtain the above information. The data are treated using the phase separation model of micellization (micelles are considered to be a separate phase in equilibrium with monomers).

The partition coefficient, P_m , between micelles and solution is given by,

$$P_m = \frac{C_3^m}{C_3^a}, \quad (3.4)$$

where C_3^m is the moles solubilize per mole of micellar surfactant and C_3^a is the mole of free solubilize per mole of water.

Equation (3.4) does not include the volumes of the micellar or aqueous phase, which can be obtained from the partial molar values of the surfactant. A better expression is,

$$P_m = \frac{D_b/V}{D_f/(1-V)}, \quad (3.5)$$

where D_b and D_f are the amount of solute in the micellar and aqueous phases respectively and V is the volume of micellar phase and $(1 - V)$ is the volume fraction of the aqueous phase.

An alternative method of expressing solubilization data is,

$$\frac{D_t}{D_f} = 1 + k[C], \quad (3.6)$$

where D_t is the total solute concentration and $[C]$ is the surfactant concentration. k is a measure of the binding capacity of the surfactant. It is given by the slope of plotting D_t/D_f versus $[C]$.

An alternative expression that treats solubilization as a process of “binding” of solute molecules to binding sites on the surfactant is,

$$r = \frac{nK[D_f]}{1 + K[D_f]}, \quad (3.7)$$

where r is the molar ratio of bound solute to total surfactant,

$$r = \frac{[D_b]}{[C]} \quad (3.8)$$

n is the total number of independent binding sites on the surfactant micelle. K is an intrinsic dissociation constant for the binding of solute molecules to one of the sites. Equation (3.7) is a form of a Langmuir isotherm.

In some cases, plots of r/D_f are curved, indicating more than one adsorption site and this requires modification of equation (3.8). For example, for two adsorption sites with dissociation constant K_1 and K_2 ,

$$r = \frac{n_1 K_1 [D_f]}{1 + K_1 [D_f]} + \frac{n_2 K_2 [D_f]}{1 + K_2 [D_f]} \quad (3.9)$$

Analysing the curves allows one to obtain n_1 , n_2 , K_1 and K_2 .

3.3.3 Determination of location of solubilize

The site of incorporation of solubilize is closely related to its chemical structure (see Fig. 3.2). Although in many cases a particular location is preferred, the lifetime of a solubilize within the micelle is long enough for a rapid interchange between different locations.

As mentioned above, for a nonionic surfactant consisting of an alkyl group R and PEO chain, one may determine the number of equivalents of alkyl chain moiety, C_R , and that of the PEO chain, C_{PEO} . The solute may be considered to be distributed between the R and PEO chain.

3.4 Quantitative methods for obtaining the exact location of solubilize

3.4.1 X-ray diffraction

This is based on application of Bragg's equation,

$$n\lambda = 2d \sin \theta, \quad (3.10)$$

where d is the distance between two parallel plates, n is an integer and θ is the angle of incidence to the plane of the X-ray beam with wavelength λ .

In addition to the diffraction caused by the solvent, three diffraction bands appear: 'S' or short spacing band giving a repeating distance of 0.4–0.5 nm, corresponding to the thickness of the hydrocarbon chain; 'M', micelle thickness band that varies with the length of the R chain (value slightly less than twice the extended length of

the R chain); 'I' or long spacing band (greater than 'M' or 'S' bands) that is sensitive to surfactant concentration. Both "M2" and 'I' bands show an increase in length of spacing with addition of apolar solubilizates, but show a little or slight increase with the addition of polar solubilizates. Assuming the micelles are spherical, their radius could be obtained from the long spacing,

$$d = \left(\frac{8\pi}{3 \cdot 2^{1/2}} \right)^{1/2} \phi - \frac{1}{3} r, \quad (3.11)$$

where r is the radius of a sphere occupying a fraction ϕ of the total volume.

An alternative X-ray technique is to plot the scattering intensity I_s versus s ($= 2\lambda \sin(\theta/2)$). The diffuse maximum in the small angle shows a shift and an increase in intensity on solubilization. These changes are attributed to the change in radii and electron density of the core and polar regions of the micelle.

3.4.2 Absorption spectrometry

The amount of vibrational fine structure in the UV absorption spectrum of a compound in solution is a function of the interaction between solvent and solute. The extent of interaction between solvent and solute increases with increasing solvent polarity, thereby decreasing the fine structure. As the micelle is characterized by regions of different polarity, UV spectra have been used as a means of obtaining information on the environment of the solubilizate in the micelle.

3.4.3 NMR methods

NMR can be used to obtain information on solubilization by measuring the shift in the peak positions on addition of the solubilizate. For example, by measuring ^1H NMR shift for a compound with an aromatic ring versus the concentration of a surfactant that contains no aromatic ring, e.g. SDS, one can determine the location of the solubilizate. This leads to an upfield shift of the ^1H peak, indicating a more hydrophobic environment.

3.4.4 Fluorescence depolarization

This is based on the use of fluorescence probes, such as pyrene, which have been used to study the interior of the micelles. The fluorescence spectrum of pyrene shows a significant change on solubilization in the core of the micelle.

3.4.5 Electron spin resonance (ESR)

This is based on the introduction of free radical probe such as nitroxide. The ESR spectrum reflects the microenvironment of the micelle and hence on solubilization this spectrum shows significant changes.

3.5 Mobility of solubilize molecules

As with surfactant monomers, the solubilize molecules are not rigidly fixed in the micelle, but have a freedom of motion that depends on the solubilization site. The lifetime of a solubilize in the micelle is very short, usually less than 1 ms. These short relaxation times were obtained using NMR and ultrasonic techniques.

3.6 Factors affecting solubilization

3.6.1 Solubilize structure

Generalizations about the manner in which structure affects solubilization are complicated by the existence of different solubilization sites. The main parameters that may be considered when investigating solubilizes are: Polarity, polarizability, chain length and branching, molecular size and shape. The most significant effect is perhaps the polarity of the solubilize and sometimes they are classified into polar and apolar; however, difficulty exist with intermediate compounds.

Some correlation exists between hydrophilicity/lipophilicity of solubilize and partition coefficient between octanol and water (the log P number concept, the higher the value the more lipophilic the compound is).

3.6.2 Surfactant structure

For solubilizes incorporated in the hydrocarbon core, the extent of solubilization increases with increasing alkyl chain length. For the same R, solubilization increases in the order: anionics < cationics < nonionics

The solubilization power that is normally described by the ratio of moles solubilize to mole surfactant increases with increasing PEO chain length; this is due to the decrease in micelle size. With increasing PEO chain length, the aggregation number decreases and hence the number of micelles per mole surfactant increases.

3.6.3 Temperature

Mostly, solubilization increases with increasing temperature as a result of the increase in solubility of the compound and the decrease in cmc (for nonionic surfactants) with increasing temperature.

3.6.4 Addition of electrolytes and non-electrolytes

Most electrolytes cause a reduction in the cmc and they may increase the aggregation number (and size) of the micelle. This may lead to an increase in solubilization. Addition of non-electrolytes, e.g. alcohols can lead to an increase in solubilization.

The above discussion clearly demonstrates that solubilization above the cmc offers an approach to formulation of poorly soluble drugs. This approach has several limitations: Finite capacity of micelles for the drug; short- or long-term adverse effects; solubilization of other ingredients such as preservatives, flavours and colouring agents, which may cause alteration in stability and effectiveness.

Future research is required on: finding solubilizing agents that increase bio-availability; the use of co-solvents; the effects of surfactants on properties of solubilized systems and interaction with components of the body; mixed micelle formation between surface active drugs and surfactants.

3.7 Liposomes and vesicles in pharmacy

Liposomes are multilamellar structures consisting of several bilayers of lipids (several μm). They are produced by simply shaking an aqueous solution of phospholipids, e.g. egg lecithin. When sonicated, these multilayer structures produce unilamellar structures (with size range of 25–50 nm) that are referred to as liposomes. The nomenclature for liposomes is far from being clear; it is now generally accepted that “All types of lipid bilayers surrounding an aqueous phase are in the general category of liposomes” [7, 8]. The term “liposome” is usually reserved for vesicles composed, even partly, of phospholipids. The more generic term “vesicle” is to be used to describe any structure consisting of one or more bilayers of various other surfactants. In general the names “liposome” and “phospholipid vesicle” are used interchangeably. Liposomes are classified in terms of the number of bilayers, as multilamellar vesicles (MLVs > 400 nm), large unilamellar vesicles (LUVs > 100 nm) and small unilamellar vesicles (SUVs < 100 nm). Other types reported are the giant vesicles (GV), which are unilamellar vesicles of diameter between 1–5 μm and large oligolamellar vesicles (LOV) where a few vesicles are entrapped in an LUV or GV.

A schematic picture of liposomes and vesicles is given in Fig. 3.3.

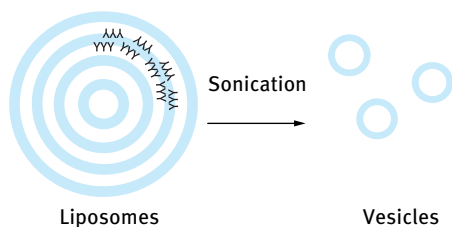


Fig. 3.3: Schematic representation of liposomes and vesicles.

Glycerol-containing phospholipids are used for the preparation of liposomes and vesicles. The structure of some lipids is shown in Fig. 3.4. The most widely used lipid for drug formulations is phosphatidylcholine that can be obtained from eggs or soybean. In most preparations, a mixture of lipids is used to obtain the most optimum structure. These liposome bilayers can be considered as mimicking models of biological membranes. They can solubilize both lipophilic active ingredients in the lipid bilayer phase, as well as hydrophilic molecules in the aqueous layers between the lipid bilayers as well as the inner aqueous phase.

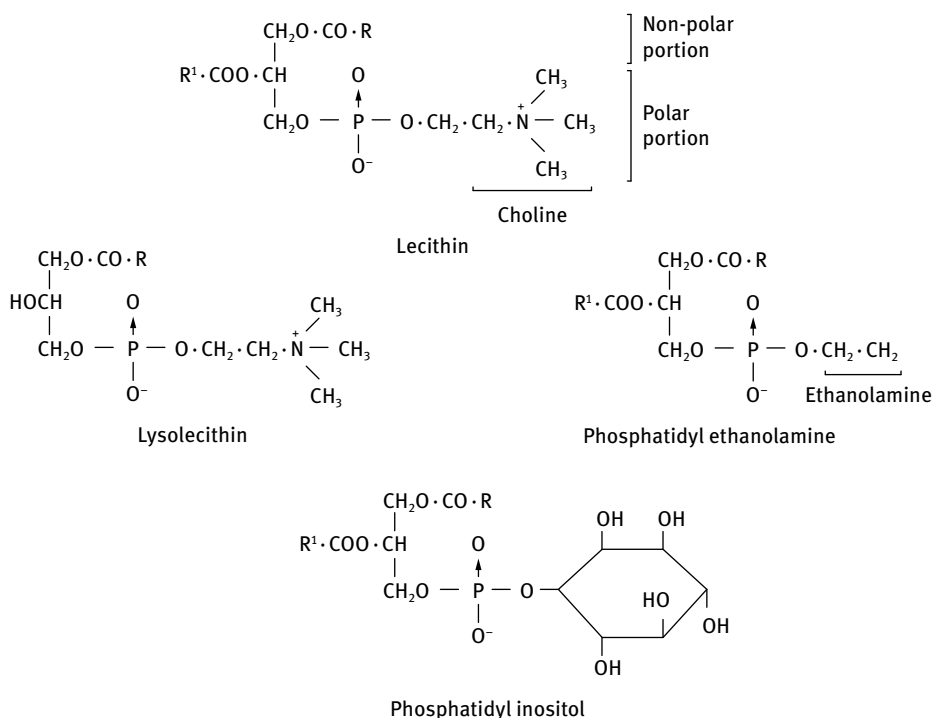


Fig. 3.4: Structure of lipids.

Liposomes and vesicles are ideal systems for drug delivery, due to their high degree of biocompatibility, in particular for intravenous delivery [5, 6]. For effective application, larger unilamellar vesicles are preferred (diameter 100–500 nm). In addition to drug delivery, liposomes have been used as model membranes, as carriers of drugs, DNA, ATP, enzymes and diagnostic agents. Both water-soluble and -insoluble drugs can be incorporated by encapsulation in the aqueous space or intercalation into the lipid bilayer.

Liposomes are capable of solubilizing both water-soluble and lipid-soluble drugs. The amount and location of a drug within a liposome is dependent on a number of factors:

- (i) The location of a drug within a liposome is based on the partition coefficient of the drug between aqueous compartments and lipid bilayers.
- (ii) The maximum amount of drug that can be entrapped within a liposome is dependent on its total solubility in each phase.
- (iii) Drugs with limited solubility in polar and nonpolar solvents cannot be encapsulated in liposomes.
- (iv) Efficient capture depends on the use of drugs at concentrations that do not exceed the saturation limit in the aqueous compartment (for polar drugs) or the lipid bilayers (for nonpolar drugs).

If liposomes are prepared by mixing the drug with the lipids, the drug will eventually partition to an extent depending on the partition coefficient of the drug and the phase volume ratio of water to bilayer. Release rates are highest when the drug has intermediate partition coefficient.

The bilayer/aqueous compartment partition coefficient is usually estimated by determining the partition coefficient between octanol and water (the log *P* number). Drug solubilization in liposomes has important biological effects:

- (i) The ultimate efficacy of a liposomal dosage depends on the control of the amount of free drug that can reach the exact “site of action”.
- (ii) Generally, the exact “site of action” is not known and one relies on attaining reproducible blood levels of the drug.
- (iii) With non-parenteral dosage forms, only the free drug is absorbed and hence one can measure the amount of drug that enters the blood as a function of time.

With parenteral, especially intravenous, administration of drugs encapsulated in liposomes requires control of the pharmacokinetics of the drug and this requires control of the following factors:

- (i) Concentration of the free drug in the blood.
- (ii) Concentration of liposomes and their entrapped drug in blood.
- (iii) Leakage rate of drug from liposome in the blood.
- (iv) Disposition of the intact drug-carrying liposomes in the blood.

To control the pharmacokinetics of these complex systems, one must separate out the leakage rate of the drug from the liposome in the blood and the disposition of the intact carrying liposomes in the blood.

One of the major problems with the application of liposomes for drug delivery is their interaction with high molecular weight substances such as albumin. The instability of liposomes in plasma appears to be the result of transfer of bilayer lipids to albumin and high-density lipoproteins (HDL). Some protein is also transferred from the lipoprotein to the liposome. Both lecithin and cholesterol can exchange with membranes of red blood cells. The susceptibility of liposomal phospholipid and phospholipase is strongly dependent on liposome size and type. Generally MLVs are most stable and SUVs are least stable. Liposomes prepared with higher chain length phospholipids are more stable in buffer and in plasma. Cholesterol and sphingomyelin are very effective in reducing instability. As we will see later, incorporation of block copolymers such as poloxamers can enhance the stability of liposomes.

In spite of the above limitations, the therapeutic promise of liposomes as a drug delivery system is becoming a reality in the following applications: parenteral administration; inhalation treatment; percutaneous administration; ophthalmics; cancer treatment and controlled-release formulations.

3.7.1 Driving force for formation of vesicles

The driving force for formation of vesicles has been described in detail by Israelachvili et al. [9–11]. From equilibrium thermodynamics, small aggregates, or even monomers, are entropically favoured over larger ones. This entropic force explains the aggregation of single-chain amphiphiles into small spherical micelles instead to bilayers or cylinders, as the aggregation number of the latter aggregates is much higher. Israelachvili et al. [9–11] attempted to describe the thermodynamic drive for vesicle formation by biological lipids. From equilibrium thermodynamics of self-assembly, the chemical potential of all molecules in a system of aggregated structures such as micelles or bilayers will be the same,

$$\mu_N^0 + \frac{kT}{N} \ln\left(\frac{X_N}{N}\right) = \text{const}; \quad N = 1, 2, 3, \dots, \quad (3.12)$$

where μ_N^0 is the free energy per molecule in the aggregate, X_N is the mole fraction of molecules incorporated into the aggregate, with an aggregation number N , k is the Boltzmann constant and T is the absolute temperature.

For monomers in solution with $N = 1$,

$$\mu_N^0 + \frac{kT}{N} \ln\left(\frac{X_N}{N}\right) = \mu_1^0 + kT \ln X_1. \quad (3.13)$$

Equation (3.12) can be written as,

$$X_N = N \left(\frac{X_M}{M} \right)^{N/M} \exp \left(\frac{N(\mu_M^0 - \mu_N^0)}{kT} \right), \quad (3.14)$$

where M is any arbitrary state of reference of aggregation number M .

The following assumptions are made to obtain the free energy per molecule:

- (i) the hydrocarbon interior of the aggregate is considered to be in a fluid-like state;
- (ii) geometric considerations and packing constrains in terms of aggregate formation are excluded;
- (iii) strong long-range forces (van der Waals and electrostatic) are neglected.

By considering the “opposing forces” approach of Tanford [12, 13], the contributions to the chemical potential, μ_N^0 , can be estimated. A balance exists between the attractive forces mainly of hydrophobic (and interfacial tension) nature and the repulsive forces due to steric repulsion (between the hydrated head group and alkyl chains), electrostatic and other forces [9]. The free energy per molecule is thus,

$$\mu_N^0 = \gamma a + \frac{C}{a}. \quad (3.15)$$

The attractive contribution (the hydrophobic free energy contribution) to μ_N^0 is γa where γ is the interfacial free energy per unit area and a is the molecular area measured at the hydrocarbon/water interface. C/a is the repulsive contribution where C is a constant term used to incorporate the charge per head group, e , and includes terms such as the dielectric constant at the head group region, ϵ , and curvature corrections.

This fine balance yields the optimum surface area, a_0 , for the polar head groups of the amphiphile molecules at the water interface, at which the total interaction free energy per molecule is a minimum,

$$\mu_N^0(\min) = \gamma a + \frac{C}{a} = 0, \quad (3.16)$$

$$\frac{\partial \mu_N^0}{\partial a} = \gamma - \frac{C}{a^2} = 0, \quad (3.17)$$

$$a = a_0 = \left(\frac{C}{\gamma} \right)^{1/2}. \quad (3.18)$$

Using the above equations, the general form relating the free energy per molecule μ_N^0 with a_0 can be expressed as,

$$\mu_N^0 = \gamma \left(a + \frac{a_0^2}{a} \right) = 2a_0\gamma + \frac{\gamma}{a} (a - a_0)^2. \quad (3.19)$$

Equation (3.19) shows that:

- (i) μ_N^0 has a parabolic (elastic) variation about the minimum energy;
- (ii) amphiphilic molecules, including phospholipids, can pack in a variety of structures in which their surface areas will remain equal or close to a_0 .

Both single-chain and double-chain amphiphiles have very much the same optimum surface area per head group ($a_0 \approx 0.5\text{--}0.7 \text{ nm}^2$), i.e. a_0 is not dependent on the nature of the hydrophobe. Thus by considering the balance between entropic and energetic contributions to the double-chain phospholipid molecule one arrives at the conclusion that the aggregation number must be as low as possible and a_0 for each polar group is of the order of $0.5\text{--}0.7 \text{ nm}^2$ (almost the same as that for a single-chain amphiphile). For phospholipid molecules containing two hydrocarbon chains of 16–18 carbon atoms per chain, the volume of the hydrocarbon part of the molecule is double the volume of a single-chain molecule, while the optimum surface area for its head group is of the same order as that of a single-chain surfactant ($a_0 \approx 0.5\text{--}0.7 \text{ nm}^2$). Thus the only way for this double-chain surfactant is to form aggregates of the bilayer sheet or the close bilayer vesicle type. This will be further explained using the critical packing parameter concept (CPP) described by Israelachvili et al. [9–11]. The CPP is a geometric expression given by the ratio of the cross-sectional area of the hydrocarbon tail(s) a to that of the head group a_0 . a is equal to the volume of the hydrocarbon chain(s) v divided by the critical chain length l_c of the hydrocarbon tail. Thus the CPP is given by [14],

$$\text{CPP} = \frac{v}{a_0 l_c}. \quad (3.20)$$

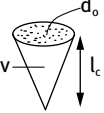

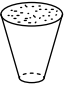
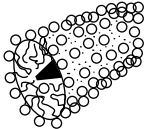

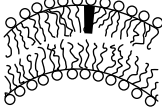

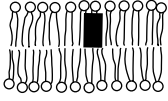

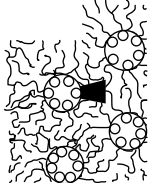
Regardless of shape, any aggregated structure should satisfy the following criterion: no point within the structure can be farther from the hydrocarbon-water surface than l_c which is roughly equal to, but less than the fully extended length l of the alkyl chain.

For a spherical micelle, the radius $r = l_c$ and from simple geometry $\text{CPP} = v/a_0 l_c \leq 1/3$. Once $v/a_0 l_c > 1/3$, spherical micelles cannot be formed and when $1/2 \geq \text{CPP} > 1/3$ cylindrical micelles are produced. When the $\text{CPP} > 1/2$ but < 1 , vesicles are produced. These vesicles will grow until $\text{CPP} \approx 1$ when planer bilayers will start forming. A schematic representation of the CPP concept is given in Tab. 3.1.

According to Israelachvili et al. [9–11], the bilayer sheet lipid structure is energetically unfavourable to the spherical vesicle, because of the lower aggregation number of the spherical structure. Without introducing packing constrains (described above), the vesicles should shrink to such a small size that they would actually form micelles. For double-chain amphiphiles there are three considerations:

- (i) an optimum a_0 (almost the same as that for single-chain surfactants) must be achieved by considering the various opposing forces;
- (ii) structures with minimum aggregation number N must be formed;
- (iii) aggregates into bilayers must be the favourite structure.

Tab. 3.1: CPP concept and various shapes of aggregates.

Lipid	Critical packing parameter v/a_0l_c	Critical packing shape	Structures formed
Single-chained lipids (surfactants) with large head-group areas: – SDS in low salt	$< 1/3$	Cone 	Spherical micelles 
Single-chained lipids with small head-group areas: – SDS and CTAB in high salt – nonionic lipids	$1/3-1/2$	Truncated cone 	Cylindrical micelles 
Double-chained lipids with large head-group areas, fluid chains: – phosphatidyl choline (lecithin) – phosphatidyl serine – phosphatidyl glycerol – phosphatidyl inositol – phosphatidic acid – sphingomyelin, DGDG ^a – dihexadecyl phosphate – dialkyl dimethyl ammonium – salts	$1/2-1$	Truncated cone 	Flexible bilayers, vesicles 
Double-chained lipids with small head-group areas, anionic lipids in high salt, saturated frozen chains: – phosphatidyl ethanamine – phosphatidyl serine + Ca^{2+}	≈ 1	Cylinder 	Planar bilayers 
Double-chained lipids with small head-group areas, nonionic lipids, poly(cis) unsaturated chains, high T : – unsat. phosphatidyl ethanolamine – cardiolipin + Ca^{2+} – phosphatidic acid + Ca^{2+} – cholesterol, MGDG ^b	> 1	Inverted truncated cone or wedge 	Inverted micelles 

a DGDG: digalactosyl diglyceride, diglucosyldiglyceride

b MGDG: monogalactosyl diglyceride, monoglucosyl diglyceride

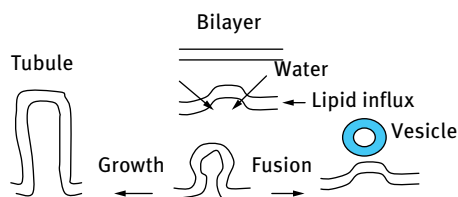


Fig. 3.5: Bilayer vesicle and tubule formation [10].

A schematic picture of the formation of bilayer vesicle and tubule structures was introduced by Israelachvili and Mitchell [10] and is shown in Fig. 3.5.

Israelachvili et al. [9–11] believe that steps A and B are energetically favourable. They considered step C to be governed by packing constraints and thermodynamics in terms of the least aggregation number. They concluded that the spherical vesicle is an equilibrium state of the aggregate in water and it is certainly more favoured over extended bilayers.

3.7.2 Stabilization of liposomes by incorporation of block copolymers

The main drawback of the application of liposomes in drug formulations is their metastability. On storage, the liposomes tend to aggregate and fuse to form larger polydisperse systems and finally the system reverses into a phospholipid lamellar phase in water. This process takes place relatively slowly because of the slow exchange between the lipids in the vesicle and the monomers in the surrounding medium. Therefore, it is essential to investigate both the chemical and physical stability of the liposomes. An examination of the aggregation process can be achieved by measuring their size as a function of time. Maintenance of the vesicle structure can be assessed using freeze fracture and electron microscopy.

Several methods have been applied to increase the rigidity and physicochemical stability of the liposome bilayer of which the following methods are the most commonly used: hydrogenation of the double bonds within the liposomes, polymerization of the bilayer using synthesized polymerizable amphiphiles and inclusion of cholesterol to rigidify the bilayer.

Other methods to increase the stability of the liposomes include modification of the liposome surface, for example by physical adsorption of polymeric surfactants onto the liposome surface (e.g. proteins and block copolymers). Another approach is to covalently bond the macromolecules to the lipids and the subsequent formation of vesicles. A third method is to incorporate the hydrophobic segments of the polymeric surfactant within the lipid bilayer. This latter approach has been successfully applied by Kostarelos et al. [15, 16] who used A–B–A block copolymers of polyethylene oxide (A) and polypropylene oxide (PPO), namely poloxamers (Pluronic). Two different techniques of adding the copolymer were attempted [15, 16]. In the first method (A), the block copolymer was added after formation of the vesicles. In the second method, the

phospholipid and copolymer are first mixed together and this is followed by hydration and formation of SUV vesicles. These two methods are briefly described below.

The formation of small unilamellar vesicles (SUVs) was carried out by sonication of 2% w/w of the hydrated lipid (for about 4 hours). This produced SUV vesicles with a mean vesicle diameter of 45 nm (polydispersity index of 1.7–2.4). This is followed by the addition of the block copolymer solution and dilution of 100 times to obtain a lipid concentration of 0.02% (method A). In the second method (I) SUV vesicles were prepared in the presence of the copolymer at the required molar ratio.

In method (A), the hydrodynamic diameter increases with increasing block copolymer concentration, particularly those with high PEO content, reaching a plateau at a certain concentration of the block copolymer. The largest increase in hydrodynamic diameter (from ≈ 43 nm to ≈ 48 nm) was obtained using Pluronic F127 (that contains a molar mass of 8330 PPO and molar mass of 3570 PEO). In method I the mean vesicle diameter showed a sharp increase with increase in %w/w copolymer reaching a maximum at a certain block copolymer concentration, after which a further increase in polymer concentration showed a sharp reduction in average diameter. For example, with Pluronic F127 the average diameter increased from ≈ 43 nm to ≈ 78 nm at 0.02%w/w block copolymer and then it decreased sharply with a further increase in polymer concentration reaching ≈ 45 nm at 0.06%w/w block copolymer. This reduction in average diameter at high polymer concentration is due to the presence of excess micelles of the block copolymer.

A schematic representation of the structure of the vesicles obtained on addition of the block copolymer using methods (A) and (I) is shown in Fig. 3.6.

With method (A), the triblock copolymer is adsorbed on the vesicle surface by both PPO and PEO blocks. These “flat” polymer layers are prone to desorption due to the weak binding onto the phospholipid surface. In contrast, with the vesicles prepared using method (I) the polymer molecules are more strongly attached to the lipid bilayer with PPO segments “buried” in the bilayer environment surrounded by the lipid fatty acids. The PEO chains remain at the vesicle surfaces free to dangle in solution and attain the preferred conformation. The resulting sterically stabilized vesicles [(I) system]

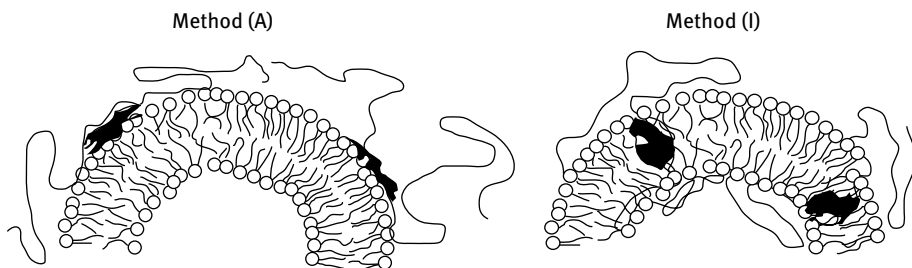


Fig. 3.6: Schematic representation of vesicle structure in the presence of triblock copolymer prepared using method (A) and (I) [4].

have several advantages over the (A) system with the copolymer simply coating their outer surface. The anchoring of the triblock copolymer using method (I) results in irreversible adsorption and lack of desorption. This is confirmed by dilution of both systems. With (A), dilution of the vesicles results in reduction of the diameter to its original bare liposome system, indicating polymer desorption. In contrast, dilution of the vesicles prepared by method (I) showed no significant reduction in diameter size indicating strong anchoring of the polymer to the vesicle. A further advantage of constructing the vesicles with bilayer-associated copolymer molecules is the possibility of increased rigidity of the lipid-polymer bilayer [3, 4].

3.8 Liquid crystalline phases and microemulsions

Apart from micelles, surfactants, block copolymers and polar lipids self-assemble to a wide range of liquid crystalline phases and microemulsions [17]. These systems offer opportunities for increased solubilization of hydrophobic drugs. Similarly, due to their water compartments, some liquid crystalline phases (e.g. cubic) are also interesting delivery systems for proteins, peptides and other biomolecular drugs. Depending on its physicochemical properties, a drug incorporated in such self-assembly systems may localize preferentially in the oil or water compartments, or at the interface between these, thereby affecting the structure and stability of the self-assembled system. Depending on its distribution within the self-assembly system, the drug may have different effects on its structure and stability. For example, if the drug is readily soluble in the oil, but sparingly soluble in water, the drug will distribute to the former and increase its effective volume. As a consequence of this, structures less curved towards the oil (or increasingly curved towards water) are favoured. Water-soluble and non-surface active drugs, on the other hand, will localize preferentially in the water domains, thereby destabilizing structures curved towards water (e.g. reversed hexagonal phase and reverse micelles). Charged water-soluble drugs may also screen electrostatic interactions as any other electrolyte, destabilizing structures highly curved towards the oil for self-assembly systems formed by charged amphiphiles. For surface active drugs, the effect of the drug on the self-assembly systems depends on a number of factors, notably the preferential location of the drug, second to that at the interface, between the water and oil compartments. Also the amount of the drug localized at the interfaces and the adsorbed layer structure play a role in this context. As these properties frequently depend on factors such as temperature, ionic strength and pH, the effect of the drug on the self-assembly structures varies with these parameters. Given the above, the structures formed in self-assembly systems are determined by the interplay between the amphiphile/oil/water and the drug. In practical terms, this means that there is no such thing as a generic self-assembly system available to use for delivery of any and all drug compounds. Instead, every delivery system has to be designed and tuned for the specific drug and application at hand.

In addition to their ability to solubilize large quantities of drugs of varying physicochemical properties, the frequently high viscosity of liquid crystalline phases allows a means for drug localization, e.g., at skin or mucosal surfaces, subcutaneously, or intramuscularly. Since the high viscosity of liquid crystalline phases makes preparation, handling, and administration of such systems difficult, focus in this context has been placed on phase transformations, from low-viscous forms, easy to prepare and administer, to the desired high-viscous liquid crystalline phase following administration. As with other self-assembly systems, such transitions may be triggered, e.g. by temperature, dilution with water, change of pH and/or ionic strength, presence of specific metabolites, degradation or external fields. For example, poly(ethylene oxide)-based surfactants and block copolymers display reduced curvature towards the oil phase with increasing temperature as a result of deteriorated solvency condition. Poly(ethylene oxide)-poly(propylene oxide)-poly(ethylene oxide) block copolymers form a particularly extensively investigated class of self-assembly system in this context. For example, Pluronic F127 (EO99-PO65-EO99) (also called Lutrol 407 or Poloxamer 407) displays a dramatic increase in stiffness on transition from micellar solution to cubic phase. The transition temperature depends on the polymer concentration, but also on the presence of cosolutes, such as homo- or block copolymers, surfactants, oils, and electrolytes. Similarly, the monoolein/water system has been extensively investigated due to its capacity for (temperature-)triggered phase transitions, allowing administration of a low viscous formulation to be combined with *in situ* formation of a (stiff) cubic liquid crystalline phase after administration.

Since the formulation is in contact with excess water after administration, dilution with water represents another triggering mechanism for self-assembly delivery systems. Thus, one may use the composition drift induced by the placement of the formulation in excess water on administration of an oil-rich formulation (e.g. a reversed micellar phase) in order to create a (transient) liquid crystalline phase formed *in situ*. An extensively investigated system in this context, offering opportunities for both temperature and dilution-induced phase transitions, is monoolein/water. For example, both the lamellar and the reversed micellar phases in this system display a transition to the cubic phase on dilution with water. Since the cubic phase is stable in equilibrium with excess water it does not dissolve by continued exposure to water, making it interesting for depot formulations. Similarly, by starting with an oil-rich and water-poor Pluronic F68/C8 oil/water/lidocaine/prilocaine formulation, dilution with water triggers a transition, first to the hexagonal phase, then to a cubic phase, and finally to a micellar solution. Another, particularly elegant, example of dilution-induced transitions for drug delivery by self-assembly systems is the Sandimmune[®] formulation for the immunosuppressive drug cyclosporine. When administered alone, oral absorption of cyclosporine is poor and highly variable, precluding safe and efficient administration. The situation may be improved by co-administration of absorption enhancers, e.g. emulsions, an effect increasing with decreasing (O/W) emulsion droplet size. By using an O/W microemulsion, even further reductions in droplet size are obtained, to

gether with improved bioavailability and reduced variability. By combining this with the utilization of a reversed micellar phase as the starting material and a dilution-induced transition after administration, much smaller volumes can be administered, and in the form of gelatin capsules, which is preferable from both logistics and patient compliance perspectives.

Injectable systems forming liquid crystalline phases *in situ* are interesting, e.g. for subcutaneous or intramuscular depot formulations, since they allow efficient and painless administration to be combined with localization and sustained release after formation. Such injectable depots have been found to be of interest, e.g. for antitumour treatment with IL-2, since toxicity related to peak serum concentration prohibits high dose treatment of IL-2. Using temperature-induced cubic phase formation in Pluronic F127 systems, an injectable depot can be achieved, displaying sustained IL-2 release, reduced peak serum concentration, and longer duration, thus reducing acute toxicity and allowing higher IL-2 concentrations to be used. Due to the need for formulation localization, administration to the oral cavity is another area where *in situ* thickening systems are of interest. In this case, localization needs to take place in a confined space, e.g. in a periodontal pocket, and the formulation able to withstand mechanical stress. An example of phase-transforming self-assembly systems used in this context are Pluronic F127/Pluronic F68, which have been employed for administration of e.g. lidocaine/prilocaine intended for local anaesthetics in the oral cavity in relation to scaling procedures, or vancomycin for reduction of oral infections.

Yet another area where phase-transformations in self-assembly systems are of interest in drug delivery is topical administration. In particular, temperature-thickening block copolymer systems have showed promise as (burn) wound dressings. Such dressings should be easily and painlessly administered, should adhere tightly but yet be easy and painless to remove, should be able to absorb exudate fluid without undergoing phase changes, and should provide a bacterial barrier. Again, temperature-induced cubic phase induction in Pluronic F127 has been found to meet these requirements, particularly when containing an additional antimicrobial agent, such as silver nitrate and silver lactate.

As mentioned above, liposomes have attracted interest as drug delivery systems, e.g. due to their ability to solubilize/encapsulate both oil-soluble and water-soluble drugs. As with other types of delivery systems, responsive transitions are of interest also for liposomes. For example, temperature-sensitive liposomes may be designed, which display melting or other phase transitions to allow for triggered drug release on temperature increase after administration. These are of interest for example in the treatment of localized infections or in directed chemotherapy. While liposomes have attracted broad drug delivery interest, including e.g. gene delivery and topical delivery, perhaps the most extensive efforts in this context have been directed to parenteral administration of liposomes, notably for cancer therapy. As with other colloidal drug delivery systems, liposomes are cleared rapidly from bloodstream circulation after administration by the reticuloendothelial system, RES, and accumulate in

tissues such as liver, spleen and marrow. This causes low bioavailability in non-RES tissues, and results in dose-limiting local toxicity in RES-related tissues. Blood clearance is achieved primarily by macrophages, initiated by the adsorption of key serum proteins (opsonins) at the liposomes. By reducing opsonin adsorption at liposome surfaces, which is particularly efficiently done through inclusion of poly(ethylene oxide) derivatives, opsonin adsorption is dramatically reduced (see below), resulting in prolonged bloodstream circulation, decreased accumulation in RES-related tissues, and an increased drug accumulation of the drug in non-RES tissues/cells. Through this, enhanced antitumour capacity and reduced toxicity can be reached.

In analogy to liposomes, lipid nanoparticles may be obtained through dispersion of liquid crystalline phases other than the lamellar phase, e.g. cubic (cubosomes), hexagonal (hexosomes), or L3 (flexosomes) phases. They may also be prepared by simple mixing in the presence of a suitable hydrotrope, e.g. ethanol. For example, by addition of water to a system of monoolein, water, and ethanol, both isotropic solutions and emulsions may be transformed to dispersed cubosome systems with only marginal energy input. Since the particles obtained are small and display significant solubilization capacity of both hydrophobic and hydrophilic drugs, such lipid nanoparticles are interesting for parenteral administration, particularly when the particles are stabilized by poly(ethylene oxide)-containing block copolymers to prolong bloodstream circulation time and reduce RES uptake (cf. micelles and liposomes). However, cubosomes have been found to also offer advantages in other drug delivery contexts. For example, Gan et al. investigated monoolein cubosomes containing dexamethasone as an ophthalmic delivery system, and found a dramatic increase in effective permeation, prolongation of ocular retention time, and increased bioavailability compared to an aqueous dexamethasone solution. Similarly, monoolein cubosomes loaded with indomethacin for percutaneous administration have been applied [17], and shown higher anti-inflammatory effect, as well as higher stratum corneum concentrations of indomethacin for the cubosome formulation compared to that of a control carbomer formulation of indomethacin.

References

- [1] McBain EL, Hutchinson E. Solubilisation and related phenomena. New York: Academic Press; 1955.
- [2] Florence AT. In: Yalkowsky S, editor. Techniques of solubilization of drugs. New York: Marcel Dekker; 1982.
- [3] Higuchi WI. *J Pharm Sci.* 1964;55:532.
- [4] Higuchi WI. *J Pharm Sci.* 1967;56:315.
- [5] Liberman HA, Rieger MM, Banker GS, editors. *Pharmaceutical dosage forms: Disperse systems*, Vols. 1 and 2. New York: Marcel Dekker; 1988.
- [6] Cartensen JT. *Theory of pharmaceutical systems*. London, New York: Academic Press; 1973.

- [7] Tadros T. Colloid aspects of cosmetic formulations. In: Tadros T, editor. *Colloids in cosmetics and personal care*. Weinheim: Wiley-VCH; 2008.
- [8] Tadros T. *Nanodispersions*. Berlin: De Gruyter; 2016.
- [9] Israelachvili JN, Mitchell DJ, Ninham BW. *J Chem Soc Faraday Trans II*. 1976;72:1525.
- [10] Israelachvili JN, Marcelja S, Horn RG. *Q Rev Biophys*. 1980;13(2):121.
- [11] Israelachvili JN. *Intermolecular and surface forces*. San Diego: Academic Press; 1991.
- [12] Tanford C. *The hydrophobic effect*. 2nd edition. New York: Wiley; 1980.
- [13] Tanford C. In: *Biomembranes*. *Proc Int Sch Phys Enrico Ferm*. 1985;90:547.
- [14] Israelachvili JN, Mitchell DJ. *Biochim Biophys Acta*. 1975;389:13.
- [15] Kostarelos K. PhD Thesis. Imperial College, London; 1995.
- [16] Kostarelos K, Tadros TF, Luckham PF. *Langmuir*. 1999;15:369.
- [17] Tadros T. *Interfacial phenomena and colloid stability*, Vol. 2. Berlin: De Gruyter; 2015.

4 Solid lipid nanoparticles, polymer gels and capsules

4.1 Solid lipid nanoparticles (SLN)

A special type of lipid-based nanoparticle of interest in drug delivery are the so-called solid lipid nanoparticles (SLN) [1]. SLN may be prepared in several different ways. In one of these, an O/W emulsion is prepared, containing the drug (with or without additional lipid) dissolved in a volatile solvent, followed by solvent evaporation and solidification of the lipid matrix. In another, a (solvent-free) O/W emulsion is prepared by high pressure homogenization at elevated temperature, followed by cooling and solidification of the lipid droplets. To some extent, the size of SLN can be determined by the droplet size of the precursor emulsion system, and the concentration of volatile solvent, although complex relationships are frequently observed. In addition, the degree of crystallinity may also be controlled to some extent in SLN systems. In particular, for dispersed melts or oil phases with low solvent content, crystallization is frequently kinetically hindered, thus the crystallinity in SLN is frequently lower than that of the corresponding macroscopic lipid sample. With increasing storage temperature, however, crystallization increases, and SLN typically become less stable than at low temperature, in analogy to many O/W emulsions. SLN are interesting drug delivery systems for several reasons. For example, they have a high loading capacity for hydrophobic drugs, and hydrolytic degradation is limited. Furthermore, the drug release rate can be controlled by the particle size and composition, and burst release is largely absent. The latter is particularly interesting for toxic drugs, where high peak concentrations must be avoided. Due to this, and the hydrophobic nature of several anticancer drugs, SLN offer opportunities for cancer therapy, for example.

4.2 Polymer gels, microgels and capsules

A gel is a “semi-solid” consisting of a “network” in which the solvent is “entrapped”. It may be classified as a “liquid-in-solid” dispersion [2]. One of the most effective techniques to characterize a gel is to investigate its rheological (viscoelastic) behaviour, in particular under conditions of low deformation [2, 3]. Three methods can be applied to investigate the viscoelastic properties of a gel. (i) Stress relaxation (after sudden application of strain). Consider a “gel” with the components in some sort of a “three-dimensional” structure. To deform it instantly, a stress is required and energy is stored in the system (high energy structure). To maintain the new shape (constant deformation), the stress required becomes smaller since the components of the “gel” undergo some diffusion resulting in a lower energy structure to be approached (structural or

<https://doi.org/10.1515/978311055257-005>

stress relaxation). Over a long time deformation becomes permanent with complete relaxation of the structure (new low energy structure) and viscous flow will occur. The exponential decay of the stress with time allows one to obtain the stress relaxation time τ of the gel. A useful way to distinguish between the various gels is to consider the Deborah number De that is given by the ratio of the relaxation time τ with the experimental time t_e . For a gel that shows “solid-like” behaviour (“three-dimensional structure”) De is large when compared with a weaker gel that behaves as a viscoelastic liquid.

The second rheological technique that can be applied to characterize gel strength is constant stress (creep) measurement. In this case a constant stress σ is applied and the strain (deformation) γ or compliance $J (= \gamma/\sigma, \text{Pa}^{-1})$ is followed as a function of time [2]. A gel that consists of a strong “three-dimensional” structure (e.g. crosslinked) behaves as a viscoelastic solid showing a small deformation on application of stress and this behaviour may occur up to high applied stresses. In other words, the critical stress above which significant deformation occurs can be quite high. A weaker gel (produced for example by high molecular weight polymers that are physically attached) behaves as a viscoelastic liquid. In this case viscoelastic solid behaviour only occurs at much lower stresses than that observed with the crosslinked gels.

The third rheological technique that can be applied to characterize a gel is dynamic (oscillatory) measurements. In this case, a sinusoidal strain (or stress) with amplitude γ_0 and frequency ω (rad s^{-1}) is applied on the system and the resulting stress (or strain) with amplitude σ_0 is simultaneously measured [2]. The strain and stress oscillate with the same frequency but the sine waves are shifted by a time Δt . The product of Δt with ω gives the phase angle shift δ . For any gel, $\delta < 90^\circ$ and the smaller the value of δ the stronger the gel.

In pharmaceuticals, gels find use as delivery systems for oral administration, as gels proper or as capsule shells made from gelatin. For topical drugs, gels are applied directly to the skin, mucous membrane or eye and for long acting forms of drugs injected intramuscularly. Gelling agents are also useful as binders in tablet granulations, protective colloids in suspensions, thickeners in oral liquids and suppository bases.

Several classes of gels can be identified [1, 2]:

- (i) Gels produced as a result of repulsive interaction, e.g. expanded double layers.
- (ii) Self-structured systems, whereby one induces weak flocculation to produce a “gel” by the particles or droplets. This requires control of the particle size and shape, volume fraction of the dispersion and depth of the secondary minimum.
- (iii) Thickeners consisting of high molecular weight polymers or finely divided particulate systems that interact in the continuous phase forming a “three-dimensional” structure.
- (iv) Self-assembled structures such as associative thickeners.
- (v) Crosslinked polymers (chemical gels).
- (vi) Liquid crystalline structures of the hexagonal, cubic or lamellar phases.

The most commonly used materials to produce a gel-network are polymers, both natural and synthetic. However, many colloidal particulate solids can form gels by some specific interactions between the particles. High concentrations of nonionic surfactants can also produce clear gels in systems containing up to 15 % mineral oil.

Natural gums have been used for a long time as gelling agents. These gums are typically branched-chain polysaccharides, mostly anionic although some, such as guar gum, are uncharged. Unfortunately these gums are subject to microbial degradation and they require the addition of a preservative. An important gum that is used to produce gels is xanthan gum, which is produced from sugar by microbiological preparation.

Several other gums have been used to produce gels, of which alginates, carrageenan, tragacanth, pectin, gelatine and agar are probably the most important. Alginates are derived from brown seaweeds in the form of monovalent and divalent salts. Sodium alginate is the most widely used gum. Gelation occurs by reduction of pH or reaction with divalent cations. Carrageenan is produced by extraction from red seaweeds and it is a mixture of sodium, potassium, ammonium, calcium and magnesium sulphate esters of polymerized galactose and 3,6-anhydrogalactose. The main copolymer types are labelled kappa-, iota- and lambda-carrageenan. They are all anionic in nature. Alpha and iota fractions form thermally reversible gels in water. At high temperatures, the copolymers exist as random coils and on cooling they result in the formation of double helices which act as crosslinks.

Tragacanth is produced by extraction from special plants grown in the Middle East. It is a complex material composed chiefly of an acidic polysaccharide (tragacanthic acid) containing calcium, magnesium and potassium, as well as a smaller amount of neutral polysaccharide (tragacanthin). The gum swells in water and concentration of 2% or above of a "high quality" gum produces a gel. Hydration takes place over a period of time so that development of maximum gel strength requires several hours.

Pectin is a polysaccharide extracted from the inner rind of citrus fruits or apple pomace. The gel is formed at an acid pH in aqueous solution containing calcium and possibly other agents that act to dehydrate the gum.

Gelatin is used as a bodying agent and gel former in the food industry and occasionally in pharmaceutical products. Agar can be used to make firm gels; it is most frequently used in culture media. Gellan gum has been more recently used as a substitute for agar.

Several synthetic gel-forming materials have been developed for various applications. Cellulose derivatives (such as hydroxyethyl cellulose and carboxymethyl cellulose) are frequently used as gelling agents in several disperse systems (such as suspensions and emulsions). Cellulose is a natural structural polymer found in plants. Treatment in the presence of various active substances results in breakdown of the cellulose backbone as well as substitution of a portion of its hydroxyl moieties. The major factors affecting the gel characteristics (and rheological properties) of the resulting material are the nature of the substituent, degree of substitution and average molecu-

lar weight of the resultant polymer. The cellulose derivatives are subject to enzymatic degradation and sterilization of the aqueous system and/or addition of preservatives are employed to prevent viscosity reduction resulting from depolymerization due to enzyme production by microorganisms.

For both physical and chemical gels, swelling transitions allow triggered exposure of a drug encapsulated in the gel to the surrounding aqueous solution and resulting drug release [1]. For example, polyacids are uncharged at low pH (e.g. in the stomach), resulting in a low degree of swelling, protection against acid-catalysed hydrolysis, and in slow drug release. At higher pH, on the other hand (e.g. in the small intestine), the polymer swells as a result of increased charging and resulting electrostatic interactions, thereby facilitating drug release in a region where it is absorbed more effectively, and where it is more stable against hydrolytic degradation. Similarly, polymer gels may be triggered by reversed temperature solubility, since such systems can be loaded at a high degree of swelling at low temperature, and then achieve a sustained release after administration due to a temperature-induced collapse of the polymer network. As with self-assembly delivery systems, the physicochemical properties of the drug frequently influence the properties of the carrier, which therefore needs to be tuned to the drug and the application at hand. In addition, polysaccharide gels have received considerable interest in drug delivery, since these may be designed to respond to various external stimuli. Examples of this include alginate and gellan gum, which form gels in the presence of Ca^{2+} and other divalent cations. Through varying the Ca^{2+} concentration, the effective 'crosslinking' density of the gels, as well as drug diffusion rate, may be tailored. Furthermore, polysaccharide degradation by microbial enzymes in the large intestine allows localized drug release, of interest e.g. for colon cancer or Crohn's disease, but also systemic absorption of e.g. peptide and protein drugs.

As with macroscopic polymer gels, microgels may be designed to respond to a number of stimuli, including pH, ionic strength, temperature, presence of specific metabolites, and external fields. Given the small size of these gel particles (≈ 100 nm), some of these have potential also in areas where macroscopic polymer gels have not found use, e.g. in parenteral administration, and also provide advantageous effects in other administration routes, e.g. in oral and nasal administration, due to their small size and faster response. As with macroscopic gels, microgels have particular potential as delivery systems for protein and other biomacromolecular drugs, since they are generally hydrophilic and contain a lot of water, which allows proteins to be incorporated into the microgels with only moderate conformational changes and with limited aggregation, thus facilitating maintained biological effect of the protein drug. Of the different response triggers for microgels, temperature is probably the most extensively investigated one. Several different types of polymers exhibit temperature-dependent swelling-deswelling transitions, including systems based on poly(ethylene oxide) derivatives and those including variants of poly(N-isopropyl acrylamide). In common for all these systems is a reduced solvency with increasing temperature, resulting in a dramatic deswelling with increasing temperature. Thermally responsive

microgels may also be combined with magnetic (e.g. $\alpha\text{-Fe}_2\text{O}_3$ or Fe_3O_4) or optically responsive (e.g. gold) nanoparticles. On exposing such composite microgels to a magnetic field or UV light, respectively, heat is generated, in turn triggering a deswelling transition in the microgel network. By localizing the magnetic field or the UV exposure, localized drug release can therefore be obtained for such systems.

From variations of the microgel charged group density, a correlation could be established between the microgel loading capacity for protons and the amount of cationic drug loaded. With increasing pH, acrylic acid dissociation causes network expansion (screened by increasing ionic strength), in turn causing faster release of the incorporated drug. Furthermore, pH-responsive microgels consisting of poly(N-isopropyl acrylamide) and poly(N-isopropyl acrylamide-acrylic acid) have been studied in the context of cancer targeting, and showed specific doxorubicin delivery to HeLa cells. Since doxorubicin causes toxic side effects, including cardiotoxicity and myelosuppression, such targeted delivery with the drug encapsulated is interesting. Also focusing on doxorubicin delivery, an encapsulated system in a pH-sensitive poly(ethylene oxide)-modified system based on diethylamino ethyl methacrylate was investigated, and showed that such doxorubicin-loaded microgels did not display any burst release, again advantageous from a toxicity perspective. Furthermore, doxorubicin release was strongly dependent on pH, which is interesting for endosomal release of the drug during acidification.

Microgels may also be designed to respond to the concentration of a specific metabolite. Insulin has received particular attention in this context, and a number of different systems have been designed to obtain glucose-triggered insulin release. For example, concanavalin A (ConA) is a tetravalent lectin able to effectively “crosslink” polysaccharide derivatives. At suitable polysaccharide/ConA concentration ratios, insulin can be incorporated into such composite microgels. When the latter are exposed to an increased glucose concentration, rupture of the gel crosslinks occurs as a result of competitive binding to ConA, thereby causing insulin release. In analogy, RNA/DNA base and antigen-antibody pairs have been used in the same way, typically with semi-interpenetrating networks prepared by grafting the two components in a recognition pair at the different networks, and forming the gel particles by mixing these together. In the presence of free antibody/antigen (or similarly DNA/RNA), competition results in “crosslink” inactivation, and resulting swelling/dissolution of the network. Triggered response in microgels may also be obtained from programmable degradation. In general, such systems involve degradable microgels, sometimes surrounded by an impermeable shell. Demonstrating this, acrylamide-based gels with acetal crosslinks were prepared, thereby obtaining biodegradation triggered at pH as a result of acid-catalysed acetal hydrolysis. Such systems display a pH-dependent release of incorporated proteins, but also pH-triggered potency of protein-based vaccines. Of course, these chemically degradable microgels are analogous to physically crosslinked microgels using specific interactions. In all these cases, as well as in e.g. cyclodextrin-based microgels, “biodegradation” can be caused also by rupturing of

physical “crosslinks” within the microgel particles, either by competition with specific solutes, or as a response to physical parameters related to the latter.

Although elaborate in preparation, polyelectrolyte multilayer capsules are also receiving increasing attention as drug delivery systems [1]. These consist of alternating anionic and cationic polyelectrolytes, surrounding a (solution or solid) core containing the drug. When suitable, the drug may also be incorporated in the multilayer structure itself. The main feature of such capsules is their barrier function generated by the multilayer, which may be controlled e.g. by the number of shell layers. In addition, polymer multilayer capsules may be triggered by much the same triggering factors as those used for microgels. For example, Nolan et al. investigated layer-by-layer structures formed by poly(acrylic acid) and poly(N-isopropyl acrylamide). Through the temperature-dependence of the latter component, such structures allow the incorporated drug to be released by increasing temperature. Furthermore, polyelectrolyte capsules formed by poly(styrene sulfonate) and poly(allylamine hydrochloride) were studied, and showed fluorescein permeability to increase with ionic strength and decrease with increasing pH. As with microgels, polyelectrolyte multilayer microcapsules may be designed to respond also to specific metabolites. Apart from the polysaccharide/ConA approach discussed above, an example of this are capsules containing phenylboronic acids, which form covalent complexes with polyol compounds such as glucose. By including phenylboronic acid compounds in polyelectrolyte multilayer capsules, a glucose-triggered permeability increase of the capsule can therefore be achieved, interesting e.g. for glucose-triggered insulin release. Also in analogy to microgel particles, drug release may be triggered by programmed capsule degradation. For example, microcapsules containing disulphide “crosslinks”, were prepared, the stability of which may be controlled by the reducing environment, which also provide a self-degradation route of the microcapsules. The opportunities offered by such degradation-mediated swelling in localized drug delivery was realized e.g. by Bromberg et al., who could demonstrate swelling triggered by cleavage of the azoaromatic crosslinks by azoreductases from the rat intestinal cecum. Such systems are therefore of interest e.g. in colon-specific drug delivery.

4.3 Solid polymer nanoparticles

Among nanoparticles not formed by self-assembly, those formed by biodegradable polymers have attracted particular attention in drug delivery. Such solid polymer nanoparticles (lattices) can be loaded with drugs in a several different ways, including:

- (i) adsorption of the drug at the particle surface;
- (ii) particle swelling by solvent and subsequent drug incorporation through passive diffusion;
- (iii) pressure-enhanced drug incorporation in pre-formed polymer particles;

- (iv) incorporation of the drug during the particle polymerization;
- (v) mixing the drug in a polymer melt or a polymer solution, followed by spray cooling or spray drying, respectively.

A number of polymers used in pharmaceutical applications are biodegradable, either by chemical or enzymatic action, or both [1]. In particular, polyesters, e.g. poly(lactide), have received considerable attention as biodegradable polymers for drug delivery. Such polymers undergo hydrolysis in aqueous environment, the rate of which can be controlled, e.g. by monomer structure and monomer mixture composition, crystallinity, and polymer structure formation, but also by temperature, pH and presence of a drug. For biodegradable polymer particles, the drug release rate can be controlled by the particle degradation rate, which may be controlled over orders of magnitude, from minutes to years. Similarly to other types of delivery systems, drug release from polymer particles also depends on drug hydrophobicity, charge, and size. In addition, incorporated drugs can also affect the degradation rate of the polymer particles. For example, basic drugs may behave as base catalysts, thereby enhancing the degradation and resulting release rate. They may, however, also neutralize terminal carboxyl residues of polyesters, thereby reducing the autocatalysis due to the acidic end groups, and therefore also the degradation rate and the release rate. Taken together, this means that the drug release rate in biodegradable polymer nanoparticle systems may be quite complex.

Both oral and parenteral uptake of polymer nanoparticles depends on particle properties (see below). For parenteral administration, their RES uptake depends on factors such as size, surface hydrophobicity, charge, and chemical functionality, in much the same manner as for liposomes, micelles, and other nanoparticulate delivery systems. The oral uptake of polymer nanoparticles, in turn, has been found to occur by several different mechanisms and through different parts of the gastrointestinal tract, including villus tip persorption, phagocytosis by intestinal macrophages, enterocyte endocytosis, and transparacellular uptake in Peyer's patches. It has also been found to depend on a number of factors, including particle size and surface properties. In relation to the latter, it could be noted that the uptake in Peyer's patches, frequently dominating in particle uptake, increases with decreasing particle size. Also the surface properties of the particles play an important role for the oral uptake of particles. For example, the more hydrophobic the particles, the more pronounced the particle uptake. Interesting in relation to oral drug delivery of particulate drug carriers is also the possibility to increase bioadhesion of polymer nanoparticles to mucosal surfaces in order to increase residence time and bioavailability. Since mucins, the main constituent in mucosa, are negatively charged and contain hydrophobic domains, increased bioadhesion can be achieved for example by positively charged particles, hydrophobic particles, or particles not colloidally stable at the conditions present at the administration site. Such approaches to reach mucoadhesion have indeed been found to result in beneficial results in oral administration, but also at other mucosal surfaces. Using e.g. the

positively charged polyelectrolyte chitosan, has been found to result in a significantly improved bioavailability of particle-based drug delivery systems, and chitosan particles have been found to display prolonged residence time through bioadhesion [1]. In parallel, chitosan-coated alginate beads have been found to adhere more to (negatively charged) stomach and other tissues than the corresponding uncoated alginate beads.

Another area where biodegradable polymeric drug carriers have been found promising is in oral vaccines. There are several reasons for this. First, stomach acidity causes rapid degradation of the compounds typically used for immunization, such as peptides, proteins, cells, and viruses. By encapsulation in polymer particles, such degradation can be reduced or eliminated. In addition, particles may be beneficial for immunization by adjuvant action. Since orally administered particles are taken up by Peyer's patches, a beneficial localization effect may also occur. The most frequently used polymer particles for oral vaccination are those consisting of biodegradable polyesters, such as poly(lactic acid), poly(glycolic acid), and their copolymers. These are taken up efficiently by Peyer's patches, are readily biodegradable with readily resorbable degradation products, and have been found to stimulate both mucosal (sIgA) and systemic (IgG) antibodies.

References

- [1] Malmsten M. Pharmacy. In: Tadros T, editor. Encyclopedia of colloid and interface science. Berlin: Springer; 2013.
- [2] Tadros T. Rheology of Dispersions. Weinheim: Wiley-VCH; 2010.
- [3] Goodwin JW, Hughes RW. Rheology for Chemists. Cambridge: Royal Society of Chemistry Publication; 2000.

5 Drug delivery and drug targeting

5.1 Introduction

The concept of delivering a drug to its pharmaceutical site of action in a controlled manner has attracted much attention in the pharmaceutical industry in recent years. A great deal of research is being carried out since the site delivery of a drug can be controlled at a rate and concentration that optimizes the therapeutic activity, while minimizing the adverse toxic effects [1, 2].

The use of biodegradable colloidal nanoparticles offers a number of advantages over more conventional dosage forms [2, 3]. Due to their small size (20–200 nm) they are suitable for intravenous administration, they can be applied as long circulating drug depots and for targeting specific organs or sites. Several other advantages of nanoparticles can be listed: protection of drugs against metabolism or recognition by the immune system, reduction of toxic effects especially for chemotherapeutic drugs and improved patient compliance by avoiding repetitive administration [3]. Various biodegradable colloidal drug carriers have been developed, of which polymeric nanoparticles are the most widely used systems.

5.2 Polymeric nanoparticles

The most widely used polymeric nanoparticles are those of the A–B and A–B–A block copolymer type. Block copolymers of the B–A and B–A–B types are known to form micelles that can be used as drug carriers [3]. These block copolymers consist of a hydrophobic B block that is insoluble in water and one or two A blocks which are very soluble in water and strongly hydrated by its molecules. In aqueous media the block copolymer will form a core of hydrophobic chains and a shell of hydrophilic chains. These self-assembled structures are referred to as micelles and they are schematically illustrated in Fig. 5.1. The core-shell structure is ideal for drug delivery where the water-insoluble drug is incorporated in the core and the hydrophilic shell provides effective steric stabilization, thus minimizing adsorption of the blood plasma components and preventing adhesion to phagocytic cells.

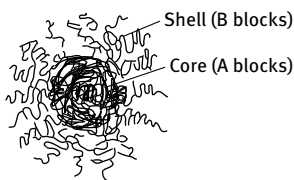


Fig. 5.1: Core-shell structure of block copolymers.

<https://doi.org/10.1515/978311055257-006>

Polymeric nanoparticles with the drug entrapped within the polymer matrix have some advantages in terms of their stability both in storage and in *in vivo* applications [3]. The choice of a polymer is restricted by its biodegradability. Both model non-biodegradable and biodegradable and these nanoparticles have been used for studies on their use of these as drug carriers.

Regardless of the type of the nanoparticle, these colloidal systems are recognized as foreign bodies after administration to the systemic circulation. They can be quickly removed by the phagocytic cells (macrophages) of the reticuloendothelial system (RES), in particular by the Kupffer cells of the liver. The main approach is to design nanoparticles that avoid RES recognition. This can be achieved by controlling the size and surface properties of the nanoparticle. If the nanoparticles remain in circulation for a prolonged period of time, and avoid liver deposition, there is the possibility of redirecting the particles to other organs/tissues. Long circulating nanoparticles can potentially be actively directed to a particular site by the use of targeting moieties such as antibodies or sugar residues that can be specifically recognized by cell surface receptors [3].

Following intravenous (i.v.) injection, the colloidal nanoparticles are recognized as foreign bodies and they may be removed from the blood circulation by the phagocyte cells of the RES. Within five minutes after i.v. injection $\approx 60\text{--}90\%$ of the nanoparticles can be phagocytosed by the macrophages of the liver and spleen. Site specific delivery to other organs must avoid this process taking place. The design of any nanoparticle system with long circulation requires understanding of the mechanism of phagocytosis. The clearance of nanoparticles is mediated by adsorption of blood components to the surface of the particles, a process referred to as opsonization that is described below.

The adsorption of proteins (a component of blood) at the surface of the nanoparticles can result in the surface becoming hydrophobic and this may lead to enhanced phagocytosis. The hydrophobic segments of a protein molecule may adsorb on a hydrophobic surface. While on the surface, the protein may be denatured due to the loss of configurational liability. There may be also a gain in configurational entropy on going from a globular to a more extended state. However, the process of protein adsorption is quite complex due to the presence of more than one type in the blood plasma.

Opsonins refer to proteins that enhance phagocytosis, whereas dyopsonins are molecules that suppress phagocytosis. This depends on the hydrophobic/hydrophilic nature of the protein. Opsonins are immunoglobulin molecules that adsorb on the particle surface, thus making them more “palatable” to macrophages. Dyopsonins are immunoglobulin molecules that render the surface of the particles more hydrophilic thus suppressing phagocytosis. The interaction of the blood components with the nanoparticles is a complex process, although its control is the key to avoiding phagocytosis [3].

When considering nanoparticles as drug delivery systems one must consider three main characteristics:

- (i) Particle size, which determines the deposition of colloidal nanoparticles containing the drug following intravenous administration.
- (ii) Surface charge, which determines the interaction between the nanoparticles and the macrophages.
- (iii) Surface hydrophobicity, which determines the interaction of the serum components with the nanoparticle surface. This determines the degree of opsonization.

A description of each of the above characteristics is given below [3].

(i) Influence of particle size: Particles $> 7 \mu\text{m}$ are larger than the blood capillaries ($\approx 6 \mu\text{m}$) and they become entrapped in the capillary beds of the lungs. Thus, aggregated or flocculated particles tend to accumulate in the lung with fatal consequences. Most of the particles that pass the lung capillary bed become accumulated by the RES of the spleen, liver and bone marrow. The degree of splenic uptake increases with increasing particle size. The splenic removal of particles and liposomes $> 200 \text{ nm}$ is due to a non-phagocytic process whereby the splenic architecture acts as a sieve or filter bed. As the particle size is reduced below 200 nm , the extent of splenic uptake decreases and the majority of particles are mostly cleared by the liver. Colloidal particles not cleared by the RES can exit the blood circulation via the sinusoidal fenestrations of the liver and bone marrow provided they are smaller than 150 nm .

(ii) Influence of surface charge: The surface charge determines the electrostatic repulsion between the colloidal nanoparticles and the blood components or a cell surface. However, the range of electrostatic repulsion decreases with increasing ionic strength. The blood has an ionic strength of $\approx 0.15 \text{ mol dm}^{-3}$ and hence the range of electrostatic repulsion is less than 1 nm . This means the surface charge only influences the protein-protein or particle-macrophage interactions at very short distances. Thus the effect of surface charge on phagocytosis is not due to its effect on electrostatic repulsion, but due to its influence on hydrophobicity of the particles that can determine protein adsorption.

(iii) Influence of surface hydrophobicity: As mentioned above, the hydrophobic sites on a nanoparticle determines the adsorption of the serum components. Increasing surface hydrophobicity increases protein adsorption, thus increasing the degree of opsonization. It has been shown by *in vitro* studies that the increased adsorption of proteins on a hydrophobic surface leads to enhanced uptake by phagocytic cells. As will be shown later, the surface modification of nanoparticles by adsorbed or grafted polymers can affect their surface hydrophobicity and hence their ability to be captured by the phagocytic cells.

The surface of polystyrene latex particles is relatively hydrophobic and can be easily modified by adsorbed nonionic polymers. Poloxamers and poloxamines are composed of a central poly(propylene oxide) (PPO) block and terminal poly(ethylene oxide) (PEO) chains. The general structure of poloxamers and poloxamines is given in

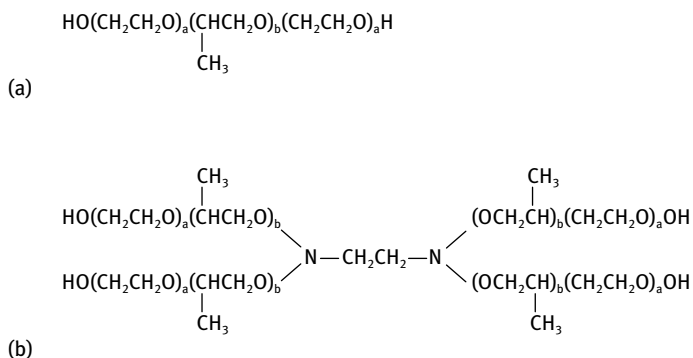


Fig. 5.2: General structure of poloxamers (a) and poloxamines (b).

Fig. 5.2. As mentioned above, the hydrophobic central PPO chain anchors the copolymer to the surface of the particle, whereas the hydrophilic PEO blocks provide the required hydrophilic steric barrier. In general, the thickness of the adsorbed layer increases with increasing length of the PEO chains [3, 4].

The coating of polystyrene particles with poloxamers and poloxamines dramatically reduces their sequestration by the liver. The thickness of the PEO layer is crucial to altering the biological fate of the nanoparticles. Poloxamers with short PEO chains, such as Poloxamer 108 (M_w of the PEO is 1800 Dalton) do not provide an effective steric barrier against *in vitro* phagocytosis. In contrast, Poloxamer 338 (M_w of the PEO is 5600 Dalton) is sufficient to suppress *in vitro* phagocytosis in the presence of serum and dramatically reduce the liver/spleen uptake of 60 nm polystyrene nanoparticles from 90 % to 45 % following *i.v.* injection. Coating with Poloxamine 908 (M_w of the PEO is 5200 Dalton) had a more pronounced effect, decreasing the amount cleared to less than 25 %.

The presence of a hydrated PEO layer alone does not necessarily prolong the circulatory half-life of all drug carriers. The particle size plays a major role. Particles >200 nm in diameter coated with Poloxamine 908 enhanced spleen uptake and decreased blood levels following *i.v.* administration to rats. Polystyrene particles with 60 and 150 nm diameters and coated with Poloxamer 407 were redirected to the sinusoidal endothelial cells of the rabbit bone marrow following *i.v.* administration. In contrast, Poloxamer 407 particles with diameter 250 nm were mostly sequestered by the liver and spleen and only a small portion reached the bone marrow [3, 4].

Polystyrene particles with chemically grafted PEO chains (M_w of the PEO is 2000 Dalton) were prepared with different surface densities of PEO. *In vitro* cell interaction studies demonstrated that particle uptake by non-parenchymal rat liver cells (primary Kupffer cells) decreased with increasing PEO surface density until an optimum density is reached. *In vivo* studies showed that only particles with very low PEO surface density result in considerable liver deposition. However, the results

showed that the liver avoidance and blood circulation was not improved above that obtained with Poloxamine 908, even though the surface density of the grafted PEO particles was higher than that of Poloxamine 908.

As mentioned above, studies using polystyrene nanoparticles as model drug carriers have demonstrated that by optimizing the particle size and modifying the surface using a hydrophilic PEO layer (as a steric barrier) can result in an increase in circulation life-time and to some extent selective targeting may be achieved.

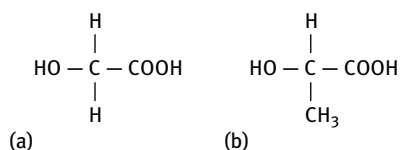
5.3 Biodegradable nanoparticles

For practical applications in drug targeting, polymeric nanoparticles that are constructed from biodegradable and biocompatible materials must be constructed [3, 4]. These polymeric nanoparticles can act as drug carriers by incorporation of the active substance in the core of the nanoparticle. Natural materials such as albumin and gelatin are poorly characterized and in some cases can produce an adverse immune response. This has led to the use of synthetic, chemically well-defined biodegradable polymers which do not cause any adverse immune response. A list of these biodegradable polymers is given in Tab. 5.1.

Tab. 5.1: Biodegradable polymers for drug carriers.

Poly(lactic acid)/poly(lactic-co-glycolic acid) – PLA/PLGA
 Poly(anhydrides)
 Poly(caprolactone)
 Poly(ortho esters)
 Poly(β -maleic acid-co-benzyl malate)
 Poly(alkylcyanoacrylate)

The most widely used biodegradable polymers are the aliphatic polyesters based on lactic and glycolic acid which have the following structures:



Poly(lactic acid) (PLA) and poly(lactic acid-co-glycolic acid) (PLGA) have been used in the production of a wide range of drug carrier nanoparticles. PLA and PLGA degrade by bulk hydrolysis of the ester linkages. The polymers degrade to lactic and glycolic acids which are eliminated in the body, primarily as carbon dioxide and urine.

The preparation of biodegradable nanoparticles with a diameter less than 200 nm (to avoid splenic uptake) remains a technical challenge. Particle formation by in situ emulsion polymerization (that is commonly used for the preparation of polystyrene latex) is not applicable to biodegradable polymers such as polyesters. Instead, the biodegradable polymer is directly synthesized by chemical polymerization methods. The polymer is dissolved in a water immiscible solvent such as dichloroethane which is then emulsified into water using a convenient emulsifier such as poly(vinyl alcohol) (PVA). Nanoemulsions can be produced by sonication or homogenization and the organic solvent is then removed by evaporation. Using this procedure, nanoparticles of PLA and PLGA with a diameter ≈ 250 nm could be produced. Unfortunately, the emulsifier could not be completely removed from the particle surface and hence this procedure was abandoned.

To overcome the above problem nanoparticles were prepared using a surfactant-free method. In this case the polymer is dissolved in a water miscible solvent such as acetone. The acetone solution is carefully added to water while stirring [4]. The polymer precipitates out as nanoparticles which are stabilized against flocculation by electrostatic repulsion (resulting from the presence of COOH groups on the particle surface). Using this procedure surfactant-free nanoparticles with diameter < 150 nm could be prepared. Later, the procedure was modified by incorporation of poloxamers or poloxamines in the aqueous phase. These block copolymers are essential for surface modification of the nanoparticle as is discussed below.

Following the encouraging in vivo results using polystyrene latex with surface modification using poloxamer and poloxamine, investigations were carried out using surfactant-free PLGA, ≈ 140 nm diameter, which was surface modified using the following block copolymers: water-soluble poly(lactic)–poly(ethylene) glycol (PLA–PEG); poloxamers, poloxamines. The results showed that both PLA–PEG 2:5 (M_w of PLA is 2000 Dalton and M_w of PEO is 5000 Dalton) Poloxamine 908 form an adsorbed layer of 10 nm. The coated PLGA nanoparticles were effectively sterically stabilized towards electrolyte-induced flocculation and in vivo studies demonstrated a prolonged systemic circulation and reduced liver/spleen accumulation when compared with the uncoated particles. The main drawback of the polymer adsorption approach is the possibility of desorption in vivo by the blood components. Chemical attachment of the PEG chain to the biodegradable carrier would certainly be beneficial [4].

The best approach is to use block copolymer assemblies as colloidal drug carriers [1–3, 5–10]. Block copolymers of the B–A and B–A–B types are known to form micelles that can be used as drug carriers. These block copolymers consist of a hydrophobic B block that is insoluble in water and one or two A blocks which are very soluble in water and strongly hydrated by its molecules. In aqueous media the block copolymer will form a core of hydrophobic chains and a shell of the hydrophilic chains. These self-assembled structures are referred to as micelles and they were schematically illustrated in Fig. 5.1. The core-shell structure is ideal for drug delivery where the

water-insoluble drug is incorporated in the core and the hydrophilic shell provides effective steric stabilization, thus minimizing adsorption of the blood plasma components and preventing adhesion to phagocytic cells [4].

The critical micelle concentration (cmc) of block copolymers is much lower than that obtained with surfactants. Typically, the cmc is of the order of 10^{-5} g ml⁻¹ or less. The aggregation number *N* (number of copolymer molecules forming a micelle) is typically several tens or even hundreds. This results in assemblies of the order of 10–30 nm which are ideal as drug carriers. The thermodynamic tendency for micellization to occur is significantly higher for block copolymers when compared with low molecular weight surfactants.

The inherent core-shell structure of aqueous block copolymer micelles enhances their potential as a colloidal drug carrier. As mentioned before, the hydrophobic core can be used to solubilize water-insoluble substances such as hydrophobic drug molecules. The core acts as a reservoir for the drug which also can be protected against *in vivo* degradation. Drugs may be incorporated by covalent or non-covalent binding, such as hydrophobic interaction. The hydrophilic shell minimizes the adsorption of blood plasma components. It also prevents the adhesion of phagocytic cells and influences the pharmacokinetics and biodistribution of micelles. The stabilizing chains (PEG) are chemically grafted to the core surface, thus eliminating the possibility of desorption or displacement by serum components. The size of the block copolymer micelles is advantageous for drug delivery [4].

The water solubility of PLA-PEG and PLGA-PEG copolymers depends on the molecular weight of the hydrophobic (PLGA-PEG) and hydrophilic (PEG) blocks. Water-soluble PLA-PEG copolymers with relatively low molecular weight PLA blocks self-disperse in water to form block copolymer micelles. For example, water-soluble PLA-PEG 2 : 5 (*M_w* of PLA is 2000 Da and *M_w* of PEO is 5000 Dalton) form spherical micelles ≈ 25 nm in diameter. These micelles solubilize model and anticancer drugs by micellar incorporation. However, *in vivo*, the systemic lifetimes produced were relatively short and the clearance rate was significantly faster when the micelles were administered at low concentration. This suggests micellar dissociation at concentrations below the cmc.

By increasing the PLA/PLGA core molecular weight, the block copolymer becomes insoluble in water and hence it cannot self-disperse to form micelles. In this case the block copolymer is dissolved in a water immiscible solvent such as dichloromethane and the solution is emulsified into water using an emulsifier such as PVA. The solvent is removed by evaporation resulting in the formation of self-assembled nanoparticles with a core-shell structure. Using this procedure, nanoparticles of PLGA-PEG copolymers (*M_w* of PLGA block of 45 000 Da and *M_w* of PEO of 5000, 12 000 or 20 000 Da) can be obtained. High drug loading (up to 45 % by nanoparticle weight) and entrapment efficiencies (more than 95 % of the initial drug used) can be achieved.

The PLGA-PEG nanoparticles shows prolonged blood circulation times and reduced liver deposition when compared with the uncoated PLGA nanoparticles. The

adsorption of plasma proteins onto the surfaces of the PEG-coated particles is substantially reduced, in comparison with the uncoated PLGA nanoparticles. The qualitative composition of the adsorbed plasma protein is also altered by the presence of the PEG layer. Substantially reduced adsorption of opsonin proteins such as fibrinogen, immunoglobulin G and some apolipoproteins is achieved. These results clearly show the importance of the presence of the hydrophilic PEG chains on the surface of the nanoparticles which prevents opsonization [1–3, 5–11].

The particle size and surface properties are strongly dependent on the emulsification conditions and the choice of emulsifier. By using a water miscible solvent such as acetone, the nanoparticles can be directly precipitated and the solvent is removed by evaporation. Using this procedure one can produce a series of PLA–PEG nanoparticles. The blood circulation of the nanoparticles (e.g. PLA–PEG 30 : 2) is considerably increased when compared with albumin-coated PLA nanoparticles. The albumin molecules are rapidly displaced by the protein in the plasma leading to phagocytosis by Kupffer cells in the liver. The PLA–PEG nanoparticles show a low deposition of proteins on the particle surface.

Functionality is introduced in the core-forming A block in the form of polymers such as poly(L-lysine) or poly(aspartic acid). Both these polymers are biodegradable but not hydrophobic. Hydrophobicity is imparted by covalent or ionic attachment of the drug molecule. In this way potent anticancer drugs can be coupled to the aspartic acid residues of poly(aspartic acid)–poly(ethylene glycol) (P(asp)–PEG) copolymer. In aqueous media the block copolymer–drug conjugate forms micelles, but some of the drug may become physically entrapped in the core of the micelle. These P(asp)–PEG micelles (≈ 40 nm diameter) remain in the vascular system for prolonged periods, with 68% of the injected dose remaining 4 hours after intravenous administration. These systems offer a promising route for drug delivery.

The mechanism of action of the hydrophilic PEG chains can be explained in terms of steric interaction that is well known in the theory of steric stabilization. Before considering the steric interaction one must know the polymer configuration at the particle/solution interface. The hydrophilic PEG chains can adopt a random coil (mushroom) or an extended (brush) configuration [15]. This depends on the graft density of the PEG chains as will be discussed below. The conformation of the PEG chains on the nanoparticle surface determines the magnitude of steric interaction. This configuration determines the interaction of the plasma proteins with the nanoparticles.

The hydrophilic PEG B chains (buoy blocks) can be regarded as chains terminally attached or grafted to the micellar core (A blocks). If the distance between the grafting points D is much greater than the radius of gyration R_G , the chains will assume a “mushroom” type conformation, as illustrated in Fig. 5.3 (a). The extension of the mushroom from the surface will be of the order of $2R_G$ and the volume fraction of the polymer exhibits a maximum away from the surface, as illustrated in Fig. 5.4 (a). If the graft density reaches a point where $D < R_G$, the chains stretch in solution forming a “brush”. A constant segment density throughout the brush with all chains ending a

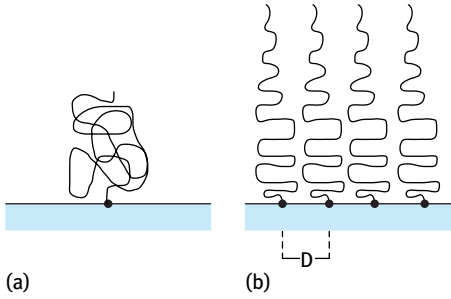


Fig. 5.3: Schematic representation of the conformation of terminally attached PEG chains.

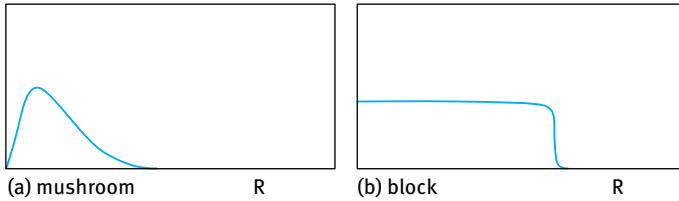


Fig. 5.4: Volume fraction profile for (a) mushroom (b) brush.

distance Δ (the layer thickness) from the surface and the volume fraction of the polymer shows a step function, as illustrated in Fig. 5.4 (b).

The thickness of the block “brush” Δ for a grafted chain of N bonds of length ℓ is given by,

$$\frac{\Delta}{\ell} \approx N \left(\frac{\ell}{D} \right)^{2/3}. \quad (5.1)$$

This means that for terminally-attached chains at high graft density (brush) Δ depends linearly on N . This is in contrast to polymer chains in free solutions where $R_G \approx N^{3/5}$ or $R_G \approx N^{1/2}$. In the case of micellar structures, the distance between grafting points D is determined by the aggregation number. Unless high aggregation numbers and hence grafting densities can be achieved, a weaker dependence of Δ on chain length is expected.

For a brush on a flat surface, the attached chain is confined to a cylindrical volume of radius $D/2$ and height Δ . If the individual chains of the brush are attached to a spherical core (as is the case with nanoparticles), then the volume accessible to each chain increases and the polymer chains have an increased freedom to move laterally resulting in a smaller thickness Δ . This is schematically illustrated in Fig. 5.5 which shows the difference between particles with high surface curvature (Fig. 5.5 (a)) and that for a surface with low surface curvature (Fig. 5.5 (b)). The curvature effect was illustrated for PEO and poloxamer block copolymers using polystyrene latex particles with different sizes. An increase in the layer thickness with increasing particle radius was observed [4].

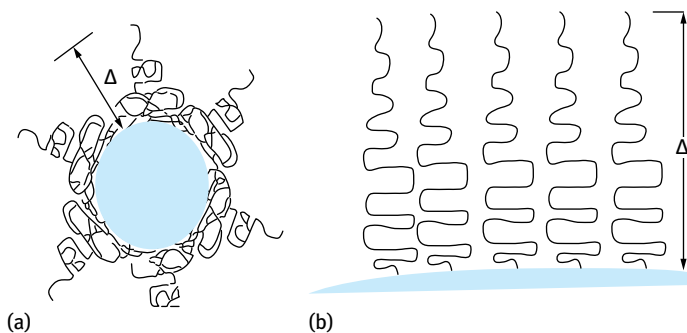


Fig. 5.5: Effect of surface curvature on the adsorbed layer thickness Δ . (a) High surface curvature; (b) low surface curvature.

Most studies with model non-biodegradable and biodegradable systems showed that the presence of a hydrated PEG steric barrier significantly increased the blood circulation of the nanoparticles following intravenous administration. The hydrophilic PEG layer minimizes the interaction with phagocytic cells and prevents the adsorption of opsonins. Hydrophilicity is necessary but not sufficient for achieving these two effects. This was demonstrated using dextran (which is considerably hydrophilic) coated liposomes which showed shorter circulation times when compared with their PEG counterparts. This clearly showed that chain flexibility is the second prerequisites for inhibiting phagocytic clearance [4].

PEG chains only have a weak tendency to interact hydrophobically with the surrounding proteins. As the protein approaches the stabilizing PEG chains, the configurational entropy of both molecules is reduced. The more mobile the stabilizing PEG chains, the greater the loss in entropy and the more effective the repulsion from the surface. At sufficiently high surface density, the flexible PEG chains form an impermeable barrier, preventing the interaction of the opsonins with the particle surface. This repulsion is referred to as elastic interaction, G_{el} . On approach of a second surface to a distance h smaller than the adsorbed layer thickness Δ , a reduction in configurational entropy of the chain occurs [12–14].

Four different types of interaction between a protein molecule and hydrophobic substrate can be considered [14–16]:

- (i) Hydrophobic attraction between the protein and substrate.
- (ii) Steric repulsion (osmotic and elastic effects).
- (iii) Van der Waals attraction between the protein and substrate.
- (iv) Van der Waals attraction between the protein and PEG chains.

These interactions are schematically represented in Fig. 5.6. The interaction of plasma proteins with the PEG steric layer is dependent on the conformation of the chains which is determined by the surface curvature as discussed above.

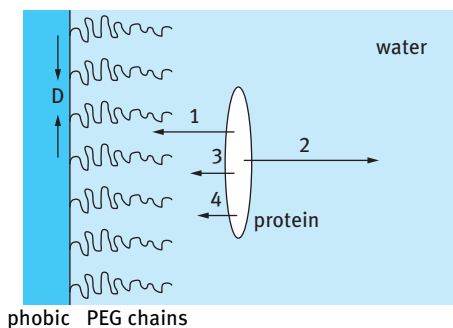


Fig. 5.6: Schematic representation of the various interactions between the PEG layer and protein molecules.

There is ample evidence to suggest that high surface coverage of long brush-like PEG chains is necessary for preventing serum protein adsorption. However, the precise surface characteristics required for successful PES avoidance is not well established and more research is still required. In vitro phagocytosis of poloxamer-coated polystyrene (PS) nanoparticles (60 and 250 nm in diameter) decreases with increasing PEG molecular weight and hence its thickness. However, increasing the PEG molecular weight above 2000 Da did not improve the ability of the coated nanoparticles to avoid phagocytosis. Similar results were obtained in vivo for both coated PS particles and liposomes of phosphatidylamine-PEG. However, results using PLGA-PEG nanoparticles showed an increase in performance when the PEG chain molecular weight was increased from 5000 to 20 000 Da.

The colloid stability of the PLA-PEG nanoparticles can be assessed by the addition of an electrolyte such as Na_2SO_4 which is known to reduce the solvency of the medium for the PEO chains [4]. This reduction in solvency results in an increase of the Flory-Huggins parameter χ (from its value in water of < 0.5) and when χ reaches 0.5 (the θ condition) flocculation occurs. In this way one can determine the critical flocculation point, CFPT. The CFPT can be easily determined by following the turbidity of the nanoparticle dispersion as a function of Na_2SO_4 concentration. At the CFPT a sharp increase in turbidity is observed. The reversibility of flocculation can be assessed by diluting the flocculated dispersion with water and observing if the flocs can be redispersed by gentle shaking. The effect of the presence of serum protein on nanodispersion stability can also be studied by firstly coating the nanoparticles with the protein and then determining the CFPT using Na_2SO_4 .

The hydrodynamic diameter of the nanoparticles and their polydispersity index are determined using PCS. The PEG molar mass is fixed at 5000 Da while gradually increasing the PLA molar mass. The nanoparticle composition is expressed as a ratio of PLA : PEG; for example PLA-PEG 2 : 5 refers to a nanoparticle with PLA molar mass of 2000 and PEG molar mass of 5000. For comparison, the hydrodynamic diameter of PLA is also determined at a given molar mass. The zeta potential of the nanoparticles in 1 mM HEPES buffer (adjusted to pH 7.4 by addition of HCl) is also determined.

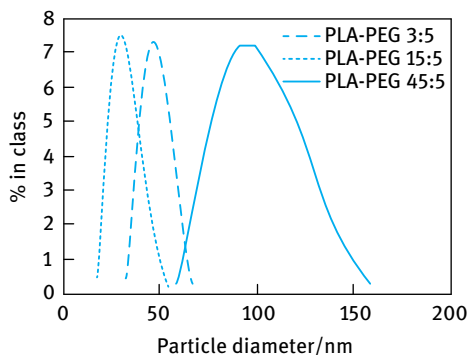
A summary of the results is given in Tab. 5.2.

Tab. 5.2: Hydrodynamic diameter, polydispersity index and zeta potential of PLA and PLA-PEG nanoparticles.

Polymer	Hydrodynamic diameter, D_{hyd} (nm) mean \pm SD	Polydispersity index mean \pm SD	Zeta potential 1 mM HEPES (mV)
PLA (M_w 35 kDa)	124.6 \pm 2.5	0.11 \pm 0.03	-49.6 \pm 0.7
PLGA-PEG 2 : 5	26.0 \pm 1.6	0.19 \pm 0.01	—
PLGA-PEG 3 : 5	28.2 \pm 0.6	0.14 \pm 0.01	—
PLGA-PEG 6 : 5	41.1 \pm 1.8	0.10 \pm 0.04	—
PLGA-PEG 15 : 5	50.6 \pm 2.0	0.06 \pm 0.01	-6.5 \pm 0.7
PLGA-PEG 30 : 5	63.8 \pm 1.8	0.08 \pm 0.02	-6.4 \pm 1.5
PLGA-PEG 45 : 5	80.7 \pm 4.8	0.10 \pm 0.01	-6.1 \pm 0.4
PLGA-PEG 75 : 5	118.7 \pm 4.9	0.10 \pm 0.01	-14.2 \pm 0.6
PLGA-PEG 110 : 5	156.6 \pm 5.0	0.13 \pm 0.02	-28.0 \pm 0.4

The results of Tab. 5.2 show that the nanoparticles have a relatively low polydispersity index. They suggest that the particle size distribution is monomodal, as illustrated in Fig. 5.7. This is confirmed by absence of subpopulations as shown in Fig. 5.7. Particles prepared from PLA ($M_w = 35\,000$) are significantly larger than those prepared with a near equivalent PLA block (30 : 5). The effect of increasing the polymer concentration in the acetone solution on the particle size is shown in Fig. 5.8 for PLA-PEG copolymers and in Fig. 5.9 for PLA homopolymer. The results of Fig. 5.8 show that up to PLA-PEG 30 : 5, the hydrodynamic diameter is independent of polymer concentration. In contrast, the results of Fig. 5.9 for the PLA homopolymer show a significant increase in particle diameter with increasing polymer concentration. It appears that the PEG block moderates the association of the PLA-PEG copolymer.

The results shown in Tab. 5.2 clearly indicate that the PLA nanoparticles have a high negative zeta potential of 49.6 mV. This is probably due to the presence of ionic carboxylic groups on the nanoparticle surface. At pH 7.4 (which is above the pK_a of

**Fig. 5.7:** Particle size distribution of PLA-PEG nanoparticles (intensity weighted CONTIN analysis).

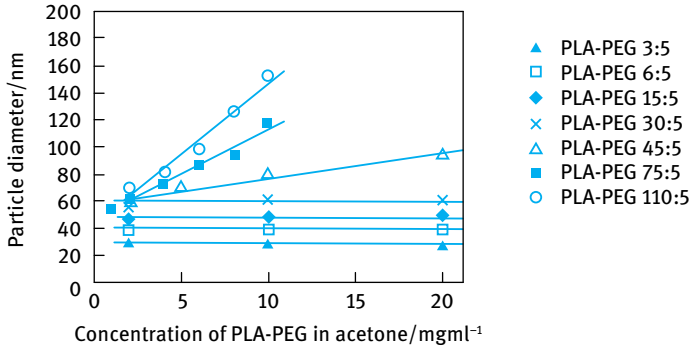


Fig. 5.8: Effect of PLA-PEG concentration on nanoparticle diameter.

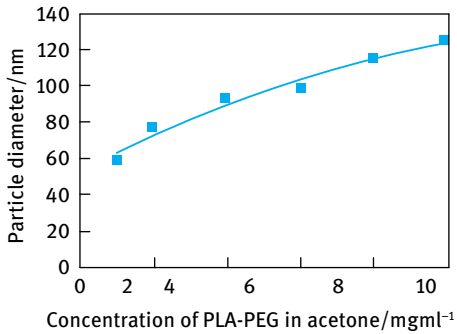


Fig. 5.9: Effect of PLA concentration on nanoparticle diameter.

COOH groups) and low ionic strength, a high negative surface charge is produced. This negative charge provides electrostatic stabilization of the nanoparticles.

The zeta potential of the PLA-PEG nanoparticles is significantly reduced (to ≈ -6 mV) up to a PLA:PEG ratio of 45:5. This reduction is due to the presence of the PEG layer that cause a significant shift in shear plane and hence reduction of ζ . However, when the PLA:PEG ratio is increased above 45:5, ζ starts to increase since the PEG layer thickness become relatively smaller to the core of PLA.

Fig. 5.10 shows the variation of turbidity with Na_2SO_4 concentration. Above a critical Na_2SO_4 concentration the turbidity shows a rapid increase with a further increase in electrolyte concentration. This critical concentration is defined as the critical flocculation point (CFPT). The CFPT decreases with increasing PLA blocks in the nanoparticle. The results are expected for a sterically stabilized dispersion and show that at the CFPT the medium becomes θ -solvent for the chains at which the Flory-Huggins interaction parameter χ become 0.5, and this is the onset of incipient flocculation. Above the CFPT χ become higher than 0.5, i.e. the medium becomes worse than a θ -solvent for the chains.

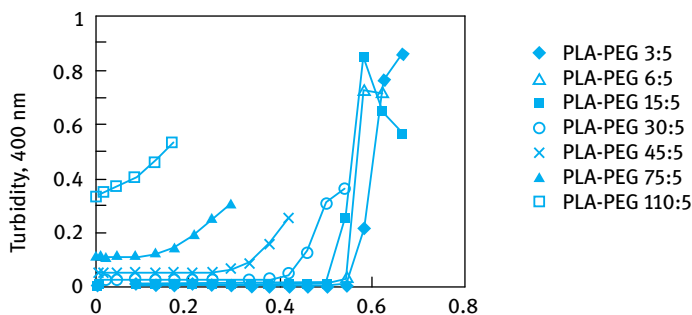


Fig. 5.10: CFPT of PLA-PEG nanoparticles determined by turbidity method.

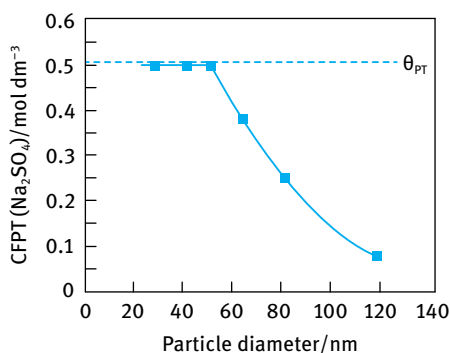


Fig. 5.11: CFPT of PLA-PEG (with increasing amounts of PLA, 3 : 5 to 75 : 5) as a function of particle diameter.

The effect of the PLA core on the CFPT is illustrated in Fig. 5.11 which shows the variation of CFPT with particle diameter.

The results of Fig. 5.11 clearly show that nanoparticles with PLA blocks of $M_w < 15\,000$ give a CFPT close to the θ -point of the PEG chain. When the PLA block M_w is $> 15\,000$, the nanoparticles give a CFPT below the θ -point of the PEG chain. The CFPT decreases with increasing PLA block M_w . This discrepancy between the CFPT and θ -point of the PEG chain may be due to the decrease in surface coverage of the nanoparticles with the PEG chains when the PLA block M_w exceeds a certain value. This reduction in surface coverage leads to lateral movement of the PEG chains which results in a smaller layer thickness. This smaller PEG thickness can result in a deep attractive minimum, causing flocculation under conditions of better than the θ -point of the PEG chain [4].

Increasing the concentration of the PLA-PEG copolymer used during the preparation by the solvent/precipitation method results in an increase in the nanoparticle size. This is illustrated in Fig. 5.12 for PLA-PEG 45 : 5, which shows the variation of CFPT with particle diameter. The results show a linear increase of the CFPT with increasing particle diameter approaching the θ -point for the PEG chain when the diameter reaches 94 nm (obtained when the concentration of the PLA-PEG reaches

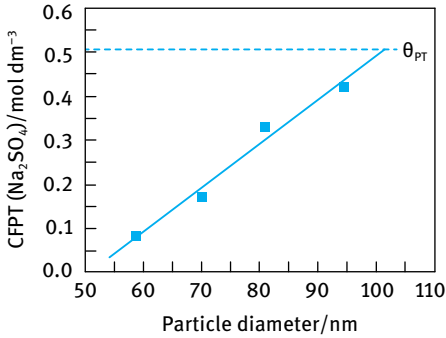


Fig. 5.12: CFPT of PLA–PEG 45 : 5 nanoparticles as a function of particle diameter.

20 mg ml⁻¹). This increase in the stability of the nanoparticle dispersion with increasing particle diameter may be due to the increased surface coverage of the particles with PEG chains as particle size is increased.

The aggregation number of the PLA–PEG copolymer in aqueous solution determines the properties of the micellar-like structures of the nanoparticles. The aggregation number is the number of copolymer units per micelle and this emphasizes the self-assembly of PLA–PEG of the nanoparticle [4]. The process is irreversible with no dynamic equilibrium between the self-assembled structure and unimers. Thus, the process is different from that of surfactant micelles in which a dynamic equilibrium exists between the micelle and the surfactant molecule.

The micellar aggregation number scales with increasing number of monomeric units in the core-forming block N_A ,

$$N_{\text{agg}} \approx N_A^\beta \quad (5.2)$$

The value of the exponent β depends on the composition of the micelle-forming copolymer. In the large core limit (“crew-cut” micelles, $N_A \gg N_B$) mean density models may be used. The volume fraction of B segments in the corona, ϕ_B , is assumed to be independent of the distance from the core and N_{agg} is predicted to be proportional to N_A ($\beta = 1$). If $N_B \gg N_A$ (star model which assumes a concentration profile for ϕ_B) $N_{\text{agg}} \approx N_A^{4/5}$.

Fig. 5.13 shows the variation of aggregation number N_{agg} and hydrodynamic radius R_{hyd} with the number of monomeric units of PLA, N_{PLA} . Fig. 5.14 shows log-log plots of N_{agg} versus N_{PLA} . For comparison, results for N_{agg} of PLA : PEG with a lower molecular weight PEG, namely 1800, are shown in the same figure. For copolymers with relatively low PLA to PEG weight ratio (2 : 5–6 : 5), there is a sharp increase in the micellar aggregation number as the molar mass of PLA is increased. This trend can be rationalized in terms of the thermodynamics of micelle formation as discussed below.

Tab. 5.3: Molar mass and aggregation numbers of PLA–PEG micellar-like nanoparticles.

PLA–PEG ^a	N_{PLA}	$R_{\text{hyd}}^{\text{b}}$ (nm)	$\overline{M}_{\text{w,mic}}$ (Da)	N_{agg}	$S_{\text{t}}/N_{\text{agg}}$ (nm ²)
2 : 5	28	13.0	2.01×10^5	29	73
3 : 5	42	14.1	3.13×10^5	39	64
4 : 5	56	17.5	7.02×10^5	78	49
6 : 5	83	20.6	1.99×10^6	180	30
9 : 5	125	23.4	2.85×10^6	203	34
15 : 5	208	25.3	5.57×10^6	278	29
30 : 5	417	31.9	1.31×10^7	375	34
45 : 5 (2 mg ml ⁻¹)	625	30.3	1.19×10^7	238	49
45 : 5 (10 mg ml ⁻¹)	625	40.4	3.37×10^7	674	30
45 : 5 (20 mg ml ⁻¹)	625	48.0	5.67×10^7	1134	26

a All prepared using 10 mg ml⁻¹ solutions of PLA–PEG in acetone unless otherwise stated.

b Results from PCS measurements.

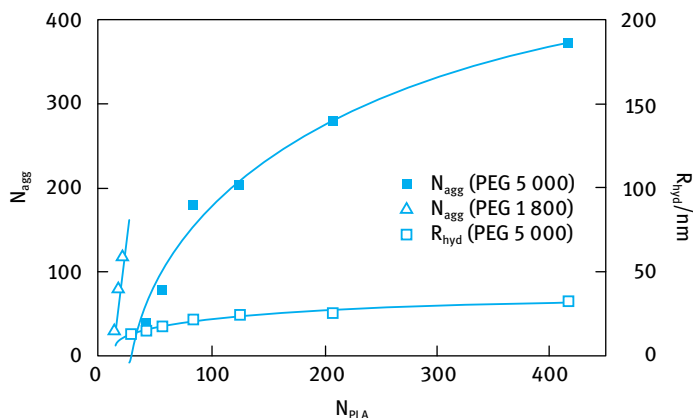


Fig. 5.13: Variation of aggregation number and hydrodynamic radius of PLA–PEG micellar-like nanoparticles with number of monomeric units of PLA.

In a selective solvent, where the block of the copolymer B is in a good solvent (PEO, $\chi_{\text{BS}} < 0.5$) but the other segments of A are in a worse than θ -solvent (PLA, $\chi_{\text{AS}} > 0.5$) there will be strong attraction between the A segments. These attractive hydrophobic interactions (enthalpic) must overcome the repulsive (entropic) forces between B chains in the corona. PLA–PEG copolymers with very low PLA to PEG ratios (e.g. 400 : 1800) do not form micelles in aqueous media. The PLA–PEG 2 : 5 copolymer has the shortest PLA block and although the block copolymer is water soluble with least number of unfavourable interactions between the lactic acid units and the aqueous solvent, yet it still spontaneously forms micellar structures. Since the interactions

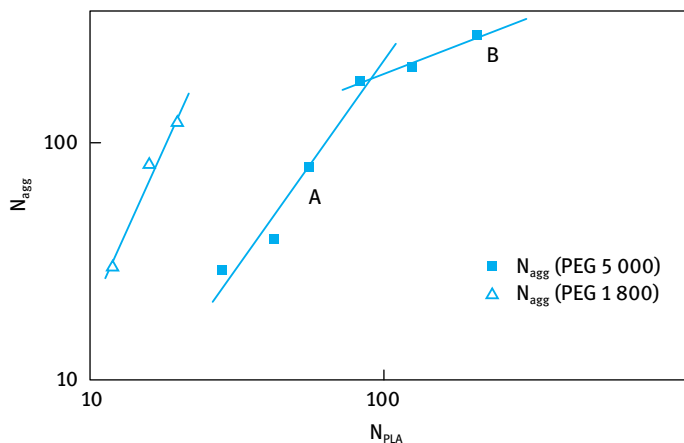


Fig. 5.14: Log-log plots of N_{agg} versus N_{PLA} .

between the low molecular weight PLA chains within the core of the micelle are weak, the 2 : 5 PLA : PEG copolymers form loosely packed micellar assemblies with a lot of free space (solvent) within the corona region. This can be demonstrated by calculating the surface area per copolymer unit (S_t/N_{agg}) at the outer surface of the micelle.

A schematic picture of the PLA : PEG micelle is shown in Fig. 5.15. The external surface area of the 2 : 5 micelle ($4\pi R_{hyd}^2$) is 2124 nm^2 and its aggregation number is 29. The area per PEG block in the micelle is $(2124/29) = 73 \text{ nm}^2$. This area may be compared with the cross-sectional area of a PEG chain of molar mass of 5 kDa in a good solvent. The radius of gyration R_g of PEG is related to its molar mass by [4],

$$R_g = 0.0215M_w^{0.583}. \quad (5.3)$$

This gives an R_g of 3.1 nm, which in free solution occupies a sphere with maximum cross-sectional area (πR_g^2) of 30 nm^2 . This clearly shows the high area per block copolymer (73 nm^2) in the 2 : 5 PLA : PEG micelle. The loosely packed nature of the micellar-like nanoparticles can be confirmed by ^1H NMR studies on nanoparticles in D_2O .

Increasing the length of the hydrophobic PLA block from 2 to 6 kDa increases the number of unfavourable interactions between the lactic acid units of the PLA chains and the aqueous media. This makes the copolymer water-insoluble and it is forced to assemble into nanoparticles by precipitation into water from a water miscible solvent (e.g. acetone). The number of attractive hydrophobic interactions between the lactic acid units of the associating PLA chains increases with increasing length of the chain. This results in an increased packing density of the PLA–PEG subunits and a sharp increase in the micellar aggregation number, as illustrated in Fig. 5.16. The surface area per copolymer unit at the outer surface of the micelle (S_t/N_{agg}) falls rapidly as the molar mass of the PLA block is increased from 2 to 6 kDa (Tab. 5.3). (S_t/N_{agg}) appears to tend towards a value that is consistent with the maximum cross-sectional area of a

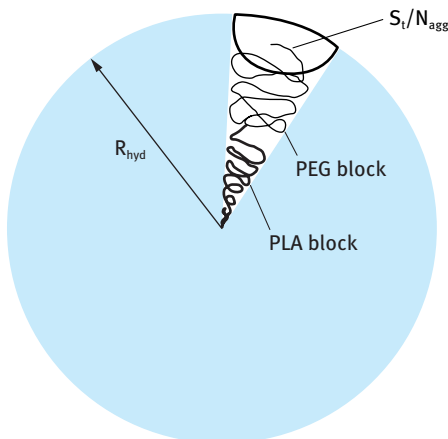


Fig. 5.15: Schematic representation of PLA-PEG micellar-like nanoparticles.

PEG 5 kDa in solution ($\approx 30 \text{ nm}^2$). The increasing aggregation number and decreasing surface curvature results in a decrease in the conical volume available to each of the coronal PEG chain [4].

The log-log plots of $N_{\text{agg}} - N_{\text{PLA}}$ shown in Fig. 5.14 give the following scaling relationship [4],

$$N_{\text{agg}} \approx N_{\text{PLA}}^{1.74}. \quad (5.4)$$

The scaling exponent (1.74) is larger than that predicted theoretically for both “crew-cut” and “star” models. This points to a third class of block copolymer micelles, characterized by blocks of different chemical composition or polarity (strongly aggregated). This class predicts an N_A^2 dependency of the micellar aggregation number.

If the micelle core is strongly segregated, then the area and volume of the core are given by,

$$4\pi R_c^2 = N_{\text{agg}} D^2, \quad (5.5)$$

$$\frac{4}{3}\pi R_c^3 = \frac{N_{\text{agg}} N_A}{\rho_{\text{bulk}}}, \quad (5.6)$$

$$N_{\text{agg}} = \frac{36\pi N_A^2}{D^6 \rho_{\text{bulk}}}, \quad (5.7)$$

where R_c is the core radius, D^2 is the interfacial area per chain and ρ_{bulk} is the mass density of the core.

The particle size of nanoparticles produced from the PLA-PEG 45 : 5 copolymer depends on the concentration of the polymer dissolved in acetone [4]. Fig. 5.16 shows the variation of the aggregation number and hydrodynamic radius with copolymer concentration. Increasing the concentration of the acetonic copolymer solution increases the local concentration of PLA-PEG units available to aggregate at any particle formation site, following precipitation into water. A significant increase in the aggregation number from 238 to 674 occurs when the copolymer concentration is increased from 2

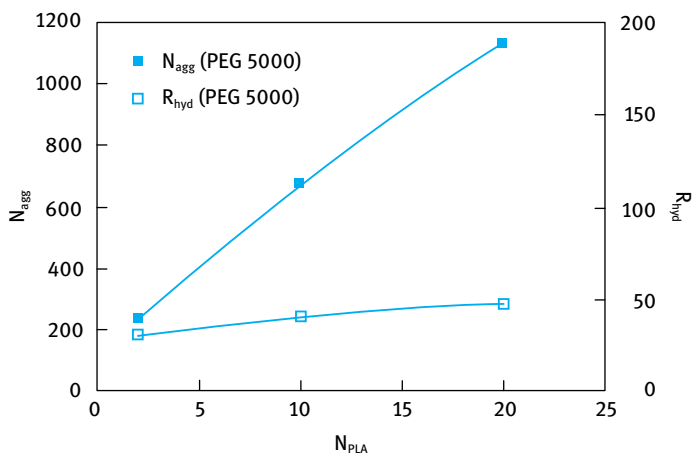


Fig. 5.16: Variation of aggregation number and hydrodynamic radius of PLA–PEG 45 : 5 nanoparticles with block copolymer concentration in the organic phase.

to 10 mg ml^{-1} . At 2 mg ml^{-1} small nanoparticles are produced with a high surface area (S_t/N_{agg}) per PEG block at the outer boundary of the micelle of 49 nm^2 that is similar to that of the smaller PLA–PEG 2 : 5–4 : 5 copolymers. These smaller PLA–PEG 45 : 5 nanoparticles have a loosely packed structure with a lot of solvent in the corona region. The particle radius of these 45 : 5 nanoparticles (30.3 nm) is considerably greater than that of those produced by the smaller 2 : 5 PLA–PEG block copolymer (13 nm). The largest PLA–PEG 45 : 5 nanoparticles have a low (S_t/N_{agg}) (26 nm^2) comparable to that of the PLA–PEG 6 : 5 micellar-like nanoparticles (30 nm^2). This implies that the largest PLA–PEG 45 : 5 nanoparticles have a high PEG surface coverage, which gives them high colloid stability.

The main objective of using PLA–PEG nanoparticles for drug delivery is to have long-circulating particulate carriers and minimize opsonization by means of high coverage of brush-like PEG chains. On the basis of this rationale, copolymers with an intermediate PLA to PEG ratio (e.g. PLA–PEG 15 : 5) would appear to form assemblies with optimal protein-resistant surface properties [4].

To test the above hypothesis, PLA and PLA–PEG nanoparticles were radiolabelled for in vivo studies by incorporation of the hydrophobic gamma-emitter, ^{111}In -oxine (8-hydroxy quinoline). In vitro studies showed that ^{111}In -oxine is released from PLA and PLA–PEG nanoparticles on incubation with rat serum [4].

For each PLA/PLA–PEG system, a group of three male Wistar rats ($150 \pm 10 \text{ g}$) was injected intravenously via the lateral tail vein with 0.3 ml (equivalent to 1 mg of solid material) of the nanoparticle dispersion. A group of control rats was injected with 10 kBq of unincorporated (free) ^{111}In -oxine. Blood samples of $20 \mu\text{l}$ were taken from the contralateral tail vein at various time intervals after administration ($5, 15, 30, 60, 120$ and 180 minutes). The animals were sacrificed after three hours by intravenous in-

jection of phenobarbitone solution, and the liver, spleen lungs and kidneys removed. The organ- and blood-associated activity was counted using a gamma counter. The carcass-associated radioactivity was determined using a well counter. A total blood volume of 75 % of the body weight was assumed. The results for the blood- and organ-associated activity are expressed as a percentage of the injected dose and are mean values for the three rats \pm standard deviation. The data for the lung and kidney are not presented, since the radioactivity associated with these organs was negligible (less than 1 % of the administered dose).

The results for the blood circulation and organ distribution showed some interesting trends [4]. The PLA nanoparticles (uncoated with PEG) were rapidly cleared from the blood circulation, with only 13 % of the injected dose still circulating after 5 minutes. After 3 hours, 70 % of the i.v. administered nanoparticles had been removed by the liver. This is attributed to rapid opsonization of the particle surface and subsequent phagocytosis by the Kupffer cells of the liver. The smallest of the PLA-PEG nanoparticles studied *in vivo* (PLA-PEG 6 : 5, \approx 40 nm in diameter) was cleared from the circulation, with a high percentage of the radioactivity (\approx 70 %) having accumulated in the liver three hours after the i.v. injection. However, the blood clearance rate was significantly slower than that found for the PLA nanoparticles. An increase in the length of the PLA block produced larger particles which exhibited prolonged circulation times and a reduced liver uptake. For example, in the case of PLA-PEG 110 : 5 nanoparticles (\approx 160 nm), 43 % of the injected dose still remained in the systemic circulation after 3 hours, whilst only 23 % of the injected dose accumulated in the liver. Despite avoiding recognition by the Kupffer cells of the liver, 11 % of the injected dose of the PLA-PEG 110 : 5 nanoparticles was found to accumulate in the spleen.

The prolonged circulation times and reduced deposition of the larger PLA-PEG nanoparticles are surprising in view of the low PEG surface coverage of these systems, which are actually stabilized by the presence of adsorbed serum components. It appears that such low PEG coverage is sufficient for restricting the adsorption of the high molecular weight opsonins. The layer thickness of terminally attached PEG chain with a molecular weight of 5 kDa is approximately 6.2 nm, which may adequately prohibit the adhesion of phagocytic cells.

It is surprising that the smaller micellar-like assemblies prepared from PLA-PEG copolymers with a low molecular weight PLA block were fairly rapidly cleared from the circulation and accumulated in the liver. These nanoparticles are the most colloidally stable of the PLA-PEG assemblies studied and hence the notion that effective steric stabilization is the most crucial effect for achieving blood circulation longevity is now questionable. It appears likely that the short circulation lifetime of the small PLA-PEG micelle-like nanoparticles is partly due to their ability to penetrate deep into the interstitial space of the liver [4].

It seems from the above discussion that the circulatory lifetime of PLA-PEG nanoparticles *in vivo* does not correlate with their colloid stability *in vitro*. It seems that the particle size of the PLA assembly is crucial in determining its biological fate.

The presence of even a low surface coverage of hydrated PEG chains is sufficient to enable relatively large (> 100 nm) PLA–PEG particles to remain in systemic circulation. Regardless of the characteristics of the PEG layer, small nanoparticles (≈ 40 nm) are cleared by the liver to a higher degree, with their small size possibly permitting access to all cell types [4].

References

- [1] Mills SN, Davis SS. Controlled drug delivery. In: Illum L, Davis SS, editors. *Polymers in controlled drug delivery*. Bristol: IOP Publishing; 1987. p. 1–14.
- [2] Krueter J. *Colloidal drug delivery systems*. New York: Marcel Dekker; 1994.
- [3] Muller RH. *Colloidal carriers for controlled drug delivery: Modification, characterisation and in vivo distribution*. Stuttgart: Wiss. Verl-Ges.; 1990.
- [4] Riley T. PhD thesis. Nottingham University; 1999.
- [5] Krueter J. Nanoparticle based drug delivery systems. *J Control Rel.* 1991;16:169–176.
- [6] Illum L, Davis SS. The organ uptake of intravenously administered colloidal particles can be altered using a non-ionic surfactant (poloxamer 338). *FEBS Lett.* 1984;167:72–82.
- [7] Muir IS, Moghimi SM, Illum L, Davis SS, Davies MC. The effect of block copolymer on the uptake of model polystyrene microspheres by Kupfer cells – in vitro and in vivo studies. *Biochem Soc Trans.* 1991;19:329S.
- [8] Illum L, Davis SS, Muller RH, Mak E, West P. The organ distribution and circulation life-time of intravenously injected colloidal carriers stabilized with a block copolymer poloxamine 908. *Life Sci.* 1987;40:367–374.
- [9] Chasin M, Langer R, editors. *Biodegradable polymers as drug delivery systems*. New York: Marcel Dekker; 1990.
- [10] Stolnik S, Dunn SE, Davies MC, Coombes AGA, Taylor DC, Irving MP, Purkiss SC, Tadros TF, Davis SS, Illum L. Surface modification of poly(lactide-co-glycolide) nanospheres by biodegradable poly(lactide)-poly(ethylene glycol) copolymers. *Pharm Res.* 1994;11:1800–1808.
- [11] Kwon GS, Kataoka K. Block copolymer micelles as long circulating drug vehicles. *Advan Drug Del Rev.* 1995;16:295–309.
- [12] de Gennes PG. *Scaling concepts of polymer physics*. Ithaca: Cornell University Press; 1979.
- [13] Napper DH. *Polymeric stabilisation of colloidal dispersions*. London: Academic Press; 1983.
- [14] Fleer GJ, Cohen-Stuart MA, Scheutjens JM, Cosgrove T, Vincent B. *Polymers at interfaces*. London: Chapman and Hall; 1993.
- [15] Jeon SI, Lee JH, Andrade JD, de Gennes PG. Protein surface interaction in the presence of polyethylene oxide. I. Simplified theory. *J Colloid Interface Sci.* 1991;142:149–158.
- [16] Jeon SI, Andrade JD. Protein surface interaction in the presence of polyethylene oxide. *J Colloid Interface Sci.* 1991;142:159–166.

Part II: Colloid and interface science in cosmetics and personal care

6 Surfactants used in cosmetic and personal care formulations, their properties and surfactant–polymer interaction

6.1 Surfactant classes

Surfactants used in cosmetic formulations must be completely free of allergens, sensitizers and irritants. To minimize medical risks, cosmetic formulators tend to use polymeric surfactants which are less likely to penetrate beyond the stratum corneum and hence they are less likely to cause any damage.

Conventional surfactants of the anionic, cationic, amphoteric and nonionic types are used in cosmetic systems [1–3]. Besides the synthetic surfactants that are used in the preparation of cosmetic systems such as emulsions, creams, suspensions, etc., several other naturally occurring materials have been introduced and there is a trend in recent years to use such natural products more widely, in the belief that they are safer for application. As mentioned above, polymeric surfactants of the A–B, A–B–A and BA_n are also used in many cosmetic formulations. Several synthetic surfactants that are applied in cosmetics may be listed as shown below.

Anionic surfactants are widely used in many cosmetic formulations. The hydrophobic chain is a linear alkyl group with a chain length in the region of 12–16 C atoms and the polar head group should be at the end of the chain. Linear chains are preferred since they are more effective and more degradable than the branched chains. The most commonly used hydrophilic groups are carboxylates, sulphates, sulphonates and phosphates. A general formula may be ascribed to anionic surfactants as follows:

- Carboxylates: $C_nH_{2n+1}COO^-X^+$
- Sulphates: $C_nH_{2n+1}OSO_3^-X^+$
- Sulphonates: $C_nH_{2n+1}SO_3^-X^+$
- Phosphates: $C_nH_{2n+1}OPO(OH)O^-X^+$

with n being the range 8–16 atoms and the counterion X^+ is usually Na^+ .

Several other anionic surfactants are commercially available such as sulphosuccinates, isethionates (esters of isothionic acid with the general formula $R'COOCH_2-CH_2-SO_3Na$) and taurates (derivatives of methyl taurine with the general formula $R'CON(R'')CH_2-CH_2-SO_3Na$), sarchosinates (with the general formula $R'CON(R'')COONa$) and these are sometimes used for special applications.

The carboxylates are perhaps the earliest known surfactants, since they constitute the earliest soaps, e.g. sodium or potassium stearate, $C_{17}H_{35}COONa$, sodium myristate, $C_{14}H_{29}COONa$. The alkyl group may contain unsaturated portions, e.g. sodium oleate, which contains one double bond in the C_{17} alkyl chain. Most commercial soaps will be a mixture of fatty acids obtained from tallow, coconut oil, palm oil, etc. They are simply

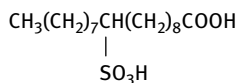
prepared by saponification of the triglycerides of the oils and fats. The main attraction of these simple soaps is their low cost, their ready biodegradability and low toxicity. Their main disadvantage is their ready precipitation in water containing bivalent ions such as Ca^{2+} and Mg^{2+} . To avoid their precipitation in hard water, the carboxylates are modified by introducing some hydrophilic chains, e.g. ethoxy carboxylates with the general structure $\text{RO}(\text{CH}_2\text{CH}_2\text{O})_n\text{CH}_2\text{COO}^-$, ester carboxylates containing hydroxyl or multi-COOH groups, sarcosinates which contain an amide group with the general structure $\text{RCON}(\text{R}')\text{COO}^-$. The addition of the ethoxylated group results in increased water solubility and enhanced chemical stability (no hydrolysis). The modified ether carboxylates are also more compatible with electrolytes. They are also compatible with other nonionic, amphoteric and sometimes even cationic surfactants. The ester carboxylates are very soluble in water, but they suffer from the problem of hydrolysis. The sarcosinates are not very soluble in acid or neutral solutions but they are quite soluble in alkaline media. They are compatible with other anionics, nonionics and cationics. The phosphate esters have very interesting properties being intermediate between ethoxylated nonionics and sulphated derivatives. They have good compatibility with inorganic builders and they can be good emulsifiers.

The sulphates are the largest and most important class of synthetic surfactants, which are produced by reaction of an alcohol with sulphuric acid, i.e. they are esters of sulphuric acid. In practice, sulphuric acid is seldom used and chlorosulphonic or sulphur dioxide/air mixtures are the most common methods of sulphating the alcohol. The properties of sulphate surfactants depend on the nature of the alkyl chain and the sulphate group. The alkali metal salts show good solubility in water, but they tend to be affected by the presence of electrolytes. The most common sulphate surfactant is sodium dodecyl sulphate (abbreviated as SDS and sometimes referred to as sodium lauryl sulphate) which is extensively used in many cosmetic formulations. At room temperature ($\approx 25^\circ\text{C}$) this surfactant is quite soluble and 30 % aqueous solutions are fairly fluid (low viscosity). However, below 25°C , the surfactant may separate out as a soft paste as the temperature falls below its Krafft point (the temperature above which the surfactant shows a rapid increase in solubility with a further increase in temperature). The latter depends on the distribution of chain lengths in the alkyl chain, the wider the distribution the lower the Krafft temperature. Thus, by controlling this distribution one may achieve a Krafft temperature of $\approx 10^\circ\text{C}$. As the surfactant concentration is increased to 30–40 % (depending on the distribution of chain lengths in the alkyl group), the viscosity of the solution increases very rapidly and may produce a gel, but then falls at about 60–70 % to give a pourable liquid, after which it increases again to a gel. The concentration at which the minimum occurs varies according to the alcohol sulphate used, and also the presence of impurities such as unsaturated alcohol. The viscosity of the aqueous solutions can be reduced by addition of short chain alcohols and glycols. The critical micelle concentration (cmc) of SDS (the concentration above which the properties of the solution show abrupt changes, see below) is

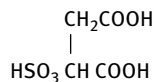
$8 \times 10^{-3} \text{ mol dm}^{-3}$ (0.24 %). The alkyl sulphates give good foaming properties with an optimum at C_{12} – C_{14} .

As with the carboxylates, the sulphate surfactants are also chemically modified to change their properties. The most common modification is to introduce some ethylene oxide units in the chain, usually referred to as alcohol ether sulphates that are commonly used in shampoos. These are made by sulphation of ethoxylated alcohols. For example, sodium dodecyl 3-mole ether sulphate, which is essentially dodecyl alcohol reacted with 3 mol EO, is sulphated and neutralized by NaOH. The presence of PEO confers improved solubility when compared with the straight alcohol sulphates. In addition, the surfactant becomes more compatible with electrolytes in aqueous solution. The ether sulphates are also more chemically stable than the alcohol sulphates. The cmc of the ether sulphates is also lower than the corresponding surfactant without the EO units. The viscosity behaviour of aqueous solutions is similar to that of alcohol sulphates, giving gels in the range 30–60 %. The ether sulphates show a pronounced salt effect, with a significant increase in viscosity of a dilute solution on addition of electrolytes such as NaCl. The ether sulphates are commonly used in hand dish-washing liquids and in shampoos in combination with amphoteric surfactants.

With sulphonates, the sulphur atom is directly attached to the carbon atom of the alkyl group and this gives the molecule stability against hydrolysis, when compared with the sulphates (where the sulphur atom is indirectly linked to the carbon of the hydrophobe via an oxygen atom). As with the sulphates, some chemical modification is obtained by introducing ethylene oxide units. These surfactants have excellent water solubility and biodegradability. They are also compatible with many aqueous ions. Another class of sulphonates is the α -olefin sulphonates which are prepared by reacting linear α -olefin with sulphur trioxide, typically yielding a mixture of alkene sulphonates (60-70 %), 3- and 4-hydroxyalkane sulphonates (\approx 30 %) and some disulphonates and other species. The two main α -olefin fractions used as starting material are C_{12} – C_{16} and C_{16} – C_{18} . Fatty acid and ester sulphonates are produced by sulphonation of unsaturated fatty acids or esters. A good example is sulphonated oleic acid,



A special class of sulphonates are sulphosuccinates which are esters of sulphosuccinic acid,



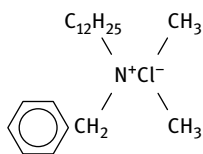
Both mono- and diesters are produced. A widely used diester in many formulations is sodium di(2-ethylhexyl)sulphosuccinate (that is sold commercially under the trade name Aerosol OT). The cmc of the diesters is very low, in the region of 0.06 % for C₆–C₈ sodium salts and they give a minimum surface tension of 26 mN m⁻¹ for the C₈ diester. Thus these molecules are excellent wetting agents. The diesters are soluble both in water and in many organic solvents. They are particularly useful for the preparation of water-in-oil (W/O) microemulsions.

Isethionates are esters of isethionic acid HOCH₂CH₂SO₃H. They are prepared by reaction of acid chloride (of the fatty acid) with sodium isethionate. The sodium salt of C₁₂–C₁₄ are soluble at high temperature (70 °C) but they have very low solubility (0.01 %) at 25 °C. They are compatible with aqueous ions and hence they can reduce the formation of scum in hard water. They are stable at pH 6–8 but they undergo hydrolysis outside this range. They also have good foaming properties.

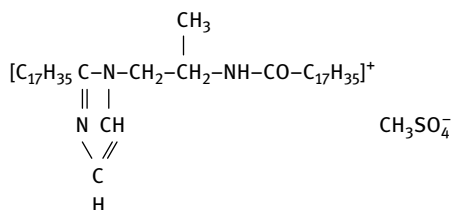
Taurates are derivatives of methyl taurine CH₂–NH–CH₂–CH₂–SO₃. The latter is made by reaction of sodium isethionate with methyl amine. The taurates are prepared by the reaction of fatty acid chloride with methyl taurine. Unlike the isethionates, the taurates are not sensitive to low pH. They have good foaming properties and they are good wetting agents.

Phosphate-containing anionic surfactants are also used in many cosmetic formulations. Both alkyl phosphates and alkyl ether phosphates are made by treating the fatty alcohol or alcohol ethoxylates with a phosphorylating agent, usually phosphorous pentoxide, P₄O₁₀. The reaction yields a mixture of mono- and diesters of phosphoric acid. The ratio of the two esters is determined by the ratio of the reactants and the amount of water present in the reaction mixture. The physicochemical properties of the alkyl phosphate surfactants depend on the ratio of the esters. They have properties intermediate between ethoxylated nonionics (see below) and the sulphated derivatives. They have good compatibility with inorganic builders and good emulsifying properties.

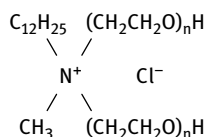
The most common cationic surfactants are the quaternary ammonium compounds with the general formula R'R''R'''R''''N + X⁻, where X⁻ is usually a chloride ion and R represents alkyl groups. These quaternaries are made by reacting an appropriate tertiary amine with an organic halide or organic sulphate. A common class of cationics is alkyl trimethyl ammonium chloride, where R contains 8–18 C atoms, e.g. dodecyl trimethyl ammonium chloride, C₁₂H₂₅(CH₃)₃NCl. Another widely used cationic surfactant class is that containing two long chain alkyl groups, i.e. dialkyl dimethyl ammonium chloride, with the alkyl groups having a chain length of 8–18 C atoms. These dialkyl surfactants are less soluble in water than the monoalkyl quaternary compounds, but they are sometimes used as hair conditioners. A widely used cationic surfactant is alkyl dimethyl benzyl ammonium chloride (sometimes referred to as benzalkonium chloride and widely used as bactericide), having the structure,



Imidazolines can also form quaternaries, the most common product being the ditallow derivative quaternized with dimethyl sulphate,



Cationic surfactants can also be modified by incorporating polyethylene oxide chains, e.g. dodecyl methyl polyethylene oxide ammonium chloride having the structure,



Cationic surfactants are generally water soluble when there is only one long alkyl group. When there are two or more long chain hydrophobes, the product becomes dispersible in water and soluble in organic solvents. They are generally compatible with most inorganic ions and hard water, but they are incompatible with metasilicates and highly condensed phosphates. They are also incompatible with protein-like materials. Cationics are generally stable to pH changes, both acid and alkaline. They are incompatible with most anionic surfactants, but they are compatible with nonionics. These cationic surfactants are insoluble in hydrocarbon oils. In contrast, cationics with two or more long alkyl chains are soluble in hydrocarbon solvents, but they become only dispersible in water (sometimes forming bilayer vesicle type structures). They are generally chemically stable and can tolerate electrolytes. The cmc of cationic surfactants is close to that of anionics with the same alkyl chain length. For example, the cmc of benzalkonium chloride is 0.17 %. The prime use of cationic surfactants is their tendency to adsorb at negatively charged surfaces, e.g. hair, and they can be applied as hair conditioners.

Amphoteric (zwitterionic) surfactants are those containing both cationic and anionic groups. The most common amphoteric are the N-alkyl betaines which are derivatives of trimethyl glycine $(\text{CH}_3)_3\text{NCH}_2\text{COOH}$ (that was described as betaine). An example of betaine surfactant is lauryl amido propyl dimethyl betaine

$C_{12}H_{25}CON(CH_3)_2CH_2COOH$. These alkyl betaines are sometimes described as alkyl dimethyl glycinates. The main characteristic of amphoteric surfactants is their dependency on the pH of the solution in which they are dissolved. In acid pH solutions, the molecule acquires a positive charge and it behaves like a cationic, whereas in alkaline pH solutions, they become negatively charged and behave like an anionic. A specific pH can be defined at which both ionic groups show equal ionization (the isoelectric point of the molecule). This can be described by the following scheme,



Amphoteric surfactants are sometimes referred to as zwitterionic molecules. They are soluble in water, but the solubility shows a minimum at the isoelectric point. Amphoterics show excellent compatibility with other surfactants, forming mixed micelles. They are chemically stable both in acids and alkalis. The surface activity of amphoterics varies widely and it depends on the distance between the charged groups, showing a maximum at the isoelectric point.

Another class of amphoterics are the N-alkyl amino propionates having the structure $R-NHCH_2CH_2COOH$. The NH group is reactive and can react with another acid molecule (e.g. acrylic) to form an amino dipropionate $R-N(CH_2CH_2COOH)_2$. Alkyl imidazoline-based product can also be produced by reacting alkyl imidazoline with a chloro acid. However, the imidazoline ring breaks down during the formation of the amphoteric.

The change in charge with pH of amphoteric surfactants affects their properties, such as wetting, foaming, etc. At the isoelectric point (IEP), the properties of amphoterics resemble those of nonionics very closely. Below and above the IEP, the properties shift towards those of cationic and anionic surfactants respectively. Zwitterionic surfactants have excellent dermatological properties. They also exhibit low eye irritation and they are frequently used in shampoos and other personal care products (cosmetics). Due to their mild characteristics, i.e. low eye and skin irritation, amphoterics are widely used in shampoos. They also provide antistatic properties to hair, good conditioning and boost foam.

The most common nonionic surfactants are those based on ethylene oxide, referred to as ethoxylated surfactants. Several classes can be distinguished: alcohol ethoxylates, fatty acid ethoxylates, monoalkaolamide ethoxylates, sorbitan ester ethoxylates, fatty amine ethoxylates and ethylene oxide-propylene oxide copolymers (sometimes referred to as polymeric surfactants). Another important class of nonionics are the multihydroxy products such as glycol esters, glycerol (and polyglycerol) esters, glucosides (and polyglucosides) and sucrose esters. Amine oxides and sulphinyl surfactants represent nonionics with a small head group.

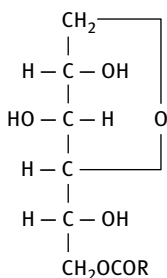
The alcohol ethoxylates are generally produced by ethoxylation of a fatty chain alcohol such as dodecanol. Several generic names are given to this class of surfactants

such as ethoxylated fatty alcohols, alkyl polyoxyethylene glycol, monoalkyl polyethylene oxide glycol ethers, etc. A typical example is dodecyl hexaoxyethylene glycol monoether with the chemical formula $C_{12}H_{25}(OCH_2CH_2O)_6OH$ (sometimes abbreviated as $C_{12}E_6$). In practice, the starting alcohol will have a distribution of alkyl chain lengths and the resulting ethoxylate will have a distribution of ethylene oxide (EO) chain lengths. Thus the numbers listed in the literature refer to average numbers.

The cmc of nonionic surfactants is about two orders of magnitude lower than that of the corresponding anionics with the same alkyl chain length. At a given alkyl chain length, the cmc decreases with decreasing number of EO units. The solubility of the alcohol ethoxylates depends both on the alkyl chain length and the number of ethylene oxide units in the molecule. Molecules with an average alkyl chain length of 12 C atoms and containing more than 5 EO units are usually soluble in water at room temperature. However, as the temperature of the solution is gradually raised, the solution becomes cloudy (as a result of dehydration of the PEO chain and the change in the conformation of the PEO chain) and the temperature at which this occurs is referred to as the cloud point (CP) of the surfactant. At a given alkyl chain length, the CP increases with increasing the EO chain of the molecule. The CP changes with a change in concentration of the surfactant solution and the trade literature usually quotes the CP of a 1% solution. The CP is also affected by the presence of electrolyte in the aqueous solution. Most electrolytes lower the CP of a nonionic surfactant solution. Nonionics tend to have maximum surface activity near to the cloud point. The CP of most nonionics increases markedly on addition of small quantities of anionic surfactants. The surface tension of alcohol ethoxylate solutions decreases with increasing its concentration, until it reaches its cmc, after which it remains constant with any further increase in its concentration. The minimum surface tension reached at and above the cmc decreases with decreasing number of EO units of the chain (at a given alkyl chain). The viscosity of a nonionic surfactant solution increases gradually with increasing its concentration, but at a critical concentration (which depends on the alkyl and EO chain lengths) its viscosity shows a rapid increase and ultimately a gel-like structure appears. This results from the formation of liquid crystalline structures of the hexagonal type. In many cases, the viscosity reaches a maximum after which it shows a decrease due to the formation of other structures (e.g. lamellar phases) (see below).

The fatty acid ethoxylates are produced by reaction of ethylene oxide with a fatty acid or a polyglycol and they have the general formula $RCOO-(CH_2CH_2O)_nH$. When a polyglycol is used, a mixture of mono- and diesters $RCOO-(CH_2CH_2O)_n-OCOR$ is produced. These surfactants are generally soluble in water provided there are enough EO units and the alkyl chain length of the acid is not too long. The mono-esters are much more soluble in water than the diesters. In the latter, a longer EO chain is required to render the molecule soluble. The surfactants are compatible with aqueous ions, provided there is not much unreacted acid. However, these surfactants undergo hydrolysis in highly alkaline solutions.

The sorbitan esters and their ethoxylated derivatives (Spans and Tweens) are perhaps one of the most commonly used nonionics. The sorbitan esters are produced by reaction of sorbitol with a fatty acid at a high temperature (> 200 °C). The sorbitol dehydrates to 1,4-sorbitan and then esterification takes place. If one mole of fatty acid is reacted with one mole of sorbitol, one obtains a mono-ester (some diester is also produced as a by-product). Thus, sorbitan mono-ester has the following general formula,



The free OH groups in the molecule can be esterified, producing di- and tri-esters. Several products are available depending on the nature of the alkyl group of the acid and whether the product is a mono-, di- or tri-ester. Some examples are given below,

- Sorbitan monolaurate – Span 20
- Sorbitan monopalmitate – Span 40
- Sorbitan monostearate – Span 60
- Sorbitan monooleate – Span 80
- Sorbitan tristearate – Span 65
- Sorbitan trioleate – Span 85

The ethoxylated derivatives of Spans (Tweens) are produced by reaction of ethylene oxide on any hydroxyl group remaining on the sorbitan ester group. Alternatively, the sorbitol is first ethoxylated and then esterified. However, the final product has different surfactant properties to the Tweens. Some examples of Tween surfactants are given below,

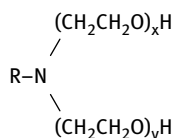
- Polyoxyethylene (20) sorbitan monolaurate – Tween 20
- Polyoxyethylene (20) sorbitan monopalmitate – Tween 40
- Polyoxyethylene (20) sorbitan monostearate – Tween 60
- Polyoxyethylene (20) sorbitan monooleate – Tween 80
- Polyoxyethylene (20) sorbitan tristearate – Tween 65
- Polyoxyethylene (20) sorbitan tri-oleate – Tween 85

The sorbitan esters are insoluble in water, but soluble in most organic solvents (low HLB number surfactants). The ethoxylated products are generally soluble in water

and they have relatively high HLB numbers. One of the main advantages of the sorbitan esters and their ethoxylated derivatives is their approval in cosmetics and some pharmaceutical preparations.

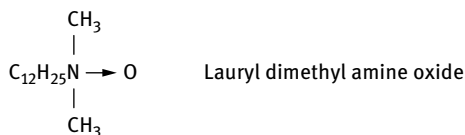
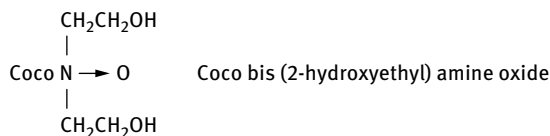
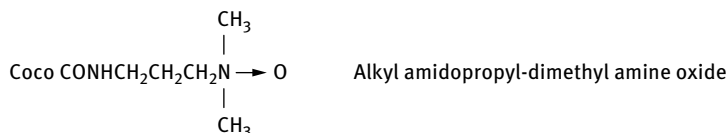
Ethoxylated fats and oils are also used in some cosmetic formulations, e.g. castor oil ethoxylates, which are good solubilizers for water-insoluble ingredients.

The amine ethoxylates are prepared by addition of ethylene oxide to primary or secondary fatty amines. With primary amines both hydrogen atoms on the amine group react with ethylene oxide and therefore the resulting surfactant has the structure,



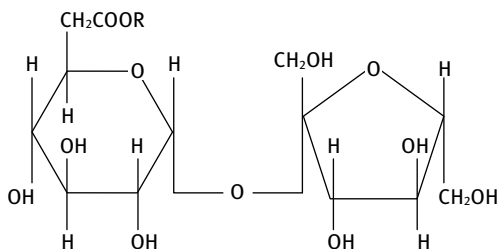
The above surfactants acquire a cationic character if the EO units are small in number and if the pH is low. However, at high EO levels and neutral pH they behave very similarly to nonionics. At low EO content, the surfactants are not soluble in water, but become soluble in an acid solution. At high pH, the amine ethoxylates are water-soluble provided the alkyl chain length of the compound is not long (usually a C₁₂ chain is adequate for reasonable solubility at sufficient EO content).

Amine oxides are prepared by oxidizing a tertiary nitrogen group with aqueous hydrogen peroxide at temperatures in the region 60–80 °C. Several examples can be quoted: N-alkyl amidopropyl-dimethyl amine oxide, N-alkyl bis(2-hydroxyethyl) amine oxide and N-alkyl dimethyl amine oxide. They have the general formula,



In acid solutions, the amino group is protonated and acts as a cationic surfactant. In neutral or alkaline solution the amine oxides are essentially nonionic in character. Alkyl dimethyl amine oxides are water soluble up to C16 alkyl chain. Above pH 9, amine oxides are compatible with most anionics. At pH 6.5 and below some anionics tend to interact and form precipitates. In combination with anionics, amine oxides can be foam boosters (e.g. in shampoos).

Several surfactants have been synthesized starting from mono- or oligosaccharides by reaction with the multifunctional hydroxyl groups: alkyl glucosides, alkyl polyglucosides, sugar fatty acid esters and sucrose esters, etc. The technical problem is one of joining a hydrophobic group to the multihydroxyl structure. Several surfactants have been made, e.g. esterification of sucrose with fatty acids or fatty glycerides to produce sucrose esters having the following structure,



The most interesting sugar surfactants are the alkyl polyglucosides (APG), which are synthesized using a two-stage transacetalization process. In the first stage, the carbohydrate reacts with a short chain alcohol, e.g. butanol or propylene glycol. In the second stage, the short chain alkyl glucoside is transacetalized with a relatively long chain alcohol (C₁₂₋₁₄-OH) to form the required alkyl polyglucoside. This process is applied if oligo- and polyglucoses (e.g. starch, syrups with a low dextrose equivalent, DE) are used. In a simplified transacetalization process, syrups with high glucose content (DE > 96 %) or solid glucose types can react with short-chain alcohols under normal pressure. Commercial alkyl polyglucosides (APG) are complex mixtures of species varying in the degree of polymerization (DP, usually in the range 1.1–3) and in the length of the alkyl chain. When the latter is shorter than C₁₄, the product is water soluble. The cmc values of APGs are comparable to nonionic surfactants and they decrease with increasing alkyl chain length.

APG surfactants have good solubility in water and they have high cloud points (> 100 °C). They are stable in neutral and alkaline solutions but are unstable in strong acid solutions. APG surfactants can tolerate high electrolyte concentrations and they are compatible with most types of surfactants. They are used in personal care products for cleansing formulations as well as for skincare and hair products.

An important naturally-occurring class of surfactants widely used in cosmetic formulations are the lipids, of which phosphatidylcholine (lecithin), lysolecithin, phosphatidylethanolamine and phosphatidylinositol are the most commonly used surfac-

tants. The structure of these lipids is given in Fig. 6.1. These lipids are used as emulsifiers as well as for producing liposomes or vesicles for skincare products. The lipids form coarse turbid dispersions of large aggregates (liposomes), which on ultrasonic irradiation form smaller units or vesicles. The liposomes are smectic mesophases of phospholipids organized into bilayers which assume a multilamellar or unilamellar structure. The multilamellar species are heterogeneous aggregates, most commonly prepared by dispersal of a thin film of phospholipid (alone or with cholesterol) into water. Sonication of the multilamellar units can produce the unilamellar liposomes, sometimes referred to as vesicles. The net charge of liposomes can be varied by incorporating a long chain amine, such as stearyl amine (to give a positively charged vesicle) or dicetyl phosphate (giving negatively charged species). Both lipid-soluble and water-soluble actives can be entrapped in liposomes. The liposoluble actives are solubilized in the hydrocarbon interiors of the lipid bilayers, whereas the water-soluble actives are intercalated in the aqueous layers.

The polymeric surfactants possess considerable advantages for use in cosmetic ingredients. The most commonly used materials are the A–B–A block copolymers, with A being poly(ethylene oxide) and B poly(propylene oxide) (Pluronic). On the whole, polymeric surfactants have much lower toxicity, sensitization and irritation

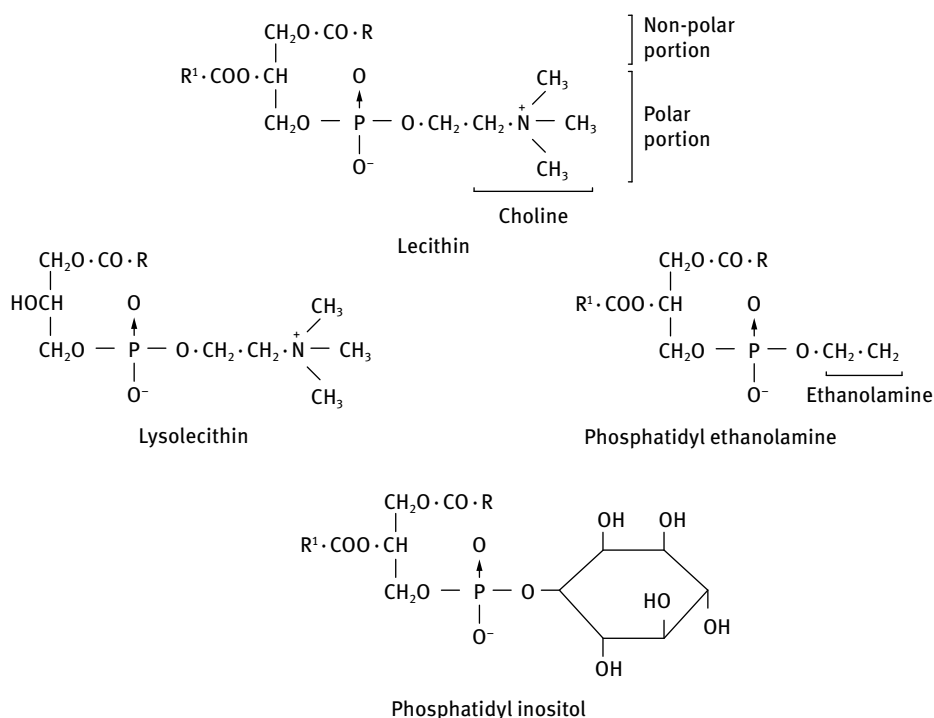


Fig. 6.1: Structure of lipids.

potentials, provided they are not contaminated with traces of the parent monomers. These molecules provide greater stability and in some cases they can be used to adjust the viscosity of the cosmetic formulation.

In recent years, there has been a great trend towards using silicone oils for many cosmetic formulations. In particular, volatile silicone oils have found application in many cosmetic products, owing to the pleasant dry sensation they impart to the skin. These volatile silicones evaporate without unpleasant cooling effects or without leaving a residue. Due to their low surface energy, silicone help spread the various active ingredients over the surface of hair and skin.

The chemical structure of the silicone compounds used in cosmetic preparations varies according to the application. As an illustration, Fig. 6.2 shows some typical structures of cyclic and linear silicones. The backbones can carry various attached “functional” groups, e.g. carboxyl, amine, sulfhydryl, etc. While most silicone oils can be emulsified using conventional hydrocarbon surfactants, there has been a trend in recent years to use silicone surfactants for producing the emulsion. Typical structures of siloxane-polyethylene oxide and siloxane polyethylene amine copolymers are shown in Fig. 6.2. The surface activity of these block copolymers depends on the relative length of the hydrophobic silicone backbone and the hydrophilic (e.g. PEO) chains. The attraction of using silicone oils and silicone copolymers is their relatively small medical and environmental hazards, when compared to their hydrocarbon counterparts.

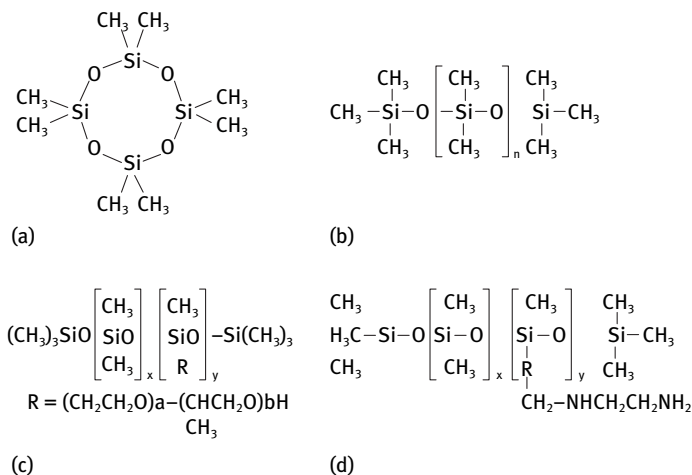


Fig. 6.2: Structural formulae of typical silicone compounds used in cosmetic formulations: (a) cyclic siloxane; (b) linear siloxane; (c) siloxane–polyethylene oxide copolymer; (d) siloxane–polyethylene amine copolymer.

6.2 Physical properties of surfactant solutions and the process of micellization

The physical properties of surface active agent solutions differ from those of non-amphiphatic molecule solutions (such as sugars) in one major aspect, namely the abrupt changes in their properties above a critical concentration [4]. This is illustrated in Fig. 6.3 which shows plots of several physical properties (osmotic pressure, surface tension, turbidity, solubilization, magnetic resonance, equivalent conductivity and self-diffusion) as a function of concentration for an anionic surfactant. At low concentrations, most properties are similar to those of a simple electrolyte. One notable exception is the surface tension, which decreases rapidly with increasing surfactant concentration. However, all the properties (interfacial and bulk) show an abrupt change at a particular concentration, which is consistent with the fact that at and above this concentration, surface active molecules or ions associate to form larger units. These associated units are called micelles (self-assembled structures) and the first formed aggregates are generally approximately spherical in shape. A schematic representation of a spherical micelle is given in Fig. 6.4.

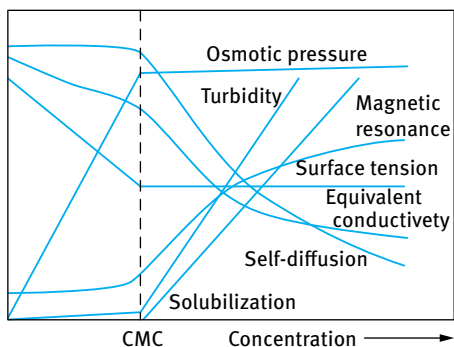


Fig. 6.3: Variation of solution properties with surfactant concentration.

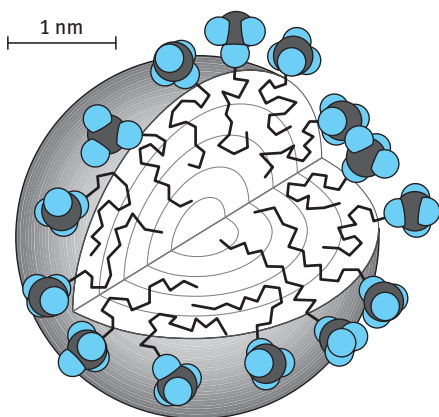


Fig. 6.4: Illustration of a spherical micelle for dodecyl sulphate [4].

The concentration at which this association phenomenon occurs is known as the critical micelle concentration (cmc). Each surfactant molecules has a characteristic cmc value at a given temperature and electrolyte concentration. The most common technique for measuring the cmc is surface tension, γ , which shows a break at the cmc, after which γ remains virtually constant with any further increase in concentration. However, other techniques such as self-diffusion measurements, NMR and fluorescence spectroscopy can be applied. A compilation of cmc values was given in 1971 by Mukerjee and Mysels [5], which is clearly not an up-to-date text, but is an extremely valuable reference. As an illustration, the cmc values of a number of surface active agents are given in Tab. 6.1, to show some of the general trends [1–3]. Within any class of surface active agent, the cmc decreases with increasing chain length of the hydrophobic portion (alkyl group). As a general rule, the cmc decreases by a factor of 2 for ionics (without added salt) and by a factor of 3 for nonionics on adding one methylene group to the alkyl chain. With nonionic surfactants, increasing the length of the hydrophilic group (polyethylene oxide) causes an increase in cmc.

Tab. 6.1: Critical micelle concentration of surfactant classes.

Surface active agent	cmc (mol dm ⁻³)
<i>(A) Anionic</i>	
Sodium octyl-l-sulphate	1.30×10^{-1}
Sodium decyl-l-sulphate	3.32×10^{-2}
Sodium dodecyl-l-sulphate	8.39×10^{-3}
Sodium tetradecyl-l-sulphate	2.05×10^{-3}
<i>(B) Cationic</i>	
Octyl trimethyl ammonium bromide	1.30×10^{-1}
Decetyl trimethyl ammonium bromide	6.46×10^{-2}
Dodecyl trimethyl ammonium bromide	1.56×10^{-2}
Hexactyltrimethyl ammonium bromide	9.20×10^{-4}
<i>(C) Nonionic</i>	
Octyl hexaoxyethylene glycol monoether C ₈ E ₆	9.80×10^{-3}
Decyl hexaoxyethylene glycol monoether C ₁₀ E ₆	9.00×10^{-4}
Decyl nonaoxyethylene glycol monoether C ₁₀ E ₉	1.30×10^{-3}
Dodecyl hexaoxyethylene glycol monoether C ₁₂ E ₆	8.70×10^{-5}
Octylphenyl hexaoxyethylene glycol monoether C ₈ E ₆	2.05×10^{-4}

In general, nonionic surfactants have lower cmc values than their corresponding ionic surfactants of the same alkyl chain length. Incorporating a phenyl group in the alkyl group increases its hydrophobicity to a much smaller extent than increasing its chain length with the same number of carbon atoms. The valency of the counterion in ionic surfactants has a significant effect on the cmc. For example, increasing the valency of the counterion from 1 to 2 causes a reduction of the cmc by roughly a factor of 4.

The cmc of anionic surfactants is, to a first approximation, independent of temperature. However, nonionic surfactants of the ethoxylate type show a monotonic decrease [1–3] in cmc with increasing temperature. The effect of addition of cosolutes, e.g. electrolytes and nonelectrolytes, on the cmc can be very striking. For example, addition of 1 : 1 electrolyte to a solution of anionic surfactant gives a dramatic lowering of the cmc, which may amount to one order of magnitude. The effect is moderate for short-chain surfactants, but is much larger for long-chain ones. At high electrolyte concentrations, the reduction in cmc with increasing number of carbon atoms in the alkyl chain is much stronger than without added electrolyte. This rate of decrease at high electrolyte concentrations is comparable to that of nonionics. The effect of added electrolyte also depends on the valency of the added counterions. In contrast, for nonionics, addition of electrolytes causes only small variation in the cmc.

Nonelectrolytes such as alcohols can also cause a decrease in the cmc [1–3]. The alcohols are less polar than water and are distributed between the bulk solution and the micelles. The more preference they have for the micelles, the more they stabilize them. A longer alkyl chain leads to a less favourable location in water and more favourable location in the micelles

The presence of micelles can account for many of the unusual properties of solutions of surface active agents. For example, it can account for the near constant surface tension value above the cmc (See Fig. 6.3). It also accounts for the reduction in molar conductance of the surface active agent solution above the cmc, which is consistent with the reduction in mobility of the micelles as a result of counterion association. The presence of micelles also accounts for the rapid increase in light scattering or turbidity above the cmc. The presence of micelles was originally suggested by McBain [6], who suggested that below the cmc most of the surfactant molecules are unassociated, whereas in the isotropic solutions immediately above the cmc, micelles and surfactant ions (molecules) are thought to co-exist, the concentration of the latter changing very slightly as more surfactant is dissolved. However, the self-association of an amphiphile occurs in a stepwise manner with one monomer added to the aggregate at a time. For a long chain amphiphile, the association is strongly cooperative up to a certain micelle size where counteracting factors became increasingly important. Typically, the micelles have a closely spherical shape in a rather wide concentration range above the cmc. Originally, it was suggested by Adam [7] and Hartley [8] that micelles are spherical in shape and have the following properties:

- (i) the association unit is spherical with a radius approximately equal to the length of the hydrocarbon chain;
- (ii) the micelle contains about 50–100 monomeric units; aggregation number generally increases with increase in alkyl chain length;
- (iii) with ionic surfactants, most counterions are bound to the micelle surface, thus significantly reducing the mobility from the value to be expected from a micelle with non-counterion bonding;

- (iv) micellization occurs over a narrow concentration range as a result of the high association number of surfactant micelles;
- (v) the interior of the surfactant micelle essentially has the properties of a liquid hydrocarbon.

This is confirmed by the high mobility of the alkyl chains and the ability of the micelles to solubilize many water-insoluble organic molecules, e.g. dyes and agrochemicals. To a first approximation, micelles can, over a wide concentration range above the cmc, be viewed as microscopic liquid hydrocarbon droplets covered with polar head groups, which interact strongly with water molecules. It appears that the radius of the micelle core constituted of the alkyl chains is close to the extended length of the alkyl chain, i.e. in the range 1.5–3.0 nm. As we will see later, the driving force for micelle formation is the elimination of the contact between the alkyl chains and water. The larger a spherical micelle, then the more efficient this is, since the volume-to-area ratio increases. It should be noted that the surfactant molecules in the micelles are not all extended. Only one molecule needs to be extended to satisfy the criterion that the radius of the micelle core is close to the extended length of the alkyl chain. The majority of surfactant molecules are in a disordered state. In other words, the interior of the micelle is close to that of the corresponding alkane in a neat liquid oil. This explains the large solubilization capacity of the micelle towards a broad range of nonpolar and weakly polar substances. At the surface of the micelle, associated counterions (in the region of 50–80 % of the surfactant ions) are present. However, simple inorganic counterions are very loosely associated with the micelle. The counterions are very mobile (see below) and there is no specific complex formed with a definite counterion–head group distance. In other words, the counterions are associated by long-range electrostatic interactions.

A useful concept for characterizing micelle geometry is the critical packing parameter, CPP [9]. The aggregation number N is the ratio between the micellar core volume, V_{mic} , and the volume of one chain, v ,

$$N = \frac{V_{\text{mic}}}{v} = \frac{(4/3)\pi R_{\text{mic}}^3}{v}, \quad (6.1)$$

where R_{mic} is the radius of the micelle.

The aggregation number, N , is also equal to the ratio of the area of a micelle, A_{mic} , to the cross-sectional area, a , of one surfactant molecule,

$$N = \frac{A_{\text{mic}}}{a} = \frac{4\pi R_{\text{mic}}^2}{a}. \quad (6.2)$$

Combining equations (6.1) and (6.2),

$$\frac{v}{R_{\text{mic}}a} = \frac{1}{3}. \quad (6.3)$$

Since R_{mic} cannot exceed the extended length of a surfactant alkyl chain, l_{max} ,

$$l_{\text{max}} = 1.5 + 1.265n_c. \quad (6.4)$$

This means that for a spherical micelle,

$$\frac{v}{l_{\max}a} \leq \frac{1}{3}. \quad (6.5)$$

The ratio $v/(l_{\max}a)$ is denoted as the critical packing parameter (CPP).

Although the spherical micelle model accounts for many of the physical properties of solutions of surfactants, a number of phenomena remain unexplained, without considering other shapes. For example, McBain [10] suggested the presence of two types of micelles, spherical and lamellar in order to account for the drop in molar conductance of surfactant solutions. The lamellar micelles are neutral and hence they account for the reduction in conductance. Later, Harkins et al. [11] used McBain's model of lamellar micelles to interpret his X-ray results in soap solutions. Moreover, many modern techniques such as light scattering and neutron scattering indicate that in many systems the micelles are not spherical. For example, Debye and Anacker [12] proposed a cylindrical micelle to explain light scattering results from hexadecyl trimethyl ammonium bromide in water. Evidence for disc-shaped micelles has also been obtained under certain conditions. A schematic representation of the spherical, lamellar and rod-shaped micelles, suggested by McBain, Hartley and Debye is given in Fig. 6.5. Many ionic surfactants show dramatic temperature-dependent solubility as illustrated in Fig. 6.6. The solubility first increases gradually with rising temperature, and then, above a certain temperature, there is a sudden increase of solubility with a further increase in temperature. The cmc increases gradually with increasing temperature. At a particular temperature, the solubility becomes equal to the cmc, i.e. the solubility curve intersects the cmc and this temperature is referred to as the Krafft temperature. At this temperature an equilibrium exists between solid hydrated surfactant, micelles and monomers (i.e. the Krafft temperature is a "triple point"). Surfactants with ionic head groups and long straight alkyl chains have high Krafft temperatures. The Krafft temperature increases with increasing alkyl chain length of the surfactant molecule. It can be reduced by introducing branching in the alkyl

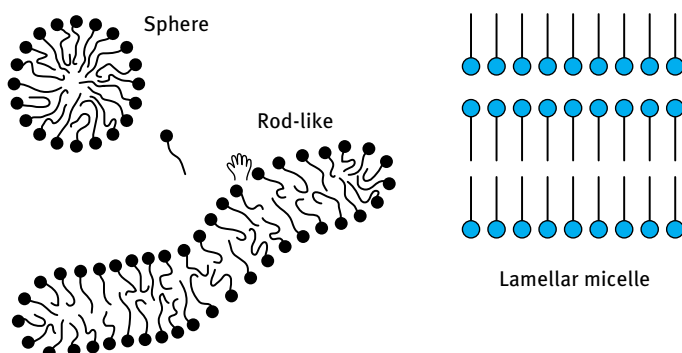


Fig. 6.5: Shape of micelles.

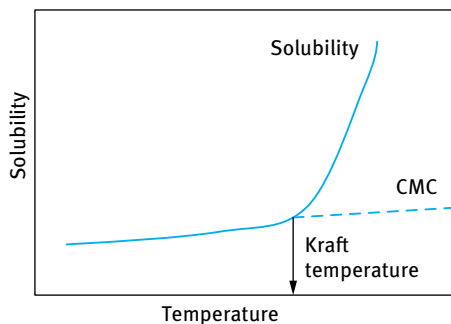


Fig. 6.6: Variation of solubility and critical micelle concentration (cmc) with temperature.

chain. The Krafft temperature is also reduced by using alkyl chains with a wide distribution of the chain length. Addition of electrolytes causes an increase in the Krafft temperature.

With nonionic surfactants of the ethoxylate type, increasing the temperature of a solution at a given concentration causes dehydration of the PEO chains and at a critical temperature the solution become cloudy. This is illustrated in Fig. 6.7 which shows the phase diagram of $C_{12}E_6$. Below the cloud point (CP) curve one can identify different liquid crystalline phases hexagonal – cubic – lamellar which are schematically shown in Fig. 6.8.

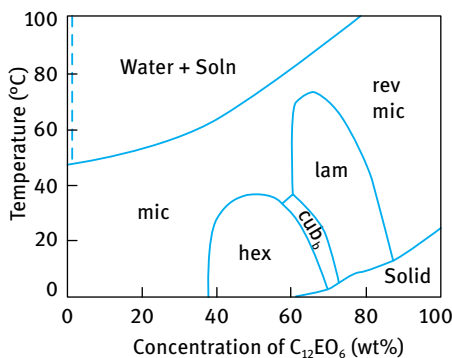


Fig. 6.7: Phase diagram of $C_{12}E_6$.

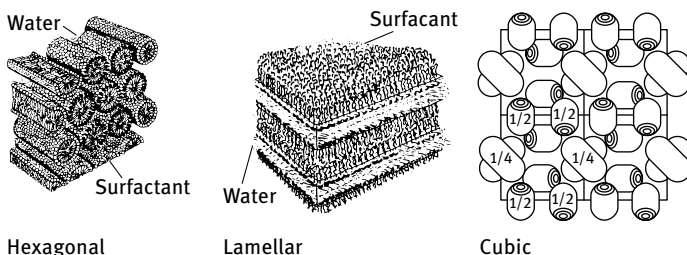


Fig. 6.8: Schematic picture of liquid crystalline phases.

6.3 Thermodynamics of micellization

The process of micellization is one of the most important characteristics of surfactant solution and hence it is essential to understand its mechanism (the driving force for micelle formation). This requires analysis of the dynamics of the process (i.e. the kinetic aspects) as well as the equilibrium aspects whereby the laws of thermodynamics may be applied to obtain the free energy, enthalpy and entropy of micellization.

Micellization is a dynamic phenomenon in which n monomeric surfactant molecules associate to form a micelle S_n , i.e.,



Hartley [8] envisaged a dynamic equilibrium whereby surface active agent molecules are constantly leaving the micelles whilst other molecules from solution enter the micelles. The same applies to the counterions with ionic surfactants, which can exchange between the micelle surface and bulk solution.

Experimental investigations using fast kinetic methods such as stop flow, temperature and pressure jumps, and ultrasonic relaxation measurements have shown that there are two relaxation processes for micellar equilibrium [13–19] characterized by relaxation times τ_1 and τ_2 . The first relaxation time, τ_1 , is of the order of 10^{-7} s (10^{-8} to 10^{-3} s) and represents the lifetime of a surface active molecule in a micelle, i.e. it represents the association and dissociation rate for a single molecule entering and leaving the micelle, which may be represented by the equation,



where K^+ and K^- represent the association and dissociation rate respectively for a single molecule entering or leaving the micelle.

The slower relaxation time τ_2 corresponds to a relatively slow process, namely the micellization-dissolution process represented by equation (6.6). The value of τ_2 is of the order of milliseconds (10^{-3} – 1 s) and hence can be conveniently measured by stopped flow methods. The fast relaxation time τ_1 can be measured using various techniques depending on its range. For example, τ_1 values in the range of 10^{-8} – 10^{-7} s are accessible to ultrasonic absorption methods, whereas τ_1 in the range of 10^{-5} – 10^{-3} s can be measured by pressure jump methods. The value of τ_1 depends on surfactant concentration, chain length and temperature. τ_1 increases with increasing chain length of surfactants, i.e. the residence time increases with increasing chain length.

The above discussion emphasizes the dynamic nature of micelles and it is important to realize that these molecules are in continuous motion and that there is a constant interchange between micelles and solution. The dynamic nature also applies to the counterions which exchange rapidly with lifetimes in the range 10^{-9} – 10^{-8} s. Furthermore, the counterions appear to be laterally mobile and not to be associated with (single) specific groups on the micelle surfaces.

Various approaches have been employed in tackling the problem of the thermodynamics of micelle formation. The simplest approach treats micelles as a single phase, and this is referred to as the phase separation model. In this model, micelle formation is considered as a phase separation phenomenon and the cmc is then the saturation concentration of the amphiphile in the monomeric state whereas the micelles constitute the separated pseudophase. Above the cmc, a phase equilibrium exists with a constant activity of the surfactant in the micellar phase. The Krafft point is viewed as the temperature at which solid hydrated surfactant, micelles and a solution saturated with undissociated surfactant molecules are in equilibrium at a given pressure.

Consider an anionic surfactant, in which n surfactant anions, S^- , and n counterions M^+ associate to form a micelle, i.e.,



The micelle is simply a charged aggregate of surfactant ions plus an equivalent number of counterions in the surrounding atmosphere and is treated as a separate phase. The chemical potential of the surfactant in the micellar state is assumed to be constant, at any given temperature, and this may be adopted as the standard chemical potential, μ_m^0 , by analogy to a pure liquid or a pure solid. Considering the equilibrium between micelles and monomer, then,

$$\mu_m^0 = \mu_1^0 + RT \ln a, \quad (6.9)$$

where μ_1 is the standard chemical potential of the surfactant monomer and a_1 is its activity which is equal to $f_1 x_1$, where f_1 is the activity coefficient and x_1 the mole fraction. Therefore, the standard free energy of micellization per mol of monomer, ΔG_m^0 , is given by,

$$\Delta G_m^0 = \mu_m^0 - \mu_1^0 = RT \ln a_1 \approx RT \ln x_1, \quad (6.10)$$

where f_1 is taken as unity (a reasonable value in very dilute solution). The cmc may be identified with x_1 so that

$$\Delta G_m^0 = RT \ln[\text{cmc}]. \quad (6.11)$$

In equation (6.10), the cmc is expressed as a mole fraction, which is equal to $C/(55.5 + C)$, where C is the concentration of surfactant in mol dm^{-3} , i.e.,

$$\Delta G_m^0 = RT \ln C - RT \ln(55.5 + C). \quad (6.12)$$

It should be stated that ΔG^0 should be calculated using the cmc expressed as a mole fraction as indicated by equation (6.12). However, most cmc's quoted in the literature are given in mol dm^{-3} and in many cases ΔG^0 values have been quoted when the cmc was simply expressed in mol dm^{-3} . Strictly speaking, this is incorrect, since ΔG^0 should be based on x_1 rather than on C . The value of ΔG^0 , when the cmc is expressed in mol dm^{-3} is substantially different from the ΔG^0 value when the cmc is

expressed in mole fraction. For example, dodecyl hexaoxyethylene glycol, the quoted cmc value is $8.7 \times 10^{-5} \text{ mol dm}^{-3}$ at 25 °C. Therefore,

$$\Delta G^0 = RT \ln \frac{8.7 \times 10^{-5}}{55.5 + 8.7 \times 10^{-5}} = -33.1 \text{ kJ mol}^{-1} \quad (6.13)$$

when the mole fraction scale is used. On the other hand,

$$\Delta G^0 = RT \ln 8.7 \times 10^{-5} = -23.2 \text{ kJ mol}^{-1} \quad (6.14)$$

when the molarity scale is used.

A convenient solution for relating ΔG_m^0 to [cmc] was given by Phillips [18] for ionic surfactants who arrived at the following expression,

$$\Delta G_m^0 = \{2 - (p/n)\} RT \ln[\text{cmc}], \quad (6.15)$$

where p is the number of free (unassociated) surfactant ions and n is the total number of surfactant molecules in the micelle. For many ionic surfactants, the degree of dissociation $(p/n) \approx 0.2$ so that,

$$\Delta G_m^0 = 1.8RT \ln[\text{cmc}]. \quad (6.16)$$

Comparison with equation (6.11) clearly shows that for similar ΔG_m , the [cmc] is about two orders of magnitude higher for ionic surfactants when compared with nonionic surfactant of the same alkyl chain length (see Tab. 6.1).

In the presence of excess added electrolyte, with mole fraction x , the free energy of micellization is given by the expression,

$$\Delta G_m^0 = RT \ln[\text{cmc}] + \{1 - (p/n)\} \ln x. \quad (6.17)$$

Equation (6.17) shows that as x increases, the [cmc] decreases.

It is clear from equation (6.15) that as $p \rightarrow 0$, i.e. when most charges are associated with counterions,

$$\Delta G_m^0 = 2RT \ln[\text{cmc}], \quad (6.18)$$

whereas when $p \approx n$, i.e. the counterions are bound to micelles,

$$\Delta G_m^0 = RT \ln[\text{cmc}] \quad (6.19)$$

which is the same equation for nonionic surfactants.

The enthalpy of micellization can be calculated from the variation of cmc with temperature. This follows from,

$$-\Delta H^0 = RT^2 \frac{d \ln[\text{cmc}]}{dT}. \quad (6.20)$$

The entropy of micellization can then be calculated from the relationship between ΔG^0 and ΔH^0 , i.e.,

$$\Delta G^0 = \Delta H^0 - T\Delta S^0. \quad (6.21)$$

Therefore ΔH^0 may be calculated from the surface tension–log C plots at various temperatures. Unfortunately, the errors in locating the cmc (which in many cases is not a sharp point) leads to a large error in the value of ΔH^0 . A more accurate and direct method of obtaining ΔH^0 is microcalorimetry.

The results of thermodynamic analysis show that ΔG^0 is large and negative, indicating that micelle formation is spontaneous and the micellar solution is thermodynamically stable at a given temperature. However, ΔH^0 is positive, indicating that the process is endothermic. In addition, $T\Delta S^0$ is large and positive which implies that in the micellization process there is a net increase in entropy. This positive enthalpy and entropy points to a different driving force for micellization from that encountered in many aggregation processes.

Until recently, the formation of micelles was regarded primarily as an interfacial energy process, analogous to the process of coalescence of oil droplets in an aqueous medium. If this were the case, micelle formation would be a highly exothermic process, as the interfacial free energy has a large enthalpy component. As mentioned above, experimental results have clearly shown that micelle formation involves only a small enthalpy change and is often endothermic. The negative free energy of micellization is the result of a large positive entropy. This led to the conclusion that micelle formation must be a predominantly entropy driven process.

Two main sources of entropy have been suggested. The first is related to the so-called “hydrophobic effect”. This was first established from a consideration of the free energy enthalpy and entropy of transfer of hydrocarbon from water to a liquid hydrocarbon. Some results are listed in Tab. 6.2. This table also lists the heat capacity change ΔC_p on transfer from water to a hydrocarbon, as well as $C_p^{0, \text{gas}}$, i.e. the heat capacity in the gas phase. It can be seen from Tab. 6.2 that the principal contribution to the value of ΔG^0 is the large positive value of ΔS^0 , which increases with increasing hydrocarbon chain length, whereas ΔH^0 is positive, or small and negative.

Tab. 6.2: Thermodynamic parameters for transfer of hydrocarbons from water to liquid hydrocarbon at 25 °C.

Hydrocarbon	ΔG^0 (kJ mol ⁻¹)	ΔH^0 (kJ mol ⁻¹)	ΔS^0 (kJ mol ⁻¹ K ⁻¹)	ΔC_p^0 (kJ mol ⁻¹ K ⁻¹)	$C_p^{0, \text{gas}}$ (kJ mol ⁻¹ K ⁻¹)
C ₂ H ₆	-16.4	10.5	88.2	—	—
C ₃ H ₈	-20.4	7.1	92.4	—	—
C ₄ H ₁₀	-24.8	3.4	96.6	-273	-143
C ₅ H ₁₂	-28.8	2.1	105.0	-403	-172
C ₆ H ₁₄	-32.5	0	109.2	-441	-197
C ₆ H ₆	-19.3	-2.1	58.8	-227	-134
C ₆ H ₅ CH ₃	-22.7	-1.7	71.4	-265	-155
C ₆ H ₅ C ₂ H ₅	-26.0	-2.0	79.8	-319	-185
C ₆ H ₅ C ₃ H ₈	-29.0	-2.3	88.2	-395	—

To account for this large positive entropy of transfer several authors [21–23] suggest that the water molecules around a hydrocarbon chain are ordered, forming “clusters” or “icebergs”. On transfer of an alkane from water to a liquid hydrocarbon, these clusters are broken thus releasing water molecules which now have a higher entropy. This accounts for the large entropy of transfer of an alkane from water to a hydrocarbon medium. This effect is also reflected in the much higher heat capacity change on transfer, ΔC_p^0 , when compared with the heat capacity in the gas phase, C_p^0 . This effect is also operative on transfer of surfactant monomer to a micelle, during the micellization process. The surfactant monomers will also contain “structured” water around their hydrocarbon chain. On transfer of such monomers to a micelle, these water molecules are released and they have a higher entropy.

In most cosmetic and personal care applications, more than one surfactant molecule is used in the formulation. It is, therefore, necessary to predict the type of possible interactions and whether this leads to some synergistic effects. Two general cases may be considered: surfactant molecules with no net interaction (with similar head groups) and systems with net interaction [1–3]. The first case is that when mixing two surfactants with the same head group but with different chain lengths. In analogy with the hydrophilic-lipophilic balance (HLB) for surfactant mixtures, one can also assume that the cmc of a surfactant mixture (with no net interaction) to be an average of the two cmc’s of the single components [1–3],

$$\text{cmc} = x_1 \text{cmc}_1 + x_2 \text{cmc}_2, \quad (6.22)$$

where x_1 and x_2 are the mole fractions of the respective surfactants in the system. However, the mole fractions should not be those in the whole system, but those inside the micelle. This means that equation (6.22) should be modified,

$$\text{cmc} = x_1^m \text{cmc}_1 + x_2^m \text{cmc}_2. \quad (6.23)$$

The superscript ‘m’ indicates that the values are inside the micelle. If x_1 and x_2 are the solution composition, then,

$$\frac{1}{\text{cmc}} = \frac{x_1}{\text{cmc}_1} + \frac{x_2}{\text{cmc}_2}. \quad (6.24)$$

The molar composition of the mixed micelle is given by,

$$x_1^m = \frac{x_1 \text{cmc}_2}{x_1 \text{cmc}_2 + x_2 \text{cmc}_1}. \quad (6.25)$$

Fig. 6.9 shows the calculated cmc and the micelle composition as a function of solution composition using equations (6.24) and (6.25) for three cases where $\text{cmc}_2/\text{cmc}_1 = 1, 0.1$ and 0.01 . As can be seen, the cmc and micellar composition change dramatically with solution composition when the cmc’s of the two surfactants vary considerably, i.e. when the ratio of cmc’s is far from 1. This fact is used when preparing micro-emulsions where the addition of medium chain alcohol (like pentanol or hexanol)

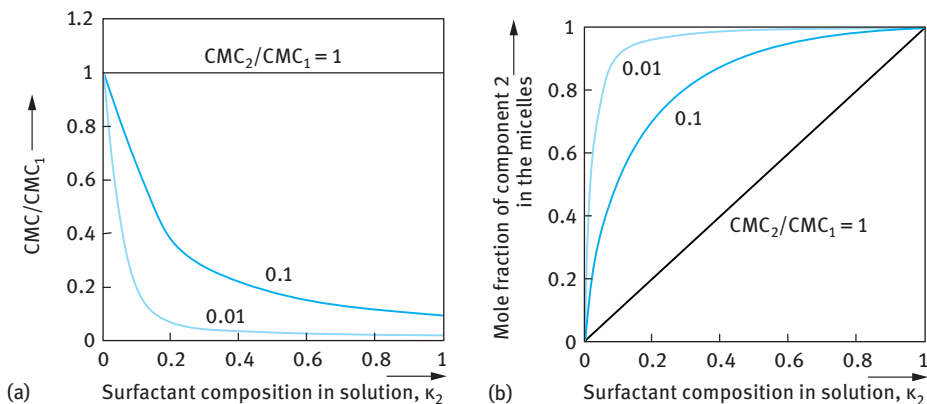


Fig. 6.9: Calculated cmc (a) and micellar composition (b) as a function of solution composition for three ratios of cmc's.

changes the properties considerably. If component 2 is much more surface active, i.e. $cmc_2/cmc_1 \ll 1$, and it is present in low concentrations (x_2 is of the order of 0.01), then from equation (6.25) $x_1^m \approx x_2^m \approx 0.5$, i.e. at the cmc of the systems the micelles are up to 50 % composed of component 2. This illustrates the role of contaminants in surface activity, e.g. dodecyl alcohol in sodium dodecyl sulphate (SDS).

Fig. 6.10 shows the cmc as a function of molar composition of the solution and in the micelles for a mixture of SDS and nonylphenol with 10 mol ethylene oxide (NP-E₁₀). If the molar composition of the micelles is used as the x -axis, the cmc is more or less the arithmetic mean of the cmc's of the two surfactants. If, on the other hand, the molar composition in the solution is used as the x -axis (which at the cmc is equal to the total molar concentration), then the cmc of the mixture shows a dramatic decrease at low fractions of NP-E₁₀. This decrease is due to the preferential absorption of NP-E₁₀ in the micelle. This higher absorption is due to the higher hydrophobicity of the NP-E₁₀ surfactant when compared with SDS.

With many cosmetic and personal care formulations, surfactants of different kinds are mixed together, for example anionics and nonionics. The nonionic surfactant molecules shield the repulsion between the negative head groups in the micelle and hence there will be a net interaction between the two types of molecules. Another example is the case when anionic and cationic surfactants are mixed, whereby very strong interaction will take place between the oppositely charged surfactant molecules. To account for this interaction, equation (6.25) has to be modified by introducing activity coefficients of the surfactants, f_1^m and f_2^m in the micelle,

$$cmc = x_1^m f_1^m cmc_1 + x_2^m f_2^m cmc_2. \quad (6.26)$$

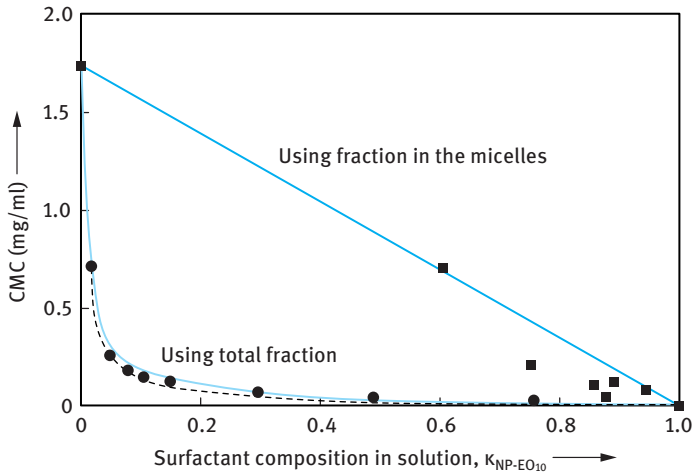


Fig. 6.10: cmc as a function of surfactant composition, x_1 , or micellar surfactant composition, x_1^m for the system SDS + NP-E₁₀.

An expression for the activity coefficients can be obtained using the regular solutions theory [1–3],

$$\ln f_1^m = (x_2^m)^2 \beta, \quad (6.27)$$

$$\ln f_2^m = (x_1^m)^2 \beta, \quad (6.28)$$

where β is an interaction parameter between the surfactant molecules in the micelle. A positive β value means that there is a net repulsion between the surfactant molecules in the micelle, whereas a negative β value means a net attraction.

The cmc of the surfactant mixture and the composition x_1 are given by the following equations,

$$\frac{1}{\text{cmc}} = \frac{x_1}{f_1^m \text{cmc}_1} + \frac{x_2}{f_2^m \text{cmc}_2}, \quad (6.29)$$

$$x_1^m = \frac{x_1 f_2^m \text{cmc}_2}{x_1 f_2^m \text{cmc}_2 + x_2 f_1^m \text{cmc}_1}. \quad (6.30)$$

Fig. 6.11 shows the effect of increasing the β parameter on the cmc and micellar composition for two surfactants with a cmc ratio of 0.1. This Fig. shows that as β becomes more negative, the cmc of the mixture decreases. β values in the region of -2 are typical for anionic/nonionic mixtures, whereas values in the region of -10 to -20 are typical for anionic/cationic mixtures. With increasing the negative value of β , the mixed micelles tend towards a mixing ratio of 50 : 50, which reflects the mutual electrostatic attraction between the surfactant molecules. The predicted cmc and micellar composition depends both on the ratio of the cmc's as well as the value of β .

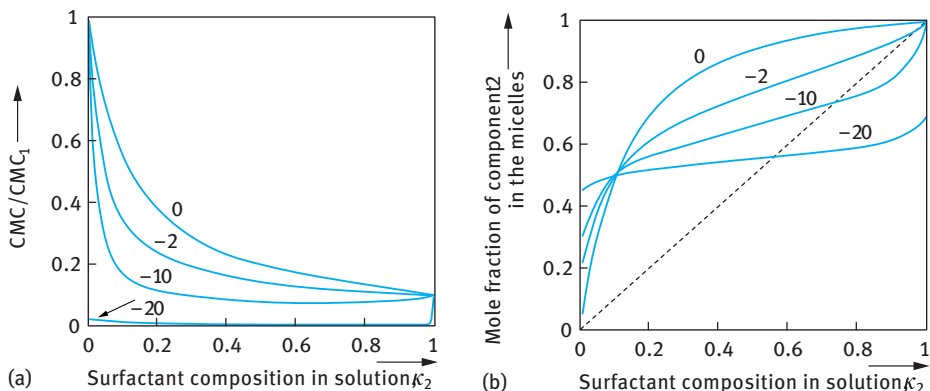


Fig. 6.11: cmc (a) and micellar composition (b) for various values of β for a system with a cmc ratio cmc_2/cmc_1 of 0.1.

When the cmc's of the single surfactants are similar, the predicted value of the cmc is very sensitive to small variations in β . On the other hand, when the ratio of the cmc's is large, the predicted value of the mixed cmc and the micellar composition are insensitive to variation of the β parameter. For mixtures of nonionic and ionic surfactants, the β decreases with increasing electrolyte concentration. This is due to the screening of the electrostatic repulsion on the addition of electrolyte. With some surfactant mixtures, the β decreases with increasing temperature, i.e. the net attraction decreases with increasing temperature.

6.4 Surfactant–polymer interaction

Mixtures of surfactants and polymers are very common in many cosmetic and personal care formulations. With many suspension and emulsion systems stabilized with surfactants, polymers are added for a number of reasons. For example, polymers are added as suspending agents (“thickeners”) to prevent sedimentation or creaming of these systems. Water-soluble polymers are added for enhancing the function of the system, e.g. in shampoos, hair sprays, lotions and creams. The interaction between surfactants and water-soluble polymers results in some synergistic effects, e.g. enhancing the surface activity, stabilizing foams and emulsions, etc. It is, therefore, important to study the interaction between surfactants and water-soluble polymers in a systematic way.

One of the earliest studies of surfactant/polymer interaction came from surface tension measurements. Fig. 6.12 shows some typical results for the effect of addition of polyvinylpyrrolidone (PVP) on the γ -log C curves of SDS [24].

In a system of fixed polymer concentration and varying surfactant concentrations, two critical concentrations appear, denoted by T_1 and T_2 . T_1 represents the concen-

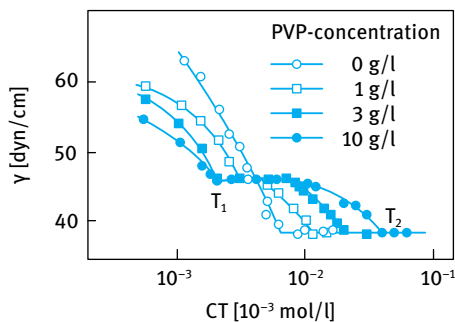


Fig. 6.12: γ -log C curves for SDS solutions in the presence of different concentrations of PVP.

tration at which interaction between the surfactant and polymer first occurs. This is sometimes termed the critical aggregation concentration (CAC), i.e. the onset of association of surfactant to the polymer. Because of this there is no further increase in surface activity and thus no lowering of surface tension. T_2 represents the concentration at which the polymer becomes saturated with surfactant. Since T_1 is generally lower than the cmc of the surfactant in the absence of polymer, then “adsorption” or “aggregation” of SDS on or with the polymer is more favourable than normal micellization. As the polymer is saturated with surfactant (i.e. beyond T_2) the surfactant monomer concentration and the activity start to increase again and there is lowering of γ until the monomer concentration reaches the cmc, after which γ remains virtually constant and normal surfactant micelles begin to form.

The above picture is confirmed if the association of surfactant is directly monitored (e.g. by using surfactant selective electrodes, by equilibrium dialysis or by some spectroscopic technique). The binding isotherms are illustrated in Fig. 6.13.

At low surfactant concentration, there is no significant interaction (binding). At the CAC, a strongly cooperative binding is indicated and at higher concentrations a plateau is reached. Further increasing surfactant concentration produces “free” surfactant molecules until the surfactant activity or concentration joins the curve obtained in the absence of polymer. The binding isotherms of Fig. 6.13 show the strong analogy with micelle formation and the interpretation of these isotherms in terms of a depression of the cmc.

Several conclusions could be drawn from the experimental binding isotherms of mixed surfactant/polymer solutions:

- (i) The CAC/cmc is only weakly dependent on polymer concentration over wide ranges;
- (ii) CAC/cmc is, to a good approximation, independent of polymer molecular weight down to low values. For very low molecular weight the interaction is weakened;
- (iii) the plateau binding increases linearly with polymer concentration;
- (iv) anionic surfactants show a marked interaction with most homopolymers (e.g. PEO and PVP) while cationic surfactants show a weaker but still significant interaction.

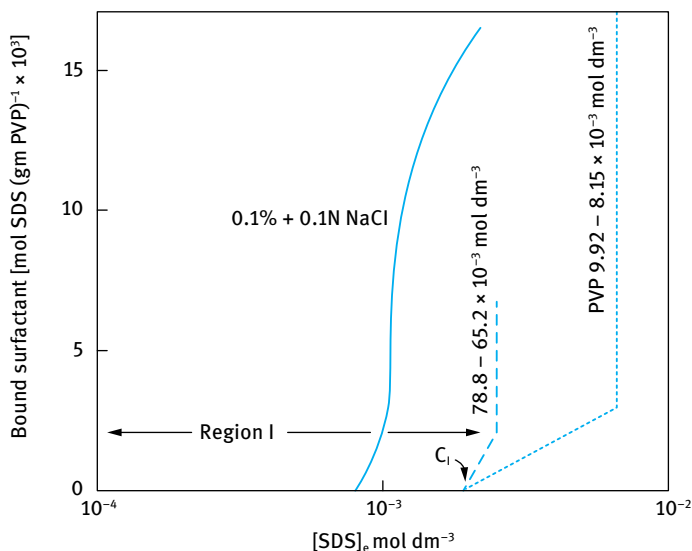


Fig. 6.13: Binding isotherms of a surfactant to a water-soluble polymer.

Nonionic and zwitterionic surfactants only rarely show a distinct interaction with homopolymers.

A schematic representation of the association between surfactants and polymers for a wide range of concentrations of both components [25] is shown in Fig. 6.14. It can be seen that at low surfactant concentration (region I) there is no significant association at any polymer concentration. Above the CAC (region II) association increases up to a surfactant concentration which increases linearly with increasing polymer concentration. In region III, association is saturated and the surfactant monomer concentration increases until region IV is reached where there is co-existence of surfactant aggregates at the polymer chains and free micelles.

Several factors influence the interaction between surfactant and polymer and these are summarized as follows.

- (i) Temperature; increasing temperature generally increases the CAC, i.e. the interaction becomes less favourable.
- (ii) Addition of electrolyte; this generally decreases the CAC, i.e. it increases the binding.
- (iii) Surfactant chain length; increasing the alkyl chain length decreases the CAC, i.e. it increases association. A plot of $\log \text{CAC}$ versus the number of carbon atoms, n , is linear (similar to the $\log \text{cmc} - n$ relationship obtained for surfactants alone).
- (iv) Surfactant structure; alkyl benzene sulphonates are similar to SDS, but introduction of EO groups in the chain weakens the interaction.

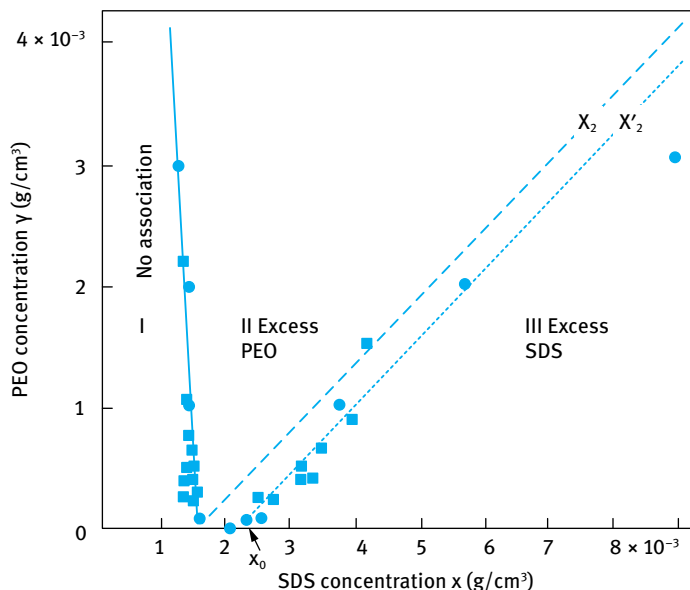


Fig. 6.14: Association between surfactant and homopolymer in different concentration domains [25].

- (v) Surfactant classes; weaker interaction is generally observed with cationics when compared to anionics. However, the interaction can be promoted by using a strongly interacting counterion for the cationic (e.g. CNS^-). Interaction between ethoxylated surfactants and nonionic polymers is weak. The interaction is stronger with alkyl phenol ethoxylates.
- (vi) Polymer molecular weight; a minimum molecular weight of ≈ 4000 for PEO and PVP is required for “complete” interaction.
- (vii) Amount of polymer; the CAC seems to be insensitive to (or slightly lower) with increasing polymer concentration. T_2 increases linearly with increasing polymer concentration.
- (viii) Polymer structure and hydrophobicity; several uncharged polymers such as PEO, PVP and polyvinyl alcohol (PVOH) interact with charged surfactants.

Many other uncharged polymers interact weakly with charged surfactants, e.g. hydroxyethyl cellulose (HEC), dextran and polyacrylamide (PAAm). For anionic surfactants, the following order of increased interaction has been listed: PVOH < PEO < MEC (methyl cellulose) < PVAc (partially hydrolyzed polyvinyl acetate) < PPO \approx PVP. For cationic surfactants, the following order was listed: PVP < PEO < PVOH < MEC < PVAc < PPO. The position of PVP can be explained by the slight positive charge on the chain which causes repulsion with cations and attraction with anionics.

The driving force for polymer/surfactant interaction is the same as that for the process of micellization (see above). As with micelles, the main driving force is the

reduction of hydrocarbon/water contact area of the alkyl chain of the dissolved surfactant. A delicate balance between several forces is responsible for the surfactant/polymer association. For example, aggregation is resisted by the crowding of the ionic head groups at the surface of the micelle. Packing constraints also resist association. Molecules that screen the repulsion between the head groups, e.g. electrolytes and alcohol, promote association. A polymer molecule with hydrophobic and hydrophilic segments (which is also flexible) can enhance association by ion-dipole association between the dipole of the hydrophilic groups and the ionic head groups of the surfactant. In addition, contact between the hydrophobic segments of the polymer and the exposed hydrocarbon areas of the micelles can enhance association. With SDS/PEO and SDS/PVP, the association complexes are approximately three monomer units per molecule of aggregated surfactant.

Generally speaking, there are two alternative pictures of mixed surfactant/polymer solutions, one describing the interaction in terms of a strongly cooperative association or binding of the surfactant to the polymer chain and one in terms of a micellization of surfactant on or in the vicinity of the polymer chain. For polymers with hydrophobic groups the binding approach is preferred, whereas for hydrophilic homopolymers the micelle formation picture is more likely. The latter picture has been suggested by Cabane [25, 26] who proposed a structure in which the aggregated SDS is surrounded by macromolecules in a loopy configuration. A schematic picture of this structure, that is sometimes referred to as “pearl-necklace model”, is given in Fig. 6.15.

The consequences of this model are:

- (i) More favourable free energy of association ($CAC < cmc$) and increased ionic dissociation of the aggregates.
- (ii) An altered environment of the CH_2 groups of the surfactant near the head group.

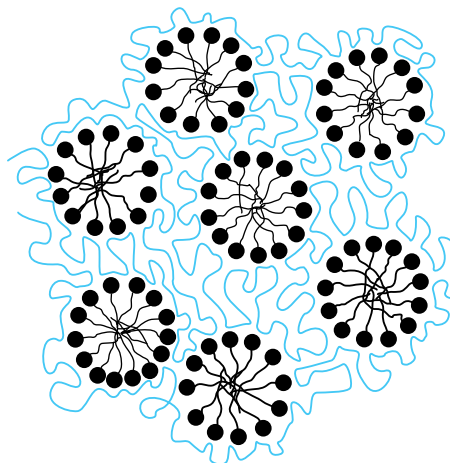


Fig. 6.15: Schematic representation of the topology of surfactant/polymer complexes according to Cabane [25, 26].

The micelle sizes are similar with polymer present and without, and the aggregation numbers are typically similar or slightly lower than those of the micelles forming in the absence of a polymer. In the presence of a polymer, the surfactant chemical potential is lowered with respect to the situation without polymer [27].

Many cosmetic and personal care products contain hydrophobically modified (HM) polymers. The water-soluble polymers are modified by grafting a low amount of hydrophobic groups (of the order of 1% of the monomers reacted in a typical molecule) resulting in the formation of “associative structures”. These molecules are referred to as associative thickeners and are used as rheology modifiers in many cosmetic and personal care products. An added surfactant will interact strongly with the hydrophobic groups of the polymer, leading to a strengthened association between the surfactant molecules and the polymer chain. A schematic picture for the interaction between SDS and hydrophobically modified hydroxyethyl cellulose (HM-HEC) is shown in Fig. 6.16 which shows the interaction at various surfactant concentrations [1–3].

Initially the surfactant monomers interact with the hydrophobic groups of the HM polymer and at some surfactant concentration (CAC), the micelles can crosslink the polymer chains. At higher surfactant concentrations, the micelles which are now abundant will no longer be shared between the polymer chains, i.e. the crosslinks are broken. These effects are reflected in the variation of viscosity with surfactant concentration for HM polymer, as illustrated in Fig. 6.17. The viscosity of the polymer increases with increasing surfactant concentration, reaching a maximum at an optimum concentration (maximum crosslinks) and then decreases with any further increase in surfactant concentration (Fig. 6.16). For the unmodified polymer, the changes in viscosity are relatively small.

The interaction between surfactants and polymers with opposite charge is employed in hair conditioners (surfactant/polyelectrolyte interaction). As an illustration, the interaction between SDS and cationically modified cellulosic polymer (Polymer JR, Union Carbide), used as a hair conditioner, is shown in Fig. 6.18 using surface tension γ measurements [28]. The γ - $\log C$ curves for SDS in the presence and absence of the polyelectrolyte are shown in Fig. 6.18 which also shows the appearance of the solutions. At low surfactant concentration, there is a synergistic lowering of surface tension, i.e. the surfactant/polyelectrolyte complex is more surface active. The low surface tension is also present in the precipitation zone. At high surfactant concentrations, γ approaches that of the polymer-free surfactant in the micellar region. These trends are schematically illustrated in Fig. 6.19.

Surfactant/polyelectrolyte interaction has several consequences on applications in hair conditioners. The most important effect is the high foaming power of the complex. Maximum foaming occurs in the region of highest precipitation, i.e. maximum hydrophobization of the polymer. It is likely that the precipitate stabilizes the foam. Direct determination of the amount of surfactant bound to the polyelectrolyte chains revealed a number of interesting features. The binding occurs at very low surfactant

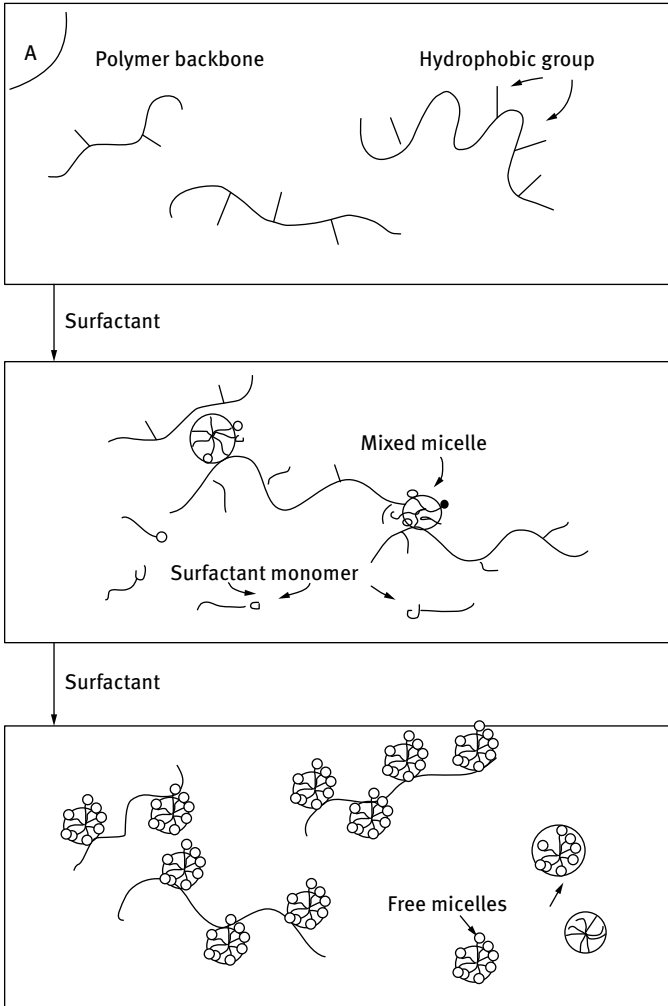


Fig. 6.16: Schematic representation of the interaction between surfactant and HM polymer.

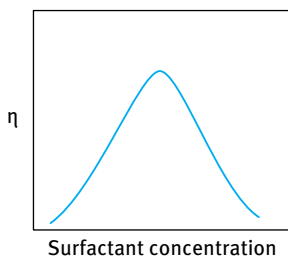


Fig. 6.17: Viscosity–surfactant concentration relationship for HM modified and unmodified polymer solutions.

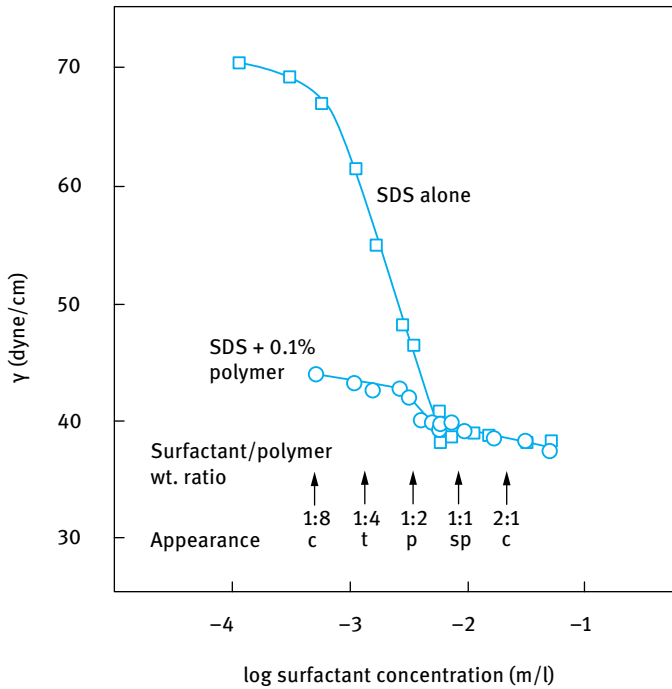


Fig. 6.18: γ -log C curves of SDS with and without addition of polymer (0.1% JR 400) – c (clear), t (turbid), p (precipitate), sp (slight precipitate).

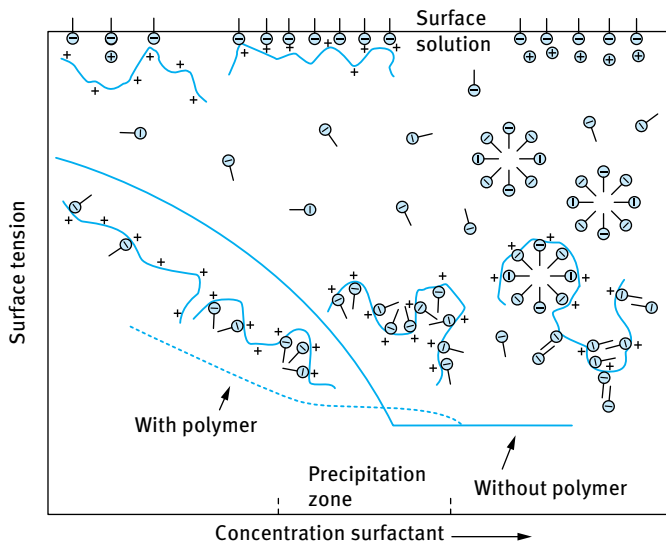


Fig. 6.19: Schematic representation of surfactant/polyelectrolyte interaction.

concentration (1/20th of the cmc). The degree of binding β reached a value of 0.5 ($\beta = 1$ corresponds to a bound DS^- ion for each ammonium group). β versus SDS concentration curves were identical for polymeric homologues with a degree of cationic substitution (CS) > 0.23. Precipitation occurred when $\beta = 1$.

The binding of cationic surfactants to anionic polyelectrolytes also showed a number of interesting features. The binding affinity depends on the nature of the polyanion. Addition of electrolytes increases the steepness of binding, but the binding occurs at higher surfactant concentration as the electrolyte concentration is increased. Increasing the alkyl chain length of the surfactant increases binding, a process that is similar to micellization.

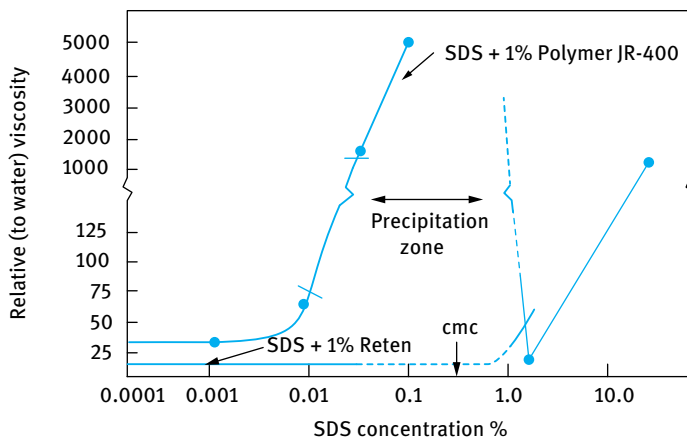


Fig. 6.20: Relative viscosity of 1% JR and 1% Reten as a function of SDS concentration.

Viscometric measurements showed a rapid increase in the relative viscosity at a critical surfactant concentration. However, the behaviour depends on the type of polyelectrolyte used. As an illustration, Fig. 6.20 shows the viscosity-SDS concentration curves for two types of cationic polyelectrolyte: JR 400 (cationically modified cellulosic) and Reten (an acrylamide/ β -methylacryloxy trimethyl ammonium chloride copolymer, ex Hercules).

The difference between the two polyelectrolytes is striking and it suggests little change in the conformation of Reten on addition of SDS, but strong intermolecular association between polymer JR 400 and SDS.

References

- [1] Tadros T. Formulations: In cosmetics and personal care. Berlin: De Gruyter; 2016.
- [2] Tadros T. Cosmetics. In: Tadros T, editor. Encyclopedia of colloid and interface science. Berlin: Springer; 2013.
- [3] Tadros T. An introduction to surfactants. Berlin: De Gruyter; 2014.
- [4] Holmberg K, Jonsson B, Kronberg B, Lindman B. Surfactants and polymers in aqueous solution. 2nd edition. John Wiley & Sons, USA; 2003.
- [5] Mukerjee P, Mysels KJ. Critical micelle concentrations of aqueous surfactant systems. Washington DC: National Bureau of Standards Publication; 1971.
- [6] McBain JW. *Trans Faraday Soc.* 1913;9:99.
- [7] Adam NK. *J Phys Chem.* 1925;29:87.
- [8] Hartley GS. Aqueous solutions of paraffin chain salts. Paris: Hermann and Cie; 1936.
- [9] Israelachvili JN. Intermolecular and surface forces, with special applications to colloidal and biological systems. London: Academic Press; 1985. p. 251.
- [10] McBain JW. *Colloid science.* Boston: Heath; 1950.
- [11] Harkins WD, Mattoon WD, Corrin ML. *J Amer Chem Soc.* 1946;68:220; *J Colloid Sci.* 1946;1:105.
- [12] 12. Debye P, Anaker EW. *J Phys Colloid Chem.* 1951;55:644.
- [13] Anainsson EAG, Wall SN. *J Phys Chem.* 1974;78:1024; 1975;79:857.
- [14] Anainsson EAG, Wall SN, Almagren M, Hoffmann H, Kielmann I, Ulbricht W, Zana R, Lang J, Tondre C. *J Phys Chem.* 1976;80:905.
- [15] Rassing J, Sams PJ, Wyn-Jones E. *J Chem Soc. Faraday II,* 1974;70:1247.
- [16] Jaycock MJ, Ottewill RH, Fourth Int. Congress Surface Activity. 1964;2:545.
- [17] Okub T, Kitano H, Ishiwatari T, Isem N. *Proc Royal Soc.* 1979;A36:81.
- [18] Phillips JN. *Trans Faraday Soc.* 1955;51:561.
- [19] Kahlweit M, Teubner M. *Adv Colloid Interface Sci.* 1980;13:1.
- [20] Rosen ML. Surfactants and interfacial phenomena. New York: Wiley-Interscience; 1978.
- [21] Tanford C. The hydrophobic effect. 2nd edition. New York: Wiley; 1980.
- [22] Stainsby G, Alexander AE. *Trans Faraday Soc.* 1950;46:587.
- [23] Arnow RH, Witten L. *J Phys Chem.* 1960;64:1643.
- [24] Robb ID. *Chemistry and Industry.* 1972:530–535.
- [25] Cabane B, Duplessix R. *J Phys (Paris).* 1982;43:1529.
- [26] Cabane B. *J Phys Chem.* 1977;81:1639.
- [27] Evans DF, Winnerstrom H. The colloidal domain. Where physics, chemistry, biology and technology meet. New York: John Wiley and Sons Inc. VCH; 1994. p. 312.
- [28] Goddard ED. *Colloids and Surfaces.* 1986;19:301.

7 Cosmetic emulsions

7.1 Introduction

Cosmetic emulsions need to satisfy a number of benefits. For example, such systems should deliver a functional benefit such as cleaning (e.g. hair, skin, etc.), provide a protective barrier against water loss from the skin and in some cases they should screen out damaging UV light (in which case a sunscreen agent such as titania is incorporated in the emulsion). These systems should also impart a pleasant odour and make the skin feel smooth. Both oil-in-water (O/W) and water-in-oil (W/O) emulsions are used in cosmetic applications [1–3]. As will be discussed in Chapter 9, more complex systems such as multiple emulsions have been applied in recent years.

The main physicochemical characteristics that need to be controlled in cosmetic emulsions are their formation and stability on storage as well as their rheology, which controls spreadability and skin feel. The life span of most cosmetic and toiletry brands is relatively short (3–5 years) and hence development of the product should be fast. For this reason, accelerated storage testing is needed for predicting stability and change of rheology with time. These accelerated tests represent a challenge to the formulation chemist [1–3].

The main criterion for any cosmetic ingredient should be medical safety (free of allergens, sensitizers and irritants and impurities that have systemic toxic effects). These ingredients should be suitable for producing stable emulsions that can deliver the functional benefit and the aesthetic characteristics. The main composition of an emulsion is the water and oil phases and the emulsifier. Several water-soluble ingredients may be incorporated in the aqueous phase and oil-soluble ingredients in the oil phase. Thus, the water phase may contain functional materials such as proteins, vitamins, minerals and many natural or synthetic water-soluble polymers. The oil phase may contain perfumes and/or pigments (e.g. in make-up). The oil phase may be a mixture of several mineral or vegetable oils. Examples of oils used in cosmetic emulsions are lanolin and its derivatives, paraffin and silicone oils. The oil phase provides a barrier against water loss from the skin.

7.2 Thermodynamics of emulsion formation

The process of emulsion formation is determined by the property of the interface, in particular the interfacial tension, which is determined by the concentration and type of the emulsifier [3–7].

Consider a system in which an oil is represented by a large drop 2 of area A_1 immersed in a liquid 2, which is now subdivided into a large number of smaller droplets with total area A_2 ($A_2 \gg A_1$), as shown in Fig. 7.1. The interfacial tension γ_{12} is the

<https://doi.org/10.1515/9783110555257-008>

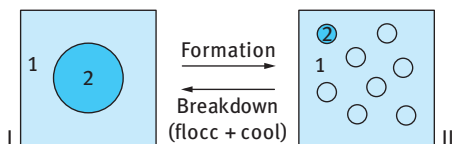


Fig. 7.1: Schematic representation of emulsion formation and breakdown.

same for the large and smaller droplets since the latter are generally in the region of 0.1 to few μm .

The change in free energy in going from state I to state II is made up of two contributions: A surface energy term (that is positive) that is equal to $\Delta A\gamma_{12}$ (where $\Delta A = A_2 - A_1$) and an entropy of dispersions term, which is also positive (since producing a large number of droplets is accompanied by an increase in configurational entropy) and is equal to $T\Delta S^{\text{conf}}$.

From the second law of thermodynamics,

$$\Delta G^{\text{form}} = \Delta A\gamma_{12} - T\Delta S^{\text{conf}}. \quad (7.1)$$

In most cases $\Delta A\gamma_{12} \gg T\Delta S^{\text{conf}}$, which means that ΔG^{form} is positive, i.e. the formation of emulsions is non-spontaneous and the system is thermodynamically unstable. In the absence of any stabilization mechanism, the emulsion will break by flocculation, coalescence, Ostwald ripening or a combination of all these processes. This is illustrated in Fig. 7.2, which shows several paths for emulsion breakdown processes.

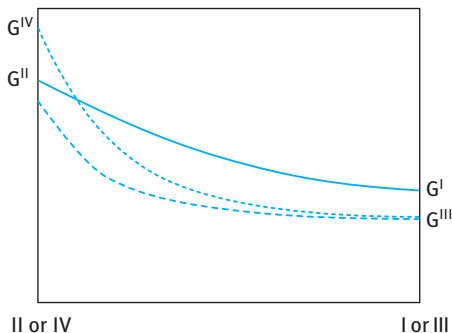


Fig. 7.2: Free energy path in emulsion breakdown: —, flocc. + coal., ---, flocc. + coal. + sed., ..., flocc. + coal. + sed. + Ostwald ripening.

In the presence of a stabilizer (surfactant and/or polymer), an energy barrier is created between the droplets and therefore the reversal from state II to state I becomes non-continuous as a result of the presence of these energy barriers. This is illustrated in Fig. 7.3. In the presence of the above energy barriers, the system becomes kinetically stable.

Several emulsifiers, mostly nonionic or polymeric, are used for the preparation of O/W or W/O emulsions and their subsequent stabilization. For W/O emulsions, the hydrophilic-lipophilic balance (HLB) range (see below) of the emulsifier is in the range 3–6, whereas for O/W emulsions this range is 8–18.

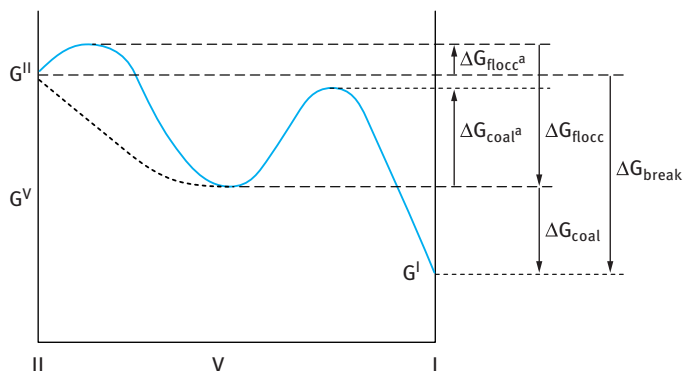


Fig. 7.3: Schematic representation of free energy path for breakdown (flocculation and coalescence) for systems containing an energy barrier.

The HLB number is based on the relative percentage of hydrophilic to lipophilic (hydrophobic) groups in the surfactant molecule(s) as will be discussed below. For an O/W emulsion droplet, the hydrophobic chain resides in the oil phase whereas the hydrophilic head group resides in the aqueous phase. For a W/O emulsion droplet, the hydrophilic group(s) reside in the water droplet, whereas the lipophilic groups reside in the hydrocarbon phase.

7.3 Emulsion breakdown processes and their prevention

Several breakdown processes may occur on storage depending on: particle size distribution and density difference between the droplets and the medium; magnitude of the attractive versus repulsive forces which determines flocculation; solubility of the disperse droplets and the particle size distribution which determine Ostwald ripening; stability of the liquid film between the droplets that determines coalescence; phase inversion, where the two phases exchange, e.g. an O/W emulsion inverting to a W/O emulsion and vice versa. Phase inversion can be catastrophic as is the case when the oil phase in an O/W emulsion exceeds a critical value. The inversion can be transient when for example the emulsion is subjected to a temperature increase.

The various breakdown processes are illustrated in Fig. 7.4. The physical phenomena involved in each breakdown process are not simple and analysis of the various surface forces involved is required. In addition, the above processes may take place simultaneously rather than consecutively and this complicates the analysis.

A summary of each of the above breakdown processes is given below, including details of each process and methods for its prevention.

Creaming and sedimentation with no change in droplet size result from external forces, usually gravitational or centrifugal. When such forces exceed the thermal

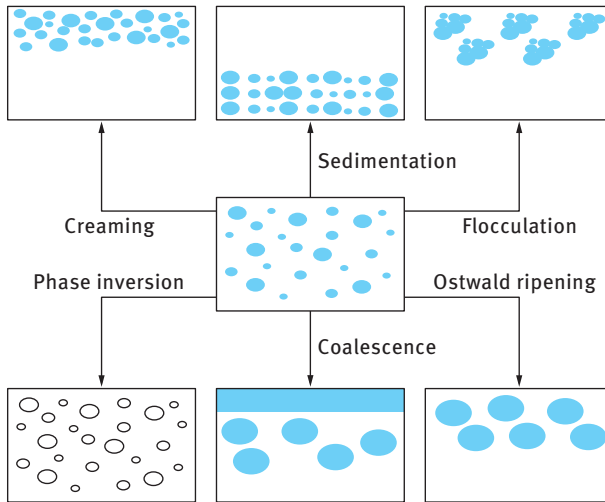


Fig. 7.4: Schematic representation of the various breakdown processes in emulsions.

motion of the droplets (Brownian motion), a concentration gradient builds up in the system with the larger droplets moving faster to the top (if their density is lower than that of the medium) or to the bottom (if their density is larger than that of the medium) of the container. In the limiting cases, the droplets may form a close-packed (random or ordered) array at the top or bottom of the system with the remainder of the volume occupied by the continuous liquid phase.

The most commonly used method for preventing creaming or sedimentation is to add a rheology modifier, sometimes referred to as a thickener, usually a high molecular weight polymer such as hydroxyethyl cellulose, associative thickener (hydrophobically modified polymer) or a microgel such as Carbopol (crosslinked polyacrylate which on neutralization with alkali forms a microgel). All these systems give a non-Newtonian system (see section on rheology of cosmetic emulsions) with a very high viscosity at low shear rate (referred to as residual or “zero-shear” viscosity $\eta(0)$). This high viscosity (usually above 10 Pa s) prevents any creaming or sedimentation of the emulsion.

Flocculation refers to aggregation of the droplets (without any change in primary droplet size) into larger units. It is the result of the van der Waals attraction which is universal with all disperse systems. The main force of attraction arises from the London dispersion force that results from charge fluctuations of the atoms or molecules in the disperse droplets. The van der Waals attraction increases with decreasing separation distance between the droplets and at small separation distances the attraction becomes very strong, resulting in droplet aggregation or flocculation. The latter occurs when there is not sufficient repulsion to keep the droplets apart to distances where the van der Waals attraction is weak. Flocculation may be “strong” or “weak”,

depending on the magnitude of the attractive energy involved. In cases where the net attractive forces are relatively weak, an equilibrium degree of flocculation may be achieved (so-called weak flocculation), associated with the reversible nature of the aggregation process. The exact nature of the equilibrium state depends on the characteristics of the system. One can envisage the build-up of aggregate size distribution and an equilibrium may be established between single droplets and large aggregates. With a strongly flocculated system, one refers to a system in which all the droplets are present in aggregates due to the strong van der Waals attraction between the droplets.

Two main rules can be applied for reducing (eliminating) flocculation depending on the stabilization mechanism:

- (i) With charge stabilized emulsions, e.g. using ionic surfactants, the most important criterion is to make the energy barrier in the energy–distance curve, G_{\max} , as high as possible. This is achieved by three main conditions: high surface or zeta potential, low electrolyte concentration and low valency of ions.
- (ii) For sterically stabilized emulsions four main criteria are necessary:
 - (a) Complete coverage of the droplets by the stabilizing chains.
 - (b) Firm attachment (strong anchoring) of the chains to the droplets. This requires the chains to be insoluble in the medium and soluble in the oil. However, this is incompatible with stabilization which requires a chain that is soluble in the medium and strongly solvated by its molecules. These conflicting requirements are solved by the use of A–B, A–B–A block or BA_n graft copolymers (B is the “anchor” chain and A is the stabilizing chain(s)). Examples for the B chains for O/W emulsions are polystyrene, polymethylmethacrylate, polypropylene oxide and alkyl polypropylene oxide. For the A chain(s), polyethylene oxide (PEO) or polyvinyl alcohol are good examples. For W/O emulsions, PEO can form the B chain, whereas the A chain(s) could be polyhydroxy stearic acid (PHS), which is strongly solvated by most oils.
 - (c) Thick adsorbed layers; the adsorbed layer thickness should be in the region of 5–10 nm. This means that the molecular weight of the stabilizing chains could be in the region of 1000–5000.
 - (d) The stabilizing chain should be maintained in good solvent conditions (the Flory–Huggins interaction parameter $\chi < 0.5$) under all conditions of temperature change on storage.

Ostwald ripening (disproportionation) results from the finite solubility of the liquid phases. Liquids referred to as being immiscible often have mutual solubilities which are not negligible. With emulsions, which are usually polydisperse, the smaller droplets will have larger solubility when compared with the larger ones (due to curvature effects). With time, the smaller droplets disappear and their molecules diffuse to the bulk and become deposited on the larger droplets. With time the droplet size distribution shifts to larger values.

Two general methods may be applied to reduce Ostwald ripening [1–3]:

- (i) Addition of a second disperse phase component which is insoluble in the continuous medium (e.g. squalane). In this case partitioning between different droplet sizes occurs, with the component having low solubility expected to be concentrated in the smaller droplets. During Ostwald ripening in a two component system, equilibrium is established when the difference in chemical potential between differently sized droplets (which results from curvature effects) is balanced by the difference in chemical potential resulting from partitioning of the two components. This effect reduces further growth of droplets.
- (ii) Modification of the interfacial film at the O/W interface: reduction in γ results in a reduction of Ostwald ripening rate. By using surfactants that are strongly adsorbed at the O/W interface (i.e. polymeric surfactants) and which do not desorb during ripening (by choosing a molecule that is insoluble in the continuous phase), the rate could be significantly reduced. An increase in the surface dilational modulus $\epsilon (= dy/d \ln A)$ and decrease in γ would be observed for the shrinking drop and this tends to reduce further growth [1–3].

A–B–A block copolymers such as PHS–PEO–PHS (which is soluble in the oil droplets but insoluble in water) can be used to achieve the above effect. Similar effects can also be obtained using a graft copolymer of hydrophobically modified inulin, namely INUTEC[®] SP1 (ORAFTEI, Belgium). This polymeric surfactant adsorbs with several alkyl chains (which may dissolve in the oil phase) leaving loops and tails of strongly hydrated inulin (polyfructose) chains. The molecule has limited solubility in water and hence it resides at the O/W interface. These polymeric emulsifiers enhance the Gibbs elasticity, thus significantly reducing the Ostwald ripening rate.

Coalescence refers to the process of thinning and disruption of the liquid film between the droplets which may be present in a creamed or sedimented layer, in a floc or simply during droplet collision, with the result of fusion of two or more droplets into larger ones. This process of coalescence results in a considerable change to the droplet size distribution, which shifts to larger sizes. The limiting case for coalescence is the complete separation of the emulsion into two distinct liquid phases. The thinning and disruption of the liquid film between the droplets is determined by the relative magnitudes of the attractive versus repulsive forces. To prevent coalescence, the repulsive forces must exceed the van der Waals attraction, thus preventing film rupture.

Several methods may be applied to achieve the above effects:

- (i) Use of mixed surfactant films. In many cases using mixed surfactants, say anionic and nonionic or long chain alcohols, can reduce coalescence as a result of several effects: high Gibbs elasticity; high surface viscosity; hindered diffusion of surfactant molecules from the film.
- (ii) Formation of lamellar liquid crystalline phases at the O/W interface. Surfactant or mixed surfactant film can produce several bilayers that “wrap” the droplets. As a result of these multilayer structures, the potential drop is shifted to longer

distances thus reducing the van der Waals attraction. For coalescence to occur, these multilayers have to be removed “two-by-two” and this forms an energy barrier preventing coalescence.

Phase inversion refers to the process in which there is an exchange between the disperse phase and the medium. For example, an O/W emulsion may with time or change of conditions invert to a W/O emulsion. In many cases, phase inversion passes through a transition state in which multiple emulsions are produced. For example with an O/W emulsion, the aqueous continuous phase may become emulsified in the oil droplets forming a W/O/W multiple emulsion. This process may continue until all the continuous phase is emulsified into the oil phase thus producing a W/O emulsion.

7.4 Selection of emulsifiers

7.4.1 The hydrophilic-lipophilic balance (HLB) concept

The hydrophilic-lipophilic balance (HLB number) is a semi-empirical scale for selecting surfactants developed by Griffin [8]. This scale is based on the relative percentage of hydrophilic to lipophilic (hydrophobic) groups in the surfactant molecule(s). For an O/W emulsion droplet, the hydrophobic chain resides in the oil phase whereas the hydrophilic head group resides in the aqueous phase. For a W/O emulsion droplet, the hydrophilic group(s) reside in the water droplet, whereas the lipophilic groups reside in the hydrocarbon phase.

Tab. 7.1 gives a guide to the selection of surfactants for a particular application. The HLB number depends on the nature of the oil. As an illustration, Tab. 7.2 gives the required HLB numbers to emulsify various oils. Examples of HLB numbers of a list of surfactants are given in Tab. 7.3.

The relative importance of the hydrophilic and lipophilic groups was first recognized when using mixtures of surfactants containing varying proportions of low and high HLB number. The efficiency of any combination (as judged by phase separation) was found to pass a maximum when the blend contained a particular proportion of the surfactant with the higher HLB number. This is illustrated in Fig. 7.5, which shows the

Tab. 7.1: Summary of HLB ranges and their applications.

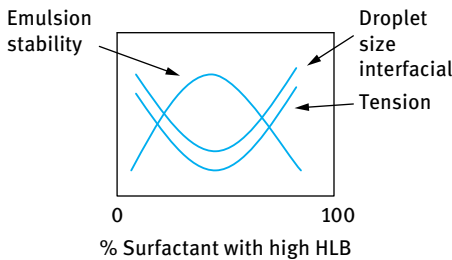
HLB range	Application
3–6	W/O emulsifier
7–9	Wetting agent
8–18	O/W emulsifier
13–15	Detergent
15–18	Solubilizer

Tab. 7.2: Required HLB numbers to emulsify various oils.

Oil	W/O emulsion	O/W emulsion
Paraffin oil	4	10
Beeswax	5	9
Lanolin, anhydrous	8	12
Cyclohexane	—	15
Toluene	—	15
Silicone oil (volatile)	—	7–8
Isopropyl myristate	—	11–12
Isohexadecyl alcohol	—	11–12
Castor oil	—	14

Tab. 7.3: HLB numbers of some surfactants.

Surfactant	Chemical name	HLB
Span 85	Sorbitan trioleate	1.8
Span 80	Sorbitan monooleate	4.3
Brij 72	Ethoxylated (2 mol ethylene oxide) stearyl alcohol	4.9
Triton X-35	Ethoxylated octylphenol	7.8
Tween 85	Ethoxylated (20 mol ethylene oxide) sorbitan trioleate	11.0
Tween 80	Ethoxylated (20 mol ethylene oxide) sorbitan monooleate	15.0

**Fig. 7.5:** Variation of emulsion stability, droplet size and interfacial tension with percentage surfactant with high HLB number.

variation of emulsion stability, droplet size and interfacial tension with % surfactant with high HLB number.

The average HLB number may be calculated from additivity,

$$HLB = x_1 HLB_1 + x_2 HLB_2. \quad (7.2)$$

x_1 and x_2 are the weight fractions of the two surfactants with HLB_1 and HLB_2 .

Griffin [8] developed simple equations for calculating the HLB number of relatively simple nonionic surfactants. For a polyhydroxy fatty acid ester,

$$HLB = 20 \left(1 - \frac{S}{A} \right). \quad (7.3)$$

S is the saponification number of the ester and A is the acid number. For a glyceryl monostearate, $S = 161$ and $A = 198$; the HLB is 3.8 (suitable for a W/O emulsion).

For a simple alcohol ethoxylate, the HLB number can be calculated from the weight percent of ethylene oxide (E) and polyhydric alcohol (P),

$$\text{HLB} = \frac{E + P}{5}. \quad (7.4)$$

If the surfactant contains PEO as the only hydrophilic group, the contribution from one OH group can be neglected,

$$\text{HLB} = \frac{E}{5}. \quad (7.5)$$

For a nonionic surfactant $\text{C}_{12}\text{H}_{25}\text{-O-(CH}_2\text{-CH}_2\text{-O)}_6$, the HLB is 12 (suitable for an O/W emulsion).

The above simple equations cannot be used for surfactants containing propylene oxide or butylene oxide. Nor can they be applied for ionic surfactants. Davies [9, 10] devised a method for calculating the HLB number for surfactants from their chemical formulae, using empirically determined group numbers. A group number is assigned to various component groups. A summary of the group numbers for some surfactants is given in Tab. 7.4.

The HLB is given by the following empirical equation,

$$\text{HLB} = 7 + \sum(\text{hydrophilic group numbers}) - \sum(\text{lipophilic group numbers}). \quad (7.6)$$

Davies has shown that the agreement between HLB numbers calculated from the above equation and those determined experimentally is quite satisfactory.

Various other procedures have been developed to obtain a rough estimate of the HLB number. Griffin found good correlation between the cloud point of 5% solution of various ethoxylated surfactants and their HLB number.

Tab. 7.4: HLB group numbers.

	Group number
<i>Hydrophilic</i>	
$-\text{SO}_4\text{Na}^+$	38.7
$-\text{COOK}$	21.2
$-\text{COONa}$	19.1
N (tertiary amine)	9.4
Ester (sorbitan ring)	6.8
$-\text{O}-$	1.3
$\text{CH-(sorbitan ring)}$	0.5
<i>Lipophilic</i>	
$(-\text{CH}-), (-\text{CH}_2-), \text{CH}_3$	0.475
<i>Derived</i>	
$-\text{CH}_2-\text{CH}_2-\text{O}$	0.33
$-\text{CH}_2-\text{CHCH}_3-\text{O}-$	0.11

Davies [9, 10] attempted to relate the HLB values to the selective coalescence rates of emulsions. Such correlations were not realized since it was found that the emulsion stability and even its type depend to a large extent on the method of dispersing the oil into the water and vice versa. At best, the HLB number can only be used as a guide for selecting optimum compositions of emulsifying agents.

One may take any pair of emulsifying agents, which fall at opposite ends of the HLB scale, e.g. Tween 80 (sorbitan monooleate with 20 mol EO, HLB = 15) and Span 80 (sorbitan monooleate, HLB = 5), using them in various proportions to cover a wide range of HLB numbers. The emulsions should be prepared in the same way, with a few percent of the emulsifying blend. For example, a 20 % O/W emulsion is prepared by using 4 % emulsifier blend (20 % with respect to oil) and 76 % water. The stability of the emulsions is then assessed at each HLB number from the rate of coalescence or qualitatively by measuring the rate of oil separation. In this way one may be able to find the optimum HLB number for a given oil. For example with a given oil, the optimum HLB number is found to be 10.3. The latter can be determined more exactly by using mixtures of surfactants with narrower HLB range, say between 9.5 and 11. Having found the most effective HLB value, various other surfactant pairs are compared at this HLB value, to find the most effective pair. This is illustrated in Fig. 7.6 which schematically shows the difference between three chemical classes of surfactants. Although the different classes give a stable emulsion at HLB 12, mixture A gives the best emulsion stability.

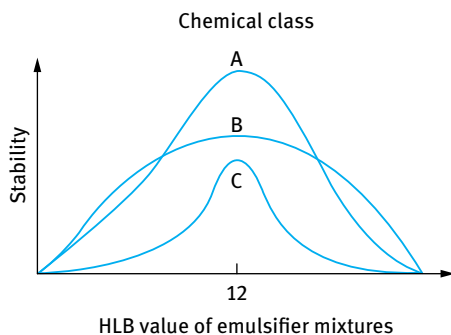


Fig. 7.6: Stabilization of emulsion by different classes of surfactants as a function of HLB.

The HLB value of a given magnitude can be obtained by mixing emulsifiers of different chemical types. The “correct” chemical type is as important as the “correct” HLB number. This is illustrated in Fig. 7.7, which shows that an emulsifier with unsaturated alkyl chain such as oleate (ethoxylated sorbitan monooleate, Tween 80) is more suitable for emulsifying an unsaturated oil [1–3]. An emulsifier with saturated alkyl chain (stearate in Tween 60) is better for emulsifying a saturated oil).

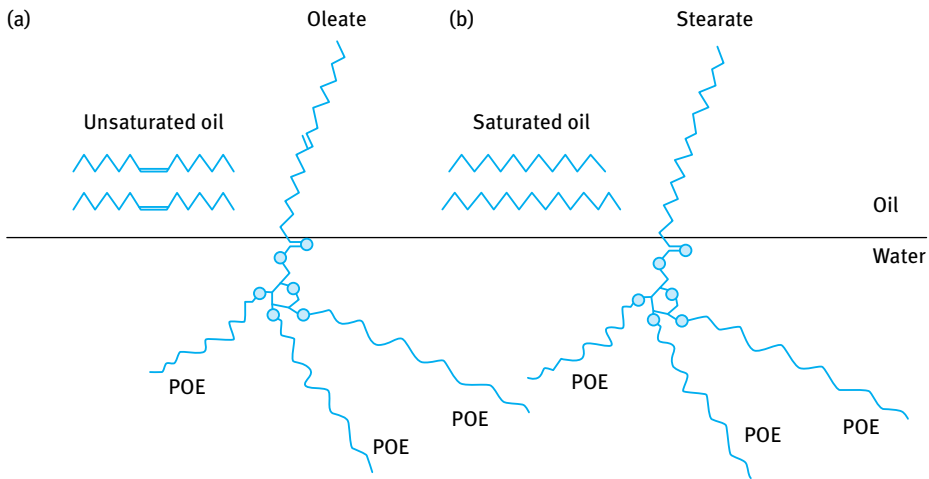


Fig. 7.7: Selection of Tween type to correspond to the type of the oil to be emulsified.

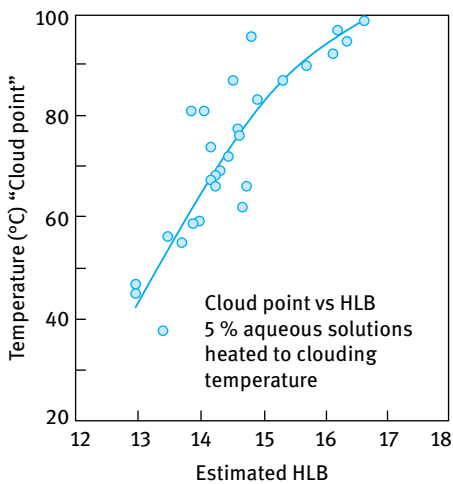


Fig. 7.8: Relationship between cloud point and HLB number.

Various procedures have been developed to determine the HLB of different surfactants. Griffin [8] found a correlation between the HLB and the cloud points of 5% aqueous solution of ethoxylated surfactants as illustrated in Fig. 7.8.

A titration procedure was developed [7] for estimating the HLB number. In this method, a 1% solution of surfactant in benzene plus dioxane is titrated with distilled water at constant temperature until a permanent turbidity appears. The researchers found a good linear relationship between the HLB number and the water titration value for polyhydric alcohol esters as shown in Fig. 7.9. However, the slope of the line depends on the class of material used.

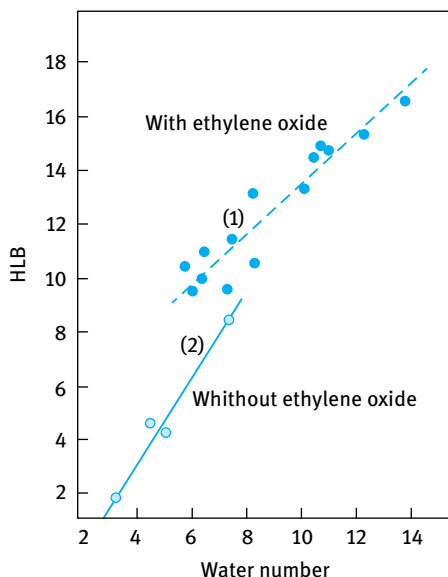


Fig. 7.9: Correlation of HLB with water number.

Gas liquid chromatography (GLC) could also be used to determine the HLB number [7]. Since in GLC the efficiency of separation depends on the polarity of the substrate with respect to the components of the mixture, it should be possible to determine the HLB directly by using the surfactant as the substrate and passing an oil phase down the column. Thus, when a 50 : 50 mixture of ethanol and hexane is passed down a column of a simple nonionic surfactant, such as sorbitan fatty acid esters and polyoxyethylated sorbitan fatty acid esters, two well defined peaks, corresponding to hexane (which appears first) and ethanol, appear on the chromatograms. A good correlation was found between the retention time ratio R_t (ethanol/hexane) and the HLB value. This is illustrated in Fig. 7.10. Statistical analysis of the data gave the following empirical

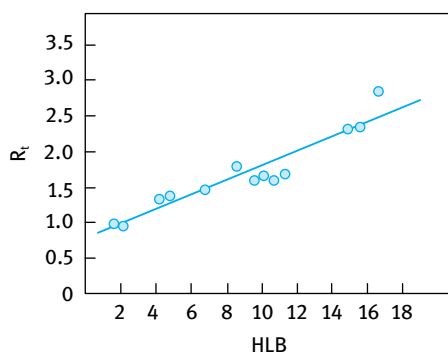


Fig. 7.10: Correlation between retention time and HLB of sorbitan fatty acid esters and polyoxyethylated fatty acid esters.

relationship between R_t and HLB,

$$\text{HLB} = 8.55R_t - 6.36, \quad (7.7)$$

$$R_t = \frac{R_t^{\text{ETOH}}}{R_t^{\text{hexane}}}. \quad (7.8)$$

7.4.2 The phase inversion temperature (PIT) concept

Shinoda and co-workers [11, 12] found that many O/W emulsions stabilized with non-ionic surfactants undergo a process of inversion at a critical temperature (PIT). The PIT can be determined by following the emulsion conductivity (small amount of electrolyte is added to increase the sensitivity) as a function of temperature as illustrated in Fig. 7.11. The conductivity of the O/W emulsion increases with increasing temperature until the PIT is reached, above which there will be a rapid reduction in conductivity (W/O emulsion is formed). Shinoda and co-workers [11, 12] found that the PIT is influenced by the HLB number of the surfactant as shown in Fig. 7.12. For any given oil, the PIT increases with increasing HLB number. The size of the emulsion droplets was found to depend on the temperature and HLB number of the emulsifiers. The droplets are less stable towards coalescence close to the PIT. However, by rapid cooling of the emulsion a stable system may be produced. Relatively stable O/W emulsions were obtained when the PIT of the system was 20–65 °C higher than the storage temperature. Emulsions prepared at a temperature just below the PIT followed by rapid cooling generally have smaller droplet sizes. This can be understood if one considers the change of interfacial tension with temperature as illustrated in Fig. 7.13. The interfacial tension decreases with increasing temperature, reaching a minimum close to the PIT, after which it increases.

Thus, the droplets prepared close to the PIT are smaller than those prepared at lower temperatures. These droplets are relatively unstable towards coalescence near the PIT, but by rapid cooling of the emulsion one can retain the smaller size. This procedure may be applied to prepare mini- (nano)emulsions.

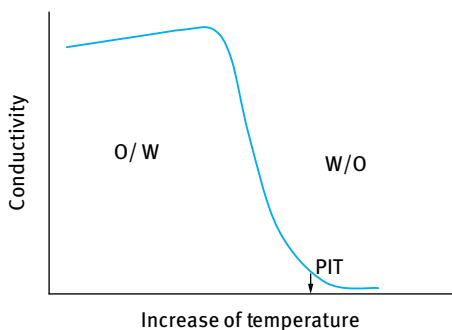


Fig. 7.11: Variation of conductivity with temperature for an O/W emulsion.

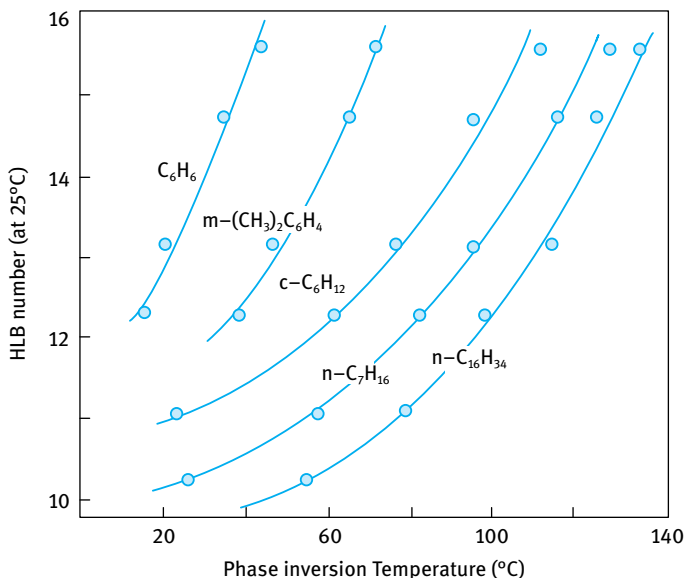


Fig. 7.12: Correlation between HLB number and PIT for various O/W (1:1) emulsions stabilized with nonionic surfactants (1.5 wt%).

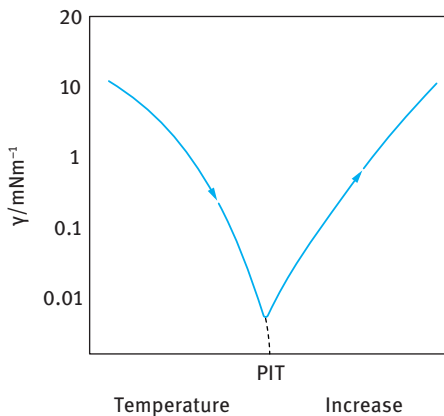


Fig. 7.13: Variation of interfacial tension with temperature increase for an O/W emulsion.

The optimum stability of the emulsion was found to be relatively insensitive to changes in the HLB value or the PIT of the emulsifier, but instability was very sensitive to the PIT of the system.

It is essential, therefore, to measure the PIT of the emulsion as a whole (with all other ingredients).

At a given HLB value, stability of the emulsion against coalescence increases markedly as the molar mass of both the hydrophilic and lipophilic components increases. The enhanced stability using high molecular weight surfactants (polymeric

surfactants) can be understood from a consideration of steric repulsion which produces more stable films. Films produced using macromolecular surfactants resist thinning and disruption, thus reducing the possibility of coalescence. The emulsions showed maximum stability when the distribution of the PEO chains was broad. The cloud point is lower but the PIT is higher than in the corresponding case for narrow size distributions. The PIT and HLB number are directly related parameters.

Addition of electrolytes reduces the PIT and hence an emulsifier with a higher PIT value is required when preparing emulsions in the presence of electrolytes. Electrolytes cause dehydration of the PEO chains and in effect this reduces the cloud point of the nonionic surfactant. One needs to compensate for this effect by using a surfactant with higher HLB. The optimum PIT of the emulsifier is fixed if the storage temperature is fixed.

In view of the above correlation between PIT and HLB and the possible dependence of the kinetics of droplet coalescence on the HLB number, Sherman and co-workers suggested the use of PIT measurements as a rapid method for assessing emulsion stability. However, one should be careful in using such methods for assessment of the long-term stability since the correlations were based on a very limited number of surfactants and oils.

Measurement of the PIT can at best be used as a guide for preparation of stable emulsions. Assessment of the stability should be evaluated by following the droplet size distribution as a function of time using a Coulter Counter or light diffraction techniques. Following the rheology of the emulsion as a function of time and temperature may also be used for assessment of the stability against coalescence. Care should be taken in analysing the rheological results. Coalescence results in an increase in droplet size and this is usually followed by a reduction in the viscosity of the emulsion. This trend is only observed if the coalescence is not accompanied by flocculation of the emulsion droplets (which results in an increase in the viscosity). Ostwald ripening can also complicate the analysis of the rheological data.

7.5 Mechanism of emulsification

This can be considered from a consideration of the energy required to expand the interface, $\Delta A\gamma$ (where ΔA is the increase in interfacial area when the bulk oil with area A_1 produces a large number of droplets with area A_2 ; $A_2 \gg A_1$ and γ is the interfacial tension). Since γ is positive, the energy to expand the interface is large and positive; this energy term cannot be compensated by the small entropy of dispersion $T\Delta S^{\text{conf}}$ (which is also positive) and the total free energy of formation of an emulsion, ΔG^{form} , given by equation (7.1) is positive. Thus, emulsion formation is non-spontaneous and energy is required to produce the droplets.

The formation of large droplets (few μm) as is the case for macroemulsions is fairly easy and hence high speed stirrers such as the Ultra-Turrax or Silverson Mixer are suffi-

cient to produce the emulsion. In contrast, the formation of small drops (submicron as is the case with nanoemulsions) is difficult and this requires a large amount of surfactant and/or energy. The high energy required for formation of nanoemulsions can be understood from a consideration of the Laplace pressure Δp (the difference in pressure between inside and outside the droplet) as given by equations (7.9) and (7.10),

$$\Delta p = \gamma \left(\frac{1}{r_1} + \frac{1}{r_2} \right), \quad (7.9)$$

where r_1 and r_2 are the two principal radii of curvature.

For a perfectly spherical droplet $r_1 = r_2 = r$ and

$$\Delta p = \frac{2\gamma}{r}. \quad (7.10)$$

To break up a drop into smaller ones, it must be strongly deformed and this deformation increases Δp . Consequently, the stress needed to deform the drop is higher for a smaller drop. Since the stress is generally transmitted by the surrounding liquid via agitation, higher stresses need more vigorous agitation, and hence more energy is needed to produce smaller drops.

Surfactants play major roles in the formation of emulsions [3–7]: By lowering the interfacial tension, Δp is reduced and hence the stress needed to break up a drop is reduced. Surfactants also prevent coalescence of newly formed drops (see below).

To describe emulsion formation one has to consider two main factors: hydrodynamics and interfacial science. In hydrodynamics one has to consider the type of flow: laminar flow and turbulent flow. This depends on the Reynolds number as will be discussed below.

To assess emulsion formation, one usually measures the droplet size distribution using for example laser diffraction techniques. If the number frequency of droplets as a function of droplet diameter d is given by $f(d)$, the n -th moment of the distribution is,

$$S_n = \int_0^{\infty} d^n f(d) \partial d. \quad (7.11)$$

The mean droplet size is defined as the ratio of selected moments of the size distribution,

$$d_{nm} = \left[\frac{\int_0^{\infty} d^n f(d) \partial d}{\int_0^{\infty} d^m f(d) \partial d} \right]^{1/(n-m)}, \quad (7.12)$$

where n and m are integers, $n > m$ and typically n does not exceed 4.

Using equation (7.12) one can define several mean average diameters:

- The Sauter mean diameter with $n = 3$ and $m = 2$,

$$d_{32} = \left[\frac{\int_0^{\infty} d^3 f(d) \partial d}{\int_0^{\infty} d^2 f(d) \partial d} \right]; \quad (7.13)$$

- The mass mean diameter,

$$d_{43} = \left[\frac{\int_0^{\infty} d^4 f(d) \partial d}{\int_0^{\infty} d^3 f(d) \partial d} \right]; \quad (7.14)$$

- The number mean diameter,

$$d_{10} = \left[\frac{\int_0^{\infty} d^1 f(d) \partial d}{\int_0^{\infty} f(d) \partial d} \right]. \quad (7.15)$$

In most cases d_{32} (the volume/surface average or Sauter mean) is used. The width of the size distribution can be given as the variation coefficient c_m , which is the standard deviation of the distribution weighted with d_m divided by the corresponding average d . Generally, C_2 will be used which corresponds to d_{32} .

Another is the specific surface area A (surface area of all emulsion droplets per unit volume of emulsion),

$$A = \pi S_2 = \frac{6\phi}{d_{32}}. \quad (7.16)$$

Surfactants lower the interfacial tension γ and this causes a reduction in droplet size. The latter decreases with decreasing γ . For laminar flow, the droplet diameter is proportional to γ ; for turbulent inertial regime, the droplet diameter is proportional to $\gamma^{3/5}$.

The surfactant can lower the interfacial tension γ_0 of a clean oil–water interface to a value γ and,

$$\pi = \gamma_0 - \gamma \quad (7.17)$$

where π is the surface pressure. The dependency of π on the surfactant activity a or concentration C is given by the Gibbs equation,

$$d\pi = -d\gamma = RT\Gamma d \ln a = RT\Gamma d \ln C, \quad (7.18)$$

where R is the gas constant, T is the absolute temperature and Γ is the surface excess (number of moles adsorbed per unit area of the interface).

At high a , the surface excess Γ reaches a plateau value; for many surfactants it is of the order of 3 mg m^{-2} . Γ increases with increasing surfactant concentration and eventually it reaches a plateau value (saturation adsorption). The value of C needed to obtain the same Γ is much smaller for the polymer when compared with the surfactant. In contrast, the value of γ reached at full saturation of the interface is lower for a surfactant (mostly in the region of $1\text{--}3 \text{ mN m}^{-1}$ depending on the nature of surfactant and oil) when compared with a polymer (with γ values in the region of $10\text{--}20 \text{ mN m}^{-1}$ depending on the nature of polymer and oil). This is due to the much closer packing of the small surfactant molecules at the interface when compared with the much larger polymer molecule that adopts tail-train-loop-tail conformation.

Another important role of the surfactant is its effect on the interfacial dilational modulus ε ,

$$\varepsilon = \frac{d\gamma}{d \ln A}. \quad (7.19)$$

ε is the absolute value of a complex quantity, composed of an elastic and viscous terms.

During emulsification an increase in the interfacial area A takes place and this causes a reduction in Γ . The equilibrium is restored by adsorption of surfactant from the bulk, but this takes time (less time at higher surfactant activity). Thus ε is small at small a and also at large a . Because of the lack or slowness of equilibrium with polymeric surfactants, ε will not be the same for expansion and compression of the interface.

In practice, emulsifiers are generally made of surfactant mixtures, often containing different components these have pronounced effects on γ and ε . Some specific surfactant mixtures give lower γ values than either of the two individual components. The presence of more than one surfactant molecule at the interface tends to increase ε at high surfactant concentrations. The various components vary in surface activity. Those with the lowest γ tend to predominate at the interface, but if present at low concentrations, it may take more time before reaching the lowest value. Polymer-surfactant mixtures may show some synergetic surface activity.

During emulsification, surfactant molecules are transferred from the solution to the interface and this leaves an ever lower surfactant activity [3–7]. Consider for example an O/W emulsion with a volume fraction $\phi = 0.4$ and a Sauter diameter $d_{32} = 1 \mu\text{m}$. According to equation (7.16), the specific surface area is $2.4 \text{ m}^2 \text{ ml}^{-1}$ and for a surface excess Γ of 3 mg m^{-2} , the amount of surfactant at the interface is 7.2 mg ml^{-1} emulsion, corresponding to 12 mg ml^{-1} aqueous phase (or 1.2%). Assuming that the concentration of surfactant, C_{eq} (the concentration left after emulsification), leading to a plateau value of Γ equals 0.3 mg ml^{-1} , then the surfactant concentration decreases from 12.3 to 0.3 mg ml^{-1} during emulsification. This implies that the effective γ value increases during the process. If insufficient surfactant is present to leave a concentration C_{eq} after emulsification, even the equilibrium γ value would increase.

Another aspect is that the composition of surfactant mixture in solution may alter during emulsification. If some minor components are present that give a relatively small γ value, this will predominate at a macroscopic interface, but during emulsification, as the interfacial area increases, the solution will soon become depleted of these components. Consequently, the equilibrium value of γ will increase during the process and the final value may be markedly larger than what is expected on the basis of the macroscopic measurement.

During droplet deformation, its interfacial area is increased. The drop will commonly have acquired some surfactant, and it may even have a Γ value close to the equilibrium at the prevailing (local) surface activity. The surfactant molecules may distribute themselves evenly over the enlarged interface by surface diffusion or by

spreading. The rate of surface diffusion is determined by the surface diffusion coefficient D_s that is inversely proportional to the molar mass of the surfactant molecule and also inversely proportional to the effective viscosity felt. D_s also decreases with increasing Γ . Sudden extension of the interface or sudden application of a surfactant to an interface can produce a large interfacial tension gradient and in such a case spreading of the surfactant can occur.

Surfactants allow the existence of interfacial tension gradients, which are crucial for formation of stable droplets. In the absence of surfactants (clean interface), the interface cannot withstand a tangential stress; the liquid motion will be continuous across a liquid interface.

If the γ -gradient can become large enough, it will arrest the interface [3–7]. The largest value attainable for $d\gamma$ equals about π_{eq} , i.e. $\gamma_0 - \gamma_{\text{eq}}$. If it acts over a small distance, a considerable stress can develop, of the order of 10 kPa.

Interfacial tension gradients are very important in stabilizing the thin liquid film between the droplets, which is very important during the beginning of emulsification when films of the continuous phase may be drawn through the disperse phase or when collision of the still large deformable drops causes the film to form between them. The magnitude of the γ -gradients and of the Marangoni effect depends on the surface dilational modulus ε , which for a plane interface with one surfactant-containing phase, is given by the expressions,

$$\varepsilon = \frac{-dy/d \ln \Gamma}{(1 + 2\xi + 2\xi^2)^{1/2}}, \quad (7.20)$$

$$\xi = \frac{dm_C}{d\Gamma} \left(\frac{D}{2\omega} \right)^{1/2}, \quad (7.21)$$

$$\omega = \frac{d \ln A}{dt}, \quad (7.22)$$

where D is the diffusion coefficient of the surfactant and ω represents a timescale (time needed for doubling the surface area) that is roughly equal to τ_{def} .

During emulsification, ε is dominated by the magnitude of the numerator in equation (7.20) because ξ remains small. The value of $dm_C/d\Gamma$ tends to go to very high values when Γ reaches its plateau value; ε goes to a maximum when m_C is increased. However, during droplet deformation Γ will always remain smaller. Taking reasonable values for the variables; $dm_C/d\Gamma = 10^2 - 10^4 \text{ m}^{-1}$, $D = 10^{-9} - 10^{-11} \text{ m}^2 \text{ s}^{-1}$ and $\tau_{\text{def}} = 10^{-2} - 10^{-6} \text{ s}$, $\xi < 0.1$ at all conditions. The same conclusion can be drawn for values of ε in thin films, e.g. between closely approaching drops. It may be concluded that for conditions that prevail during emulsification, ε increases with m_C and follows the relation,

$$\varepsilon \approx \frac{d\pi}{d \ln \Gamma}, \quad (7.23)$$

except for very high surfactant concentration, where π is the surface pressure ($\pi = \gamma_0 - \gamma$).

The presence of a surfactant means that during emulsification the interfacial tension need not be the same everywhere. This has two consequences:

- (i) the equilibrium shape of the drop is affected;
- (ii) any γ -gradient formed will slow down the motion of the liquid inside the drop (this diminishes the amount of energy needed to deform and break up the drop).

Another important role of the emulsifier is to prevent coalescence during emulsification. This is certainly not due to the strong repulsion between the droplets, since the pressure at which two drops are pressed together is much greater than the repulsive stresses. The counteracting stress must be due to the formation of γ -gradients. When two drops are pushed together, liquid will flow out from the thin layer between them, and the flow will induce a γ -gradient.

$$\tau_{\Delta\gamma} \approx \frac{2|\Delta\gamma|}{(1/2)d}. \quad (7.24)$$

The factor 2 follows from the fact that two interfaces are involved. Taking a value of $\Delta\gamma = 10 \text{ mN m}^{-1}$, the stress amounts to 40 kPa (which is of the same order of magnitude as the external stress). The stress due to the γ -gradient cannot as such prevent coalescence, since it only acts for a short time, but it will greatly slow down the mutual approach of the droplets. The external stress will also act for a short time, and it may well be that the drops move apart before coalescence can occur. The effective γ -gradient will depend on the value of ε as given by equation (7.24).

Closely related to the above mechanism is the Gibbs–Marangoni effect [13–15], schematically represented in Fig. 7.14. The depletion of surfactant in the thin film between approaching drops results in γ -gradient without liquid flow being involved. This results in an inward flow of liquid that tends to drive the drops apart. Such a mechanism would only act if the drops are insufficiently covered with surfactant (Γ below the plateau value), as occurs during emulsification.

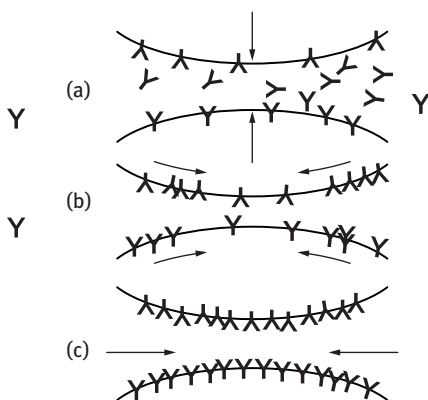


Fig. 7.14: Schematic representation of the Gibbs–Marangoni effect for two approaching drops.

The Gibbs–Marangoni effect also explains the Bancroft rule which states that the phase in which the surfactant is most soluble forms the continuous phase. If the surfactant is in the droplets, a γ -gradient cannot develop and the drops would be prone to coalescence. Thus, surfactants with $HLB > 7$ tend to form O/W emulsions and those with $HLB < 7$ tend to form W/O emulsions.

The Gibbs–Marangoni effect also explains the difference between surfactants and polymers for emulsification. Polymers give larger drops when compared with surfactants. Polymers give a smaller value of ε at small concentrations when compared to surfactants.

Various other factors should also be considered for emulsification, as will be discussed below: The disperse phase volume fraction ϕ since an increase in ϕ leads to an increase in droplet collision and hence coalescence during emulsification. With increasing ϕ , the viscosity of the emulsion increases and could change the flow from being turbulent to being laminar. The presence of many particles results in a local increase in velocity gradients. In turbulent flow, an increase in ϕ will induce turbulence depression (see below). This will result in larger droplets. Turbulence depression by adding polymers tends to remove the small eddies, resulting in the formation of larger droplets.

If the mass ratio of surfactant to continuous phase is kept constant, increasing ϕ results in a decrease in surfactant concentration and hence an increase in γ_{eq} resulting in larger droplets. If the mass ratio of surfactant to disperse phase is kept constant, the above changes are reversed.

7.6 Rheological properties of cosmetic emulsions

The rheological properties of a cosmetic emulsion that need to be achieved depend on the consumer perspective, which is very subjective. However, the efficacy and aesthetic qualities of a cosmetic emulsion are affected by their rheology. For example, with moisturizing creams one requires fast dispersion and deposition of a continuous protective oil film over the skin surface. This requires a shear thinning system (see below).

For characterization of the rheology of a cosmetic emulsion, one needs to combine several techniques, namely steady state, dynamic (oscillatory) and constant stress (creep) measurements [16–18]. A brief description of these techniques is given below.

In steady state measurements one measures the shear stress (τ)–shear rate ($\dot{\gamma}$) relationship using a rotational viscometer. A concentric cylinder or cone and plate geometry may be used depending on the emulsion consistency. Most cosmetic emulsions are non-Newtonian, usually pseudoplastic as illustrated in Fig. 7.15. In this case the viscosity decreases with applied shear rate (shear thinning behaviour in Fig. 7.15), but at very low shear rates the viscosity reaches a high limiting value (usually referred to as the residual or zero shear viscosity).

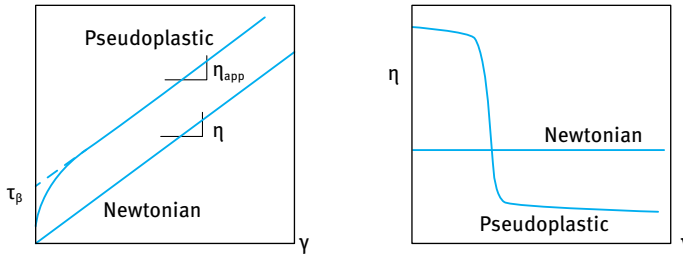


Fig. 7.15: Schematic representation of Newtonian and non-Newtonian (pseudoplastic) flow.

For the above pseudoplastic flow, one may apply a power law fluid model [12], a Bingham model [19] or a Casson model [20]. These models are represented by the following equations respectively,

$$\tau = \eta_{\text{app}} \gamma^n, \quad (7.25)$$

$$\tau = \tau_\beta + \eta_{\text{app}} \gamma, \quad (7.26)$$

$$\tau^{1/2} = \tau_c^{1/2} + \eta_c^{1/2} \gamma^{1/2}, \quad (7.27)$$

where n is the power in shear rate that is less than 1 for a shear thinning system (n is sometimes referred to as the consistency index), τ_β is the Bingham (extrapolated) yield value, η is the slope of the linear portion of the τ - γ curve, usually referred to as the plastic or apparent viscosity, τ_c is the Casson's yield value and η_c is the Casson's viscosity.

In dynamic (oscillator) measurements, a sinusoidal strain, with frequency ν in Hz or ω in rad s^{-1} ($\omega = 2\pi\nu$), is applied to the cup (of a concentric cylinder) or plate (of a cone and plate) and the stress is measured simultaneously on the bob or the cone which are connected to a torque bar. The angular displacement of the cup or the plate is measured using a transducer. For a viscoelastic system, such as is the case with a cosmetic emulsion, the stress oscillates with the same frequency as the strain, but out of phase [16]. This is illustrated in Fig. 7.16, which shows the stress and strain sine waves for a viscoelastic system. From the time shift between the sine waves of the stress and strain, Δt , the phase angle shift δ is calculated,

$$\delta = \Delta t \omega. \quad (7.28)$$

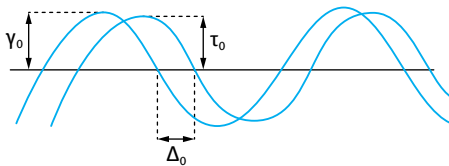


Fig. 7.16: Schematic representation of stress and strain sine waves for a viscoelastic system.

The complex modulus, G^* , is calculated from the stress and strain amplitudes (τ_0 and γ_0 respectively), i.e.,

$$G^* = \frac{\tau_0}{\gamma_0}. \quad (7.29)$$

The storage modulus, G' , which is a measure of the elastic component, is given by the following expression,

$$G' = |G^*| \cos \delta. \quad (7.30)$$

The loss modulus, G'' , which is a measure of the viscous component, is given by the following expression,

$$G'' = |G^*| \sin \delta, \quad (7.31)$$

and,

$$|G^*| = G' + iG'', \quad (7.32)$$

where i is equal to $(-1)^{-1/2}$.

The dynamic viscosity, η' , is given by the following expression,

$$\eta' = \frac{G''}{\omega}. \quad (7.33)$$

In dynamic measurements one carries out two separate experiments. Firstly, the viscoelastic parameters are measured as a function of strain amplitude, at constant frequency, in order to establish the linear viscoelastic region, where G^* , G' and G'' are independent of the strain amplitude. This is illustrated in Fig. 7.17, which shows the variation of G^* , G' and G'' with γ_0 . It can be seen that the viscoelastic parameters remain constant up to a critical strain value, γ_{cr} , above which, G^* and G' start to decrease and G'' starts to increase with any further increase in the strain amplitude. Most cosmetic emulsions produce a linear viscoelastic response up to appreciable strains ($>10\%$), indicative of structure build-up in the system (“gel” formation). If the system shows a short linear region (i.e., a low γ_{cr}), it indicates lack of a “coherent” gel structure (in many cases this is indicative of strong flocculation in the system).

Once the linear viscoelastic region is established, measurements are then made of the viscoelastic parameters, at strain amplitudes within the linear region, as a function of frequency. This is schematically illustrated in Fig. 7.18, which shows the variation of G^* , G' and G'' with ν or ω . It can be seen that below a characteristic frequency, ν^* or ω^* , $G'' > G'$. In this low frequency regime (long timescale), the system can dissipate energy as viscous flow. Above ν^* or ω^* , $G' > G''$, since in this high frequency

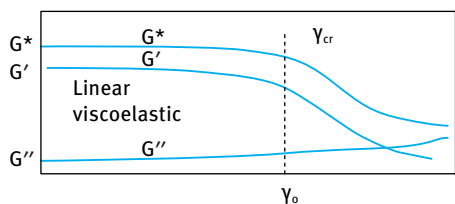


Fig. 7.17: Schematic representation of the variation of G^* , G' and G'' with strain amplitude (at a fixed frequency).

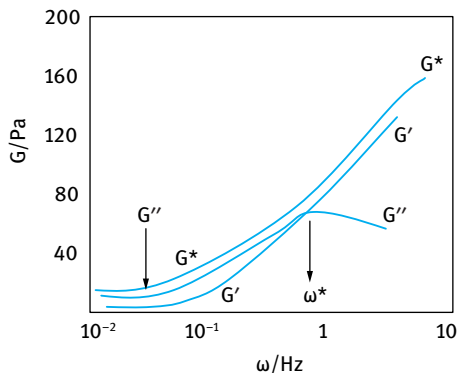


Fig. 7.18: Schematic representation of the variation of G^* , G' and G'' with ω for a viscoelastic system.

regime (short timescale) the system is able to store energy elastically. Indeed, at sufficiently high frequency G'' tends to zero and G' approaches G^* closely, showing little dependency on frequency.

The relaxation time of the system can be calculated from the characteristic frequency (the crossover point) at which $G' = G''$, i.e.,

$$t^* = \frac{1}{\omega^*}. \quad (7.34)$$

Many cosmetic emulsions behave as semi-solids with long t^* . They show only elastic response within the practical range of the instrument, i.e. $G' \gg G''$ and show low dependency on frequency. Thus, the behaviour of many emulsion creams is similar to many elastic gels. This is not surprising, since in most cosmetic emulsions systems, the volume fraction of the disperse phase is fairly high (usually > 0.5) and in many systems a polymeric thickener is added to the continuous phase for stabilizing the emulsion against creaming (or sedimentation) and to produce the right consistency for application.

In creep (constant stress) measurements [16], a stress τ is applied on the system and the deformation γ or the compliance $J = \gamma/\tau$ is followed as a function of time. A typical example of a creep curve is shown in Fig. 7.19. At $t = 0$, i.e. just after the application of the stress, the system shows a rapid elastic response characterized by an instantaneous compliance J_0 which is proportional to the instantaneous modulus G . Clearly at $t = 0$, all the energy is stored elastically in the system. At $t > 0$, the compliance shows a slow increase, since bonds are broken and reformed but at different rates. This retarded response is the mixed viscoelastic region. At sufficiently large timescales, that depend on the system, a steady state may be reached with a constant shear rate. In this region J shows a linear increase with time and the slope of the straight line gives the viscosity, η_τ , at the applied stress. If the stress is removed after the steady state is reached, J decreases and the deformation reverses sign, but only the elastic part is recovered. By carrying out creep curves at various stresses (starting from very low values depending on the instrument sensitivity), one can obtain the viscosity

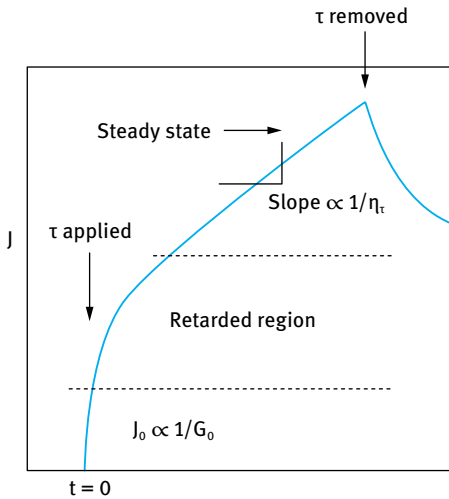


Fig. 7.19: Typical creep curve for a viscoelastic system.

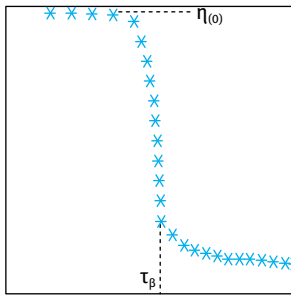


Fig. 7.20: Variation of viscosity with applied stress for a cosmetic emulsion.

of the emulsion at various stresses. A plot of η_τ versus τ shows the typical behaviour shown in Fig. 7.20. Below a critical stress, τ_β , the system shows a Newtonian region with a very high viscosity, usually referred to as the residual (or zero shear) viscosity. Above τ_β , the emulsion shows a shear thinning region and ultimately another Newtonian region with a viscosity that is much lower than $\eta(0)$ is obtained. The residual viscosity gives information on the stability of the emulsion on storage. The higher the value of $\eta(0)$ the lower the creaming or sedimentation of the emulsion. The high stress viscosity gives information on the applicability of the emulsion such as its spreading and film formation. The critical stress τ_β gives a measure of the true yield value of the system, which is an important parameter both for application purposes and the long-term physical stability of the cosmetic emulsion.

It is clear from the above discussion that rheological measurements of cosmetic emulsions are very valuable in determining the long-term physical stability of the system as well as its application. This subject has attracted considerable interest in recent years from many cosmetic manufacturers. Apart from its value in the above mentioned assessment, one of the most important considerations is to relate the rhe-

ological parameters to the consumer perception of the product. This requires careful measurement of the various rheological parameters for a number of cosmetic products and relating these parameters to the perception of expert panels who assess the consistency of the product, its skin feel, spreading, adhesion, etc. It is claimed that the rheological properties of an emulsion cream determine the final thickness of the oil layer, the moisturizing efficiency and its aesthetic properties such as stickiness, stiffness and oiliness (texture profile). Psychophysical models may be applied to correlate rheology with consumer perception and a new branch of psychorheology may be introduced.

References

- [1] Tadros T, editor. *Colloids in cosmetics and personal care*. Weinheim: Wiley-VCH; 2008.
- [2] Tadros T. *Cosmetics*. In: Tadros T, editor. *Encyclopedia of colloid and interface science*. Berlin: Springer; 2013.
- [3] Tadros T. *Formulations: In cosmetics and personal care*. Berlin: De Gruyter; 2016.
- [4] Walstra P, Smolders PEA. In: Binks BP, editor. *Modern aspects of emulsions*. Cambridge: The Royal Society of Chemistry; 1998.
- [5] Tadros T. *Applied surfactants*. Weinheim: Wiley-VCH; 2005.
- [6] Tadros T. *Emulsion formation stability and rheology*. In: Tadros T, editor. *Emulsion formation and stability*. Weinheim: Wiley-VCH; 2013. Chapter 1.
- [7] Tadros T. *Emulsions*. Berlin: De Gruyter; 2016.
- [8] Griffin WC. *J Cosmet Chemists*. 1949;1:311; 1954;5:249.
- [9] Davies JT. *Proc Int Congr Surface Activity*. 1959;1:426.
- [10] Davies JT, Rideal EK. *Interfacial phenomena*. New York: Academic Press; 1961.
- [11] Shinoda K. *J Colloid Interface Sci*. 1967;25:396.
- [12] Shinoda K, Saito H. *J Colloid Interface Sci*. 1969;30:258.
- [13] Lucassen-Reynders EH. *Colloids and Surfaces*. 1994;A91:79.
- [14] Lucassen J. In: Lucassen-Reynders EH, editor. *Anionic surfactants*. New York: Marcel Dekker; 1981.
- [15] van den Tempel M. *Proc Int Congr Surf Act*. 1960;2:573.
- [16] Tadros T. *Rheology of dispersions*. Weinheim: Wiley-VCH; 2010.
- [17] Tadros TF. *Rheological properties of emulsion systems*. In: Sjoblom J, editor. *Emulsions – A fundamental and practical approach*. NATO ASI Series, 363. London: Kluwer Academic Publishers; 1991.
- [18] Tadros TF. *Colloids and Surfaces*. 1994;91:39.
- [19] Bingham EC. *Fluidity and plasticity*. New York: McGraw Hill; 1922.
- [20] Casson N. In: Mill CC, editor. *Rheology of Disperse Systems*. New York; Pergamon Press; 1959. p. 84–104.

8 Nanoemulsions in cosmetics

8.1 Introduction

Nanoemulsions are transparent or translucent systems in the size range 20–200 nm [1, 2]. Whether the system is transparent or translucent depends on the droplet size, the volume fraction of the oil and the refractive index difference between the droplets and the medium. Nanoemulsions having diameters < 50 nm appear transparent when the oil volume fraction is < 0.2 and the refractive index difference between the droplets and the medium is not large. With increasing droplet diameter and oil volume fraction the system may appear translucent and at higher oil volume fractions the system may become turbid.

Nanoemulsions are only kinetically stable. They have to be distinguished from microemulsions (that cover the size range 5–50 nm) and are mostly transparent and thermodynamically stable. The long-term physical stability of nanoemulsions (with no apparent flocculation or coalescence) makes them unique and they are sometimes referred to as “approaching thermodynamic stability”. The inherently high colloid stability of nanoemulsions can be well understood from a consideration of their steric stabilization (when using nonionic surfactants and/or polymers) and how this is affected by the ratio of the adsorbed layer thickness to droplet radius as will be discussed below.

Unless adequately prepared (to control the droplet size distribution) and stabilized against Ostwald ripening (that occurs when the oil has some finite solubility in the continuous medium), nanoemulsions may show an increase in droplet size and an initially transparent system may become turbid on storage.

The attraction of nanoemulsions for applications in personal care and cosmetics is due to the following advantages [1]:

- (i) The very small droplet size causes a large reduction in the gravity force and the Brownian motion may be sufficient for overcoming gravity. This means that no creaming or sedimentation occurs on storage.
- (ii) The small droplet size also prevents any flocculation of the droplets. Weak flocculation is prevented and this enables the system to remain dispersed with no separation.
- (iii) The small droplets also prevent their coalescence, since these droplets are non-deformable and hence surface fluctuations are prevented. In addition, the significant surfactant film thickness (relative to droplet radius) prevents any thinning or disruption of the liquid film between the droplets.
- (iv) Nanoemulsions are suitable for efficient delivery of active ingredients through the skin. The large surface area of the emulsion system allows rapid penetration of actives.

- (v) Due to their small size, nanoemulsions can penetrate through the “rough” skin surface and this enhances penetration of actives.
- (vi) The transparent nature of the system, their fluidity (at reasonable oil concentrations) as well as the absence of any thickeners may give them a pleasant aesthetic character and skin feel.
- (vii) Unlike microemulsions (which require a high surfactant concentration, usually in the region of 20 % and higher), nanoemulsions can be prepared using reasonable surfactant concentration. For a 20 % O/W nanoemulsion, a surfactant concentration in the region of 5–10 % may be sufficient.
- (viii) The small size of the droplets allows them to deposit uniformly on substrates. Wetting, spreading and penetration may be also enhanced as a result of the low surface tension of the whole system and the low interfacial tension of the O/W droplets.
- (ix) Nanoemulsions can be applied for delivery of fragrances that may be incorporated in many personal care products. This could also be applied in perfumes, which are desirable to be formulated alcohol free.
- (x) Nanoemulsions may be applied as a substitute for liposomes and vesicles (which are much less stable) and it is possible in some cases to build lamellar liquid crystalline phases around the nanoemulsion droplets.

8.2 Colloid stability of nanoemulsions

The inherently high colloid stability of nanoemulsions when using nonionic or polymeric surfactants is due to their steric stabilization [3]. The latter arises from two main effects:

- (i) the unfavourable mixing of the surfactant or polymer chains, G_{mix} , which is positive when the stabilizing chains are in good solvent condition;
- (ii) loss of configurational entropy on considerable overlap of the adsorbed chain, this is referred to as the elastic interaction, G_{el} .

Combining G_{mix} and G_{el} with the van der Waals attraction, G_{A} , gives the total free energy of interaction, G_{T} . The variation of G_{mix} , G_{el} , G_{A} and G_{T} with separation distance between the droplets, h is illustrated in Fig. 8.1. The $G_{\text{T}}-h$ curve shows a shallow attractive minimum at separation distance comparable to twice the adsorbed layer thickness 2δ . This minimum decreases in magnitude as the ratio between adsorbed layer thickness to droplet size increases, as illustrated in Fig. 8.2. With nanoemulsions, the ratio of adsorbed layer thickness to droplet radius (δ/R) is relatively large (0.1–0.2) when compared with macroemulsions.

These systems approach thermodynamic stability against flocculation and/or coalescence. The very small size of the droplets and the dense adsorbed layers ensure lack of deformation of the interface, lack of thinning and disruption of the liquid film between the droplets and hence coalescence is also prevented.

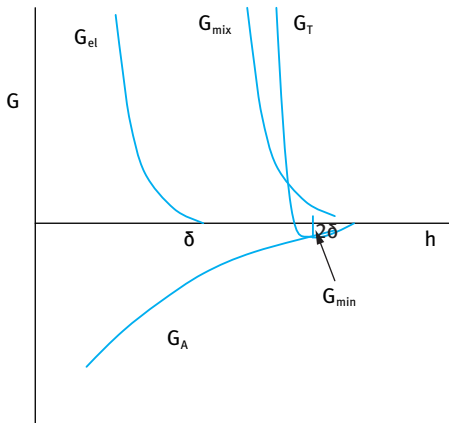


Fig. 8.1: Variation of the mixing interaction, G_{mix} , elastic interaction, G_{el} , van der Waals attraction, G_{A} , and total free energy of interaction, G_{T} , with droplet separation distance h .

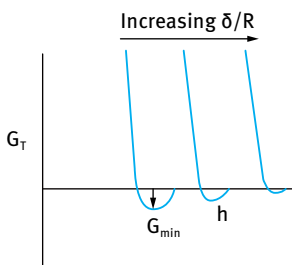


Fig. 8.2: Variation of the total free energy of interaction, G_{T} with droplet separation distance h .

One of the main problems with nanoemulsions is Ostwald ripening, which results from the difference in solubility between small and large droplets [4]. The difference in chemical potential of dispersed phase droplets between different sized droplets was given by Lord Kelvin,

$$c(r) = c(\infty) \exp\left(\frac{2\gamma V_{\text{m}}}{rRT}\right), \quad (8.1)$$

where $c(r)$ is the solubility surrounding a particle of radius r , $c(\infty)$ is the bulk phase solubility and V_{m} is the molar volume of the dispersed phase. The quantity $(2\gamma V_{\text{m}}/RT)$ is termed the characteristic length. It has an order of ≈ 1 nm or less, indicating that the difference in solubility of a $1\ \mu\text{m}$ droplet is of the order of 0.1 % or less.

Theoretically, Ostwald ripening should lead to condensation of all droplets into a single drop (i.e. phase separation). This does not occur in practice since the rate of growth decreases with increasing droplet size.

For two droplets of radii r_1 and r_2 (where $r_1 < r_2$),

$$\frac{RT}{V_m} \ln \left[\frac{c(r_1)}{c(r_2)} \right] = 2\gamma \left(\frac{1}{r_1} - \frac{1}{r_2} \right). \quad (8.2)$$

Equation (8.2) shows that the larger the difference between r_1 and r_2 , the higher the rate of Ostwald ripening.

Ostwald ripening can be quantitatively assessed from plots of the cube of the radius versus time t [4, 5],

$$r^3 = \frac{8}{9} \left[\frac{c(\infty)\gamma V_m}{\rho RT} \right] t, \quad (8.3)$$

where D is the diffusion coefficient of the disperse phase in the continuous phase.

Ostwald ripening can be reduced by incorporation of a second component which is insoluble in the continuous phase (e.g. squalane) [4–6]. In this case significant partitioning between different droplets occurs, with the component having low solubility in the continuous phase expected to be concentrated in the smaller droplets. During Ostwald ripening in a two component disperse phase system, equilibrium is established when the difference in chemical potential between different sized droplets (which results from curvature effects) is balanced by the difference in chemical potential resulting from partitioning of the two components. If the secondary component has zero solubility in the continuous phase, the size distribution will not deviate from the initial one (the growth rate is equal to zero). In the case of limited solubility of the secondary component, the distribution is the same as governed by equation (8.3), i.e. a mixture growth rate is obtained which is still lower than that of the more soluble component.

The above method is of limited application since one requires a highly insoluble oil as the second phase which is miscible with the primary phase.

Another method for reducing Ostwald ripening depends on modification of the interfacial film at the O/W interface [7]. According to equation (8.3), a reduction in γ results in a reduction in Ostwald ripening. However, this alone is not sufficient since one has to reduce γ by several orders of magnitude. It has been suggested that by using surfactants which are strongly adsorbed at the O/W interface (i.e. polymeric surfactants) and which do not desorb during ripening, the rate could be significantly reduced. An increase in the surface dilational modulus and decrease in γ would be observed for the shrinking drops. The difference in γ between the droplets would balance the difference in capillary pressure (i.e. curvature effects).

To achieve the above effect it is useful to use A–B–A block copolymers that are soluble in the oil phase and insoluble in the continuous phase. A strongly adsorbed polymeric surfactant that has limited solubility in the aqueous phase can also be used (e.g. hydrophobically modified inulin, INUTE[®] SP1 – ORAFTI, Belgium) [8, 9] as will be discussed below.

8.3 Preparation of nanoemulsions using high pressure homogenizers

The production of small droplets (submicron) requires application of high energy [1]; the process of emulsification is generally inefficient. Simple calculations show that the mechanical energy required for emulsification exceeds the interfacial energy by several orders of magnitude. For example to produce an emulsion at $\phi = 0.1$ with a volume to surface diameter (Sauter diameter) $d_{32} = 0.6 \mu\text{m}$, using a surfactant that gives an interfacial tension $\gamma = 10 \text{ mN m}^{-1}$, the net increase in surface free energy is $\Delta\gamma = 6\phi\gamma/d_{32} = 10^4 \text{ J m}^{-3}$. The mechanical energy required in a homogenizer is 10^7 J m^{-3} , i.e. an efficiency of 0.1%. The rest of the energy (99.9%) is dissipated as heat [1].

Before describing the methods that can be applied to prepare submicron droplets (nanoemulsions), it is essential to consider the thermodynamics of emulsion formation and breakdown, the role of the emulsifier in preventing coalescence during emulsification and the procedures that can be applied for selection of the emulsifier. This was described in detail in Chapter 7.

The mechanism of emulsification was described in detail in Chapter 7 and only a summary is given here. To prepare an emulsion oil, water, surfactant and energy are needed. This can be analysed from a consideration of the energy required to expand the interface, $\Delta A\gamma$ (where ΔA is the increase in interfacial area when the bulk oil with area A_1 produces a large number of droplets with area A_2 ; $A_2 \gg A_1$, γ is the interfacial tension). Since γ is positive, the energy to expand the interface is large and positive; this energy term cannot be compensated by the small entropy of dispersion $T\Delta S$ (which is also positive), and the total free energy of formation of an emulsion, ΔG , is positive. Thus, emulsion formation is non-spontaneous and energy is required to produce the droplets.

The formation of large droplets (few μm) as is the case for macroemulsions is fairly easy and hence high speed stirrers such as the Ultra-Turrax or Silverson Mixer are sufficient to produce the emulsion [1]. In contrast, the formation of small drops (submicron as is the case with nanoemulsions) is difficult and this requires a large amount of surfactant and/or energy. The high energy required for formation of nanoemulsions can be understood from a consideration of the Laplace pressure Δp (the difference in pressure between inside and outside the droplet),

$$\Delta p = \frac{2\gamma}{r}. \quad (8.4)$$

To break up a drop into smaller ones, it must be strongly deformed and this deformation increases Δp . Surfactants play major roles in the formation of emulsions: By lowering the interfacial tension, Δp is reduced and hence the stress needed to break up a drop is reduced. Surfactants also prevent coalescence of newly formed drops.

To describe emulsion formation one has to consider two main factors: hydrodynamics and interfacial science. In hydrodynamics one has to consider the type of flow: laminar flow and turbulent flow. This depends on the Reynolds number as will be discussed later.

To assess emulsion formation, one usually measures the droplet size distribution using for example laser diffraction techniques. A useful average diameter d is,

$$d_{nm} = \left(\frac{S_m}{S_n} \right)^{1/(n-m)}. \quad (8.5)$$

In most cases d_{32} (the volume/surface average or Sauter mean) is used. The width of the size distribution can be given as the variation coefficient c_m which is the standard deviation of the distribution weighted with d_m divided by the corresponding average d . Generally, C_2 will be used which corresponds to d_{32} .

An alternative way to describe the emulsion quality is to use the specific surface area A (surface area of all emulsion droplets per unit volume of emulsion),

$$A = \pi S^2 = \frac{6\phi}{d_{32}}. \quad (8.6)$$

Several procedures may be applied for emulsion preparation [1], these range from simple pipe flow (low agitation energy, L), static mixers and general stirrers (low to medium energy, L–M), high speed mixers such as the Ultra-Turrax (M), colloid mills and high pressure homogenizers (high energy, H), ultrasound generators (M–H). The method of preparation can be continuous (C) or batchwise (B): Pipe flow and static mixers – C; stirrers and Ultra-Turrax – B, C; colloid mill and high pressure homogenizers – C; ultrasound – B, C.

In all methods, there is liquid flow; unbounded and strongly confined flow. In unbounded flow any droplets is surrounded by a large amount of flowing liquid (the confining walls of the apparatus are far away from most of the droplets). The forces can be frictional (mostly viscous) or inertial. Viscous forces cause shear stresses to act on the interface between the droplets and the continuous phase (primarily in the direction of the interface). The shear stresses can be generated by laminar flow (LV) or turbulent flow (TV); this depends on the Reynolds number Re ,

$$Re = \frac{vl\rho}{\eta}, \quad (8.7)$$

where v is the linear liquid velocity, ρ is the liquid density and η is its viscosity. l is a characteristic length that is given by the diameter of flow through a cylindrical tube and by twice the slit width in a narrow slit.

For laminar flow $Re \lesssim 1000$, whereas for turbulent flow $Re \gtrsim 2000$. Thus whether the regime is linear or turbulent depends on the scale of the apparatus, the flow rate and the liquid viscosity [8–11].

If the turbulent eddies are much larger than the droplets, they exert shear stresses on the droplets. If the turbulent eddies are much smaller than the droplets, inertial forces will cause disruption (TI).

In bounded flow other relations hold. If the smallest dimension of the part of the apparatus in which the droplets are disrupted (say a slit) is comparable to droplet size, other relations hold (the flow is always laminar). A different regime prevails if the droplets are directly injected through a narrow capillary into the continuous phase (injection regime), i.e. membrane emulsification.

Within each regime, an essential variable is the intensity of the forces acting; the viscous stress during laminar flow σ_{viscous} is given by,

$$\sigma_{\text{viscous}} = \eta G, \quad (8.8)$$

where G is the velocity gradient.

The intensity in turbulent flow is expressed by the power density ε (the amount of energy dissipated per unit volume per unit time); for turbulent flow [11],

$$\varepsilon = \eta G^2. \quad (8.9)$$

The most important regimes are: laminar/viscous (LV) – turbulent/viscous (TV) – turbulent/inertial (TI). For water as the continuous phase, the regime is always TI. For higher viscosity of the continuous phase ($\eta_c = 0.1$ Pa s), the regime is TV. For still higher viscosity or a small apparatus (small l), the regime is LV. For very small apparatus (as is the case with most laboratory homogenizers), the regime is nearly always LV.

For the above regimes, a semi-quantitative theory is available that can give the timescale and magnitude of the local stress σ_{ext} , the droplet diameter d , timescale of droplets deformation τ_{def} , timescale of surfactant adsorption, τ_{ads} and mutual collision of droplets.

An important parameter that describes droplet deformation is the Weber number We (which gives the ratio of the external stress over the Laplace pressure),

$$We = \frac{G\eta_c R}{2\gamma}. \quad (8.10)$$

The viscosity of the oil plays an important role in the break-up of droplets; the higher the viscosity, the longer it will take to deform a drop. The deformation time τ_{def} is given by the ratio of oil viscosity to the external stress acting on the drop,

$$\tau_{\text{def}} = \frac{\eta_D}{\sigma_{\text{ext}}} \quad (8.11)$$

The viscosity of the continuous phase η_c plays an important role in some regimes: For the turbulent inertial regime, η_c has no effect on droplet size. For the turbulent viscous regime, larger η_c leads to smaller droplets. For the laminar viscous regime the effect is even stronger.

Surfactants lower the interfacial tension γ and this causes a reduction in droplet size. The latter decreases with decreasing γ . For laminar flow, the droplet diameter is proportional to γ ; for turbulent inertial regime, the droplet diameter is proportional to $\gamma^{3/5}$.

Another important role of the surfactant is its effect on the interfacial dilational modulus ε [12–15],

$$\varepsilon = \frac{d\gamma}{d \ln A} \quad (8.12)$$

During emulsification an increase in the interfacial area A takes place and this causes a reduction in Γ . The equilibrium is restored by adsorption of surfactant from the bulk, but this takes time (shorter times occur at higher surfactant activity). Thus ε is small at small a and also at large a . Because of the lack or slowness of equilibrium with polymeric surfactants, ε will not be the same for expansion and compression of the interface.

In practice, surfactant mixtures are used and these have pronounced effects on γ and ε . Some specific surfactant mixtures give lower γ values than either of the two individual components. The presence of more than one surfactant molecule at the interface tends to increase ε at high surfactant concentrations. The various components vary in surface activity. Those with the lowest γ tend to predominate at the interface, but if present at low concentrations, it may take a long time before reaching the lowest value. Polymer–surfactant mixtures may show some synergetic surface activity.

Apart for their effect on reducing γ , surfactants play major roles in deformation and break-up of droplets; this is summarized as follows. Surfactants allow the existence of interfacial tension gradients which are crucial for formation of stable droplets. In the absence of surfactants (clean interface), the interface cannot withstand a tangential stress; the liquid motion will be continuous

Interfacial tension gradients are very important in stabilizing the thin liquid film between the droplets, which is very important during the beginning of emulsification (films of the continuous phase may be drawn through the disperse phase and collision is very large). The magnitude of the γ -gradients and of the Marangoni effect depends on the surface dilational modulus ε given by equation (8.12).

For conditions that prevail during emulsification, ε increases with increasing surfactant concentration, m_C and it is given by the relationship,

$$\varepsilon = \frac{d\pi}{d \ln \Gamma}, \quad (8.13)$$

where π is the surface pressure ($\pi = \gamma_0 - \gamma$). Fig. 8.3 shows the variation of π with $\ln \Gamma$; ε is given by the slope of the line [16].

The SDS shows a much higher ε value when compared with β -casein and lysozyme. This is because the value of Γ is higher for SDS. The two proteins show differences in their ε values which may be attributed to the conformational changes that occur upon adsorption.

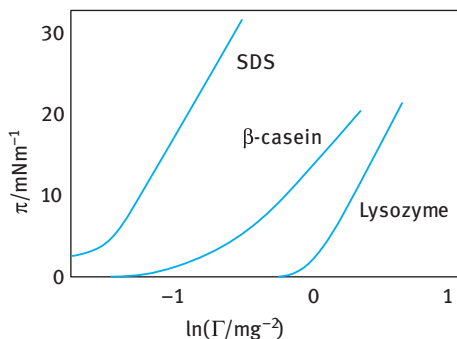


Fig. 8.3: π versus $\ln \Gamma$ for various emulsifiers.

Another important role of the emulsifier is to prevent coalescence during emulsification. This is certainly not due to the strong repulsion between the droplets, since the pressure at which two drops are pressed together is much greater than the repulsive stresses. The counteracting stress must be due to the formation of γ -gradients. When two drops are pushed together, liquid will flow out from the thin layer between them, and the flow will induce a γ -gradient. This produces a counteracting stress given by,

$$\tau_{\Delta\gamma} \approx \frac{2|\Delta\gamma|}{(1/2)d}. \quad (8.14)$$

The factor 2 follows from the fact that two interfaces are involved. Taking a value of $\Delta\gamma = 10 \text{ mN m}^{-1}$, the stress amounts to 40 kPa (which is of the same order of magnitude as the external stress).

Closely related to the above mechanism is the Gibbs–Marangoni effect [12–15], schematically represented in Fig. 8.4. The depletion of surfactant in the thin film between approaching drops results in γ -gradient without liquid flow being involved. This results in an inward flow of liquid that tends to drive the drops apart.

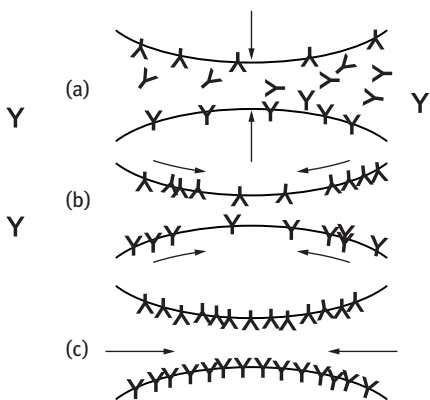


Fig. 8.4: Schematic representation of the Gibbs–Marangoni effect for two approaching drops.

The Gibbs–Marangoni effect also explains the Bancroft rule which states that the phase in which the surfactant is most soluble forms the continuous phase. If the surfactant is in the droplets, a γ -gradient cannot develop and the drops would be prone to coalescence. Thus, surfactants with $HLB > 7$ tend to form O/W emulsions and those with $HLB < 7$ tend to form W/O emulsions.

The Gibbs–Marangoni effect also explains the difference between surfactants and polymers for emulsification: Polymers give larger drops when compared with surfactants and polymers give a smaller value of ε at small concentrations when compared to surfactants (Fig. 8.3).

Various other factors should also be considered for emulsification: The disperse phase volume fraction ϕ since an increase in ϕ leads to an increase in droplet collision and hence coalescence during emulsification. With increasing ϕ , the viscosity of the emulsion increases and could change the flow from being turbulent to being laminar (LV regime).

The presence of many particles results in a local increase in velocity gradients. This means that G increases. In turbulent flow, an increase in ϕ will induce turbulence depression. This will result in larger droplets. Turbulence depression by adding polymers tends to remove the small eddies, resulting in the formation of larger droplets.

If the mass ratio of surfactant to continuous phase is kept constant, increasing ϕ results in decreasing surfactant concentration and hence an increase in γ_{eq} , resulting in larger droplets. If the mass ratio of surfactant to disperse phase is kept constant, the above changes are reversed.

General conclusions cannot be drawn since several of the above mentioned mechanism may come into play. Experiments using a high pressure homogenizer at various ϕ values at constant initial mC (regime TI changing to TV at higher ϕ) showed that with increasing ϕ (> 0.1) the resulting droplet diameter increased and the dependency on energy consumption became weaker. Fig. 8.5 shows a comparison of the average droplet diameter versus power consumption using different emulsifying machines. It can be seen that the smallest droplet diameters were obtained when using the high pressure homogenizers.

The selection of different surfactants in the preparation of either O/W or W/O was described in detail in Chapter 7. Two methods can be used for selection of emulsifiers, namely the hydrophilic-lipophilic balance (HLB), the phase inversion temperature (PIT). These methods were described in detail in Chapter 7.

As mentioned above, emulsification combines the creation of fine droplets and their stabilization against coalescence. The emulsion droplets are created by premixing the lipophilic and hydrophilic phases. The coarse droplets are then finely dispersed in the μm range or even smaller by deforming and disrupting them at high specific energy. These droplets have to be stabilized against coalescence by using an efficient emulsifier. The latter must adsorb quickly at the oil/water interface to prevent droplet coalescence during emulsification. In most cases, a synergistic mixture of emulsifiers is used.

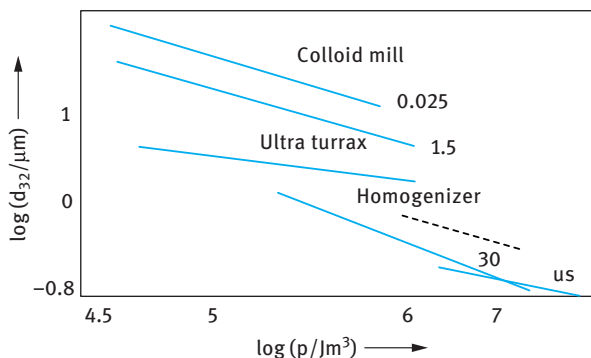


Fig. 8.5: Average droplet diameters obtained in various emulsifying machines as a function of energy consumption p . The number near the curves denotes the viscosity ratio λ . The results for the homogenizer are for $\phi = 0.04$ (solid line) and $\phi = 0.3$ (broken line) – us means ultrasonic generator.

In most cases, the nanoemulsion is produced in two stages, firstly by using a rotor-stator mixer (such as an Ultra-Turrax or Silverson) that can produce droplets in the μm range, followed by high pressure homogenization (reaching 3000 bar) to produce droplets in the nanometre size (as low as 50 nm).

The rotor-stator mixer consists of a rotating and fixed machine part [1]. Different geometries are available with various sizes and gaps between the rotor and stator. The simplest rotor stator machine is a vessel with a stirrer, which is used to produce the emulsion batchwise or quasicontinuously. The power density is relatively low and broadly distributed. Therefore, small mean droplet diameter ($< 1 \mu\text{m}$) can rarely be produced. In addition, a long residence time and emulsification for several minutes are required, often resulting in a broad droplet size distribution. Some of these problems can be overcome by reducing the disruption zone that enhances the power density, e.g. using colloid mills or toothed-disc dispersing machines.

To produce submicron droplets, high pressure homogenization is commonly used [1]. These homogenizers are operated continuously and throughputs up to several thousand litres per hour can be achieved. The homogenizer consists of essentially a high pressure pump, and a homogenization nozzle. The pump creates the pressure which is then transferred within the nozzle to kinetic energy that is responsible for droplet disintegration. The design of the homogenization nozzle influences the flow pattern of the emulsion in the nozzle and hence droplet disruption. A good example of efficient homogenization nozzles are the opposing jets that operate in the Microfluidizer. Other examples are the jet disperser (designed by Bayer) and the simple orifice valve. Droplet disruption in high pressure homogenizers is predominantly due to inertial forces in turbulent flow, shear forces in laminar elongational flow, as well as cavitation.

Droplets can also be disrupted by means of ultrasonic waves (frequency $> 18 \text{ kHz}$) which cause cavitation that induces micro-jets and zones of high microturbulence [1].

A batchwise operation at small scale has been applied in the laboratory, especially for low viscosity systems. Continuous application requires the use of a flow chamber of special design into which the ultrasound waves are introduced. Due to the limited power of sound inducers, there are technical limits for high throughput.

Another method that can be applied for droplet disintegration is the use of microchannel systems (membrane emulsification). This can be realized by pressing the disperse phase through microporous membrane pores [1]. Droplets are formed at the membrane surface and detached from it by wall shear stress of the continuous phase. Besides tubular membranes made from ceramics like aluminium oxide, special porous glasses and polymers like polypropylene, polytetrafluoroethylene (PTFE), nylon and silicon have been used. The membrane's surface wetting behaviour has a major influence; if the membrane is wetted by the continuous phase only, emulsions of very narrow droplet size distribution are produced with mean droplet sizes in the range of three times the mean droplet diameter of the pore. The pressure to be applied should ideally be a little above the capillary pressure. The membrane emulsification reduces the shear forces acting in droplet formation.

The droplets are disrupted if they are deformed over a period of time t_{def} that is longer than a critical deformation time $t_{\text{def,crit}}$ and if the deformation described by the Weber number We , equation (8.10), exceeds a critical value We_{cr} . The droplet-deforming tensions are supplied by the continuous phase.

In turbulent flow, the droplets are disrupted mostly by inertial forces that are generated by energy dissipating small eddies. Due to internal viscous forces the droplets try to regain their initial form and size. Two dimensionless numbers, the turbulent Weber number We_{turb} and the Ohnsorge number Oh , characterize the tensions working on droplets in deformation and break-up [17].

$$We_{\text{turb}} = \frac{C^2 P_v^{2/3} \rho_c^{1/3} x^{5/3}}{\gamma}, \quad (8.15)$$

$$Oh = \frac{\eta_d}{(\gamma \rho_d x)^{1/2}}. \quad (8.16)$$

C is a constant, P_v is the volumetric power density, ρ_c the continuous phase viscosity, ρ_d the droplet density and x is the droplet diameter.

The droplet disruption in laminar shear flow is restricted to a narrow range of viscosity ratio between the disperse phase and continuous phase (η_d/η_c) for single droplet disruption, or between the disperse phase and emulsion (η_d/η_e) for emulsions. For laminar shear flow,

$$x_{3,2} \propto E_v^{-1} f(\eta_d/\eta_e), \quad (8.17)$$

and for laminar elongational flow,

$$x_{3,2} \propto E_v^{-1}, \quad (8.18)$$

where E_v is the volumetric energy density or specific disruption energy.

Laminar elongational flow is successfully applied in innovative high pressure homogenization valves, where it adds to the effect of turbulent droplet disruption by predeforming the droplets. Thus, the droplet disruption efficiency of high pressure homogenization can be significantly increased, especially for droplets with high viscosities.

The intensity of the process or the effectiveness in making small droplets is often governed by the net power density ($\varepsilon(t)$).

$$p = \varepsilon(t) dt, \quad (8.19)$$

where t is the time during which emulsification occurs.

Break-up of droplets will only occur at high ε values, which means that the energy dissipated at low ε levels is wasted. Batch processes are generally less efficient than continuous processes. This shows why with a stirrer in a large vessel, most of the energy applied at low intensity is dissipated as heat. In a homogenizer, p is simply equal to the homogenizer pressure [4, 5].

Several procedures may be applied to enhance the efficiency of emulsification when producing nanoemulsions: One should optimize the efficiency of agitation by increasing ε and decreasing dissipation time. Furthermore, the emulsion is preferably prepared at high volume fraction ϕ of the disperse phase and diluted afterwards. However, very high ϕ values may result in coalescence during emulsification. Adding more surfactant would create a smaller γ_{eff} and possibly diminish recoalescence. Using a surfactant mixture that shows more reduction in γ the individual components is a further option. If possible, dissolve the surfactant in the disperse phase rather than the continuous phase; this often leads to smaller droplets. It may be useful to emulsify in steps of increasing intensity, particularly with emulsions having highly viscous disperse phase.

8.4 Low-energy methods for preparing nanoemulsions

The low-energy methods for preparing nanoemulsions are of particular interest, since they can make production more economical and offer the possibility to produce narrow droplet distribution nanoemulsions. In these methods, the chemical energy of the components is the key factor for the emulsification. The most well-known low-energy emulsification methods are direct or self-emulsification [18–20] and phase inversion methods [21–23]. Generally, emulsification by low-energy methods allows obtaining smaller and more uniform droplets.

In the so-called direct or self-emulsification methods, emulsification is achieved by a dilution process at a constant temperature, without any phase transitions (no change in the spontaneous curvature of the surfactant) taking place in the system during emulsification [18–20]. In this case, oil-in-water nanoemulsions (O/W) are obtained by the addition of water over a direct microemulsion phase, whereas water-in-

oil nanoemulsions (W/O) are obtained by the addition of oil over an indirect microemulsion phase. This method is described in detail below. This self-emulsification method uses the chemical energy of dissolution in the continuous phase of the solvent present in the initial system (which is going to constitute the disperse phase). When the intended continuous phase and the intended disperse phase are mixed, the solvent present in the later phase is dissolved into the continuous phase, dragging and dispersing the micelles of the initial system, thus giving rise to the nanoemulsion droplets.

Phase inversion methods make use of the chemical energy released during the emulsification process as a consequence of a change in the spontaneous curvature of surfactant molecules, from negative to positive (obtaining oil-in-water, O/W, nanoemulsions) or from positive to negative (obtaining water-in-oil, W/O, nanoemulsions). This change of the surfactant curvature can be achieved by a change in composition keeping the temperature constant (Phase Inversion Composition method, PIC) [21, 22], or by a rapid change in temperature with no variation in composition (phase inversion temperature method, PIT) [23]. The PIT method can only be applied to systems with surfactants sensitive to changes in temperature, i.e. the POE-type surfactants, in which changes in temperature induce a change in the hydration of the poly(oxyethylene) chains, and thus, a change of curvature [23, 24]. In the PIC method, the change in curvature is induced by the progressive addition of the intended continuous phase, which may be pure water or oil [21, 22], over the mixture of the intended disperse phase (oil or water and surfactant/s).

Studies on surfactant phase behaviour are important when the low-energy emulsification methods are used, since the phases involved during emulsification are crucial in order to obtain nanoemulsions with small droplet size and low polydispersity. In contrast, if shear methods are used, only phases present at the final composition are important.

8.4.1 Phase inversion composition (PIC) principle

A study of the phase behaviour of water/oil/surfactant systems demonstrated that emulsification can be achieved by three different low-energy emulsification methods, as schematically shown in Fig. 8.6.

- (A) Stepwise addition of oil to a water surfactant mixture.
- (B) Stepwise addition of water to a solution of the surfactant in oil.
- (C) Mixing all the components in the final composition, pre-equilibrating the samples prior to emulsification.

In these studies, the system water/Brij 30 (polyoxyethylene lauryl ether with an average of 4 mol of ethylene oxide)/decane was chosen as a model to obtain O/W emulsions. The results showed that nanoemulsions with droplet sizes of the order of 50 nm

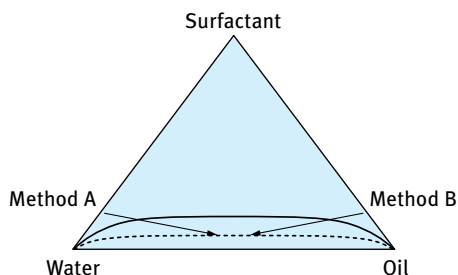


Fig. 8.6: Schematic representation of the experimental path in two emulsification methods: Method A, addition of decane to water/surfactant mixture; method B, addition of water to decane/Brij 30 solutions.

were formed only when water was added to mixtures of surfactant and oil (method B) whereby inversion from W/O emulsion to O/W nanoemulsion occurred.

8.4.2 Phase inversion temperature (PIT) principle

Phase inversion in emulsions can be one of two types: Transitional inversion induced by changing factors which affect the HLB of the system, e.g. temperature and/or electrolyte concentration or catastrophic inversion, which is induced by increasing the volume fraction of the disperse phase.

Transitional inversion can also be induced by changing the HLB number of the surfactant at constant temperature using surfactant mixtures. This is illustrated in Fig. 8.7 which shows the average droplet diameter and rate constant for attaining constant droplet size as a function of the HLB number. It can be seen that the diameter decreases and the rate constant increases as inversion is approached.

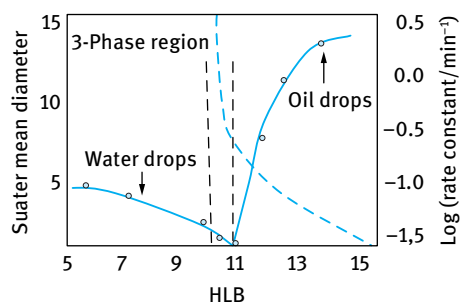


Fig. 8.7: Emulsion droplet diameters (circles) and rate constant for attaining steady size (squares) as function of HLB – cyclohexane/nonylphenol ethoxylate.

For application of the phase inversion principle one uses the transitional inversion method which has been demonstrated by Shinoda and co-workers [23, 24] using non-ionic surfactants of the ethoxylate type. These surfactants are highly dependent on temperature, becoming lipophilic with increasing temperature due to the dehydration of the polyethyleneoxide chain. When an O/W emulsion is prepared using a nonionic surfactant of the ethoxylate type and is heated, then at a critical temperature (the PIT),

the emulsion inverts to a W/O emulsion. At the PIT the droplet size reaches a minimum and the interfacial tension also reaches a minimum. However, the small droplets are unstable and they coalesce very rapidly. By rapid cooling of an emulsion prepared at a temperature near the PIT, very stable and small emulsion droplets could be produced.

A clear demonstration of the phase inversion that occurs on heating an emulsion is illustrated by a study of the phase behaviour of emulsions as a function of temperature. This is illustrated in Fig. 8.8, which schematically shows what happens when the temperature is increased [6, 25]. At low temperature, over the Winsor I region, O/W macroemulsions can be formed and are quite stable. On increasing the temperature, the O/W emulsion stability decreases and the macroemulsion finally resolves when the system reaches the Winsor III phase region (both O/W and W/O emulsions are unstable). At higher temperature, over the Winsor II region, W/O emulsions become stable.

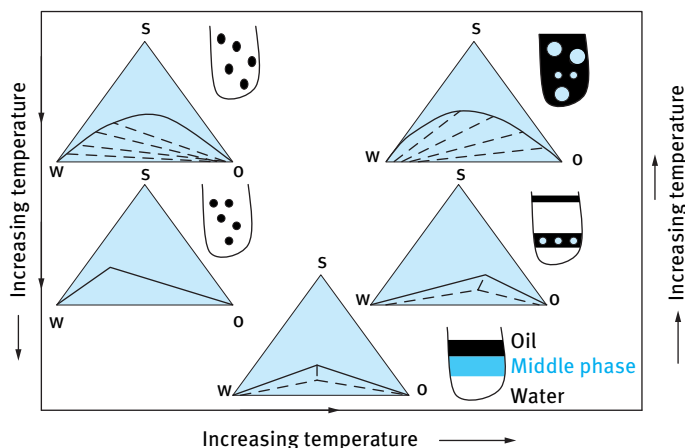


Fig. 8.8: The PIT concept.

Near the HLB temperature, the interfacial tension reaches a minimum. This is illustrated in Fig. 8.9. Thus, by preparing the emulsion at a temperature 2–4 °C below the PIT (near the minimum in γ) followed by rapid cooling of the system, nanoemulsions may be produced. The minimum in γ can be explained in terms of the change in curvature H of the interfacial region, as the system changes from O/W to W/O. For an O/W system and normal micelles, the monolayer curves towards the oil and H is given a positive value. For a W/O emulsion and inverse micelles, the monolayer curves towards the water and H is assigned a negative value. At the inversion point (HLB temperature) H becomes zero and γ reaches a minimum.

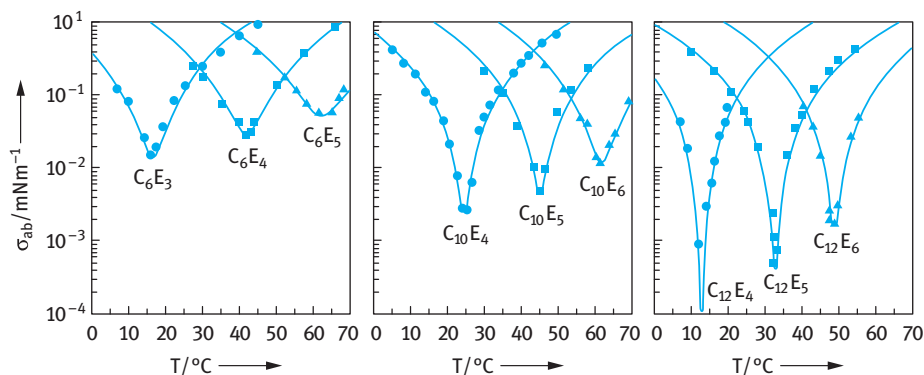


Fig. 8.9: Interfacial tensions of n-octane against water in the presence of various C_nE_m surfactants above the cmc as a function of temperature.

8.4.3 Preparation of nanoemulsions by dilution of microemulsions

A common way to prepare nanoemulsions by self-emulsification is to dilute an O/W microemulsion with water. When diluting a microemulsion with water, part of the surfactant and/or cosurfactant diffuses to the aqueous phase. The droplets are no longer thermodynamically stable, since the surfactant concentration is not high enough to maintain the ultra-low interfacial tension ($< 10^{-4} \text{ mN m}^{-1}$) for thermodynamic stability. The system becomes unstable and the droplets show a tendency to grow by coalescence and/or Ostwald ripening forming a nanoemulsion. This is illustrated in Fig. 8.10 which shows the phase diagram of the system water/SDS-Hexanol (ratio of 1:1.76)/dodecane.

Nanoemulsions can be prepared starting from microemulsions located in the inverse microemulsion domain, O_m , and in the direct microemulsion domain, W_m , at different oil:surfactant ratios ranging from 12:88 to 40:60, and coincident for both types of microemulsions. The water concentration is fixed at 20% for microemulsions in the O_m domain labelled as O_{m1} , O_{m2} , O_{m3} , O_{m4} , O_{m5} . The microemulsions in the W_m region are accordingly W_{m2} , W_{m3} , W_{m4} , W_{m5} and their water content decreases from W_{m2} to W_{m5} .

Several emulsification methods can be applied:

- addition of microemulsion into water in one step;
- addition of microemulsion into water stepwise;
- addition of water into microemulsion in one step;
- addition of water into microemulsion stepwise.

The final water content is kept constant at 98 wt%.

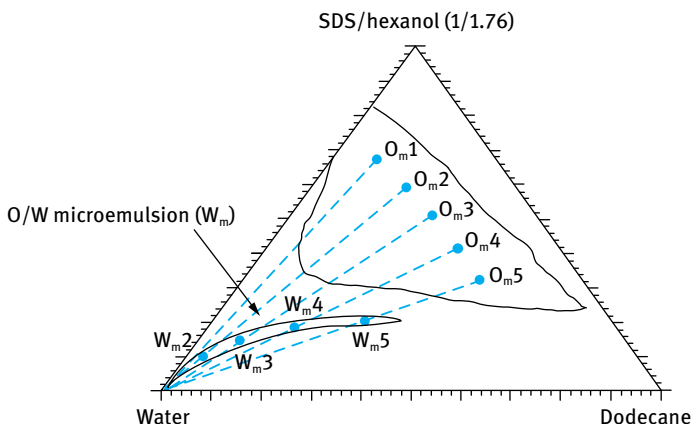


Fig. 8.10: Pseudoternary phase diagram of water/SDS/hexanol/dodecane with SDS : hexanol ratio of 1 : 1.76. Solid and dashed lines indicate the emulsification paths followed, starting from both O/W (W_m) and W/O (O_m) microemulsion domains.

Starting emulsification from W_m microemulsions, low-polydispersed nanoemulsions with droplet sizes within the range 20–40 nm are obtained regardless of the emulsification method used. When starting from O_m microemulsions, nanoemulsion formation and properties depend on the emulsification method. From an O_{m1} microemulsion, a turbid emulsion with rapid creaming is obtained whatever method is used. In this case the direct microemulsion region W_m is not crossed. Starting from O_{m2} to O_{m5} and using emulsification method (d), in which water is gradually added to the microemulsion, the nanoemulsion droplet sizes coincide with those obtained starting from microemulsions in the W_m domain for the corresponding O : S ratio. Methods (a), (b) and (c) produce coarse emulsions.

8.5 Preparation of nanoemulsions using the PIT technique

Experiments were carried out using hexadecane and isohexadecane (Arlamol HD) as the oil phase and Brij 30 ($C_{12}EO_4$) as the nonionic emulsifier [25]. The phase diagrams of the ternary system water– $C_{12}EO_4$ –hexadecane and water– $C_{12}EO_4$ –isohexadecane are shown in Fig. 8.11 and 8.12. The main features of the pseudoternary system are as follows:

- (i) O_m isotropic liquid transparent phase, which extends along the hexadecane– $C_{12}EO_4$ or isohexadecane– $C_{12}EO_4$ axis, corresponding to inverse micelles or W/O microemulsions;
- (ii) L_α lamellar liquid crystalline phase extending from the W– $C_{12}EO_4$ axis toward the oil vertex;

- (iii) the rest of the phase diagram consists of two- or three-phase regions:
- $(W_m + O)$ two-liquid-phase region, which appears along the water-oil axis;
 - $(W_m + L_\alpha + O)$ three-phase region, which consists of a bluish liquid phase (O/W microemulsion), a lamellar liquid crystalline phase (L_α) and a transparent oil phase;
 - $(L_\alpha + O_m)$ two-phase region consisting of an oil and liquid crystalline region;
 - MLC a multiphase region containing a lamellar liquid crystalline phase (L_α).

The HLB temperature was determined using conductivity measurements, whereby $10^{-2} \text{ mol dm}^{-3}$ NaCl was added to the aqueous phase (to increase the sensitivity of the conductivity measurements). The concentration of NaCl was low and hence it had little effect on the phase behaviour.

Fig. 8.13 shows the variation of conductivity versus temperature for 20% O/W emulsions at different surfactant concentrations. It can be seen that there is a sharp decrease in conductivity at the PIT or HLB temperature of the system.

The HLB temperature decreases with increasing surfactant concentration; this could be due to the excess nonionic surfactant remaining in the continuous phase. However, at a concentration of surfactant higher than 5%, the conductivity plots showed a second maximum (Fig. 8.13). This was attributed to the presence of L_α phase and bicontinuous L_3 or D' phases [25].

Nanoemulsions were prepared by rapid cooling of the system to 25 °C. The droplet diameter was determined using photon correlation spectroscopy (PCS). The results are

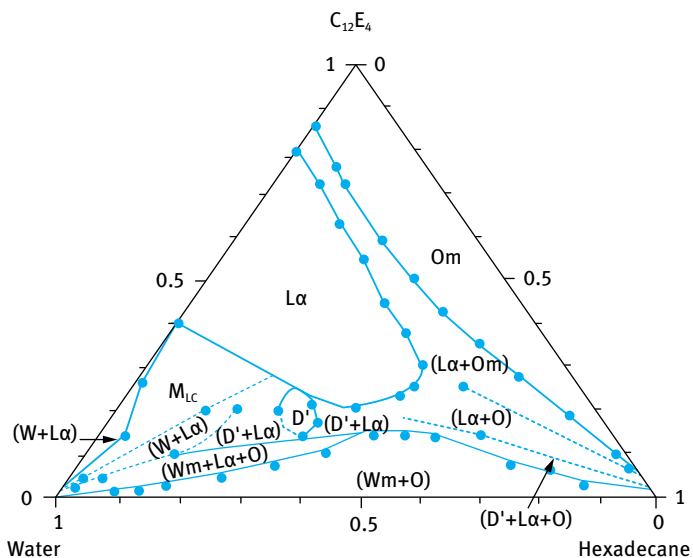


Fig. 8.11: Pseudoternary phase diagram at 25 °C of the system water– $C_{12}EO_4$ –hexadecane.

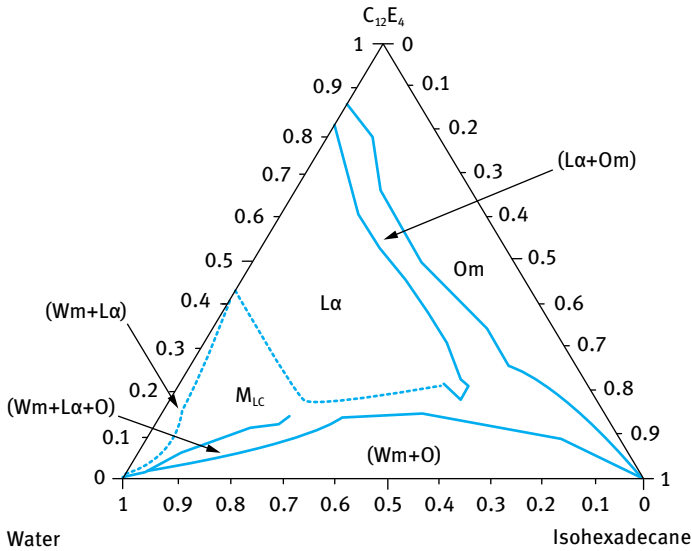


Fig. 8.12: Pseudoternary phase diagram at 25 °C of the system water– $C_{12}EO_4$ –iso-hexadecane.

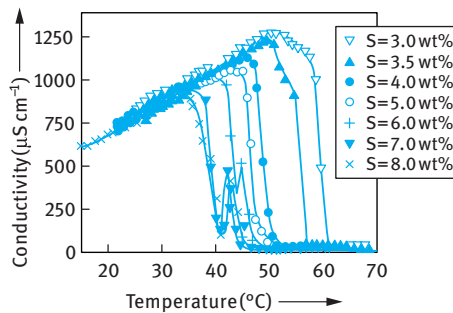


Fig. 8.13: Conductivity versus temperature for a 20 : 80 hexadecane : water emulsions at various $C_{12}EO_4$ concentrations.

summarized in Tab. 8.1, which shows the exact composition of the emulsions, HLB temperature, z-average radius and polydispersity index.

O/W nanoemulsions with droplet radii in the range 26–66 nm could be obtained at surfactant concentrations between 4 and 8 %. The nanoemulsion droplet size and polydispersity index decreases with increasing surfactant concentration. The decrease in droplet size with increasing surfactant concentration is due to the increase in surfactant interfacial area and decrease in interfacial tension, γ .

As mentioned above, γ reaches a minimum at the HLB temperature. Therefore, the minimum in interfacial tension occurs at lower temperature as the surfactant concentration increases. This temperature becomes closer to the cooling temperature as the surfactant concentration increases and this results in smaller droplet sizes.

Tab. 8.1: Composition, HLB temperature (T_{HLB}), droplet radius r and polydispersity index (pol.) for the system water–C₁₂EO₄–hexadecane at 25 °C.

Surfactant (wt%)	Water (wt%)	Oil/water	T_{HLB} (°C)	r (nm)	pol.
2.0	78.0	20.4/79.6	—	320	1.00
3.0	77.0	20.6/79.4	57.0	82	0.41
3.5	76.5	20.7/79.3	54.0	69	0.30
4.0	76.0	20.8/79.2	49.0	66	0.17
5.0	75.0	21.2/78.9	46.8	48	0.09
6.0	74.0	21.3/78.7	45.6	34	0.12
7.0	73.0	21.5/78.5	40.9	30	0.07
8.0	72.0	21.7/78.3	40.8	26	0.08

All nanoemulsions showed an increase in droplet size with time, as a result of Ostwald ripening. Fig. 8.14 shows plots of r^3 versus time for all the nanoemulsions studied. The slope of the lines gives the rate of Ostwald ripening ω ($\text{m}^3 \text{s}^{-1}$) and this showed an increase from 2×10^{-27} to $39.7 \times 10^{-27} \text{ m}^3 \text{ s}^{-1}$ as the surfactant concentration is increased from 4 to 8 wt%. This increase could be due to a number of factors:

- (i) decrease in droplet size increases the Brownian diffusion and this enhances the rate;
- (ii) presence of micelles, which increases with increasing surfactant concentration. This has the effect of increasing the solubilization of the oil into the core of the micelles. This results in an increase of the flux J of diffusion of oil molecules from different size droplets. Although the diffusion of micelles is slower than the diffusion of oil molecules, the concentration gradient ($\partial C/\partial X$) can be increased by orders of magnitude as a result of solubilization. The overall effect will be an increase in J and this may enhance Ostwald ripening;
- (iii) partition of surfactant molecules between the oil and aqueous phases. With higher surfactant concentrations, the molecules with shorter EO chains (lower HLB number) may preferentially accumulate at the O/W interface and this may result in reduction of the Gibbs elasticity, which in turn results in an increase in the Ostwald ripening rate.

The results with isohexadecane are summarized in Tab. 8.2. As with the hexadecane system, the droplet size and polydispersity index decreased with increasing surfactant concentration. Nanoemulsions with droplet radii of 25–80 nm were obtained at 3–8% surfactant concentration. It should be noted, however, that nanoemulsions could be produced at lower surfactant concentration when using isohexadecane, when compared with the results obtained with hexadecane. This could be attributed to the higher solubility of the isohexadecane (a branched hydrocarbon), the lower HLB temperature and the lower interfacial tension.

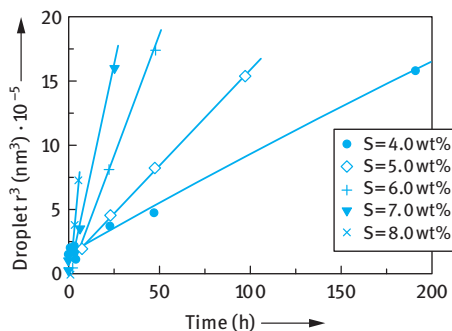


Fig. 8.14: r^3 versus time at 25°C for nanoemulsions prepared using the system water- $C_{12}EO_4$ -hexadecane.

Tab. 8.2: Composition, HLB temperature (T_{HLB}), droplet radius r and polydispersity index (pol.) at 25°C for emulsions in the system water- $C_{12}EO_4$ -isohexadecane.

Surfactant (wt%)	Water (wt%)	O/W	T_{HLB} (°C)	r (nm)	pol.
2.0	78.0	20.4/79.6	—	97	0.50
3.0	77.0	20.6/79.4	51.3	80	0.13
4.0	76.0	20.8/79.2	43.0	65	0.06
5.0	75.0	21.1/78.9	38.8	43	0.07
6.0	74.0	21.3/78.7	36.7	33	0.05
7.0	73.0	21.3/78.7	33.4	29	0.06
8.0	72.0	21.7/78.3	32.7	27	0.12

The stability of the nanoemulsions prepared using isohexadecane was assessed by following the droplet size as a function of time. Plots of r^3 versus time for four surfactant concentrations (3, 4, 5 and 6 wt%) are shown in Fig. 8.15.

The results show an increase in Ostwald ripening rate as the surfactant concentration is increased from 3 to 6% (the rate increased from 4.1×10^{-27} to $50.7 \times 10^{-27} \text{ m}^3 \text{ s}^{-1}$). The nanoemulsions prepared using 7 wt% surfactant was so unstable that they showed significant creaming after 8 hours. However, when the surfactant concentration was increased to 8 wt%, a very stable nanoemulsion could be produced with no apparent increase in droplet size over several months. This unexpected stability was attributed to the phase behaviour at such surfactant concentrations. The sample containing 8 wt% surfactant showed birefringence to shear when observed under polarized light. It seems that the ratio between the phases ($W_m + L_\alpha + O$) may play a key factor in nanoemulsion stability. Attempts were made to prepare nanoemulsions at higher O/W ratios (hexadecane being the oil phase), while keeping the surfactant concentration constant at 4 wt%. When the oil content was increased to 40 and 50%, the droplet radius increased to 188 and 297 nm respectively. In addition, the polydispersity index also increased to 0.95. These systems become so unstable that they showed creaming within few hours. This is not surprising, since the surfactant concentration is not sufficient to produce the nanoemulsion droplets

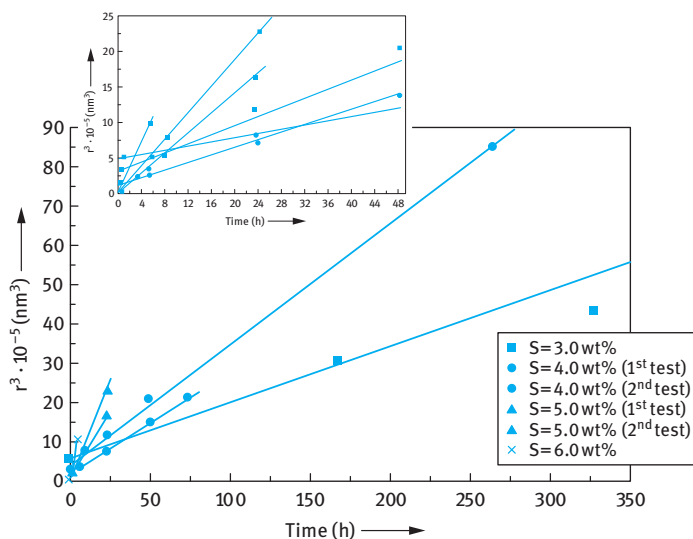


Fig. 8.15: r^3 versus time at 25 °C for the system water– $C_{12}EO_4$ –isohehexadecane at various surfactant concentration; O/W ratio 20/80.

with high surface area. Similar results were obtained with isohehexadecane. However, nanoemulsions could be produced using 30/70 O/W ratio (droplet size being 81 nm), but with high polydispersity index (0.28). the nanoemulsions showed significant Ostwald ripening.

The effect of changing the alkyl chain length and branching was investigated using decane, dodecane, tetradecane, hexadecane and isohehexadecane. Plots of r^3 versus time are shown in Fig. 8.16 for 20/80 O/W ratio and surfactant concentration of 4 wt%. As expected by reducing the oil solubility from decane to hexadecane, the rate of Ostwald ripening decreases. The branched oil isohehexadecane also show higher Ostwald ripening rate when compared with hexadecane. A summary of the results is shown in Tab. 8.3 which also shows the solubility of the oil $C(\infty)$.

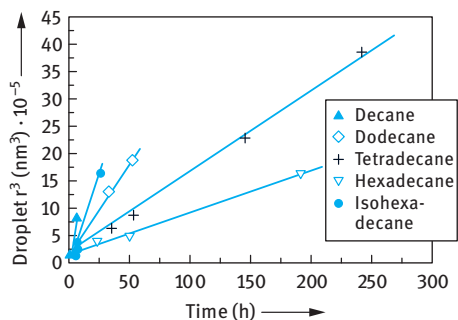


Fig. 8.16: r^3 versus time at 25 °C for nanoemulsions (O/W ratio 20/80) with hydrocarbons of various alkyl chain lengths. System water– $C_{12}EO_4$ –hydrocarbon (4 wt% surfactant).

Tab. 8.3: HLB temperature (T_{HLB}), droplet radius r , Ostwald ripening rate ω and oil solubility for nanoemulsions prepared using hydrocarbons with different alkyl chain length.

Oil	T_{HLB} (°C)	r (nm)	$\omega \times 10^{27}$ ($\text{m}^3 \text{s}^{-1}$)	$C(\infty)$ (ml ml^{-1})
Decane	38.5	59	20.9	710.0
Dodecane	45.5	62	9.3	52.0
Tetradecane	49.5	64	4.0	3.7
Hexadecane	49.8	66	2.3	0.3
Isohexadecane	43.0	60	8.0	—

As expected from Ostwald ripening theory, the rate of Ostwald ripening decreases as the oil solubility decreases. Isohexadecane has a rate of Ostwald ripening similar to that of dodecane.

As discussed before, one would expect that the Ostwald ripening of any given oil should decrease on incorporation of a second oil with much lower solubility. To test this hypothesis, nanoemulsions were made using hexadecane or isohexadecane to which various proportions of a less soluble oil, namely squalane, were added. The results using hexadecane did significantly decrease in stability on addition of 10 % squalane. This was thought to be due to coalescence rather than an increase in Ostwald ripening rate. In some cases, addition of a hydrocarbon with a long alkyl chain can induce instability as a result of change in the adsorption and conformation of the surfactant at the O/W interface.

In contrast to the results obtained with hexadecane, addition of squalane to the O/W nanoemulsion system based on isohexadecane showed a systematic decrease in Ostwald ripening rate as the squalane content was increased. The results are shown in Fig. 8.17 which shows plots of r^3 versus time for nanoemulsions containing varying amounts of squalane. Addition of squalane up to 20 % based on the oil phase showed a systematic reduction in the rate (from 8.0×10^{-27} to $4.1 \times 10^{-27} \text{ m}^3 \text{ s}^{-1}$). It should

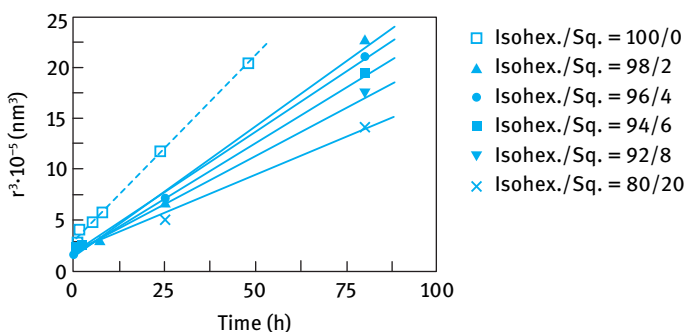


Fig. 8.17: r^3 versus time at 25 °C for the system water– C_{12}EO_4 –isohexadecane–squalane (20/80 O/W and 4 wt% surfactant).

be noted that when squalane alone was used as the oil phase, the system was very unstable and it showed creaming within 1 hour. This shows that the surfactant used is not suitable for emulsification of squalane.

The effect of HLB number on nanoemulsion formation and stability was investigated by using mixtures of $C_{12}EO_4$ (HLB = 9.7) and $C_{12}EO_6$ (HLB = 11.7). Two surfactant concentrations (4 and 8 wt%) were used and the O/W ratio was kept at 20/80. Fig. 8.18 shows the variation of droplet radius with HLB number. This figure shows that the droplet radius remain virtually constant in the HLB range 9.7–11.0, after which there is a gradual increase in droplet radius with increasing HLB number of the surfactant mixture. All nanoemulsions showed an increase in droplet radius with time, except for the sample prepared at 8 wt% surfactant with an HLB number of 9.7 (100 % $C_{12}EO_4$). Fig. 8.19 shows the variation of Ostwald ripening rate constant ω with HLB number of surfactant. The rate seems to decrease with increasing surfactant HLB number and when the latter is >10.5, the rate reaches a low value ($< 4 \times 10^{-27} \text{ m}^3 \text{ s}^{-1}$).

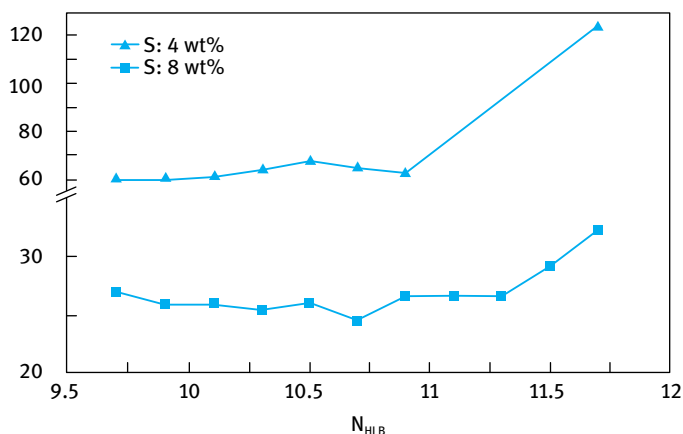


Fig. 8.18: r versus HLB number at two different surfactant concentrations (O/W ratio 20/80).

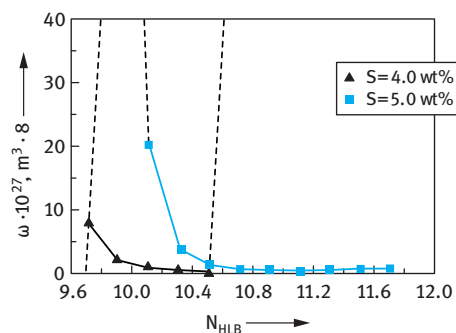


Fig. 8.19: ω versus HLB number in the system water- $C_{12}EO_4$ - $C_{12}EO_6$ -isohexadecane at two surfactant concentrations.

As discussed above, the incorporation of an oil-soluble polymeric surfactant that adsorbs strongly at the O/W interface would lead one to expect a reduction in the Ostwald ripening rate. To test this hypothesis, an A–B–A block copolymer of polyhydroxystearic acid (PHS, the A chains) and polyethylene oxide (PEO, the B chain) PHS–PEO–PHS (Arlacel P135) was incorporated in the oil phase at low concentrations (the ratio of surfactant to Arlacel was varied between 99 : 1 to 92 : 8). For the hexadecane system, the Ostwald ripening rate showed a decrease with the addition of Arlacel P135 surfactant at ratios lower than 94 : 6. Similar results were obtained using isohexadecane. However, at higher polymeric surfactant concentrations, the nanoemulsion became unstable.

As mentioned above, the nanoemulsions prepared using the PIT method are relatively polydisperse and they generally give higher Ostwald ripening rates when compared to nanoemulsions prepared using high pressure homogenization techniques. To test this hypothesis, several nanoemulsions were prepared using a Microfluidizer (that can apply pressures in the range 5000–15 000 psi or 350–1000 bar). Using an oil : surfactant ratio of 4 : 8 and O/W ratios of 20 : 80 and 50 : 50, emulsions were prepared first using the Ultra-Turrax followed by high pressure homogenization (ranging from 1500 to 15 000 psi). The best results were obtained using a pressure of 15 000 psi (one cycle of homogenization). The droplet radius was plotted versus the oil : surfactant ratio, $R(O/S)$ as shown in Fig. 8.20.

For comparison, the theoretical radii values calculated by assuming that all surfactant molecules are at the interface was calculated using the Nakajima equation [26, 27],

$$r = \left(\frac{3M_b}{AN\rho_a} \right) R + \left(\frac{3\alpha M_b}{AN\rho_b} \right) + d, \quad (8.20)$$

where M_b is the molecular weight of the surfactant, A is the area occupied by a single molecule, N is the Avogadro number, ρ_a is the oil density, ρ_b is the density of the

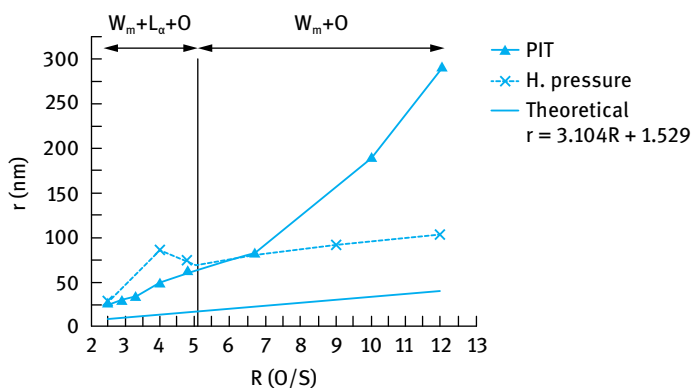


Fig. 8.20: r versus $R(O/S)$ at 25 °C for the system water– $C_{12}EO_4$ –hexadecane. W_m = micellar solution or O/W microemulsion, L_α = lamellar liquid crystalline phase; O = oil phase.

surfactant alkyl chain, α is the alkyl chain weight fraction and d is the thickness of the hydrated layer of PEO.

In all cases, there is an increase in nanoemulsion radius with increasing $R(O/S)$. However, when using the high pressure homogenizer, the droplet size can be maintained to values below 100 nm at high $R(O/S)$ values. With the PIT method, there is a rapid increase in r with increasing $R(O/S)$ when the latter exceeds 7.

As expected, the nanoemulsions prepared using high pressure homogenization showed a lower Ostwald ripening rate when compared to the systems prepared using the PIT method. This is illustrated in Fig. 8.21, which shows plots of r^3 versus time for the two systems.

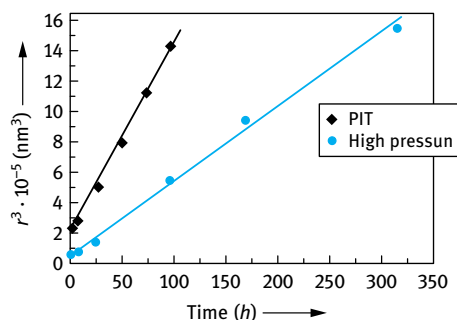


Fig. 8.21: r^3 versus time for nanoemulsion systems prepared using the PIT and Microfluidizer. 20 : 80 O/W and 4 wt% surfactant.

8.6 Nanoemulsions based on polymeric surfactants

The use of polymeric surfactants for preparing nanoemulsions is expected to significantly reduce Ostwald ripening due to the high interfacial elasticity produced by the adsorbed polymeric surfactant molecules [28]. To test this hypothesis, several nanoemulsions were formulated using a graft copolymer of hydrophobically modified inulin. The inulin backbone consists of polyfructose with a degree of polymerization > 23. This hydrophilic backbone is hydrophobically modified by attachment of several C_{12} alkyl chains [28]. The polymeric surfactant (with a trade name of INUTE[®] SP1) adsorbs with several alkyl chains that can be soluble in the oil phase or strongly attached to the oil surface, leaving the strongly hydrated hydrophilic polyfructose loops and tails “dangling” in the aqueous phase. These hydrated loops and tails (with a hydrodynamic thickness > 5 nm) provide effective steric stabilization.

Oil/water (O/W) nanoemulsions were prepared by two-step emulsification processes. In the first step, an O/W emulsion was prepared using a high speed stirrer, namely an Ultra-Turrax [1, 5]. The resulting coarse emulsion was subjected to high pressure homogenization using a Microfluidizer (Microfluidics, USA). In all cases, the pressure used was 700 bar and homogenization was carried out for 1 minute. The

Z-average droplet diameter was determined using PCS measurements as discussed before.

Fig. 8.22 shows plots of r^3 versus t for nanoemulsions of the hydrocarbon oils that were stored at 50 °C. It can be seen that paraffinum liquidum with both low and high viscosity gives almost a zero-slope, indicating absence of Ostwald ripening in this case. This is not surprising since both oils have very low solubility and the hydrophobically modified inulin, INUTEC® SP1, strongly adsorbs at the interface giving high elasticity that reduces both Ostwald ripening and coalescence. However, with the more soluble hydrocarbon oils, namely isohexadecane, there is an increase in r^3 with time, giving a rate of Ostwald ripening of $4.1 \times 10^{-27} \text{ m}^3 \text{ s}^{-1}$. The rate for this oil is almost three orders of magnitude lower than that obtained with a nonionic surfactant, namely laureth-4 (C₁₂-alkyl chain with 4 mol ethylene oxide) when stored at 50 °C. This clearly shows the effectiveness of INUTEC® SP1 in reducing Ostwald ripening. This reduction can be attributed to the enhancement of the Gibbs dilational elasticity [27] which results from the multipoint attachment of the polymeric surfactant with several alkyl groups to the oil droplets. This results in a reduction of the molecular diffusion of the oil from the smaller to the larger droplets.

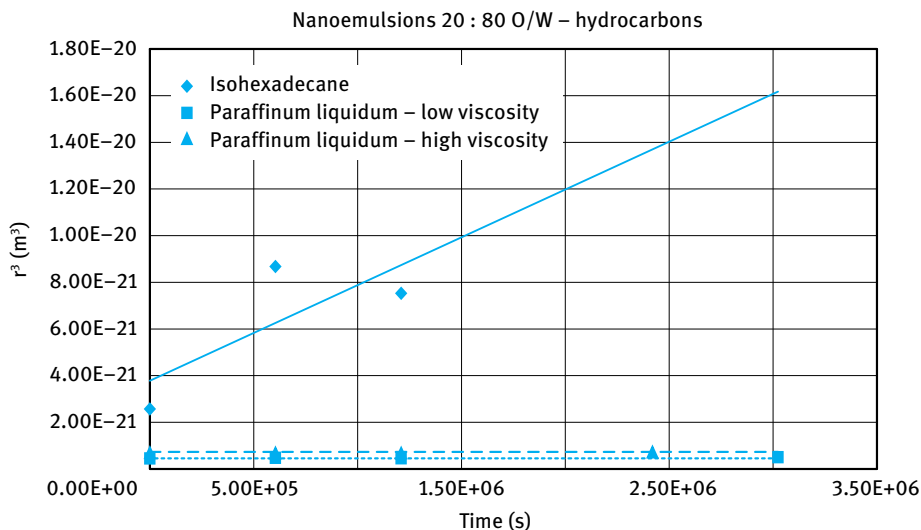


Fig. 8.22: r^3 versus t for nanoemulsions based on hydrocarbon oils.

Fig. 8.23 shows the results for the isopropylalkylate O/W nanoemulsions. As with the hydrocarbon oils, there is a significant reduction in the Ostwald ripening rate with increasing alkyl chain length of the oil. The rate constants are 1.8×10^{-27} , 1.7×10^{-27} and $4.8 \times 10^{-28} \text{ m}^3 \text{ s}^{-1}$ respectively.

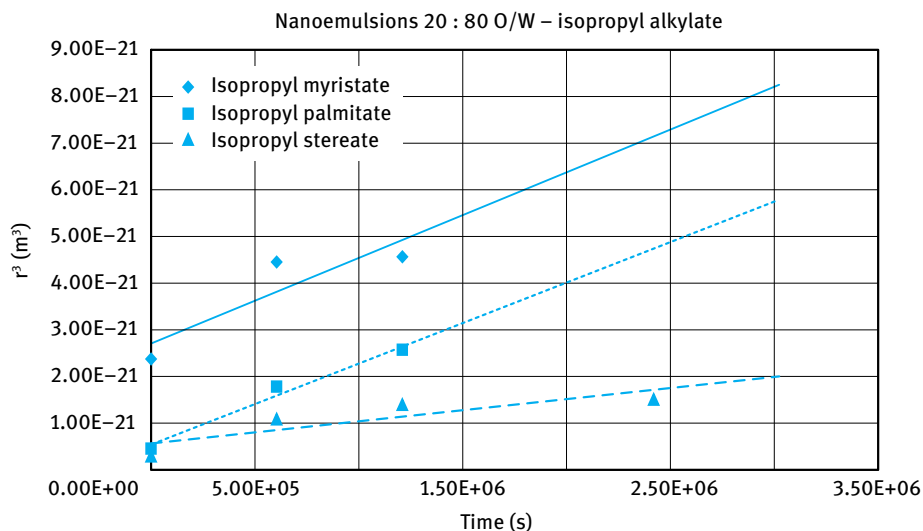


Fig. 8.23: r^3 versus t for nanoemulsions based on isopropylalkylate.

Fig. 8.24 shows the r^3-t plots for nanoemulsions based on natural oils. In all cases, the Ostwald ripening rate is very low. However, a comparison between squalene and squalane shows that rate is relatively higher for squalene (unsaturated oil) when compared with squalane (with lower solubility). The Ostwald ripening rate for these natural oils is given in Tab. 8.4.

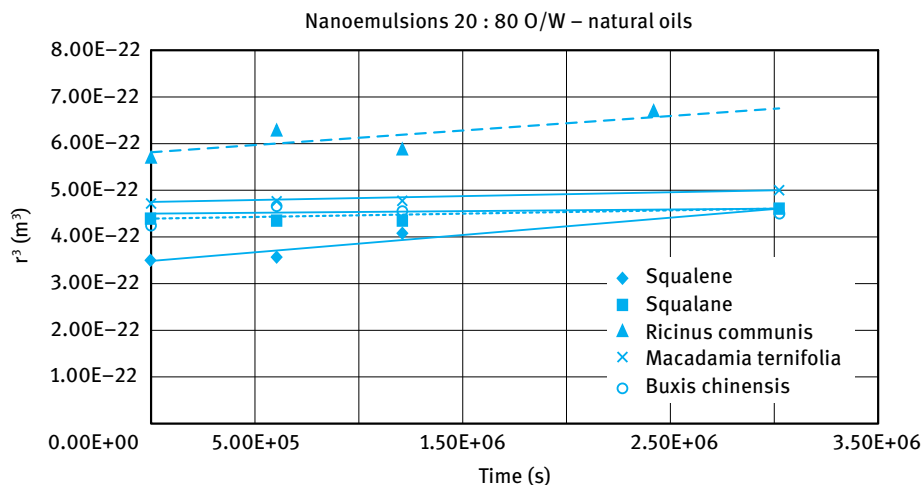


Fig. 8.24: r^3 versus t for nanoemulsions based on natural oils.

Tab. 8.4: Ostwald ripening rates for nanoemulsions based on natural oils.

Oil	Ostwald ripening rate ($\text{m}^3 \text{s}^{-1}$)
Squalene	2.9×10^{-28}
Squalane	5.2×10^{-30}
Ricinus communis	3.0×10^{-29}
Macadamia ternifolia	4.4×10^{-30}
Buxis chinensis	≈ 0

Fig. 8.25 shows the results based on silicone oils. Both dimethicone and phenyl trimethicone give an Ostwald ripening rate close to zero, whereas cyclopentasiloxane gives a rate of $5.6 \times 10^{-28} \text{ m}^3 \text{ s}^{-1}$.

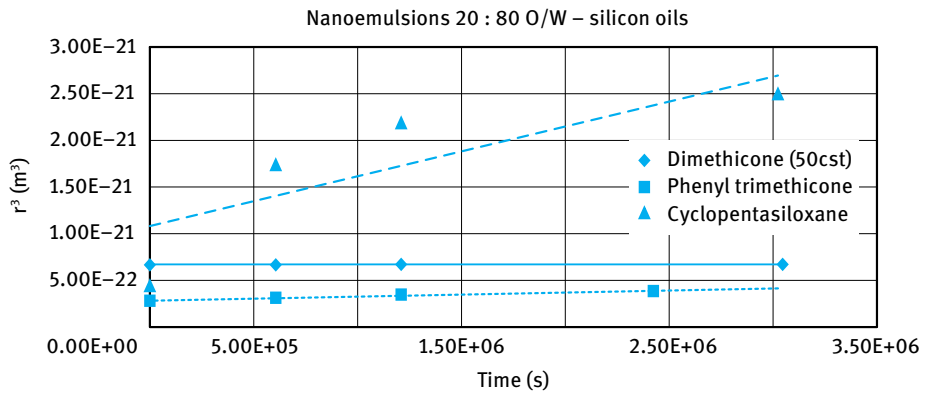
**Fig. 8.25:** r^3 versus t for nanoemulsions based on silicon oils.

Fig. 8.26 shows the results for nanoemulsions based on esters and the Ostwald ripening rates are given in Tab. 8.5. C_{12-15} alkylbenzoate seems to give the highest rate.

Tab. 8.5: Ostwald ripening rates for nanoemulsions based on esters.

Oil	Ostwald ripening rate ($\text{m}^3 \text{ s}^{-1}$)
Butyl stearate	1.8×10^{-28}
Caprylic capric triglyceride	4.9×10^{-29}
Cetearyl ethylhexanoate	1.9×10^{-29}
Ethylhexyl palmitate	5.1×10^{-29}
Cetearyl isononanoate	1.8×10^{-29}
C_{12-15} alkyl benzoate	6.6×10^{-28}

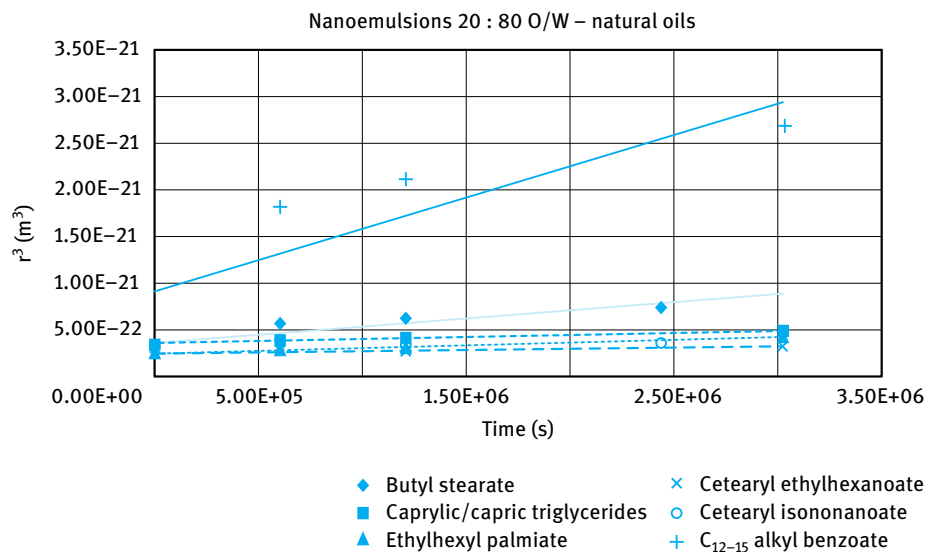


Fig. 8.26: r^3 versus t for nanoemulsions based on esters.

Fig. 8.27 gives a comparison for two nanoemulsions based on polydecene, a highly insoluble nonpolar oil and PPG-15 stearyl ether which is relatively more polar. Polydecene gives a low Ostwald ripening rate of $6.4 \times 10^{-30} \text{ m}^3 \text{ s}^{-1}$, which is one order of magnitude lower than that of PPG-15 stearyl ether ($5.5 \times 10^{-29} \text{ m}^3 \text{ s}^{-1}$).

The influence of adding glycerol (which is sometimes added to personal care formulations as a humectant) that can be used to prepare transparent nanoemulsions (by matching the refractive index of the oil and the aqueous phase) on the Ostwald ripening rate is shown in Fig. 8.28. With the more insoluble silicone oil, addition of

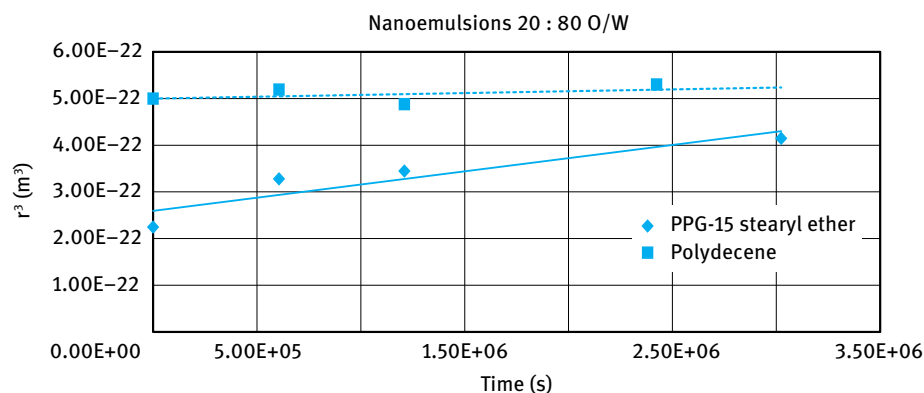


Fig. 8.27: r^3 versus t for nanoemulsions based on PPG-15 stearyl ether and polydecene.

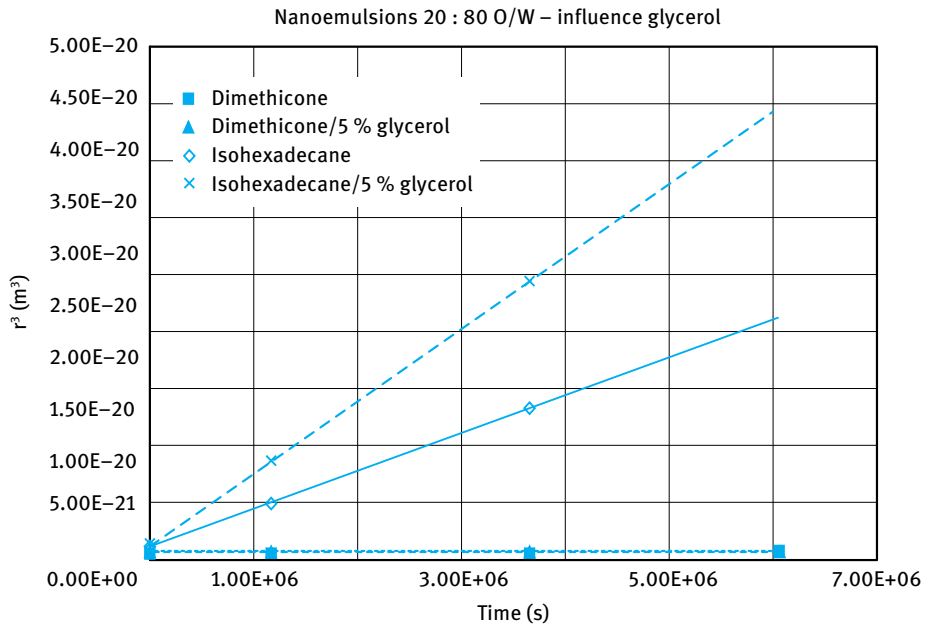


Fig. 8.28: Influence of glycerol on the Ostwald ripening rate of nanoemulsions.

5% glycerol does not show an increase in the Ostwald ripening rate, whereas for the more soluble isohexadecane oil, glycerol increases the rate.

It can be seen that hydrophobically modified inulin, HMI (INUTEC[®] SP1), reduces the Ostwald ripening rate of nanoemulsions when compared with nonionic surfactants such as laureth-4. This is due to the strong adsorption of INUTEC[®] SP1 at the oil–water interface (by multipoint attachment) and enhancement of the Gibbs dilational elasticity, both reducing the diffusion of oil molecules from the smaller to the larger droplets [7]. The present study also showed a big influence of the nature of the oil-phase with the more soluble and more polar oils giving the highest Ostwald ripening rate. However in all cases, when using INUTEC[®] SP1, the rates are reasonably low allowing one to use this polymeric surfactant in the formulation of nanoemulsions for personal care applications.

References

- [1] Tadros T. Nanodispersions. Berlin: De Gruyter; 2016.
- [2] Solans C, Izquierdo P, Nolla J, Azemar N, García-Celma M J. Nanoemulsions. *Current Opinion in Colloid & Interface Science*. 2005;10(3-4):102–110.
- [3] Tadros T, Izquierdo P, Esquena J, Solans C. Formation and stability of nanoemulsions. *Advances in Colloid and Interface Science*. 2004;108–109:303–318.

- [4] Thompson W (Lord Kelvin). *Phil Mag.* 1871;42:448.
- [5] Kabalnov AS, Schukin ED. *Adv Colloid Interface Sci.* 1992;38:69.
- [6] Kabalanov AS. *Langmuir.* 1994;10:680.
- [7] Walstra P. *Chem. Eng. Sci.* 1993;48:333.
- [8] Stone HA. *Ann Rev Fluid Mech.* 1994;226:95.
- [9] Wierenga JA, van Dieren F, Janssen JJM, Agterof WGM. *Trans Inst Chem Eng.* 1996;74-A:554.
- [10] Levich VG. *Physicochemical hydrodynamics.* Englewood Cliffs: Prentice-Hall; 1962.
- [11] Davis JT. *Turbulent phenomena.* London: Academic Press; 1972.
- [12] Lucassen-Reynders EH. In: Becher P, editor. *Encyclopedia of emulsion technology.* New York: Marcel Dekker; 1996.
- [13] Lucassen-Reynders EH. *Collids and Surfaces.* 1994;A91:79.
- [14] Lucassen J. In: Lucassen-Reynders EH, editor. *Anionic surfactants.* New York: Marcel Dekker; 1981.
- [15] van den Tempel M. *Proc Int Congr Surf Act.* 1960;2:573.
- [16] Walstra P, Smolders PEA. In: Binks BP, editor. *Modern aspects of emulsions.* Cambridge: The Royal Society of Chemistry; 1998.
- [17] Tadros T. *Emulsions.* Berlin: De Gruyter; 2016.
- [18] Ganachaud F, Katz JL. Nanoparticles and nanocapsules created using the ouzo effect: Spontaneous emulsification as an alternative to ultrasonic and high-shear devices. *Chem Phys Chem.* 2005;6:209–216.
- [19] Bouchemal K, Briançon S, Perrier E, Fessi H. Nanoemulsion formulation using spontaneous emulsification: Solvent, oil and surfactant optimisation. *Int J Pharm.* 2004;280:241–251.
- [20] Vitale SA, Katz JL, Liquid droplet dispersions formed by homogeneous liquid-liquid nucleation: “The ouzo effect”. *Langmuir.* 2003;19:4105–4110.
- [21] Forgiarini A, Esquena J, Gonzalez C, Solans C. Formation of nanoemulsions by low-energy emulsification methods at constant temperature. *Langmuir.* 2001;17(7):2076–2083.
- [22] Izquierdo P, Esquena J, Tadros T, Dederen C, Garcia MJ, Azemar N, Solans C. Formation and stability of nanoemulsions prepared using the phase inversion temperature method. *Langmuir.* 2002;18(1)26–30.8.
- [23] Shinoda K. *J Chem Soc Japan.* 1968;89:435.
- [24] Shinoda K, Saito H. *J Colloid Interface Sci.* 1969;30:258.
- [25] Izquierdo P. *Studies on nanoemulsion formation and stability [thesis].* University of Barcelona, Spain; 2002.
- [26] Nakajima H, Tomomossa S, Okabe M. *First Emulsion Conference.* Paris; 1993.
- [27] Nakajima H. In: Solans C, H. Konieda H, editors. *Industrial applications of microemulsions.* New York: Marcel Dekker; 1997.
- [28] Tadros T, editor. *Colloids in cosmetics and personal care.* Weinheim: Wiley-VCH; 2008.

9 Multiple emulsions in cosmetics

9.1 Introduction

Multiple emulsions are complex systems of “emulsions of emulsions” [1–3]. Two main types can be distinguished:

- (i) Water-in-oil-in-water (W/O/W) multiple emulsions in which the dispersed oil droplets contain emulsified water droplets;
- (ii) oil-in-water-in-oil (O/W/O) multiple emulsions in which the dispersed water droplets contain emulsified oil droplets.

The most commonly used multiple emulsions are the W/O/W which may be considered as water/water emulsions in which the internal water droplets are separated by an “oily layer” (membrane). The internal droplets could also consist of a polar solvent such glycol or glycerol which may contain a dissolved or dispersed active ingredient (AI). The O/W/O multiple emulsion can be considered as an oil/oil emulsion separated by an “aqueous layer” (membrane). Application of multiple emulsions in pharmacy for control and sustained release of drugs has been investigated over several decades using animal studies. The only successful application of multiple emulsions in industry is in the field of personal care and cosmetics. Products based on W/O/W systems have been introduced by several cosmetic companies.

Due to the oily liquid or aqueous membrane formed, multiple emulsions ensure complete protection of the entrapped active ingredient used in many cosmetic systems (e.g. anti-wrinkle agents) and controlled release of this active ingredient from the internal to the external phase. In addition, multiple emulsions offer several advantages such as protection of fragile ingredients, separation of incompatible ingredients, prolonged hydration of the skin and in some cases formation of a firm gelled structure. In addition, a pleasant skin feel like that of an O/W emulsion combined with the well-known moisturizing properties of W/O emulsions are obtained with W/O/W multiple emulsions. Multiple emulsions can be usefully applied for controlled release by controlling the rate of the breakdown process of the multiple emulsions on application. Initially, one prepares a stable multiple emulsion (with a shelf life of two years), which on application breaks down in a controlled manner thus releasing the active ingredient in a controlled manner (slow or sustained release).

For applications in personal care and cosmetics, a wider range of surfactants can be used provided these molecules satisfy some essential criteria such as lack of skin irritation, lack of toxicity on application and safety to the environment (biodegradability of the molecule is essential in this case).

9.2 Types of multiple emulsions

Florence and Whitehall [1] distinguish between three types of multiple emulsions (W/O/W) prepared using isopropyl microstate as the oil phase, 5% Span 80 to prepare the primary W/O emulsion and various surfactants to prepare the secondary emulsion:

- (A) Brij 30 (polyoxyethylene 4 lauryl ether) 2%.
- (B) Triton X-165 (polyoxyethylene (16.5) nonyl phenyl ether) 2%.
- (C) 3 : 1 Span 80 : Tween 80 mixtures.

A schematic picture of the three structures is shown in Fig. 9.1. Type A contains one large internal droplet similar to that described by Matsumoto et al. [2]. This type was produced when polyoxyethylene (4) lauryl ether (Brij 30) was used as emulsifier at 2%. Type B contains several small internal droplets. These were prepared using 2% polyoxyethylene (16.5) nonyl phenyl ether (Triton X-165). Type C drops entrap a very large number of small internal droplets. These were prepared using a 3 : 1 Span 80 : Tween 80 mixture. It should be mentioned that type A multiple emulsions are not encountered much in practice. Type C is difficult to prepare since a large number of small water internal droplets (which are produced in the primary emulsification process) results in a large increase in viscosity. Thus, the most common multiple emulsions used in practice are those of type B, whereby the large size multiple emulsion droplets (10–100 μm) contain water droplets $\approx 1 \mu\text{m}$.

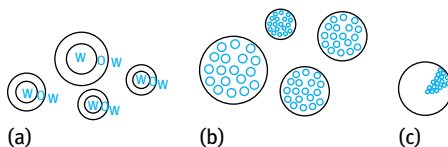


Fig. 9.1: Schematic representation of three structures of W/O/W multiple emulsions.

9.3 Breakdown processes of multiple emulsions

A schematic representation of some breakdown pathways that may occur in W/O/W multiple emulsions is shown in Fig. 9.2. One of the main instabilities of multiple emulsions is the osmotic flow of water from the internal to the external phase or vice versa [1, 2]. This leads to shrinkage or swelling of the internal water droplets respectively. This process assumes the oil layer to act as a semi-permeable membrane (permeable to water but not to solute). The volume flow of water, J_w , may be equated with the change of droplet volume with time dv/dt ,

$$J_w = \frac{dv}{dt} = -L_p A R T (g_2 c_2 - g_1 c_1). \quad (9.1)$$

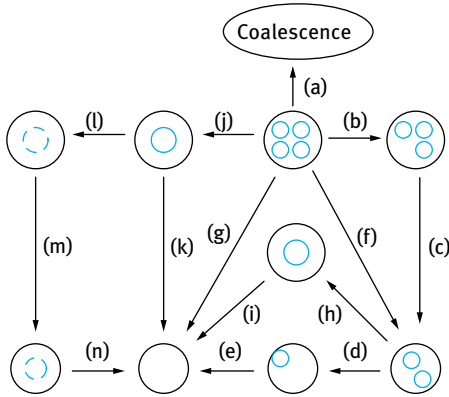


Fig. 9.2: Schematic representation of the possible breakdown pathways in W/O/W multiple emulsions: (a) coalescence; (b)–(e) expulsion of one or more internal aqueous droplets; (g) less frequent expulsion; (h), (i) coalescence of water droplets before expulsion; (j), (k) diffusion of water through the oil phase; (l)–(n) shrinking of internal droplets.

L_p is the hydrodynamic coefficient of the oil “membrane”, A is the cross-sectional area, R is the gas constant and T is the absolute temperature. g is the osmotic coefficient of electrolyte solution with concentration c .

The flux of water ϕ_W is,

$$\phi_W = \frac{J_W}{V_m}, \quad (9.2)$$

where V_m is the partial molar volume of water.

An osmotic permeability coefficient P_o can be defined,

$$P_o = \frac{L_p R T}{V_m}. \quad (9.3)$$

Combining equations (9.1)–(9.3),

$$\phi_W = -P_o A (g_2 c_2 - g_1 c_1). \quad (9.4)$$

The diffusion coefficient of water D_W can be obtained from P_o and the thickness of the diffusion layer Δx ,

$$-P_o = \frac{D_W}{\Delta x} \quad (9.5)$$

For isopropyl myristate W/O/W emulsions, $\Delta x \approx 8.2 \mu\text{m}$ and $D_W \approx 5.15 \times 10^{-8} \text{ cm}^2 \text{ s}^{-1}$, the value expected for diffusion of water in reverse micelles.

9.4 Preparation of multiple emulsions

Two main criteria are essential for the preparation of stable multiple emulsions:

- (i) Two emulsifiers with low and high HLB numbers. Emulsifier 1 should prevent coalescence of the internal water droplets, preferably producing a viscoelastic film which also reduces water transport. The secondary emulsifier should also produce an effective steric barrier at the O/W interface to prevent any coalescence of the multiple emulsion droplet.

- (ii) Optimum osmotic balance. This is essential to reduce water transport which is achieved by addition of electrolytes or nonelectrolytes. The osmotic pressure in the external phase should be slightly lower than that of the internal phase to compensate for curvature effects.

Four methods can be applied for preparing multiple emulsions [3] and these are summarized below.

9.4.1 The two-step process

Multiple emulsions are usually prepared in a two-stage process, which is the most widely used process. For example, a W/O/W multiple emulsion is formulated by first preparing a W/O emulsion using a surfactant with a low HLB number (5–6) using a high speed mixer (e.g. an Ultra-Turrax or Silverson). The resulting W/O emulsion is further emulsified in aqueous solution containing a surfactant with a high HLB number (9–12) using a low speed stirrer (e.g. a paddle stirrer). A schematic representation of the preparation of multiple emulsions is given in Fig. 9.3.

The W/O emulsion is prepared using a high speed stirrer (usually above 1500 rev/min) at high temperature (about 70 °C) for about 25–35 minutes until complete cooling. In the second emulsification process, the process is carried out at room temperature using low speed stirring (well below 500 rev/min) and the addition of the primary W/O emulsion to the aqueous solution of the high HLB surfactant should be carried out slowly (for about 1 hour). It is recommended to continue the slow speed stirring for about 20 minutes after complete addition of the primary emulsion to the aqueous solution of the high HLB surfactant.

The main advantage of the two-step process of preparing a multiple emulsion is the full control of the procedure. The main problem with this process is the possibility of having a highly viscous W/O emulsion (particularly at high volume fraction of the aqueous droplet) which is difficult to disperse in the aqueous solution of the high HLB surfactant. To overcome this problem, one can reduce the aqueous volume fraction in the primary emulsion.

The yield of the multiple emulsion can be determined using dialysis for W/O/W multiple emulsions. A water-soluble marker is used and its concentration in the outside phase is determined.

$$\% \text{ multiple emulsions} = \frac{C_i}{C_i + C_e} \times 100, \quad (9.6)$$

where C_i is the amount of marker in the internal phase and C_e is the amount of marker in the external phase. It has been suggested that if a yield more than 90 % is required, the lipophilic (low HLB) surfactant used to prepare the primary emulsion must be ≈ 10 times higher in concentration than the hydrophilic (high HLB) surfactant.

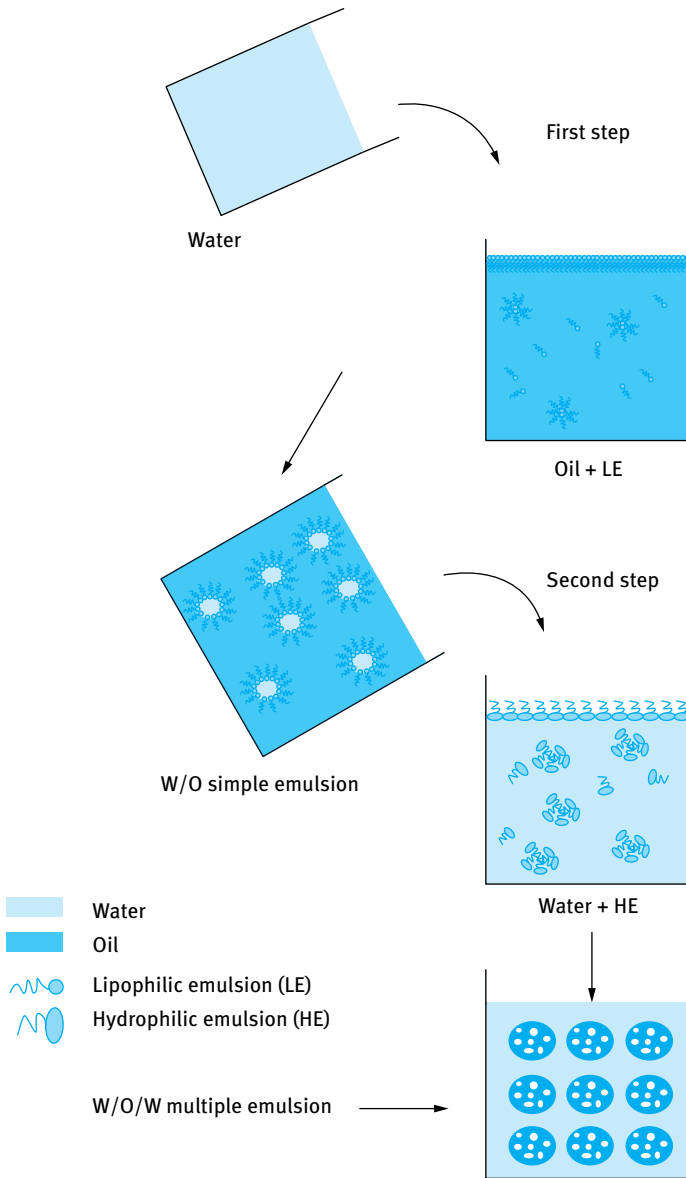


Fig. 9.3: Two-step method for preparing a W/O/W multiple emulsion.

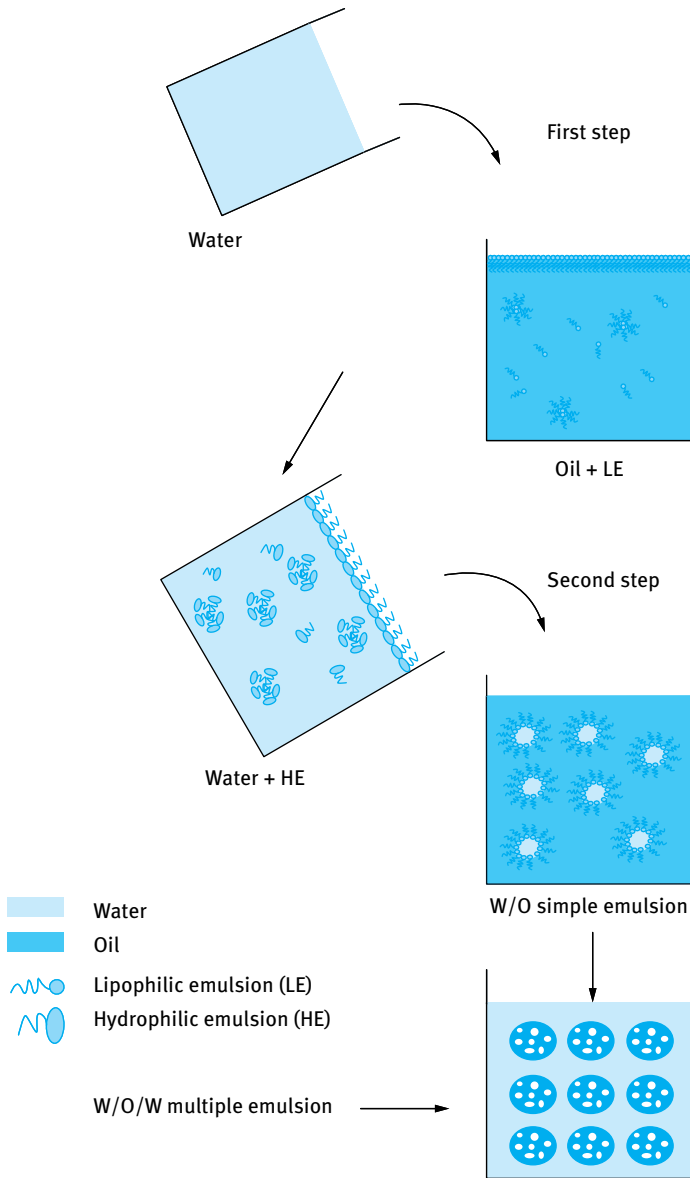


Fig. 9.4: Schematic representation of the preparation of a W/O/W multiple emulsion by phase inversion.

9.4.2 The phase inversion method

This is also a two-step process in which the lipophilic surfactant is dissolved in the oil phase and then an aqueous solution containing the hydrophilic surfactant is slowly added to the oil solution, while stirring. Initially a W/O emulsion is produced and on further addition of the solution of the hydrophilic surfactant, a W/O/W multiple emulsion may be produced. This method is schematically represented in Fig. 9.4.

The main advantage of the phase inversion method is the ease of preparation and it provides a given proportion of internal phase, exactly as in the two-step method described above. However, it suffers from the disadvantage of formation of an O/W emulsion instead of the required W/O/W multiple emulsions. Indeed, a very slight excess of water is sufficient to transform the multiple emulsion to an O/W emulsion.

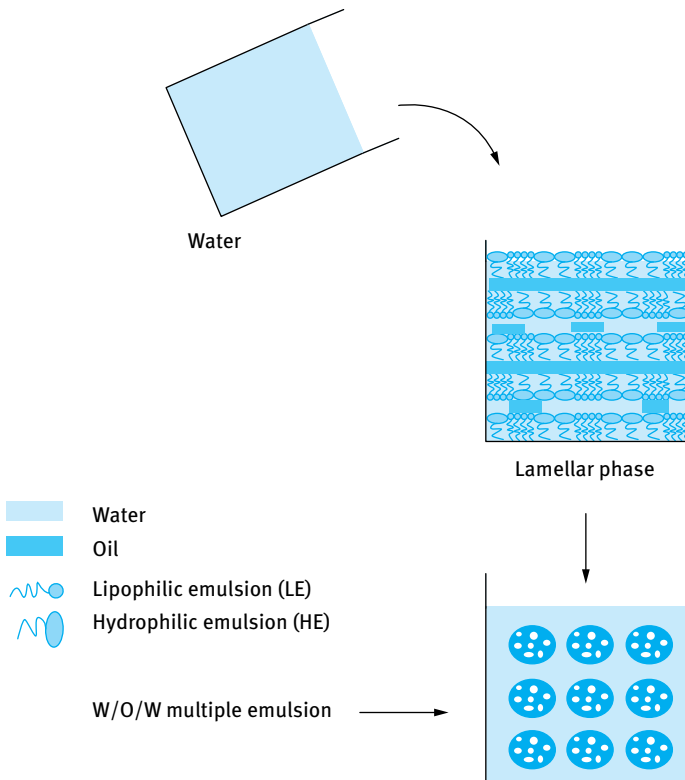


Fig. 9.5: Schematic representation of the preparation of a W/O/W multiple emulsion by lamellar phase inversion.

9.4.3 Lamellar phase dispersion process

In this case a lamellar liquid crystalline phase is prepared by mixing at 70 °C about 60 % emulsifier, 10 % oil and 30 % water-containing electrolyte. The dispersion is created, for example, by low speed stirring (at 500 rev/min) for 10 minutes. The lamellar mesophase receives a given amount of water at high stirring speed (> 1500 rev/min) until a W/O/W multiple emulsion is formed. This process is schematically represented in Fig. 9.5.

The above procedure offers the advantage of requiring a simple emulsification process. The lamellar phase formed by an ideal ratio of lipophilic and hydrophilic emulsifiers in water is thermodynamically stable and can be obtained rapidly and easily. The main limitation of the method is due to the fact that not all emulsifiers produce lamellar phases. This is particularly the case with polymeric surfactants, which are necessary to produce stable multiple emulsions. In addition, the method requires the use of high amounts of emulsifiers.

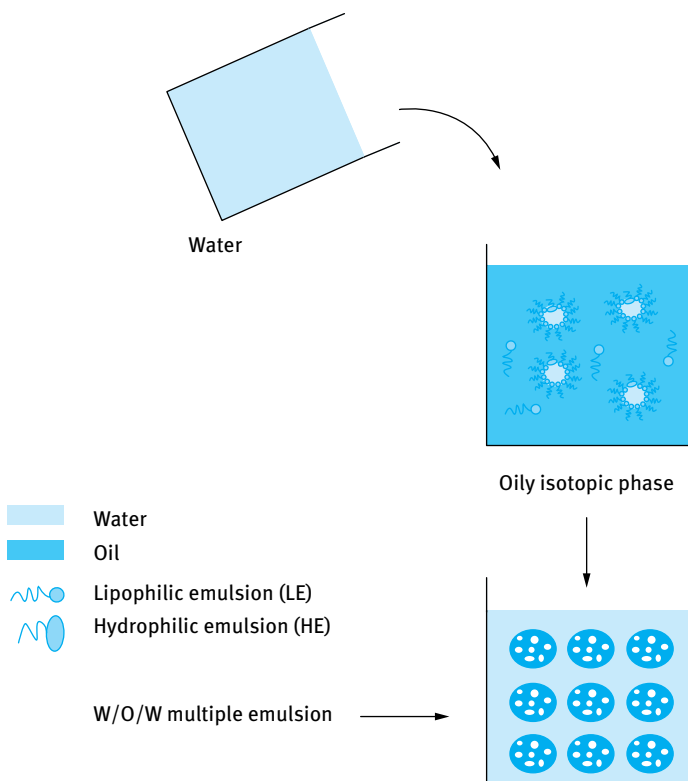


Fig. 9.6: Schematic representation of the preparation of a W/O/W multiple emulsion by the oily isotropic dispersion method.

9.4.4 The oily isotropic dispersion process

In this case an oily micellar isotropic phase (inverse micellar phase) is prepared at 70 to 80 °C for about 30 minutes at high stirring speed (about 1000 rev/min). Water is then gradually added to this oily micellar phase and the dispersion is carried out at lower speed (200–400 rev/min) for about 30 minutes. A schematic representation of this process is shown in Fig. 9.6.

This method offers the same advantages as the lamellar phase dispersion process. However, it suffers from the same disadvantage of the necessity of using high amounts of emulsifiers.

9.5 Main parameters that need to be controlled in the preparation of W/O/W multiple emulsions for cosmetic applications

9.5.1 Nature of the oil

The oils that can be used for the preparation of multiple emulsions must be cosmetically acceptable (no toxicity). The most convenient oils are vegetable oils such as soybean or safflower oil. Paraffinic oils with no toxic effect may be used. Also some polar oils such as isopropyl myristate can be applied; silicone oils can also be used.

The viscosity of the oil phase has a dominant effect on the physicochemical characteristics of the multiple emulsion [4]. Several attempts have been made to use viscous oils such as Vaseline or mixtures of oils that produce varying viscosities. For example, a mixture of viscous isoparaffinic oil with a non-viscous oil leads to increased stability with increasing oil viscosity and a decrease in the material transferred from the internal to the external phase [4]. Other additives that increase the oil viscosity, such as beeswax and palmitic acid, were found to yield more stable multiple emulsions [4].

9.5.2 Nature of the emulsifier

The low HLB emulsifiers (for the primary W/O emulsion) are mostly the sorbitan esters (Spans), but these may be mixed with other polymeric emulsifiers such as silicone emulsifiers. A very effective emulsifier for the primary W/O emulsion is Arlacel P135, an A–B–A block copolymer consisting of polyethylene oxide (PEO) chain (B) with two polyhydroxystearic acid (PHS) chains (A). The high HLB surfactant can be chosen from the Tween series, although the block copolymers PEO–PPO–PEO (Poloxamers or Pluronics) may give much better stability. The polymeric surfactant INUTEC® SP1 (hydrophobically modified inulin) can also give much higher stability.

When considering the choice of emulsifiers for multiple emulsions, one must know the adsorption and conformation of the emulsifiers at two interfaces, namely the W/O interface for the internal droplets and the O/W interface for the multiple emulsion drop. For example, when using Arlacel P135 as the primary emulsifier, the A–B–A block copolymer adsorbs strongly with the PEO chain at the W/O interface leaving the PHS A chains in the oil phase. These PHS chains are strongly solvated in most hydrocarbon solvents, thus providing an effective steric barrier to prevent any flocculation or coalescence of the water droplets [5]. When using Pluronic for stabilizing the final multiple emulsion drop, the PPO chain adsorbs strongly at the O/W interface, leaving the strongly hydrated PEO chains in the aqueous medium. These PEO chains provide effective steric stabilization [5], thus preventing any flocculation or coalescence of the multiple emulsion drops.

9.5.3 Gelling agents

In most cases a “gelling agent” is required, both for the oil and the outside external phase. For the oil phase, fatty alcohols may be used. For the aqueous continuous phase one can use the same “thickeners” that are used in emulsions, e.g. hydroxyethyl cellulose, xanthan gum, alginates, carrageenans, etc. Sometimes liquid crystalline phases are applied to stabilize the multiple emulsion droplets. These can be generated using a nonionic surfactant and long chain alcohol. “Gel” coating around the multiple emulsion droplets may also be formed to enhance stability.

9.5.4 Osmotic pressure control

As mentioned above, one of the main breakdown processes of multiple emulsions is due to the osmotic flow of water from the internal to the external phases. To prevent such flow it is essential to have nearly equal osmotic pressure between the internal and external aqueous phases. To control the osmotic pressure of the internal and external phases, electrolytes such as NaCl or nonelectrolytes such as sorbitol may be used.

9.6 Examples of W/O/W multiple emulsions

As an illustration, a typical formulation of a W/O/W multiple emulsion is described below, using two different thickeners, namely Keltrol (Xanthan Gum from Kelco) and Carbopol 980 (a crosslinked polyacrylate gel produced by BF Goodrich). These thickeners were added to reduce creaming of the multiple emulsion. A two-step process was used in both cases.

The primary W/O emulsion was prepared using an A–B–A block copolymer (where A is poly(hydroxystearic acid, PHS, and B is polyethylene oxide, PEO), i.e. PHS–PEO–PHS. 4 g of PHS–PEO–PHS were dissolved in 30 g of a hydrocarbon oil. For quick dissolution, the mixture was heated to 75 °C. The aqueous phase consisted of 65.3 g water, 0.7 g $\text{MgSO}_4 \cdot 7\text{H}_2\text{O}$ and a preservative. This aqueous solution was also heated to 75 °C. The aqueous phase was added to the oil phase slowly while stirring intensively using a high speed mixer. The W/O emulsion was homogenized for 1 minute and allowed to cool to 40–45 °C followed by further homogenization for another minute and stirring was continued until the temperature reached ambient.

The primary W/O emulsion was emulsified in an aqueous solution containing the polymeric surfactant PEO–PPO–PEO, namely Pluronic PEF127. 2 g of the polymeric surfactant were dissolved in 16.2 g water containing a preservative by stirring at 5 °C. 0.4 g $\text{MgSO}_4 \cdot 7\text{H}_2\text{O}$ were then added to the aqueous polymeric surfactant solution. 60 g of the primary W/O emulsion were slowly added to the aqueous PFE127 solution while stirring slowly at 700 rpm (using a paddle stirrer). An aqueous Keltrol solution was prepared by slowly adding 0.7 g Keltrol powder to 20.7 g water, while stirring. The resulting thickener solution was further stirred for 30–40 minutes until a homogeneous gel was produced. The thickener solution was slowly added to the multiple emulsion while stirring at low speed (400 rpm) and the whole system is homogenized for 1 minute followed by gentle stirring at 300 rpm until the thickener completely dispersed in the multiple emulsion (about 30 minutes stirring was sufficient). The final system was investigated using optical microscopy to ensure that a multiple emulsion was produced. The formulation was left standing for several months and the droplets of the multiple emulsion were investigated using optical microscopy (see below). The rheology of the multiple emulsion was also measured (see below) at various intervals to ensure that the consistency of the product remained the same on long storage.

The above multiple emulsion was made under the same conditions except using Carbopol 980 as a thickener (gel). In this case, no MgSO_4 was added, since the Carbopol gel was affected by electrolytes. The aqueous PEF127 polymeric surfactant solution was made by dissolving 2 g of the polymer in 23 g water. 15 g of 2% master gel of Carbopol were added to the PEF127 solution while stirring until the Carbopol was completely dispersed. 60 g of the primary W/O emulsion were slowly added to the aqueous solution of PEF127/Carbopol solution, while stirring thoroughly at 700 rpm. Triethanolamine was added slowly, while gently stirring until the pH of the system reached 6.0–6.5.

Another example of a W/O/W multiple emulsion was prepared using two polymeric surfactants. A W/O emulsion was prepared using an A–B–A block copolymer of PHS–PEO–PHS. This emulsion was prepared using high speed mixer giving droplet sizes in the region of 1 μm . The W/O emulsion was then emulsified in an aqueous solution of hydrophobically modified inulin (INUTEC[®] SP1) using low speed stirring to produce multiple emulsion droplets in the range 10–100 μm . The osmotic balance was achieved using 0.1 mol dm^{-3} MgCl_2 in the internal water droplets and outside contin-

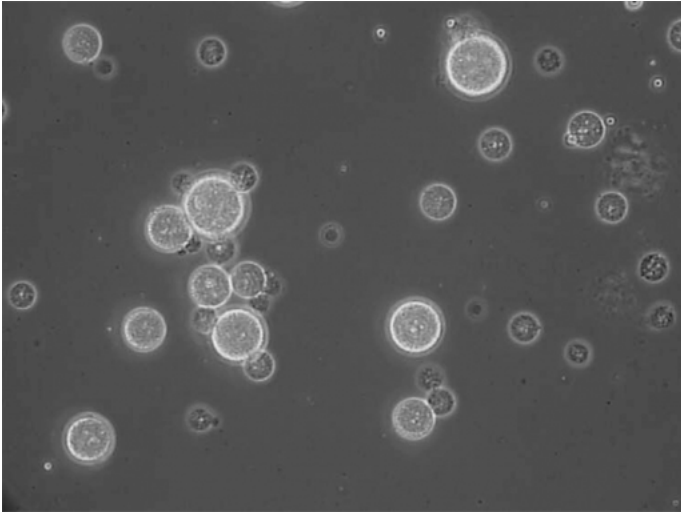


Fig. 9.7: Photomicrograph of the W/O/W multiple emulsion.

uous phase. The multiple emulsion was stored at room temperature and 50 °C and photomicrographs were taken at various intervals of time. The multiple emulsion was very stable for several months. A photomicrograph of the W/O/W multiple emulsion is shown in Fig. 9.7.

An O/W/O multiple emulsion was made by first preparing a nanoemulsion using INUTE[®] SP1. The nanoemulsion was then emulsified into an oil solution of PHS–

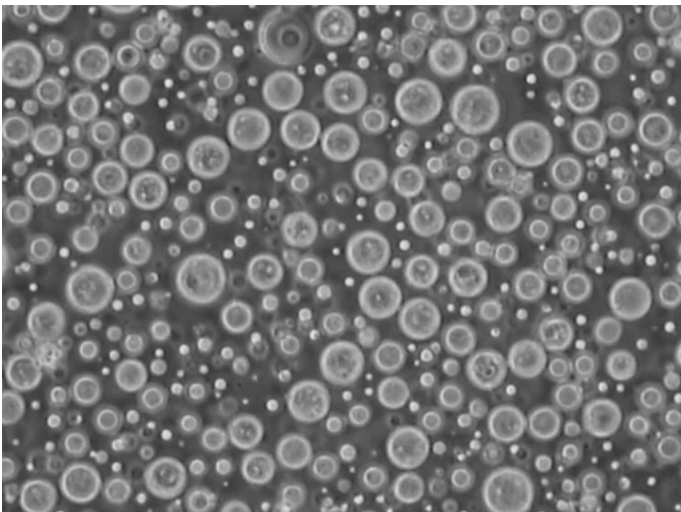


Fig. 9.8: Photomicrograph of the O/W/O multiple emulsion.

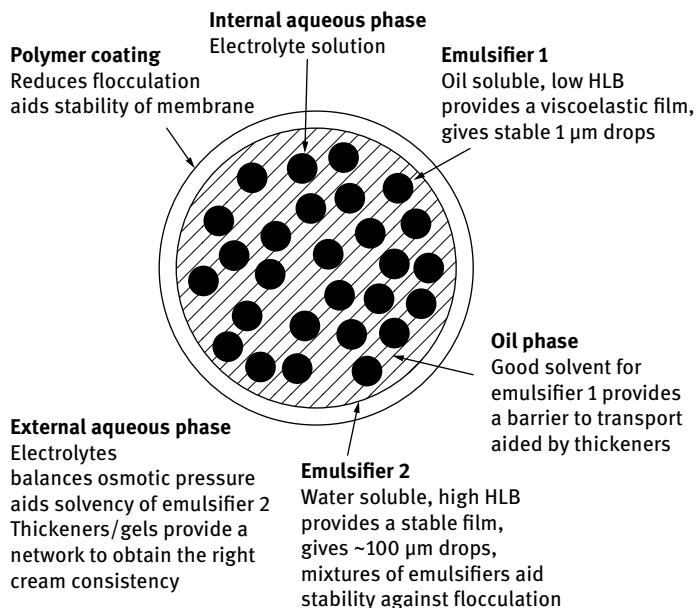


Fig. 9.9: Schematic representation of a multiple emulsion drop.

PEO-PHS using a low speed stirrer. The O/W/O multiple emulsion was stored at room temperature and 50 °C and photomicrographs taken at various intervals of time. The O/W/O multiple emulsion was stable for several months both at room temperature and 50 °C. A photomicrograph of the O/W/O multiple emulsion is shown in Fig. 9.8. A schematic representation of a drop of the W/O/W multiple emulsion is shown in Fig. 9.9.

9.7 Characterization of multiple emulsions

Several methods can be applied for characterizing multiple emulsions.

9.7.1 Droplet size analysis

The droplet size distribution of the primary emulsion (internal droplets of the multiple emulsion) is usually in the region 0.5–2 μm , with an average of ≈ 0.5 –1.0 μm . The droplet size distribution of this primary emulsion can be determined using photon correlation spectroscopy (PCS). This depends on measuring the intensity fluctuation of light scattered by the droplets as they undergo Brownian motion. Alternatively, light diffraction techniques, e.g. using the Master Sizer (Malvern, UK) can be used. The mul-

multiple emulsion droplets cover a wide range of sizes, usually 5–100 μm , with an average in the region of 5–20 μm . Optical microscopy (differential interference contrast) can be used to assess the droplets of the multiple emulsion. Optical micrographs may be taken at various storage times to assess the stability.

Freeze fracture and electron microscopy can give a quantitative assessment of the structure of the multiple emulsion droplets. Techniques can be applied to measure the droplet size of the multiple emulsion. Since the particle size is $> 5 \mu\text{m}$ (i.e. the diameter is much greater than the wavelength of light), they show light diffraction (Fraunhofer diffraction) and the Master Sizer could also be used.

9.7.2 Dialysis

As mentioned above, this could be used to measure the yield of the multiple emulsion; it can also be applied to follow any solute transfer from the inner droplets to the outer continuous phase.

9.7.3 Rheological techniques

Three rheological techniques may be applied.

9.7.3.1 Steady state shear stress (τ)–shear rate ($\dot{\gamma}$) measurements

A pseudoplastic flow is obtained, as illustrated in Fig. 9.10. This flow curve can be analysed using, for example, the Herschel–Bulkley equation [7, 8],

$$\tau = \tau_{\beta} + k\dot{\gamma}^n, \quad (9.7)$$

where τ_{β} is the “yield value”, k is the consistency index and n is the shear thinning index. This equation can be used to obtain the viscosity η as a function of shear rate.

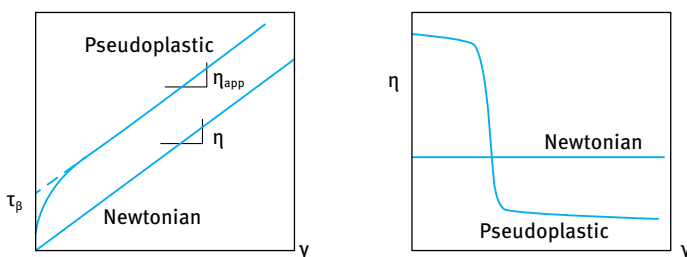


Fig. 9.10: Flow curves for Newtonian and pseudoplastic systems.

By following the change in viscosity with time, one can obtain information on multiple emulsion stability. For example, if there is water flow from the external phase to the internal water droplets (“swelling”), the viscosity will increase with time. If after some period of time, the multiple emulsion droplets begin to disintegrate forming O/W emulsion, the viscosity will drop.

9.7.3.2 Constant stress (creep) measurements

In this case, a constant stress is applied and the strain γ (or compliance $J = \gamma/\tau$) is followed as a function of time, as shown in Fig. 9.11. If the applied stress is below the yield stress, the strain will initially show a small increase and then it remains virtually constant. Once the stress exceeds the yield value, the strain shows a rapid increase with time and eventually it reaches a steady state (with constant slope). From the slopes of the creep tests one can obtain the viscosity at any applied stress, as illustrated in Fig. 9.12, which shows a plateau high value below the yield stress (residual or zero

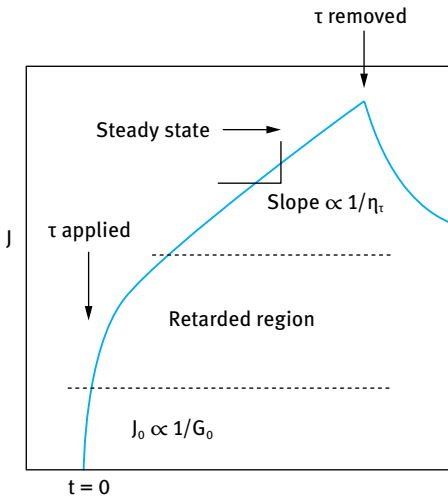


Fig. 9.11: Typical creep curve for a visco-elastic system.

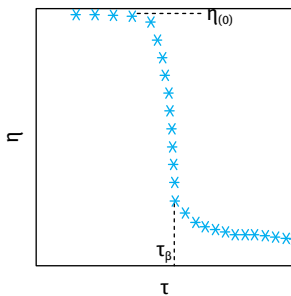


Fig. 9.12: Variation of viscosity with applied stress.

shear viscosity) followed by a rapid decrease when the yield stress is exceeded. By following the creep curves as a function of storage time one can assess the stability of the multiple emulsion. Apart from swelling or shrinking of the droplets, which cause reduction in zero shear viscosity and yield value, any separation will also show a change in the rheological parameters.

9.7.3.3 Dynamic or oscillatory measurements

In dynamic (oscillator) measurements, a sinusoidal strain, with frequency ν in Hz or ω in rad s^{-1} ($\omega = 2\pi\nu$) is applied to the cup (of a concentric cylinder) or plate (of a cone and plate) and the stress is measured simultaneously on the bob or the cone which are connected to a torque bar [5]. The angular displacement of the cup or the plate is measured using a transducer. For a viscoelastic system, such as is the case with a multiple emulsion, the stress oscillates with the same frequency as the strain, but out of phase [5]. This is illustrated in Fig. 9.13, which shows the stress and strain sine waves for a viscoelastic system. From the time shift between the sine waves of the stress and strain, Δt , the phase angle shift δ is calculated,

$$\delta = \Delta t \omega. \quad (9.8)$$

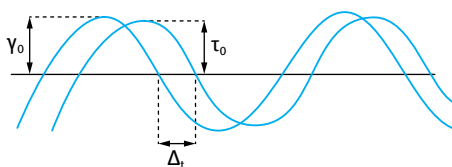


Fig. 9.13: Schematic representation of stress and strain sine waves for a viscoelastic system.

The complex modulus, G^* , is calculated from the stress and strain amplitudes (τ_0 and γ_0 respectively), i.e.,

$$G^* = \frac{\tau_0}{\gamma_0}. \quad (9.9)$$

The storage modulus, G' , which is a measure of the elastic component, is given by the following expression,

$$G' = |G^*| \cos \delta. \quad (9.10)$$

The loss modulus, G'' , which is a measure of the viscous component, is given by the following expression,

$$G'' = |G^*| \sin \delta, \quad (9.11)$$

and,

$$|G^*| = G' + iG'', \quad (9.12)$$

where i is equal to $(-1)^{1/2}$.

The dynamic viscosity, η' , is given by the following expression,

$$\eta' = \frac{G''}{\omega}. \quad (9.13)$$

In dynamic measurements one carries out two separate experiments. Firstly, the viscoelastic parameters are measured as a function of strain amplitude, at constant frequency, in order to establish the linear viscoelastic region, where G^* , G' and G'' are independent of the strain amplitude. This is illustrated in Fig. 9.14, which shows the variation of G^* , G' and G'' with γ_0 . It can be seen that the viscoelastic parameters remain constant up to a critical strain value, γ_{cr} , above which, G^* and G' start to decrease and G'' starts to increase with a further increase in the strain amplitude. Most multiple emulsions produce a linear viscoelastic response up to appreciable strains (>10%), indicative of structure build-up in the system (“gel” formation). If the system shows a short linear region (i.e., a low γ_{cr}), it indicates lack of a “coherent” gel structure (in many cases this is indicative of strong flocculation in the system).

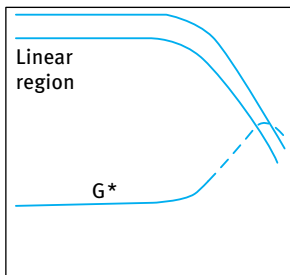


Fig. 9.14: Schematic representation of the variation of G^* , G' and G'' with strain amplitude (at a fixed frequency).

Once the linear viscoelastic region is established, measurements are then made of the viscoelastic parameters, at strain amplitudes within the linear region, as a function of frequency. This is schematically illustrated in Fig. 9.15, which shows the variation of G^* , G' and G'' with ν or ω . It can be seen that below a characteristic frequency, ν^* or ω^* , $G'' > G'$. In this low frequency regime (long timescale), the system can dissipate energy as viscous flow. Above ν^* or ω^* , $G' > G''$, since in this high frequency regime (short timescale) the system is able to store energy elastically. Indeed, at sufficiently high frequency G'' tends to zero and G' approaches G^* closely, showing little dependency on frequency. The relaxation time of the system can be calculated from the characteristic frequency (the crossover point) at which $G' = G''$, i.e.,

$$t^* = \frac{1}{\omega^*}. \quad (9.14)$$

It is clear from the above discussion that rheological measurements of multiple emulsions are very valuable in determining the long-term physical stability of the system as well as its application. This subject has attracted considerable interest in recent years

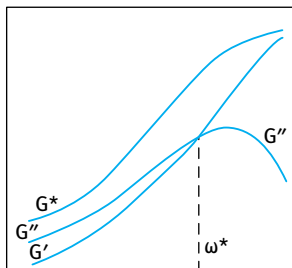


Fig. 9.15: Schematic representation of the variation of G^* , G' and G'' with ω for a viscoelastic system.

from many cosmetic manufacturers. Apart from its value in the above mentioned assessment, one of the most important considerations is to relate the rheological parameters to the consumer perception of the product. This requires careful measurement of the various rheological parameters for a number of multiple emulsions and relating these parameters to the perception of expert panels who assess the consistency of the product, its skin feel, spreading, adhesion, etc. It is claimed that the rheological properties of an emulsion cream formulated as a multiple emulsion determine the final thickness of the oil layer, the moisturizing efficiency and its aesthetic properties such as stickiness, stiffness and oiliness (texture profile). Psychophysical models may be applied to correlate rheology with consumer perception.

9.8 Summary of the factors affecting stability of multiple emulsions and criteria for their stabilization

As discussed above, the stability of a multiple emulsion is influenced by the nature of the two emulsifiers used for preparing the multiple emulsion. Most papers published in the literature on multiple emulsions are based on conventional nonionic surfactants. Unfortunately, most of these surfactant systems produce multiple emulsions with limited shelf life, particularly if the system is subjected to large temperature variations. As mentioned above, we have formulated multiple emulsions using polymeric surfactants for both the primary and multiple emulsion preparation. These polymeric surfactants proved to be superior to the conventional nonionic surfactants in maintaining the physical stability of the multiple emulsion and they now could be successfully applied for the formulation of cosmetic multiple emulsions. The key is to use polymeric surfactants that are approved by the CTA for cosmetics.

The stability of the resulting multiple emulsion depends on a number of factors:

- (i) the nature of the emulsifiers used for preparing the primary and multiple emulsion;
- (ii) the osmotic balance between the aqueous droplets in the multiple emulsion drops and that in the external aqueous phase;

- (iii) the volume fractions of the disperse water droplets in the multiple emulsion drops and the final volume fraction of the multiple emulsions;
- (iv) the temperature range to which the multiple emulsion is subjected;
- (v) the process used to prepare the system;
- (vi) the rheology of the whole system which can be modified by the addition of thickeners in the external aqueous phase.

As discussed above, the main criteria for the preparation of a stable multiple emulsion are:

- (i) Two emulsifiers, one with low (emulsifier I) and one with high (emulsifier II) HLB number.
- (ii) Emulsifier I should provide a very effective barrier against coalescence of the water droplets in the multiple emulsion drop. Emulsifier II should also provide an effective barrier against flocculation and/or coalescence of the multiple emulsion drops.
- (iii) The amount of emulsifiers used in the preparation of the primary and the multiple emulsion is critical. Excess emulsifier I in the oil phase may result in further emulsification of the aqueous phase into the multiple emulsion with the ultimate production of a W/O emulsion. Excess emulsifier II in the aqueous phase may result in solubilization of the low HLB number surfactant with the ultimate formation of an O/W emulsion.
- (iv) Optimum osmotic balance of the internal and external aqueous phases. If the osmotic pressure of the internal aqueous droplets is higher than the external aqueous phase, water will flow to the internal droplets resulting in “swelling” of the multiple emulsion drops with the ultimate production of a W/O emulsion. In contrast, if the osmotic pressure in the outside external phase is higher, water will diffuse in the opposite direction and the multiple emulsion will revert to an O/W emulsion.

Various formulation variables must be considered:

- (i) primary W/O emulsifier; various low HLB number surfactants are available of which the following may be mentioned: decaglycerol decaoleate; mixed triglycerol trioleate and sorbitan trioleate; A–B–A block copolymers of PEO and PHS;
- (ii) primary volume fraction of the W/O or O/W emulsion; usually volume fractions between 0.4 and 0.6 are produced, depending on the requirements;
- (iii) nature of the oil phase; various paraffinic oils (e.g. heptamethyl nonane), silicone oil, soybean and other vegetable oils may be used;
- (iv) secondary O/W emulsifier; high HLB number surfactants or polymers may be used, e.g. Tween 20, polyethylene oxide–polypropylene oxide block copolymers (Pluronics) may be used;
- (v) secondary volume fraction; this may be varied between 0.4 and 0.8 depending on the consistency required;

- (vi) electrolyte nature and concentration; e.g. NaCl, CaCl₂, MgCl₂ or MgSO₄;
- (vii) thickeners and other additives; in some cases a gel coating for the multiple emulsion drops may be beneficial, e.g. polymethacrylic acid or carboxymethyl cellulose. Gels in the outside continuous phase for a W/O/W multiple emulsion may be produced using xanthan gum (Keltrol or Rhodopol), Carbopol or alginates;
- (viii) process; for the preparation of the primary emulsion, high speed mixers such as Ultra-Turrax or Silverson may be used.

For preparing the secondary emulsion, a low shear mixing regime is required, in which case paddle stirrers are probably the most convenient. The mixing times, speed and order of addition need to be optimized.

References

- [1] Florence AT, Whitehill D. *J Colloid Interface Sci.* 1981;79:243.
- [2] Matsumoto S, Kita Y, Yonezawa D. *J Colloid Interface Sci.* 1976;57:353.
- [3] Seiller M, Grossiord JL, Silva-Cunha A. In: Grossiord JL, Seiller M, editors. *Multiple Emulsions: Structure, Properties and Applications*. Paris: Editions de Sante; 1998. Chapter 2.
- [4] Garti N. In: Grossiord JL, Seiller M, editors. *Multiple Emulsions: Structure, Properties and Applications*. Paris: Editions de Sante; 1998. Chapter 3.
- [5] Napper DH. *Polymeric stabilisation of colloidal dispersions*. London: Academic Press; 1981.
- [6] Tadros TF. *Int J Cosmet. Sci.* 1992;14:93.
- [7] Whorlow RW. *Rheological Techniques*. Chichester: Ellis Horwood; 1980.
- [8] Tadros T. *Rheology of dispersions*. Weinheim: Wiley-VCH; 2010.

10 Shampoos, gels and hair conditioners

10.1 Introduction

The purpose of a shampoo is to clean the hair from sebum, dead epidermal cells, residues from hair dressing, hair sprays, dust, etc. [1–4]. It must also remove greasy substances from hair oils, pomades and hair sprays. Soiled hair lacks lustre, becomes oily and unmanageable and develops an unpleasant odour. A shampoo must clean the hair and leave it in a lustrous, manageable condition. This requires the application of surfactants and hair conditioners, the so-called “two-in-one” shampoo. Shampoos can be formulated as clear, pearly or opaque liquids, gels or creams.

Shampoos should possess good, stable foaming action which depends on the surfactants used and the additives that are incorporated. Good shampoos should provide satisfactory cleaning power and easy rinsing without producing soap scum in any water hardness. They also should give a soft touch to the hair, with good manageability after shampooing. The shampoo should also have a low order of irritation to skin and eyes. In addition, for consumer appeal, the product should have an attractive colour and fragrance, and make a rich and mild foam.

Two types of shampoos are marketed, namely powder shampoo and liquid type. The latter can be a clear liquid with low, medium or high (gel form) viscosity. Alternatively, the shampoo can be an opaque liquid consisting of either a pearly liquid or milk lotion. From the point of view of function and application, the shampoo can be plain, medicated (anti-dandruff or deodorant), conditioning and low irritation (baby shampoo).

A hair conditioner is an ingredient or product that when applied to hair in its recommended use procedure and concentration improves the manageability, gloss and smooth touch of the hair [1]. Using shampoos containing anionic surfactants leaves the hair difficult to comb while wet. It also results in a static charge build-up or fly-away when the hair is combed dry. As will be discussed later, the isoelectric point of hair is approximately 3.67 and hence its surface will have a net negative charge at neutral pH. Anionic surfactants, which are also negatively charged, do not deposit (do not adsorb) on the hair and leave it in an unmanageable condition. Amphoteric surfactants that contain a positively charged nitrogen group are more substantive to hair and can impart some conditioning effect. Cationic surfactants such as stearyl benzyl dimethyl ammonium chloride, cetyltrimethylammonium chloride, distearyl dimethyl ammonium chloride or stearamidopropyl dimethyl amine and diesterquats are also effective as hair conditioners. The main problem with using cationic surfactants is their strong interaction with the anionic surfactant molecules which may cause precipitation.

As we will see later, polymeric conditioners with their high molecular weight are deposited strictly on the fibre surface or can penetrate into the cuticle or even beyond it into the cortex. The most effective hair conditioners are the cationically modified polymers (e.g. Polyquaternium-10) that will be discussed later. These polymeric compounds are incorporated into shampoos with the major goal of improving the “condition” of hair, which includes its appearance and manageability. Properties such as combability, flyaway, body and curl retention are affected by the deposition of polymers on the hair surface. Several other components can impart some conditioning effect, e.g. fatty alcohols, fatty acids, monoglycerides, lecithin, silicones, hydrolysed proteins, polyvinylpyrrolidone, gelatin, pectin, etc.

To understand the role of the conditioner it is essential to know the structure and properties of human hair with particular reference to its surface properties.

In this chapter I will discuss the following points that are relevant for formulating a conditioning shampoo:

- (i) The surfactants used in shampoo formulations.
- (ii) The desirable properties of a shampoo.
- (iii) The components that are used in the formulation.
- (iv) The role of the ingredients: mixed surfactant systems and their synergistic action to lower skin irritation, cleansing function, foam boosters, thickening agents as rheology modifiers and silicone oil emulsions in shampoos.

The subject of hair conditioners will be dealt with in the next section with particular reference to the structure and properties of human hair.

10.2 Surfactants for use in shampoo formulations [2, 3]

10.2.1 Anionic surfactants

Alkyl carboxylates or soaps, with C_{12} – C_{14} chain and counterions of potassium, di- or tri-ethanolamine are sometimes used in shampoos in combination with alkyl sulphates or polyoxyethylene ether sulphate. These carboxylates are applied as foam boosters or foam thickeners. They are seldom used alone due to the disadvantages produced by them. For example, the potassium salt of alkyl carboxylates can make the hair swell because of its alkalinity. The di- and tri-ethanolamine salts can become discoloured by heat or light. In addition, the soap-based shampoos can leave an insoluble metal salt on the hair after shampooing in hard water and cause unpleasant stickiness. The most commonly used anionic surfactants in shampoos are the alkyl sulphates and their ethoxylates (polyoxyethylene alkyl ether sulphates, AES). The alkyl sulphates are produced by sulphation of higher alcohols (C_{12} – C_{14} chain) using chlorosulphonic acid or sulphuric anhydride. Since the sodium or potassium salt of alkyl sulphates are not easily soluble in water, their uses are limited to a powder or paste shampoo base, al-

though in warm climates they can also be used as liquid shampoo base, either alone or in combination with AES. For liquid shampoos, tri-ethanolamine salt and ammonium salt are commonly used.

Alkyl sulphates exhibit good creamy foaming even with oily hair and a good soft feel after shampooing. The performance of alkyl sulphates depends on the length and the distribution of the alkyl chain as well as the nature of the counterion. The alkyl sulphate based on coconut alcohol is the most popular type. It is difficult to thicken shampoo based on alkyl sulphate by simply adding NaCl and this requires the addition of polymer thickener such as xanthan gum.

The most commonly used anionic surfactants are the ether sulphates, referred to as polyoxyethylene alkyl ether sulphate or AES. It is obtained by sulphating ethoxylated alcohols based mainly on lauryl (dodecyl) alcohol obtained from coconut or synthetic material. Unlike alkyl sulphate-based shampoos, liquid shampoos based on AES can be easily thickened by addition of inorganic salts such as NaCl. The maximum viscosity can be obtained by adding a certain amount of NaCl, regardless of the content of AES.

The solubility in water and the foaming ability of NaAES vary with the average moles of ethylene oxide (EO) and the linearity of the alcohol. The higher the number of EO units, the better the solubility and the lower the foaming ability. The more linear the alkyl group of the alcohol, the higher the foaming ability.

10.2.2 Amphoteric surfactants

The most commonly used amphoteric surfactants used in combination with anionics (AES) are the fatty alkyl betaines, e.g. lauryl amido propyl dimethyl betaine $C_{12}H_{25}CON(CH_3)_2COOH$ (dimethyl lauryl betaine). The addition of the amphoteric surfactant to the anionic surfactant lowers the critical micelle concentration (cmc) of the latter (see below) and this significantly reduces skin irritation. In addition, the amphoteric surfactant acts as a foam booster and thickener. It produces lighter and more voluminous foam. A suitable basic ingredient for baby shampoos with low irritation is imidazoline and its derivatives. It is also used as a conditioning booster when combined with a cationic polymer such as Polymer JR (see Chapter 11).

10.2.3 Nonionic surfactants

The most commonly used nonionic surfactants in shampoos are the fatty acid alkanolamides which improve foaming ability and solubility in water as well as increase viscosity when combined with anionic surfactants. Another commonly used nonionic surfactant in shampoos is the fatty acid amine oxide, which is used as foam stabilizer, thickener and for the improvement of tactile feeling of hair for shampoos based

on alkyl sulphates or alkyl ether sulphates (AES). When the pH is in the acid range, it tends to behave like a cationic surfactant and compatibility with anionic surfactants becomes poor. Occasionally, high HLB (hydrophilic-lipophilic balance) surfactants such as Tween 80 (Sorbitan monooleate with 20 mol EO) are used as solubilizing agents.

10.3 Properties of a shampoo

Several desirable properties of a shampoo can be listed [1]:

- (i) Ease of application; the shampoo should have the desirable rheology profile, enough viscosity and elasticity (reasonably high yield value) to stay in the hand before application to the hair. During application, the shampoo must spread easily and disperse quickly over the head and hair, i.e. a shear thinning system is required. This rheological profile can be achieved when using a concentrated surfactant solution that contains liquid crystalline structures (rod-shaped micelles), but in most cases a thickener (high molecular weight material) is included to arrive at the desirable high viscosity at low shear rates.
- (ii) Dense and luxurious lather: This requires the presence of a foam booster. The surfactant used for cleaning develops an abundant lacy foam in soft water, but the foam quality drops in the presence of oily soils such as sebum. A foam stabilizer is required and this could be a mixture of more than one surfactant.
- (iii) Ease of rinsing; the shampoo should not leave a residual tackiness or stickiness and it should not precipitate in hard water.
- (iv) Easy wet combing; after rinsing the hair should comb through easily without entanglement. Hair conditioners that are cationically modified polymers neutralize the charge on the hair surface (which is negatively charged) and this helps in combing the hair as will be discussed later. With long hair, a cationic cream rinse after shampooing is more effective.
- (v) Manageability; when combed dry the hair should be left in a manageable condition (no “flyaway” or frizziness). Again, charge neutralization of the hair surface by the conditioner helps in this respect.
- (vi) Lustrous; the hair should be left in a lustrous condition.
- (vii) Body; the hair should have “body” when dry, i.e. it should not be limp or over-conditioned.
- (viii) Fragrance; this should not have any objectionable odour.
- (ix) Low level of irritation; this is the most important factor in any shampoo and for this purpose amphoteric surfactants are preferred over anionics, which irritate the skin more. As will be discussed later, the use of amphoteric surfactants in combination with anionics reduces the latter’s skin irritation.
- (x) Preservatives; these should be effective against microbial and fungal contamination.

- (xi) Good stability; the product should remain stable for at least two or three years at ambient temperatures (both low and high for various regions) as well as when stored in daylight. Both physical and chemical stability should be maintained (no separation, no change in the rheology of the system and no chemical degradation on storage).

10.4 Components of a shampoo

10.4.1 Cleansing agents

Several surfactant systems are used in formulations of shampoos, as discussed in Section 10.2. These are mostly anionic surfactants which are usually mixed with amphoteric molecules. As mentioned in the introduction, the main criteria required are good cleansing from sebum, scales and other residues, as well as developing an acceptable lather. For the latter purpose, foam boosters or lather enrichers are added. The surfactant concentration in a typical shampoo is in the region of 10–20 %. This concentration is far in excess of that required to clean the hair; the sebum and other oily materials that inhibit foam formation require the use of such a high concentration. As mentioned in Section 10.2, the most widely used anionic surfactants are the alkyl sulphates $R-O-SO_3-M^+$ with R being a mixture of C_{12} and C_{14} and M^+ being sodium, ammonium, triethanolamine, diethanolamine or monoethanolamine. These anionic surfactants hydrolyse and produce the corresponding alcohol and this may result in the separation of the shampoo. The rate of hydrolysis depends on the pH of the system and this should remain in the range 5–9 to reduce the rate of hydrolysis. The sodium salt has a high Krafft temperature ($> 20^\circ C$) and separation (cloudiness) may occur when the temperature is reduced below $15^\circ C$. The ammonium and triethanolamine surfactant has a much lower Krafft temperature and this ensures good stability at low temperatures. Monoethanolamine lauryl sulphate produces very viscous shampoo and this could be considered for formulating a clear gel product. The low temperature stability can also be improved by using ether sulphates $R-O-(CH_2-CH_2-O)_nSO_4$ (with $n = 1-5$) which also reduce irritancy. Sulphosuccinates, e.g. disodium monococamido sulphosuccinate, disodium monolauramido sulphosuccinate, disodium monooleamido sulphosuccinate (and its PEG modified molecule) are commonly used in shampoos in combination with anionic surfactants. The sulphosuccinates alone do not lather well, but in combination with the anionics they result in excellent shampoos with good foam and reduced eye and skin irritation. Several other surfactants are used in combination with the anionics such as sarcosinates, glutamates, etc. As mentioned in Section 10.2, the most important class of surfactants that are used in combination with anionics are the amphoteric, e.g. amphoteric glycinates/propionates, betaines, amino/imino propionates, etc. These amphoteric surfactants impart mildness and hair conditioning properties to shampoos. Due to their low degree of eye irritation they are used to

develop baby shampoos. The pH of the system must be carefully adjusted to 6.9–7.5 (near the isoelectric point of the surfactant), since at low pH the surfactant acquires a positive charge and this leads to an increase in irritation. Several classes of amphoteric surfactants have been developed and these will be discussed in the section on the role of ingredients. Nonionic surfactants are not used alone in shampoos due to their poor foaming properties. However, they are used in mixtures with anionics to modify the primary cleansing agent, as viscosity builders, solubilizing agents, emulsifiers, lime soap dispersants, etc. They are also incorporated to reduce eye and skin irritation. The most commonly used nonionics are the polysorbates (Tweens), but in some cases Pluronics (or Poloxamers) (A–B–A block copolymers of polyethylene oxide (A) and polypropylene oxide (B)) are also used.

10.4.2 Foam boosters

Most of the surfactants used as cleansing agents develop an abundant lacy foam in soft water. However, in the presence of oily soils such as sebum, the abundance and quality of the lather drops drastically. Accordingly, one or more ingredients are added to the shampoo to improve the quality, volume and characteristics of the lather. Examples are fatty acid alkanolamides and amine oxides. As will be discussed later, these molecules stabilize the foams by strengthening the surfactant film at the air/water interface (by enhancing the Gibbs elasticity).

10.4.3 Thickening agents

As mentioned before, the viscosity of the shampoo must be carefully adjusted to give a shear thinning system. The most commonly used materials to enhance the viscosity of a shampoo are simple salts such as sodium or ammonium chloride. As will be discussed later, these salts will enhance the viscosity simply by producing rod-shaped micelles which have much higher viscosity than the spherical units. Some nonionic surfactants such as PEG distearate or PEG dioleate can also enhance the viscosity of many anionic surfactant solutions. Several other polymeric thickeners can also be used to enhance the viscosity, e.g. hydroxyethylcellulose, xanthan gum, Carbomers (crosslinked polyacrylate), etc. The mechanism of their action will be discussed later.

10.4.4 Preservatives

As shampoos are directly applied to human hair and scalp, they must be completely hygienic. Preservatives are necessary to prevent the growth of germs which can be caused by contamination during preparation or use. The most commonly used preser-

vatives are benzoic acid (0.1–0.2%), sodium benzoate (0.5–1.0%), salicylic acid (0.1–0.2%), sodium salicylate (0.5–1%) and methyl para-hydroxy benzoate (0.2–0.5%). The effects of preservatives depend upon concentration, pH and ingredients of the shampoo. Generally, shampoos of higher concentration are more resistant to germ contamination.

10.4.5 Miscellaneous additives

Many other components are also included in shampoos: Opacifying agents, e.g. ethylene glycol stearate, glyceryl monostearate, cetyl and stearyl alcohol, etc. These materials produce rich, lustrous, pearlescent texture. Clarifying agents; in many cases the perfume added may result in a slight haze and a solubilizer is added to clarify the shampoo. Buffers; these need to be added to control the pH to a value around 7 to avoid production of cationic charges.

10.5 Role of the components

10.5.1 Behaviour of mixed surfactant systems [2, 3]

As mentioned above, most shampoo formulations contain a mixed surfactant system, mostly anionic and amphoteric. For a surfactant mixture with no net interaction, mixed micelles are produced and the critical micelle concentration (cmc) of the mixture is an average of the two cmc's of the single components,

$$\text{cmc} = x_1 \text{cmc}_1 + x_2 \text{cmc}_2. \quad (10.1)$$

With most surfactant systems, there is a net interaction between the two molecules and the cmc of the mixture is not given by simple additivity. The interaction between surfactant molecules is described by an interaction parameter β which is positive when there is net repulsion and negative when there is net attraction between the molecules. In these cases the cmc of the mixture is given by the following expression,

$$\text{cmc} = x_1^m f_1^m \text{cmc}_1 + x_2^m f_2^m \text{cmc}_2, \quad (10.2)$$

where f_1^m and f_2^m are the activity coefficients which are related to the interaction parameter β ,

$$\ln f_1^m = (x_1^m)^2 \beta, \quad (10.3)$$

$$\ln f_2^m = (x_2^m)^2 \beta. \quad (10.4)$$

With mixtures of anionic and amphoteric surfactants (near the isoelectric point) there will be net attraction between the molecules and β is negative. This means that addition of the amphoteric surfactant to the anionic surfactant results in lowering of the

cmc and the mixture gives a better foam stabilization. In addition, the irritation of the mixture decreases when compared with that of the anionic surfactant alone. As mentioned above, an amphoteric surfactant that contains a nitrogen group is more substantive for the hair (better deposition).

10.5.2 Cleansing function

The main function of the surfactants in the shampoo is to clean the hair from sebum, scales, residues, dust and any oily deposits. The principal action is to remove any soil by the same mechanism as for detergency [1]. For removal of solid particles one has to replace the soil/surface interface (characterized by a tension γ_{SD}) with a solid/water interface (characterized by a tension γ_{SW}) and dirt/water interface (characterized by a tension γ_{DW}). The work of adhesion between a particle of dirt and a solid surface, W_{SD} , is given by,

$$W_{SD} = \gamma_{DW} + \gamma_{SW} - \gamma_{SD}. \quad (10.5)$$

Fig. 10.1 gives a schematic representation of dirt removal. The task of the surfactant in the shampoo is to lower γ_{DW} and γ_{SW} , which decreases W_{SD} and facilitates the removal of dirt by mechanical agitation. Nonionic surfactants are generally less effective in removal of dirt than anionic surfactants. In practice a mixture of anionic and nonionic surfactants are used. If the dirt is a liquid (oil or fat), its removal depends on the balance of contact angles. The oil or fat forms a low contact angle with the substrate (as illustrated in Fig. 10.2). To increase the contact angle between the oil and the substrate (with its subsequent removal), one has to increase the substrate/water interfacial tension, γ_{SW} . The addition of surfactant increases the contact angle at the dirt/substrate/water interface so that the dirt “rolls up” and off the substrate. Surfactants that adsorb both at the substrate/water and the dirt/water interfaces are

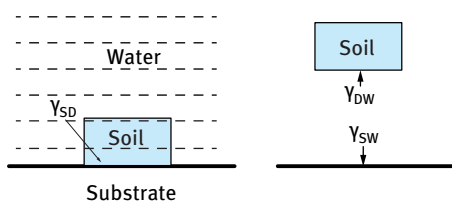


Fig. 10.1: Scheme of dirt removal.

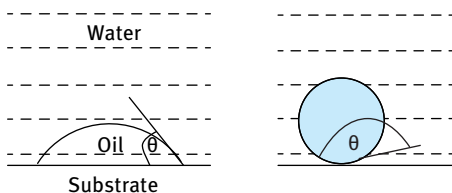


Fig. 10.2: Scheme of oil removal.

the most effective. If the surfactant adsorbs only at the dirt/water interface and lowers the interfacial tension between the oil and substrate (γ_{SD}), dirt removal is more difficult. Nonionic surfactants are the most effective in liquid dirt removal since they reduce the oil/water interfacial tension without reducing the oil/substrate tension.

10.5.3 Foam boosters

As mentioned before, with many shampoo formulations the abundance and quality of the lather may drop drastically in the presence of oily soils such as sebum and this requires the addition of a foam booster. Addition of a conditioner such as Polymer JR-400 (cationically modified hydroxyethyl cellulose) will cause a significant reduction of the surface tension of an anionic surfactant such as SDS below its cmc. This occurs even in the precipitation zone and it illustrates the high surface activity of the polymer-surfactant complex.

The polymer-surfactant complex has high surface viscosity and elasticity (i.e. surface viscoelasticity); both will enhance foam stability (see below). The amphoteric surfactants such as betaines and the phospholipid surfactants when used in conjunction with alkyl sulphates or alkyl ether sulphates can also enhance foam stability. All these molecules strengthen the film of surfactant at the air/water interface, thus modifying the lather from a loose lacy structure to a rich, dense, small bubble size, luxurious foam. Several foam boosters have been suggested and these include fatty acid alkanolamide and amine oxides. Fatty alcohol and fatty acids can also act as foam boosters when used at levels of 0.25–0.5%. Several approaches have been considered to explain foam stability:

- (i) Surface viscosity and elasticity theory: The adsorbed surfactant film is assumed to control the mechanical-dynamical properties of the surface layers by virtue of its surface viscosity and elasticity. This may be true for thick films (> 100 nm) where intermolecular forces are less dominant. Some correlations have been found between surface viscosity and elasticity and foam stability, e.g. when adding lauryl alcohol to sodium lauryl sulphate. This explains why mixed surfactant films are more effective in stabilizing foam as discussed above.
- (ii) Gibbs–Marangoni effect theory: The Gibbs coefficient of elasticity, ε , was introduced as a variable resistance to surface deformation during thinning [2, 3],

$$\varepsilon = 2(d\gamma/d \ln A) = -2(d\gamma/d \ln h), \quad (10.6)$$

where γ is the surface tension, A is the area of the interface and $d \ln h$ is the relative change in lamella thickness. ε is the “film elasticity of compression modulus” and it is a measure of the ability of the film to adjust its surface tension in a constant stress. The higher the value of ε the more stable the film; ε depends on surface concentration and film thickness and this explains the advantage of using mixed surfactant films. The diffusion of surfactant from the bulk solution, i.e. the

Marangoni effect, also plays a major role in stabilizing the film. The Marangoni effect opposes any rapid displacement of the surface and this leads to a more stable foam.

- (iii) Surface forces theory (disjoining pressure) [2, 3]: This theory operates under static (equilibrium) conditions particularly for thin liquid films (< 100 nm) in relatively dilute surfactant concentrations (e.g. during rinsing). The disjoining pressure π is made up of three contributions, namely electrostatic repulsion π_{el} , steric repulsion π_{st} (both are positive) and van der Waals attraction π_{vdw} (which is negative),

$$\pi = \pi_{el} + \pi_{st} + \pi_{vdw}. \quad (10.7)$$

For a stable film to form $\pi_{el} + \pi_{st} \gg \pi_{vdw}$. This explains the stability of foams where both electrostatic and steric repulsion exist.

- (iv) Stabilization by micelles and liquid crystalline phases: This occurs at high surfactant concentrations and in the presence of surfactant systems that can produce lamellar liquid crystalline phases. The latter, which are formed from several surfactant bilayers, “wrap” around the air bubbles and this can produce a very stable foam. This concept is very important in the formulation of shampoos containing high surfactant concentrations and several components that can produce the lamellar phases.

10.5.4 Thickeners and rheology modifiers

As mentioned above, the shampoo should be viscous enough to stay in the hand before application, but during application the viscosity must decrease enough for good spreading and dispersion over the hair and the head. This requires a shear thinning system (reduction of viscosity on application of shear). Several methods can be applied to increase the viscosity of the shampoo at low shear rates and its reduction on application of shear and these are summarized below.

10.5.4.1 Addition of electrolytes

Many surfactant systems increase their viscosity on addition of electrolytes at an optimum concentration, e.g. sodium chloride, ammonium chloride, sodium sulphate, monoethanolamine chloride, ammonium or sodium phosphate, etc. Of these, sodium chloride and ammonium chloride are the most commonly used. The mechanism by which these electrolytes increase the viscosity of the shampoo can be related to the micellar structure of the surfactant system. Before addition of electrolytes, the micelles are most likely spherical in nature, but when electrolytes are added at an optimum level, the micelles may change to cylindrical (rod-shaped) structures and the viscosity increases. This can be understood when considering the packing parameter of the surfactant system P . The packing parameter P is given by the ratio of the cross-sectional

area of the alkyl chain (v/l_c , where v is the volume of the hydrocarbon chain and l_c its extended length) to the cross-sectional area of the head group a [5–7],

$$P = v/l_c a. \quad (10.8)$$

For a spherical micelle $P \leq (1/3)$, whereas for a cylindrical (rod-shaped) micelle $P \leq (1/2)$. Addition of electrolyte reduces a (by screening the charge) and the spherical micelles change to rod-shaped micelles. This leads to an increase in viscosity. A schematic representation of the rod-shaped (thread-like) micelles and their overlap is given in Fig. 10.3. The viscosity increases gradually by increasing electrolyte concentration, reaches a maximum at an optimum electrolyte concentration and then decreases on further increase in electrolyte concentration (due to salting-out of the surfactant). The concentration of electrolyte required to reach maximum viscosity depends on the nature of the electrolyte and temperature. These surfactant systems produce viscoelastic solutions that occur at a critical surfactant concentration at which the rod-shaped micelles begin to overlap (similar to the case of polymer solutions). However, these viscoelastic solutions may not have sufficient viscosity to stay on the hand before application. This may be due to their insufficient relaxation times (note that the relaxation time is given by the ratio of viscosity to the modulus). For this reason, many shampoos contain high molecular weight polymers such as hydroxyethyl cellulose (HEC) or xanthan gum and these thickeners are discussed below.

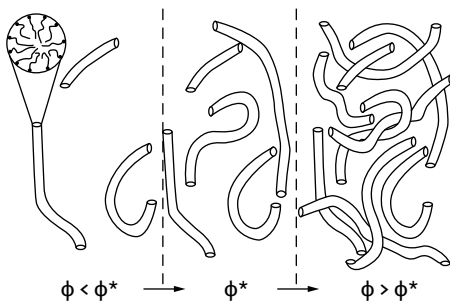


Fig. 10.3: Schematic representation of overlap of thread-like micelles.

10.5.4.2 Thickeners [8]

Most shampoos contain a high molecular weight polymer such as HEC, xanthan gum and some hydrophobically modified HEC or poly(ethylene oxide) (PEO) (associative thickeners). The concentration of the polymer required to produce a certain viscosity at low shear rates depends on its molecular weight M and structure. With HEC, several grades are commercially available, e.g. the Natrosol range with M varying between 70 000 and 250 000. The concentration of HEC required (0.5–2%) to reach a given optimum viscosity decreases with increasing M . With hydrophobically modified HEC (Natrosol Plus) a lower concentration can be used when compared with the

unmodified HEC. Hydrophobically modified PEO (HEUR) is also available. Carbomers (crosslinked polyacrylic acids) and other acrylate crosspolymers such as Carbopol 934 and 941 can produce gels when neutralized using ethanolamine (forming microgel particles by swelling due to double layer effects). Unfortunately, they have low tolerance to electrolytes (due to compression of the double layers) and hence they are seldom used in shampoos. Alternatives to Carbomers are the modified acrylate derivatives, such as acrylates/stearth-20/methacrylate copolymer that is supplied as a latex. It is added to the shampoo and then neutralized to the appropriate pH. Care should be taken with this polymer to avoid high electrolyte concentrations and low pH values that may cause its precipitation.

10.5.5 Silicone oil emulsions in shampoos

Silicone oil offers a suitable replacement to sebum that is removed during shampooing. This needs to be formulated as small oil droplets; which is not an easy task to obtain. The main advantage of silicone oil is its ability to spread and deposit uniformly on the hair surface, thus providing lubricant, lustre and softness to the hair. This stems from the low surface tension of silicone oils ($< 20 \text{ mN m}^{-1}$) thus giving a negative work of spreading W_s . The latter is given by the balance of the solid/liquid interfacial tension, γ_{SL} , the liquid/vapour interfacial tension, γ_{LV} , and the solid/vapour interfacial tensions, γ_{SV} ,

$$W_s = \gamma_{SL} - \gamma_{LV} - \gamma_{SV}. \quad (10.9)$$

For W_s to become negative, both γ_{SL} and γ_{LV} have to be reduced while keeping γ_{SV} high. The main problem when incorporating a silicone oil in the shampoo is its dispersion to small droplets and causing these small droplets to coalesce on the hair surface.

10.6 Use of associative thickeners as rheology modifiers in shampoos [9]

Associative thickeners are hydrophobically modified polymer molecules in which alkyl chains (C_{12} – C_{16}) are either randomly grafted on a hydrophilic polymer molecule, such as hydroxyethyl cellulose (HEC), or simply grafted at both ends of the hydrophilic chain. An example of hydrophobically modified HEC is Natrosol Plus (Hercules) which contains 3–4 C_{16} randomly grafted onto hydroxyethyl cellulose [9]. An example of polymer that contains two alkyl chains at both ends of the molecule is HEUR (Rohm and Haas) that is made of polyethylene oxide (PEO) that is capped at both ends with linear C_{18} hydrocarbon chains. These hydrophobically modified polymers form gels when dissolved in water. Gel formation can occur at relatively lower polymer concentrations when compared with the unmodified molecule. The

most likely explanation of gel formation is due to hydrophobic bonding (association) between the alkyl chains in the molecule. This effectively causes an apparent increase in the molecular weight. These associative structures are similar to micelles, except the aggregation numbers are much smaller.

Another example of associative thickeners is a blend of PEG-150 distearate and PEG-2-hydroxyethyl cocamide (Promidium LTS, Croda, UK) which was used in a shampoo formulation consisting of 7% sodium laureth sulphate (with 2 mol ethylene oxide), 3% cocamidopropylbetaine (CAPB) and 1% preservative (Germaben II). A comparison was made with the same shampoo thickened by addition of 1.6% NaCl, using viscoelastic measurements. The latter were investigated using dynamic (oscillatory) measurements, using a Bohlin CVO rheometer (Malvern Instruments, UK). All measurements were carried out at 25 °C, using a cone-plate geometry.

Fig. 10.4 gives typical stress-sweep results obtained at 1 Hz for the surfactant base thickened with 1.6% NaCl (Fig. 10.4 (a)) and 1.75% Promidium LTS (Fig. 10.4 (b)).

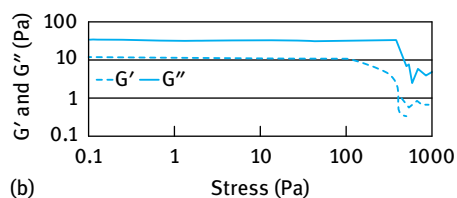
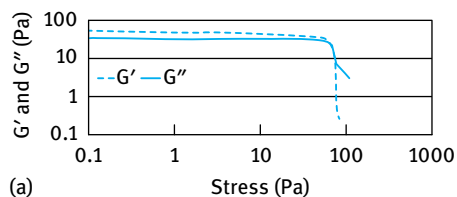


Fig. 10.4: Typical stress sweep results (1 Hz) for surfactant blends thickened with 1.6% NaCl (a) and Promidium LTS (b)

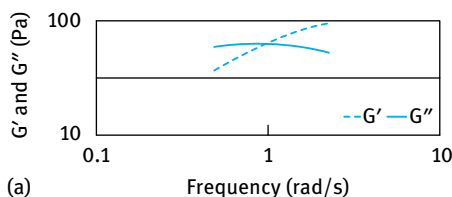
In both cases G' and G'' remained constant up to a critical stress, above which both G' and G'' start to decrease with decreasing applied stress. The region below the critical stress at which G' and G'' remain constant with increasing stress is denoted as the linear viscoelastic region. It should be mentioned that the surfactant system based on NaCl gives a lower critical stress when compared with the system thickened with Promidium LTS. This reflects the difference in “gel” structure between the two systems. It is likely that the system thickened with Promidium TLS gives a more coherent region (with a longer linear viscoelastic region) when compared with the system based on NaCl.

It can be also seen from the results in Fig. 10.4 that the surfactant base thickened with Promidium LTS (Fig. 10.4 (b)) is far more viscous than elastic ($G'' \gg G'$) when

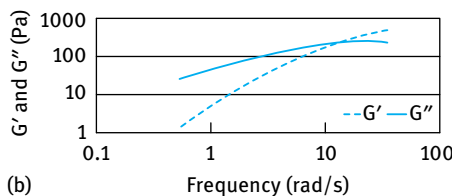
compared with the same base thickened with NaCl (Fig. 10.4 (a)) where $G' > G''$. In fact, regardless of the quantity of Promidium LTS used (and hence the final viscosity of the formula) the thickened surfactant always remains viscous dominant, even at extremely high viscosity. In the case of surfactant thickened with NaCl, at some critical concentration (in this case close to 1.6 %) the base becomes elastic dominant. This can be seen even at reasonably low viscosity.

Once the linear viscoelastic region was known it was possible to measure the effect of frequency on these surfactant bases. As an example, typical frequency sweeps for surfactant bases thickened with 2.5 % NaCl and 2.5 % Promidium LTS are given in Fig. 10.5. It can be seen from Fig. 10.5 that the crossover point (at which $G' = G''$) occurs at much higher frequency for the surfactant base thickened with Promidium LTS when compared to the same base thickened with salt. This implies that the relaxation time for the base thickened with Promidium LTS is much smaller than the values for the salt thickened system. A plot of relaxation time versus both NaCl and Promidium LTS concentration is given in Fig. 10.6.

At the high frequencies (corresponding to short timescales), the response is more elastic than viscous ($G' > G''$) for surfactants thickened with both NaCl and Promidium LTS. The high frequency modulus values are significantly higher for the bases



(a)



(b)

Fig. 10.5: Typical frequency sweeps for surfactant base thickened with 2.5 % NaCl (top) and 2.5 % Promidium LTS (bottom).

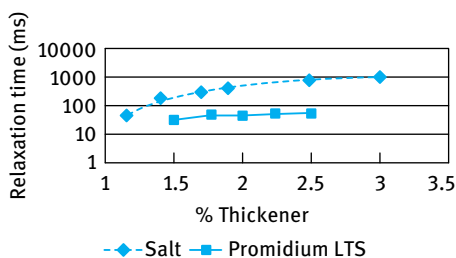


Fig. 10.6: Relaxation time versus NaCl and Promidium LTS concentration.

thickened with Promidium LTS when compared to those thickened with NaCl. However, G'' is beginning to plateau at 1.4% NaCl while Promidium LTS G'' values are continuing to rise (over the whole concentration range). Again, this implies that independent of Promidium LTS concentration, and the structure this gives, the surfactant bases thickened with this associative thickener remain viscous in behaviour. Those thickened with salt become predominantly elastic [9].

Fig. 10.7 and 10.8 show variation of G' and G'' of a high frequency oscillation that is above the G'/G'' crossover point. This is shown as a function of both NaCl concentration and Promidium LTS concentration. For NaCl, the frequency is 10 rad/s, for LTS the frequency is 50 rad/s.

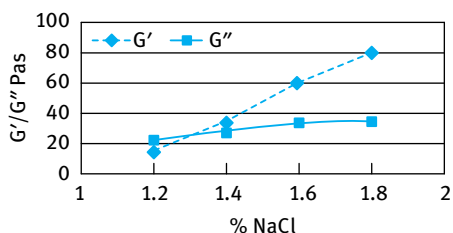


Fig. 10.7: Variation of G' and G'' (at a frequency higher than the crossover point) for surfactants thickened with NaCl.

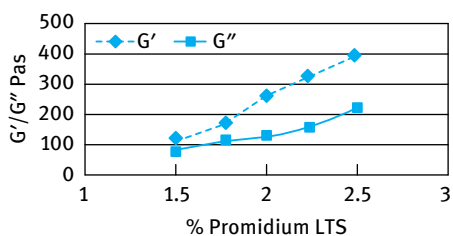


Fig. 10.8: Variation of G' and G'' (at a frequency higher than the G'/G'' crossover point) for surfactant base thickened with Promidium LTS.

The increase in the viscosity or elasticity of surfactant blends thickened with NaCl is due to the change in micellar structure from spherical to rod-shaped micelles by considering the critical packing parameter, P , given by equation (10.8). However, such structures give a more elastic than viscous response even at low frequency (long timescales), i.e. 1 Hz. This could be comparable to the timescales used in pouring, pumping and spreading during in-use application. The crossover point for such electrolyte thickened systems occurs at much lower frequencies giving long relaxation times. With increasing NaCl concentration, the relaxation time increases reaching very high values. For example, at 2.5% NaCl, the crossover point occurs at 1 rad s^{-1} (0.16 Hz) giving a relaxation time of 1 s.

As mentioned above, an alternative and more elegant way of thickening shampoos is to use associative thickeners. The associative thickener studied above consists of a hydrophilic chain of 150 ethylene oxide units (PEG 150), with two stearate chains attached, one at each end of the hydrophilic chain. This produces “micelle-

like” structures [9]. These structures are seen to have much shorter relaxation times when compared to surfactants thickened with salt (Fig. 10.6). The relaxation times are more than one order of magnitude lower than the bases thickened with salt. The crossover point for the formulations thickened using Promidium LTS occurs at much higher frequency when compared to those thickened by addition of NaCl. This means that at low frequency the system thickened with Promidium LTS is more viscous than elastic, independent of stress amplitude (Fig. 10.4). This will contribute a great degree to the sensory characteristics of the shampoo, both in terms of feel during application and also visually, i.e. a lack of stringiness and stickiness.

10.7 Morphology of hair

A schematic representation of a human hair fibre is shown in Fig. 10.9. This complex morphology [10] consists of four components, namely the cortex, the medulla, the cell membrane and the cuticle.

The major part of the interior of the fibre mass is the cortex that consists of elongated, spindle-shaped cells aligned in the direction of the fibre axis. The second component of hair morphology located in the centre of some thicker fibres and consisting of a loosely packed cellular structure is called the medulla (see Fig. 10.9). The third component fulfils the vital function of cementing the various cells of the cortex to-

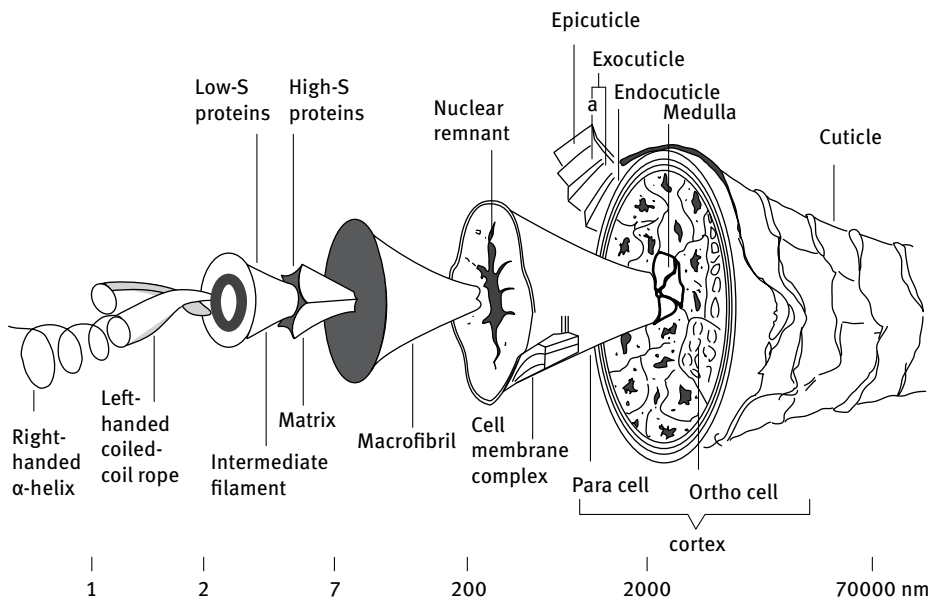


Fig. 10.9: Schematic representation of a human hair fibre.

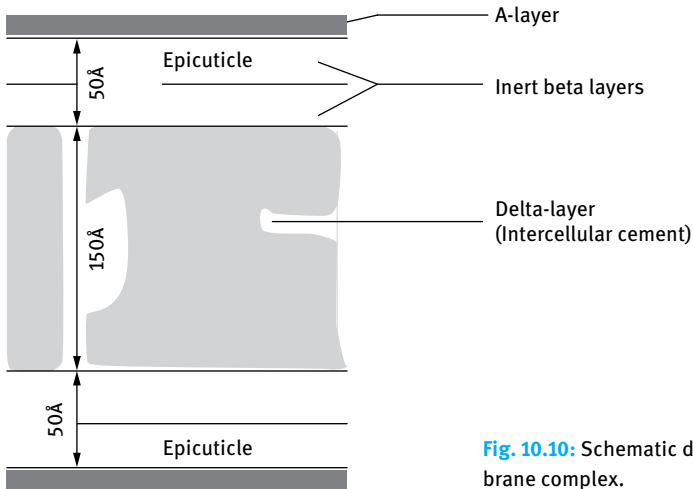


Fig. 10.10: Schematic diagram of the cell membrane complex.

gether, thus making a fibre out of a conglomerate of cells. This intercellular cement together with the cell membranes forms the cell membrane complex (illustrated in Fig. 10.10) and is assumed to be the location of transport paths into the fibre. This intercellular transport is especially important for the incorporation of polymeric molecules into the cuticle, or even for diffusion into the cortex.

On the outside of the hair, a thick covering of several layers of overlapping cuticle cells provides protection against mechanical and environmental stresses. While at the root end, up to 10 layers of cuticle cells are stacked over each other. The thickness of the cuticle layer decreases with increasing distance from the scalp as mechanical and environmental stresses cause ablation of cuticle fragments until occasionally the cuticle envelop has been totally worn away at the tip of long fibres. The cuticle cell itself is a multilayered structure as schematically illustrated in Fig. 10.11. The most important part of the cuticle from the point of view of surfactant and polymer deposition is its

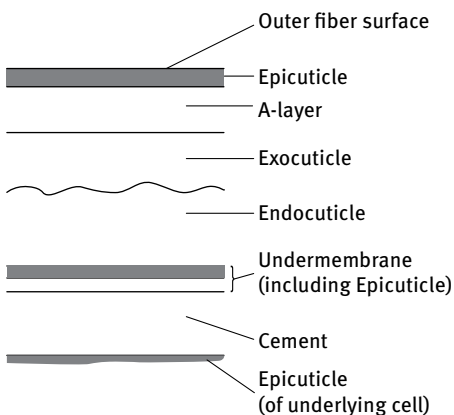


Fig. 10.11: Schematic diagram of the structure of a cuticle cell in cross section [11].

outermost surface, namely the epicuticle, which is about 2.5 nm thick [11]. It consists of 25% lipids and 75% protein, the latter having an ordered possibly β -pleated sheet structure with 12% cystine. The cystine groups are acylated by fatty acids, which form the hydrophobic surface region. A schematic representation of the epicuticle is shown in Fig. 10.12.

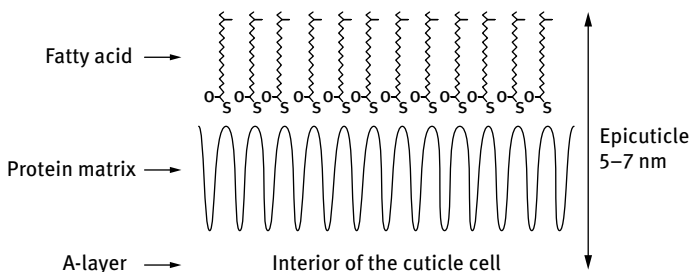


Fig. 10.12: Model of the epicuticle of keratin fibres.

10.8 Surface properties of hair

10.8.1 Wettability investigations

The surface energy of the intact human hair is determined by the outermost layer of the epicuticle which consists of covalently bound, long chain fatty acids [10]. Thus, the low-energy hydrophobic surface is not uniformly wetted by a high energy liquid like water. The most convenient method for assessing the wettability of a substrate by water is to measure the contact angle θ of a drop or air bubble on the substrate. This is illustrated in Fig. 10.13, which shows a schematic representation of a sessile drop (Fig. 10.13 (a)) and air bubble (Fig. 10.13 (b)) resting on a flat surface for a wettable surface (with $\theta < 90^\circ$, Fig. 10.13) and a non-wettable surface (with $\theta > 90^\circ$, Fig. 10.13).

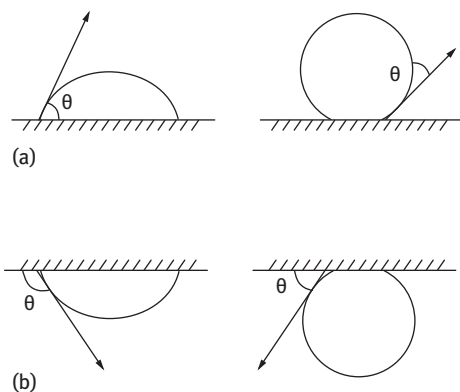


Fig. 10.13: Schematic representation of the sessile drop (a) and air bubble (b) resting on a surface.

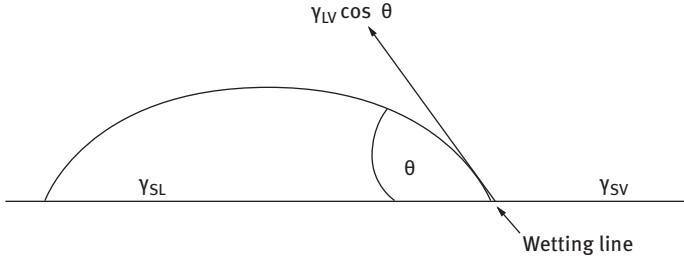


Fig. 10.14: Schematic representation of the balance of forces at the wetting line.

The equilibrium aspect of wetting can be assessed using Young's equation by considering the balance of forces at the wetting line as illustrated in Fig. 10.14. Three interfacial tensions can be identified: γ_{SV} , γ_{SL} and γ_{LV} (where 'S' refers to solid, 'V' to vapour and 'L' to liquid).

$$\gamma_{SV} = \gamma_{SL} + \gamma_{LV} \cos \theta, \quad (10.10)$$

$$\gamma_{LV} \cos \theta = \gamma_{SV} - \gamma_{SL}. \quad (10.11)$$

Clearly a hair is not a flat surface and it can be approximated as a cylinder. To measure the contact angle on the hair surface, the Wilhelmy plate method represented in Fig. 10.15 can be applied.

In the first case, the force on the plate F is given by the equation,

$$F = (\gamma_{LV} \cos \theta)p, \quad (10.12)$$

where p is the plate perimeter.

In the second case, the force is given by,

$$F = (\gamma_{LV} \cos \theta)p - \Delta\rho gV. \quad (10.13)$$

$\Delta\rho$ is the density difference between the plate and the liquid and V is the volume of liquid displaced.

A schematic representation for the set-up for measuring the wettability of a hair fibre [10] is shown in Fig. 10.16. An untreated intact hair fiber gives a contact angle θ greater than 90° and hence it produces a negative meniscus resulting in a negative wetting force w that is given by,

$$F_w = w + F_b, \quad (10.14)$$

where F_w is the recorded force and F_b is the buoyancy force.

On deposition of a hydrophilic polymer on the surface of the hair, the contact angle becomes smaller than 90° giving a positive meniscus and a positive wetting force.

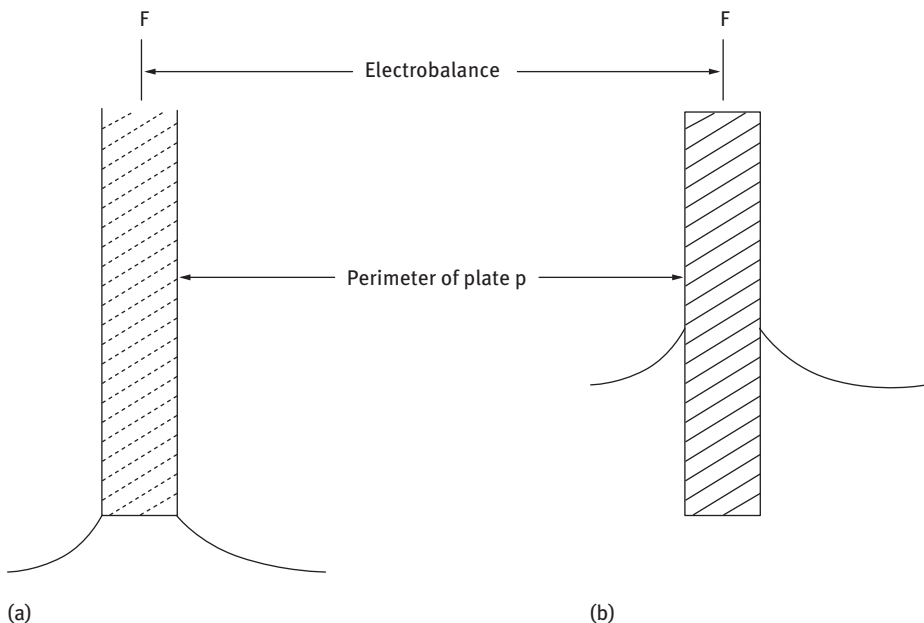


Fig. 10.15: Scheme for the Wilhelmy plate technique for measuring the contact angle: Left zero net depth; right finite depth.

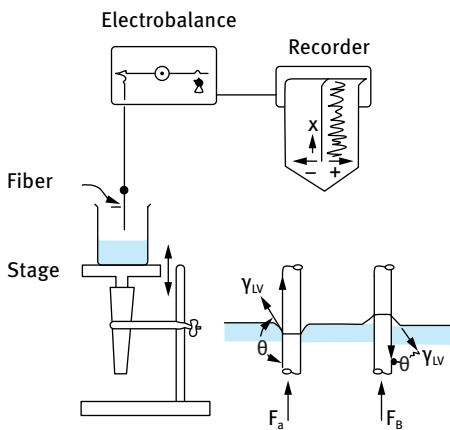


Fig. 10.16: Set-up for measuring the wettability of a hair fibre [10].

If the wetted perimeter P at the line of contact between liquid and fiber is known, the wettability W can be calculated,

$$W = w/P = \gamma_{LV} \cos \theta, \tag{10.15}$$

where γ_{LV} is the surface tension of the wetting liquid.

The perimeter of the fibre is calculated from the approximate relation,

$$P = 2\pi \left(\frac{A^2 + B^2}{2} \right)^{1/2}, \quad (10.16)$$

where A and B are the major and minor half-axes of the fibre and can be determined by laser micrometry.

Another parameter than can be used to characterize the surface is the work of adhesion A ,

$$A = \gamma_{LV}(\cos \theta + 1) = W + \gamma_{LV}. \quad (10.17)$$

The deposition, uniformity and substantivity of the hair conditioner can be characterized by scanning the wettability along the length of the fibre before and after treatment. Typical results are illustrated in Fig. 10.17 for quaternized cellulose derivative (Polymer JR-400) that is commonly used in conditioner formulations [10]. The wetting force of untreated fibre shows minor irregularities due to the scale structure and surface heterogeneity of the fibre. First immersion in the JR solution shows a spotty deposition of the polymer. The second immersion in water shows a significant reduction in the wetting peak indicating a loss of the hydrophilic polymer from the surface. No further desorption of the polymer occurs after the third immersion in water. Interaction with the anionic surfactant such as sodium lauryl sulphate or PEG ether sulphate affects the polymer deposition and the fibre wettability.

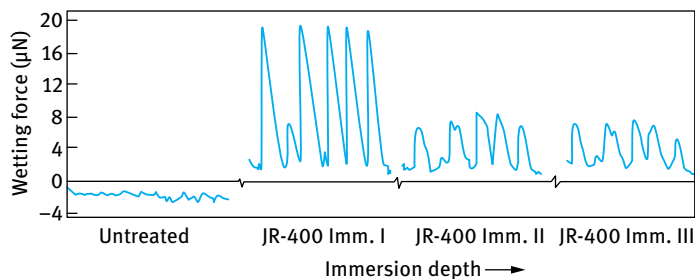


Fig. 10.17: Advanced wetting force curves in successive immersion of untreated hair fibre and the same hair fibre treated with 1% JR-400.

The interaction between anionic surfactants and the polymer cation can affect the polymer deposition. For example, with sodium lauryl sulphate below the critical micelle concentration (cmc), high levels of deposition with low substantivity are observed. However, above the cmc the wettability decreases below that of the untreated fibre. This could be due to the interaction between the surfactant micelles and the cationic polymer forming a surfactant–polymer complex with re-orientations that produce a hydrophobic surface.

10.8.2 Electrokinetic studies

The surface properties of hair can be investigated using streaming potential measurements [10], which can be applied to measure the zeta potential as a function of pH as well as the permeability of the plug (which can give information on swelling or shrinking of the fiber). A plug of hair is packed in a cell that contains two electrodes at its ends. The liquid under investigation is allowed to flow through the plug and the pressure drop P is measured. The potential difference at the electrodes is measured using an electrometer and the conductivity of the flowing liquid is simultaneously measured. This allows one to obtain the zeta potential and the permeability of the plug. Using this technique, the zeta potential–pH curves showed an isoelectric point for untreated hair of 3.7, indicating that in most practical conditions the hair surface is negatively charged (pH > 5).

10.9 Role of surfactants and polymers in hair conditioners

When using anionic surfactants alone in shampoos repulsion between the negatively charged hair and the anionic surfactant occurs, preventing deposition of the molecules on the hair surface. The electrostatic charges present on the hair surface results in difficult combing when the hair is wet [1]. In addition, when the hair is dry, the electrostatic build up on the surface of hair also makes the hair unmanageable, causing “flyaway” or frizziness [1]. These problems can be reduced in part by incorporation of amphoteric surfactants which can deposit on the hair surface, thus reducing the negative charge. However, these molecules are not very effective in conditioning the hair and various more effective cationically charged molecules have been suggested for hair conditioning. One of the earliest conditioners tried were cationic surfactants which deposit on the hair by electrostatic attraction between the negative charge on the hair surface and the cationic charge of the surfactant. However, when added to a shampoo based on anionic surfactant, interaction between the molecules occurs, resulting in associative phase-separated complexes that are incompatible with the nonionic formulation. Efforts have been made to minimize these interactions, but in general the resulting systems provide poor conditioning from a shampoo. The use of soluble cationic surfactants that form soluble ionic complexes that remain compatible in the formulation do not deposit well on the hair surface. The use of cationic surfactants that are compatible in the formulation, but form insoluble complexes on dilution also did not result in good conditioning. The breakthrough in hair conditioners came from the development of cationically modified water-soluble polymers.

The earliest studies used the cationic polymer polyethyleneimine (PEI), which could be radiolabelled (^{14}C) allowing one to accurately measure the uptake of the polymer by hair. Although this polymer was later withdrawn from hair conditioners (due to its toxicity) it can be considered as an initial model for an adsorbing polycation [12–

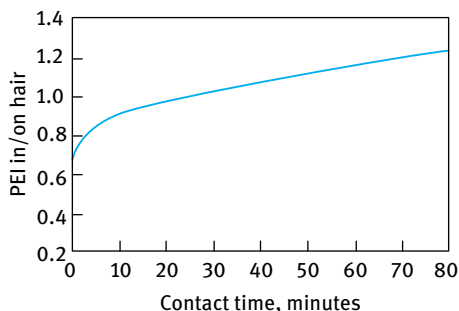


Fig. 10.18: Sorption of ^{14}C -labelled PEI 600 (expressed in % based on the weight of hair) from a 5% aqueous solution as a function of contact time.

15]. Two homopolymers of PEI with molar mass 600 and 60 000 were used in these studies. As an illustration, Fig. 10.18 shows the sorption of ^{14}C -labelled PEI 600 (expressed in % based on the weight of hair) from a 5% aqueous solution as a function of contact time.

The results in Fig. 10.18 show that sorption occurs almost immediately once the hair comes into contact with the PEI solution. This sorption increases with increasing contact time reaching more than 1% after 60 minutes. Similar results were obtained with the higher molar mass PEI and the sorption is compatible for the two polymers. Bleaching of hair increases the uptake of the polymer, in particular with the higher molar mass PEI. After 1 hour, the sorption of PEI 60 000 increases from 1.2 to 3.4 % on bleaching the hair. Reducing the concentration of PEI causes a decrease in the sorption amount (with an 80 % reduction in concentration, the sorption amount decreases by 50 %). The sorption was highest at pH 7 and it decreases when the pH is increased to 10. Reduction of the pH to 2 significantly reduces the sorption amount since at this pH the hair becomes positively charged.

Polyquaternium-10, which is a cationically modified hydroxyethyl cellulose (HEC) with the cationic groups being hydroxypropyltrimethylammonium, is commonly used as a hair conditioner in shampoos [12–15]. The grade of Polyquaternium-10 that is commonly used in shampoos has a number average molecular weight of 400 000 and about 1300 cationic sites. Several other cationically modified HEC have been developed such as Polymer-JR with three molecular weight grades of 250 000 (JR-30M), 400 000 (JR-400) and 600 000 (JR-125). These polymers have the generic formula represented in Fig. 10.19.

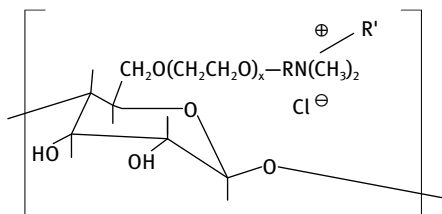


Fig. 10.19: Generic formula of Polymer JR.

The cross-sectional area of these polymers is considerably larger than that of PEI. The adsorption of HEC and JR polymers on hair was studied by Goddard [14] using radio-labelled polymers. In all experiments, the concentration of polymer was kept constant at 0.1% and the amount sorbed (mg/g) was measured as a function of time for several days. The sorption of HEC reached equilibrium in 5 minutes, whereas with the charged JR polymers it did not reach its equilibrium value even after 2 days. The results are shown in Fig. 10.20 and 10.21 which shows the variation of the amount sorbed (mg/g) with time.

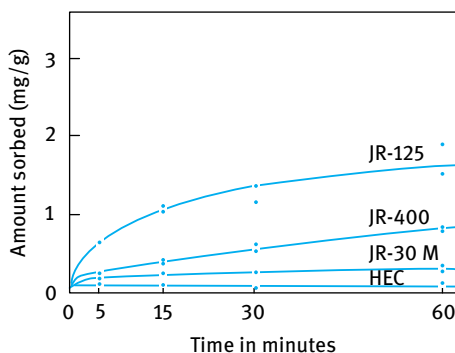


Fig. 10.20: Sorption of ¹⁴C-labelled polymer (from 0.1% solution) by virgin hair; short time experiment [14].

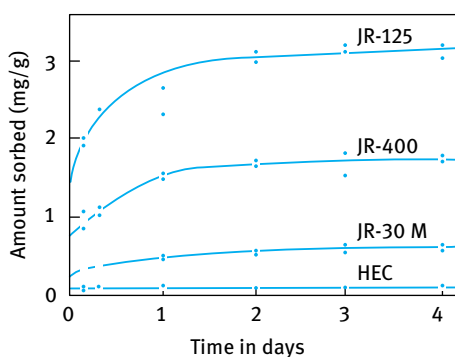


Fig. 10.21: Sorption of ¹⁴C-labelled polymer (from 0.1% solution) by virgin hair; long time experiment [14].

The amount of adsorption of HEC on hair (0.05 mg/g) corresponds to the value expected for a close-packed monolayer of the cellulose (in flat orientation) giving an area per HEC residue of $\approx 0.85 \text{ nm}^2$. The adsorption of JR polymers is higher than the corresponding amount for flat orientation. It has been suggested that the polycation diffuses in the keratinous substrate. The sorption of the polymer on bleached hair was much higher (Fig. 10.14), which shows an order of magnitude higher adsorption when compared with that of unbleached hair (Fig. 10.22). This indicates the more damaged and porous nature of the bleached fibre.

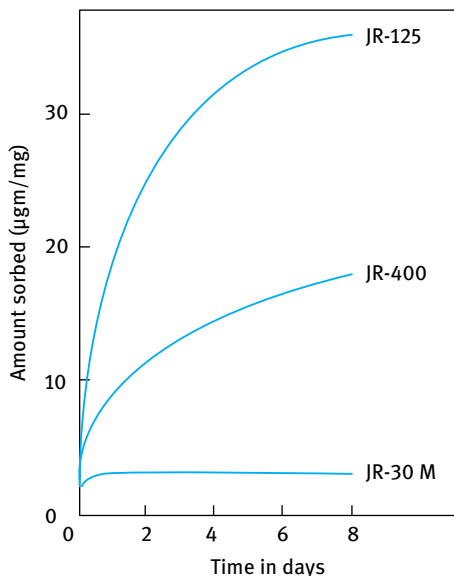


Fig. 10.22: Sorption of different grades of Polymer JR on bleached hair from 0.1% solution [14].

The electrostatic attraction between the cationic groups on the JR polymers and the negative charges on the surface of hair seems to be the driving force for the adsorption process. Evidence for this was obtained by studying adsorption in the presence of added electrolytes, 0.1 and 1% NaCl which reduced the adsorption by approximately three- and 10-fold respectively (Fig. 10.23).

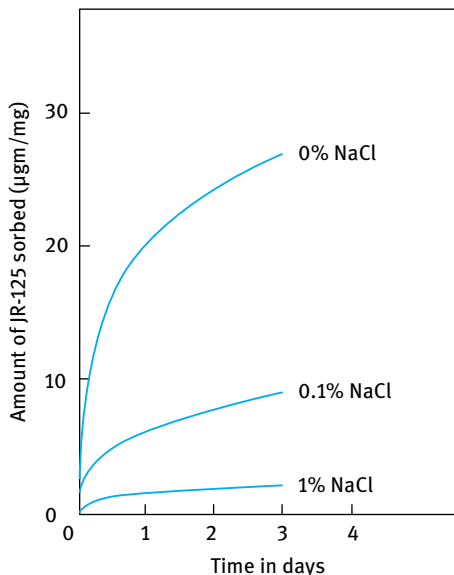


Fig. 10.23: Effect of addition of NaCl on the sorption of JR 125 by bleached hair; 0.1% polymer solution [14].

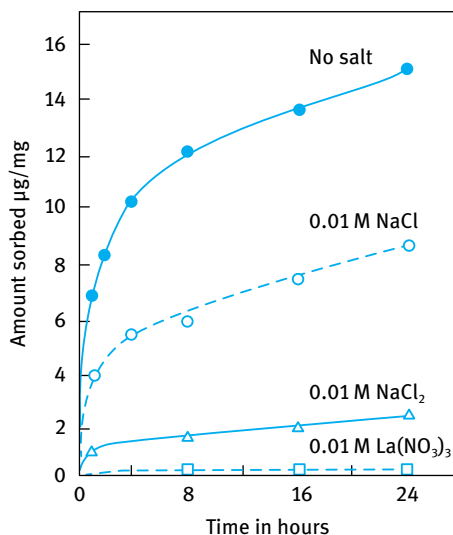


Fig. 10.24: Effect of different electrolytes on the sorption of Polymer JR 125 by bleached hair; 0.1% polymer solution [14].

For a given molarity of electrolyte, the reduction in sorption increases with increasing electrolyte valency as shown in Fig. 10.24 (in accordance with the Schultz–Hardy rule).

If electrostatic attraction between the polycation and the negatively charged hair is the driving force for adsorption, one would expect a large effect of the pH which determines the charge on the hair surface. The effect of pH on the sorption of JR 125 (expressed as the amount of sorption σ in g/g) is shown in Fig. 10.25. Initial work showed little variation of the adsorption of Polymer JR-125 on bleached hair within the pH range 4–10. However, later work showed a catastrophic reduction in the sorption of this polymer on virgin hair when the pH was reduced below the isoelectric point (pH 3.7). Under these conditions, the amount of uptake approximated that displayed by the uncharged HEC molecule. This result provides further evidence that electrostatic forces govern the adsorption of the polyelectrolyte [14].

As mentioned above, the adsorption of cationically modified polymers on hair in the presence of anionic surfactants is complicated by the polyelectrolyte-surfactant interaction. Results for the interaction between JR-400 or Reten (polycation of acrylamide/ β -methylacryloxy trimethyl ammonium chloride) and sodium dodecyl sulphate (SDS) were obtained by Goddard [12] using surface tension and viscosity measurements. Fig. 10.26 shows the viscosity results where the relative viscosity is plotted as a function of SDS concentration at a constant JR-400 or Reten concentration of 1%. With Polymer JR-400, the relative viscosity showed a rapid increase in the immediate precipitation zone. In the precipitation zone a network is invoked in which surfactant molecules bound to one polycation molecule associate with similarly linked surfactant molecules on the other polymer chains. At high SDS concentration, the solution viscosity falls since the properties are now dominated by surfactant micelles. In contrast with Reten at 1% concentration, a change in viscosity with added

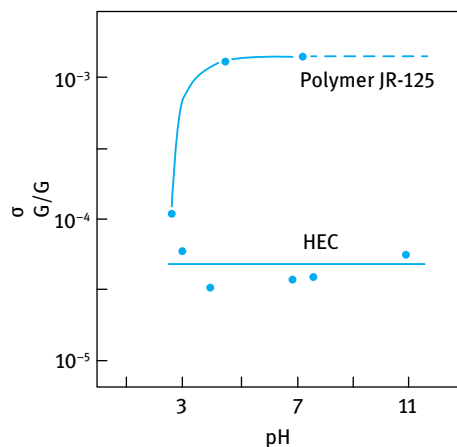


Fig. 10.25: Sorption of JR-125 onto virgin hair as a function of solution pH; 0.1% polymer solution [14].

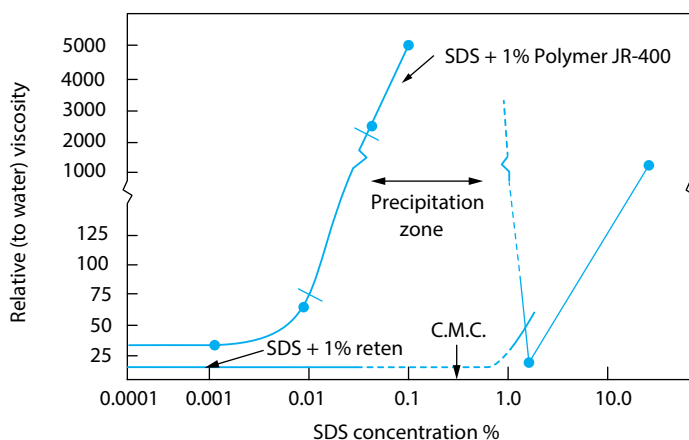


Fig. 10.26: Relative viscosity of 1% Polymer JR 400 and 1% Reten as a function of SDS concentrations [12].

SDS in the precipitation zone and only a modest increase in viscosity is observed at 1% SDS concentration.

The above interaction between the anionic surfactants and polycation has a major influence on the uptake of Polymer JR. This interaction leads to considerable reduction of polyelectrolyte deposition on hair. Nonionic surfactants such as Tergitol 15-S-9 show substantially “unimpeded” deposition of the polycation, whereas amphoteric surfactants (based on imidazoline) showed substantial deposition of the polymer. In contrast, the cationic surfactant cetyltrimethyl ammonium bromide (CTAB) virtually eliminated the polymer adsorption. This is due to the faster diffusion of CTA^+ which neutralized the negative charges on the hair.

References

- [1] Tadros T. Cosmetics. In: Tadros T, editor. Encyclopedia of colloid and interface science. Berlin: Springer; 2013.
- [2] Tadros T. Applied surfactants. Weinheim: Wiley-VCH; 2005.
- [3] Tadros T. An introduction to surfactants. Berlin: De Gruyter; 2014.
- [4] Holmberg K, Jonsson B, Kronberg B, Lindman B. Surfactants and polymers in aqueous solution. 2nd edition. John Wiley & Sons, USA; 2003.
- [5] Penfield K. IFSCC Magazine. 2005;8(2):115.
- [6] Tadros TF. Advances Colloid and Interface Science. 1996;68:97.
- [7] Israelachvili JN. Intermolecular and surface forces, with special applications to colloidal and biological systems. London: Academic Press; 1985.
- [8] Goddard ED, Gruber JV, editors. Principles of polymer science and technology in cosmetics and personal care. New York: Marcel Dekker; 1999.
- [9] Tadros T, Hously S. In: Tadros T, editor. Colloids in cosmetics and personal care. Weinheim: Wiley-VCH; 2008.
- [10] Weigman HD, Kamath Y. Evaluation methods for conditioned hair. In: Goddard DE, Gruber JV, editors. Principles of polymer science and technology in cosmetics and personal care. New York: Marcel Dekker; 1999. Chapter 12.
- [11] Robbins CR. Chemical and physical behaviour of human hair. 3rd edition. New York: Springer; 1994.
- [12] Goddard DE. Polymer/surfactant interaction, methods and mechanisms. In: Goddard DE, Gruber JV, editors. Principles of polymer science and technology in cosmetics and personal care. New York: Marcel Dekker; 1999. Chapter 4.
- [13] Goddard DE. Polymer/surfactant interaction, applied systems. In: Goddard DE, Gruber JV, editors. Principles of polymer science and technology in cosmetics and personal care. New York: Marcel Dekker; 1999. Chapter 5.
- [14] Goddard DE. Measuring and interpreting polycation adsorption. In: Goddard DE, Gruber JV, editors. Principles of polymer science and technology in cosmetics and personal care. New York: Marcel Dekker; 1999. Chapter 10.
- [15] Goddard DE. The adsorptivity of charged and uncharged cellulose ethers. In: Goddard DE, Gruber JV, editors. Principles of polymer science and technology in cosmetics and personal care. New York: Marcel Dekker; 1999. Chapter 11.

11 Sunscreens for UV protection

11.1 Introduction

The increase in skin cancers has heightened public awareness to the damaging effects of the sun and many skin preparations are now available to help protect the skin from UV radiation [1, 2]. The actives employed in these preparations are of two basic types: organics, which can absorb UV radiation of specific wavelengths due to their chemical structure and inorganics, which both absorb and scatter UV radiation. Inorganics have several benefits over organics in that they are capable of absorbing over a broad spectrum of wavelengths and they are mild and non-irritant. Both of these advantages are becoming increasingly important as the demand for *daily* UV protection against both UVB (wavelength 290–320 nm) and UVA (wavelength 320–400 nm) radiation increases. Since UVB is much more effective than UVA at causing biological damage, solar UVB contributes about 80 % towards a sunburn reaction, with solar UVA contributing the remaining 20 %. In people with white skin living in the tropics (30° N to 30° S), sun protection is necessary all year, whereas those living in temperate altitudes (40° to 60°), sun awareness is generally limited to the 6-month period encompassing the summer solstice. Several harmful effects can be quoted on prolonged exposure to UV radiation. For UVB the main effects are DNA damage, immunosuppression, sunburn and skin cancer. For UVA the main effects are generation of active oxygen species, photo-dermatoses, premature skin ageing, skin wrinkles and skin cancer.

The ability of fine particle inorganics to absorb radiation depends upon their refractive index. For inorganic semiconductors such as titanium dioxide and zinc oxide this is a complex number indicating their ability to absorb light. The band gap in these materials is such that UV light up to around 405 nm can be absorbed. They can also scatter light due to their particulate nature and their high refractive indices make them particularly effective scatterers. Both scattering and absorption depend critically on particle size [1–3]. Particles of around 250 nm for example are very effective at scattering visible light and TiO₂ of this particle size is the most widely used white pigment. At smaller particle sizes, absorption and scattering maxima shift to the UV region and at 30–50 nm UV attenuation is maximized.

The use of TiO₂ as a UV attenuator in cosmetics was, until recently, largely limited to baby sun protection products due to its poor aesthetic properties (*viz*; scattering of visible wavelengths results in whitening). Recent advances in particle size control and coatings have enabled formulators to use fine particle titanium dioxide and zinc oxide in daily skincare formulations without compromising the cosmetic elegance [3].

The benefits of a pre-dispersion of inorganic sunscreens are widely acknowledged. However, it requires an understanding of the nature of colloidal stabilization in order to optimize this pre-dispersion (for both UV attenuation and stability) and exceed the performance of powder-based formulations. Dispersion rheology and its

<https://doi.org/10.1515/9783110555257-012>

dependence on interparticle interactions is a key factor in this optimization. Optimization of sunscreen actives however does not end there; an appreciation of the end application is crucial to maintaining performance. Formulators need to incorporate the particulate actives into an emulsion, mousse or gel with due regard to aesthetics (skin feel and transparency), stability and rheology.

In this chapter, I will demonstrate how the application of colloid and interface science principles give a sound basis on which to carry out true optimization of consumer acceptable sunscreen formulations based upon particulate TiO₂. I will show that both dispersion stability and dispersion rheology depend upon adsorbed amount Γ and steric layer thickness δ (which in turn depends on oligomer molecular weight M_n and solvency χ). In order to optimize formulation, the adsorption strength χ^s must also be considered. The nature of interaction between particles, dispersant, emulsifiers and thickeners must be considered with regard to competitive adsorption and/or interfacial stability if a formulation is to deliver its required protection when spread on the skin.

11.2 Mechanism of absorbance and scattering by TiO₂ and ZnO

As mentioned in the introduction, TiO₂ and ZnO absorb and scatter UV light. They provide a broad spectrum and they are inert and safe to use. Larger particles scatter visible light and they cause whitening. The scattering and absorption depend on the refractive index (which depends on the chemical nature), the wavelength of light and the particle size and shape distribution. The total attenuation is maximized in UVB for 30–50 nm particles. A schematic representation of the scattering of light is given in Fig. 11.1 whereas Fig. 11.2 shows the effect of particle size on UVA and UVB absorption.

The performance of any sunscreen formulation is defined by a number referred to as the sun protection factor (SPF). The basic principle of calculation of the SPF [4] is based on the fact that the inverse of the UV transmission through an absorbing layer, $1/T$, is the factor by which the intensity of the UV light is reduced. Thus, at a certain wavelength λ , $1/T(\lambda)$ is regarded as a monochromatic protection factor (MPF). Since the spectral range relevant for the in vivo SPF is between 290 and 400 nm (see Fig. 11.2), the monochromatic protection factors have to be averaged over this range. This average must be weighted using the intensity of a standard sun, $S_s(\lambda)$ and the erythral action spectrum, $S_{er}(\lambda)$, leading to the following definition of SPF [4],

$$\text{SPF} = \frac{\sum_{290}^{400} S_{er}(\lambda)S_s(\lambda)}{\sum_{290}^{400} S_{er}(\lambda)S_s(\lambda)T(\lambda)}. \quad (11.1)$$

Data for $S_s(\lambda)$ and $S_{er}(\lambda)$ are available in the literature; the product of $S_s(\lambda)$ $S_{er}(\lambda)$ is called the erythral efficiency. $T(\lambda)$ has to be determined for the respective sunscreen; this can be done either via transmission measurements with special UV spectrometers using substrates and a rough surface or via the calculation of the transmission.

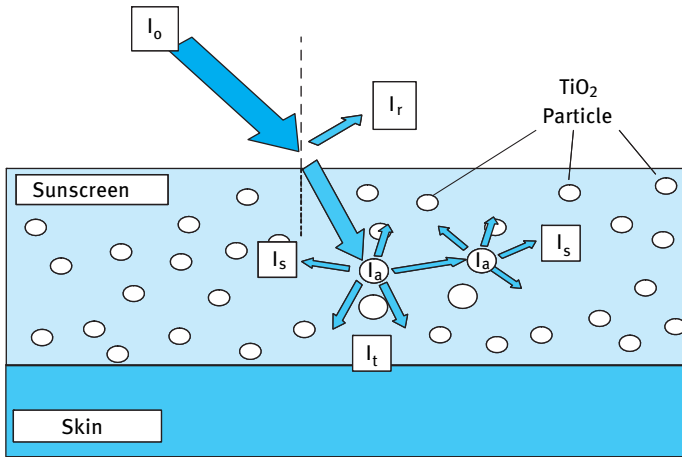


Fig. 11.1: Schematic representation of scattering of light by TiO₂ particles.

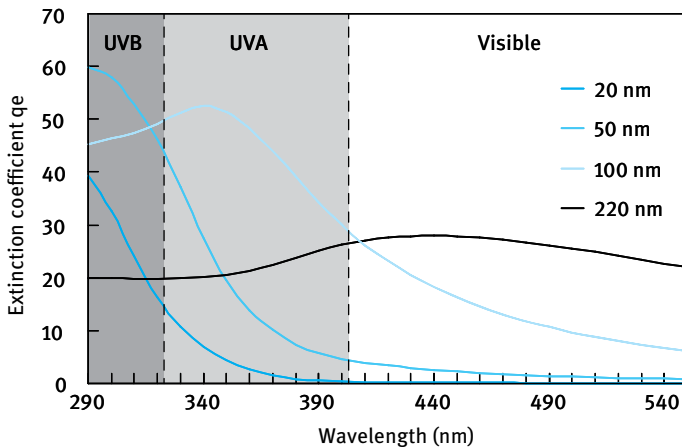


Fig. 11.2: Effect of particle size on UVA and UVB absorption.

11.3 Preparation of well-dispersed particles

To keep the particles well dispersed (as single particles) high steric repulsion is required to overcome strong van der Waals attraction. The mechanism of steric stabilization has been described in detail in Chapter 4 and only a summary is given here.

Small particles tend to aggregate as a result of the universal van der Waals attraction unless this attraction is screened by an effective repulsion between the particles. The van der Waals attraction energy $G_A(h)$ at close approach depends upon the distance, h , between particles of radius, R , and is characterized by the effective Hamaker

constant, A ,

$$G_A(h) = -\frac{AR}{12h}. \quad (11.2)$$

The effective Hamaker constant A is given by the following equation,

$$A = (A_{11}^{1/2} - A_{22}^{1/2})^2. \quad (11.3)$$

A_{11} is the Hamaker constant of the particles and A_{22} is that for the medium. For TiO_2 , A_{11} is exceptionally high so that in nonaqueous media with relatively low A_{22} the effective Hamaker constant A is high, and despite the small size of the particles a dispersant is always needed to achieve colloidal stabilization. This is usually obtained using adsorbed layers of polymers or surfactants. The most effective molecules are the A-B, A-B-A block or BA_n graft polymeric surfactants [5] where B refers to the anchor chain. For a hydrophilic particle this may be a carboxylic acid, an amine or phosphate group or other larger hydrogen bonding type block such as polyethylene oxide. The A chains are referred to as the stabilizing chains, which should be highly soluble in the medium and strongly solvated by its molecules. For nonaqueous dispersions the A chains could be polypropylene oxide, a long chain alkane, oil-soluble polyester or polyhydroxystearic acid (PHS). A schematic representation of the adsorbed layers and the resultant interaction energy–distance curve is shown in Fig. 11.3.

When two particles with an adsorbed layer of hydrodynamic thickness δ approach to a separation distance h that is smaller than 2δ , repulsion occurs as a result of two main effects:

- (i) unfavourable mixing of the A chains when these are in good solvent condition;
- (ii) reduction in configurational entropy on significant overlap.

Napper [6] derived a form for the so-called steric potential $G(h)$ which arises as polymer layers begin to overlap (equation (11.4))

$$G(h) = 2\pi kTR^2\Gamma^2 N_A \left(\frac{v_p^2}{V_s}\right) \left(\frac{1}{2} - \chi\right) \left(1 - \frac{h}{2\delta}\right)^2 + G_{\text{elastic}}, \quad (11.4)$$

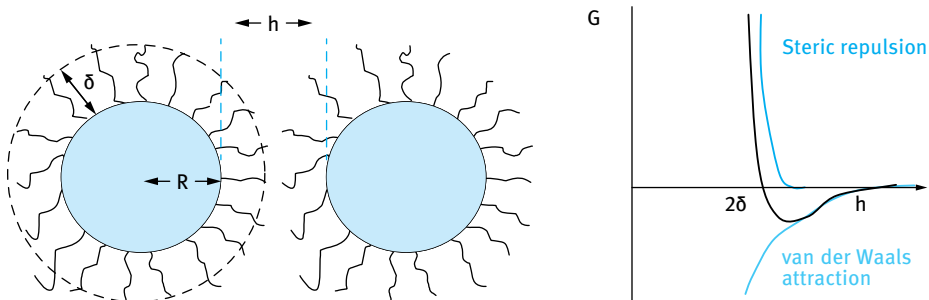


Fig. 11.3: Schematic representation of adsorbed polymer layers and resultant interaction energy G on close approach at distance $h < 2R$.

where k is the Boltzmann constant, T is temperature, R is the particle radius, Γ is the adsorbed amount, N_A the Avogadro constant, v is the specific partial volume of the polymer, V_s the molar volume of the solvent, χ is the Flory–Huggins parameter and δ is the maximum extent of the adsorbed layer.

It is useful to consider the terms in equation (11.4):

- (i) The adsorbed amount Γ ; the higher the value, the greater the interaction/repulsion.
- (ii) Solvent conditions as determined by the value of χ ; two very distinct cases emerge. Maximum interaction occurs on overlap of the stabilizing layers when the chains are in good solvent conditions, i.e. $\chi < 0.5$. Osmotic forces cause solvent to move into the highly concentrated overlap zone forcing the particles apart. If $\chi = 0.5$, a theta solvent, the steric potential goes to zero and for poor solvent conditions ($\chi > 0.5$) the steric potential becomes negative and the chains will attract, enhancing flocculation.
- (iii) Adsorbed layer thickness δ . The steric interaction starts at $h = 2\delta$ as the chains begin to overlap and increases as the square of the distance. Here it not the size of the steric potential that is important, but the distance h at which it begins.
- (iv) The final interaction potential is the superposition of the steric potential and the van der Waals attraction as shown in Fig. 11.3.

The adsorbed layer thickness depends critically on the solvation of the polymer chain and it is therefore important to gain at least a qualitative view as to the relative solubilities of a polymer in different oils employed in dispersion. In this study solubility parameters were employed to provide that comparison. Generally, the affinity between two materials is considered to be high when the chemical and physical properties of the two materials resemble each other. For example, nonpolar materials can be easily dispersed in nonpolar solvents but hardly dissolved in polar solvents and vice versa.

One of the most useful concepts for assessing solvation of any polymer by the medium is to use the Hildebrand solubility parameter δ^2 which is related to the heat of vaporization ΔH by the following equation [7],

$$\delta^2 = \frac{\Delta H - RT}{V_M}, \quad (11.5)$$

where V_M is the molar volume of the solvent.

Hansen [8] first divided Hildebrand's solubility parameter into three terms as follows:

$$\delta^2 = \delta_d^2 + \delta_p^2 + \delta_h^2, \quad (11.6)$$

where δ_d , δ_p and δ_h correspond to London dispersion effects, polar effects and hydrogen bonding effects, respectively.

Hansen and Beerbower [9] developed this approach further and proposed a stepwise approach such that theoretical solubility parameters can be calculated for any solvent or polymer based upon its component groups. In this way we can arrive at

theoretical solubility parameters for dispersants and oils. In principle, solvents with a similar solubility parameter to the polymer should also be a good solvent for it (low χ).

For sterically stabilized dispersions, the resulting energy–distance curve often shows a shallow minimum G_{\min} at particle–particle separation distance h comparable to twice the adsorbed layer thickness δ (Fig. 11.3). The depth of this minimum depends on the particle size R , Hamaker constant A and adsorbed layer thickness δ . At constant R and A , G_{\min} decreases with increasing δ/R [10]. This is illustrated in Fig. 11.4.

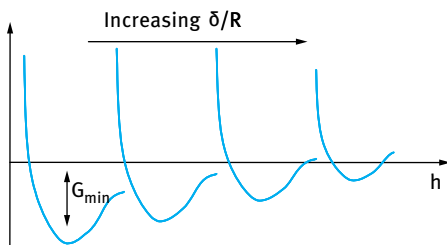


Fig. 11.4: Schematic representation of energy–distance curves at increasing δ/R ratios

When δ becomes smaller than 5 nm, G_{\min} may become deep enough to cause weak flocculation. This is particularly the case with concentrated dispersions since the entropy loss on flocculation becomes very small and a small G_{\min} would be sufficient to cause weak flocculation ($\Delta G_{\text{floc}} < 0$). This can be explained by considering the free energy of flocculation [10],

$$\Delta G_{\text{floc}} = \Delta H_{\text{floc}} - T\Delta S_{\text{floc}}. \quad (11.7)$$

Since for concentrated dispersions ΔS_{floc} is very small, then ΔG_{floc} depends only on the value of ΔH_{floc} . This in turn depends on G_{\min} , which is negative. In other words, ΔG_{floc} becomes negative causing weak flocculation. This will result in a three-dimensional coherent structure with a measurable yields stress [11]. This weak gel can be easily redispersed by gentle shaking or mixing. However, the gel will prevent any separation of the dispersion on storage. So, we can see that the interaction energies also determine the dispersion rheology.

At high solids content and for dispersions with larger δ/R , viscosity is also increased by steric repulsion. With a dispersion consisting of very small particles, as is the case with UV attenuating TiO_2 , significant rheological effects can be observed even at moderate volume fraction of the dispersion. This is due to the much higher effective volume fraction of the dispersion compared with the core volume fraction due to the adsorbed layer.

Let us for example consider a 50 % w/w TiO_2 dispersion with a particle radius of 20 nm with a 3000 molecular weight stabilizer giving an adsorbed layer thickness of ≈ 10 nm. The effective volume fraction is given by [2]:

$$\begin{aligned}
 \phi_{\text{eff}} &= \phi \left[1 + \frac{\delta}{R} \right]^3 \\
 &= \phi [1 + 10/20]^3 \\
 &\approx 3\phi.
 \end{aligned}
 \tag{11.8}$$

The effective volume fraction can be three times that of the core particle volume fraction. For a 50 % solids (w/w) TiO₂ dispersion the core volume fraction ϕ is ≈ 0.25 (taking an average density of 3 g cm^{-3} for the TiO₂ particles) which means that ϕ_{eff} is about 0.75 which is sufficient to fill the whole dispersion space producing a highly viscous material. It is important therefore to choose the minimum δ for stabilization.

In the case of steric stabilization as employed in these oil dispersions the important success criteria for well stabilized but handleable dispersions are [2]:

- (i) complete coverage of the surface – high Γ (adsorbed amount);
- (ii) Strong adsorption (or “anchoring”) of the chains to the surface;
- (iii) effective stabilizing chain, chain well solvated, $\chi < 0.5$ and adequate (but not too large) steric barrier δ .

However, a colloiddally stable dispersion does not guarantee a stable and optimized final formulation. TiO₂ particles are always surface modified in a variety of ways in order to improve dispersability and compatibility with other ingredients. It is important that we understand the impact these surface treatments may have upon the dispersion and more importantly upon the final formulation. As will be discussed below, TiO₂ is actually formulated into a suspoemulsion, i.e. a suspension in an emulsion. Many additional ingredients are added to ensure cosmetic elegance and function. The emulsifiers used are structurally and functionally not very different to the dispersants used to optimize the fine particle inorganics. Competitive adsorption may occur with some partial desorption of a stabilizer from one or other of the available interfaces. Thus one requires strong adsorption (which should be irreversible) of the polymer to the particle surface.

11.4 Experimental results for sterically stabilized TiO₂ dispersions in nonaqueous media

Dispersions of surface modified TiO₂ (Tab. 11.1) in alkyl benzoate and hexamethyl-tetracosane (Squalane) were prepared at various solids loadings using a polymeric/oligomeric polyhydroxystearic acid (PHS) surfactant of molecular weight 2500 (PHS 2500) and 1000 (PHS1000) [2]. For comparison, results were also obtained using a low molecular weight (monomeric) dispersant, namely isostearic acid, ISA. The titania particles had been coated with alumina and/or silica. The electron micrograph in Fig. 11.5 shows the typical size and shape of these rutile particles. The surface area and particle size of the three powders used are summarized in Tab. 11.1.

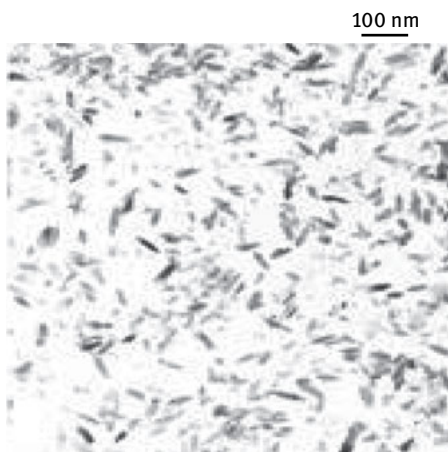


Fig. 11.5: Transmission electron micrograph of titanium dioxide particles.

Tab. 11.1: Surface modified TiO₂ powders.

Powder	Coating	Surface Area* (m ² g ⁻¹)	Particle size** (nm)
A	Alumina/silica	95	40–60
B	Alumina/stearic acid	70	30–40
C	Silica/stearic acid	65	30–40

* BET N₂, ** equivalent sphere diameter, X-ray disc centrifuge

The dispersions of the surface modified TiO₂ powder, dried at 110 °C, were prepared by milling (using a horizontal bead mill) in polymer solutions of different concentrations for 15 minutes and were then allowed to equilibrate for more than 16 hours at room temperature before making the measurements.

The adsorption isotherms were obtained by preparing dispersions of 30 % w/w TiO₂ at different polymer concentrations (C_0 , mg l⁻¹). The particles and adsorbed dispersant were removed by centrifugation at 20 000 rpm ($\approx 48\,000\text{ g}$) for 4 hours, leaving a clear supernatant. The concentration of the polymer in the supernatant was determined by acid value titration. The adsorption isotherms were calculated by mass balance to determine the amount of polymer adsorbed at the particle surface (Γ , mg m⁻²) of a known mass of particulate material (m , g) relative to that equilibrated in solution (C_e , mg l⁻¹).

$$\Gamma = \frac{(C_0 - C_e)}{mA_s}. \quad (11.9)$$

The surface area of the particles (A_s , m² g⁻¹) was determined by BET nitrogen adsorption method. Dispersions of various solids loading were obtained by milling at progressively increasing TiO₂ concentration at an optimum dispersant/solids ratio [2]. The dispersion stability was evaluated by viscosity measurement and by attenuation of UV/vis radiation. The viscosity of the dispersions was measured by subjecting the

dispersions to an increasing shear stress, from 0.03 Pa to 200 Pa over 3 minutes at 25 °C using a Bohlin CVO rheometer. It was found that the dispersions exhibited shear thinning behaviour and the zero shear viscosity, identified from the plateau region at low shear stress (where viscosity was apparently independent of the applied shear stress). The latter was used to provide an indication of the equilibrium energy of interaction that had developed between the particles.

UV-vis attenuation was determined by measuring transmittance of radiation between 250 nm and 550 nm. Samples were prepared by dilution with a 1% w/v solution of dispersant in cyclohexane to approximately 20 mg l⁻¹ and placed in a 1 cm pathlength cuvette in a UV-vis spectrophotometer. The sample solution extinction ε (l g⁻¹ cm⁻¹) was calculated from Beer's Law (equation (11.10)):

$$\varepsilon = \frac{A}{cl}, \quad (11.10)$$

where A is absorbance, c is concentration of attenuating species (g l⁻¹), l is path-length (cm).

The dispersions of powders B and C were finally incorporated into typical water-in-oil sunscreen formulations at 5% solids with an additional 2% of organic active (butyl methoxy dibenzoyl methane) and assessed for efficacy, SPF (sun protection factor) as well as stability (visual observation, viscosity). SPF measurements were made on an Optometrics SPF-290 analyser fitted with an integrating sphere, using the method of Diffey and Robson [12].

Fig. 11.6 shows the adsorption isotherms of ISA, PHS1000 and PHS2500 on TiO₂ in alkylbenzoate (Fig. 11.6 (a)) and in squalane (Fig. 11.6 (b)).

The adsorption of the low molecular weight ISA from alkylbenzoate is of low affinity (Langmuir type), indicating reversible adsorption (possibly physisorption). In contrast, the adsorption isotherms for PHS100 and PHS2500 are of the high affinity type, indicating irreversible adsorption and possible chemisorption due to acid-base interaction. From squalane, all adsorption isotherms show high affinity type and they show

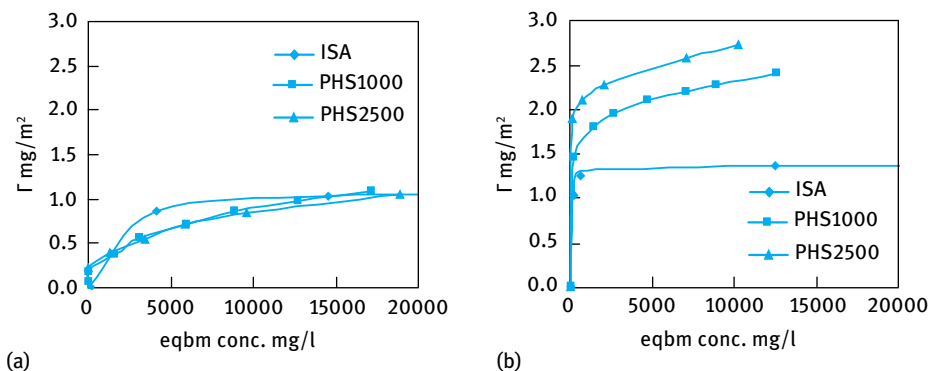


Fig. 11.6: (a) Adsorption isotherms in alkylbenzoate. (b) Adsorption isotherms in squalane.

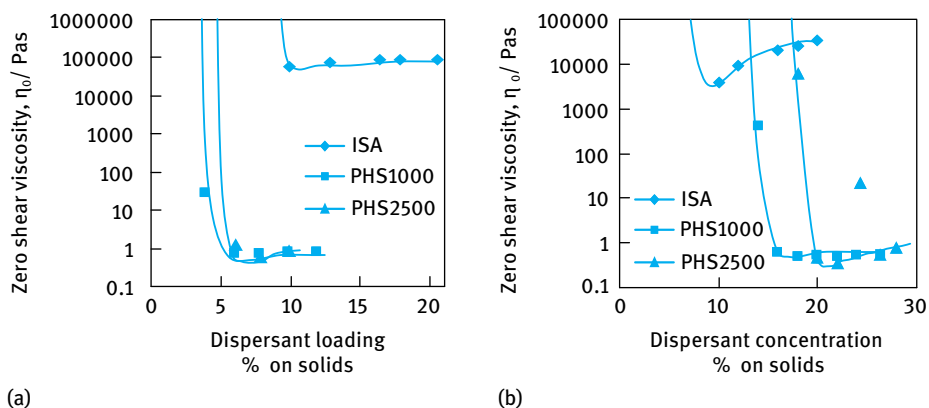


Fig. 11.7: Dispersant demand curve in alkylbenzoate (left) and squalane (right).

higher adsorption values when compared with the results using alkylbenzoate. This reflects the difference in solvency of the dispersant by the medium as will be discussed below.

Fig. 11.7 shows the variation of zero shear viscosity with dispersant loading % on solid for a 40 % dispersion. It can be seen that the zero shear viscosity decreases very rapidly with increasing dispersant loading and eventually the viscosity reaches a minimum at an optimum loading that depends on the solvent used as well as the nature of the dispersant.

With the molecular dispersant ISA, the minimum viscosity that could be reached at high dispersant loading was very high (several orders of magnitude more than the optimized dispersions) indicating poor dispersion of the powder in both solvents. Even reducing the solids content of TiO_2 to 30 % did not result in a low viscosity dispersion. With PHS1000 and PHS2500, a low minimum viscosity could be reached at 8–10 % dispersant loading in alkylbenzoate and 18–20 % dispersant loading in squalane. In the latter case the dispersant loading required for reaching a viscosity minimum is higher for the higher molecular weight PHS.

The quality of the dispersion was assessed using UV-vis attenuation measurements. At very low dispersant concentration a high solids dispersion can be achieved by simple mixing but the particles are aggregated as demonstrated by the UV-vis curves (Fig. 11.8). These large aggregates are not effective as UV attenuators. As the PHS dispersant level is increased, UV attenuation is improved and above 8 wt% dispersant on particulate mass, optimized attenuation properties (high UV, low visible attenuation) are achieved (for the PHS1000 in alkyl benzoate). However, milling is also required to break down the aggregates into their constituent nanoparticles and a simple mixture which is unmilled has poor UV attenuation, even at 14 % dispersant loading.

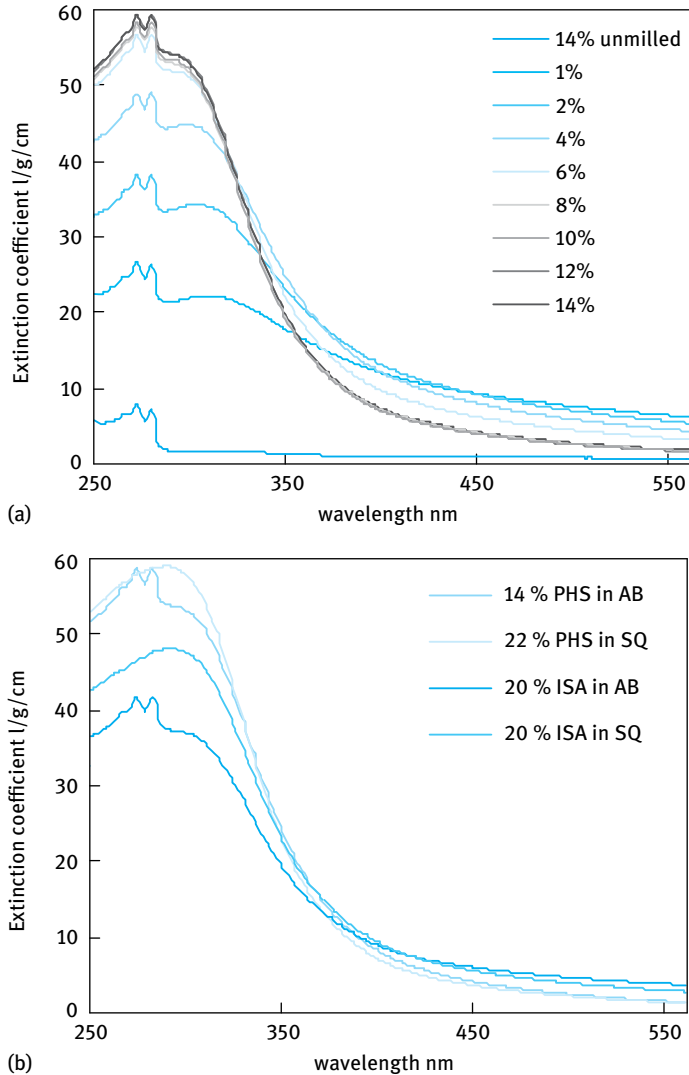


Fig. 11.8: (a) UV-vis attenuation for milled dispersions with 1-14 % PHS1000 dispersant and un-milled at 14 % dispersant on solids. (b) UV-vis attenuation for dispersions in squalane (SQ) and in alkylbenzoate (AB) using 20 % isostearic acid (ISA) as dispersant compared to optimized PHS1000 dispersions in the same oils.

The UV-vis curves obtained when monomeric isostearic acid was incorporated as a dispersant (Fig. 11.8) indicate that these molecules do not provide a sufficient barrier to aggregation, resulting in relatively poor attenuation properties (low UV, high visible attenuation).

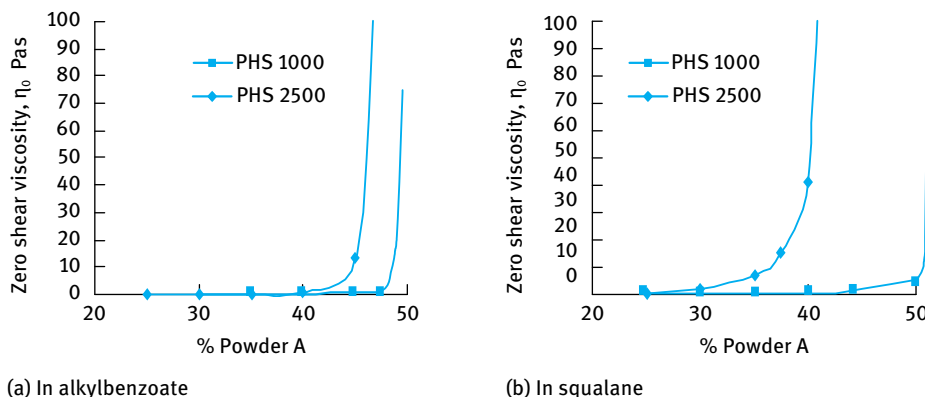


Fig. 11.9: Zero shear viscosity dependency on solids loading.

The steric layer thickness δ could be varied by altering the dispersion medium and hence the solvency of the polymer chain. This had a significant effect upon dispersion rheology. Solids loading curves (Fig. 11.9 (a) and (b)) demonstrate the differences in effective volume fraction due to the adsorbed layer (equation (11.8)).

In the poorer solvent case (squalane), the effective volume fraction and adsorbed layer thickness showed a strong dependency upon molecular weight with solids loading becoming severely limited above 35% for the higher molecular weight whereas $\approx 50\%$ could be reached for the lower molecular weight polymer. In alkyl benzoate, no strong dependency was seen with both systems achieving more than 45% solids. Solids weight fraction above 50% resulted in very high viscosity dispersions in both solvents.

The same procedure described above enabled optimized dispersion of equivalent particles with alumina and silica inorganic coatings (powders B and C). Both particles additionally had the same level of organic (stearate) modification. These optimized dispersions were incorporated into water-in-oil formulations and their stability/efficacy monitored by visual observation and SPF measurements (Tab. 11.2).

The formulation was destabilized by the addition of the powder C dispersion and poor efficacy was achieved despite an optimized dispersion before formulation. When emulsifier concentration was increased from 2 to 3.5% (emulsion 2) the formulation became stable and efficacy was restored.

Tab. 11.2: Sunscreen emulsion formulations from dispersions of powders B and C.

Emulsion	Visual observation	SPF	Emulsifier level
Powder B emulsion 1	Good homogenous emulsion	29	2.0 %
Powder C emulsion 1	Separation, inhomogeneous	11	2.0 %
Powder C emulsion 2	Good homogeneous emulsion	24	3.5 %

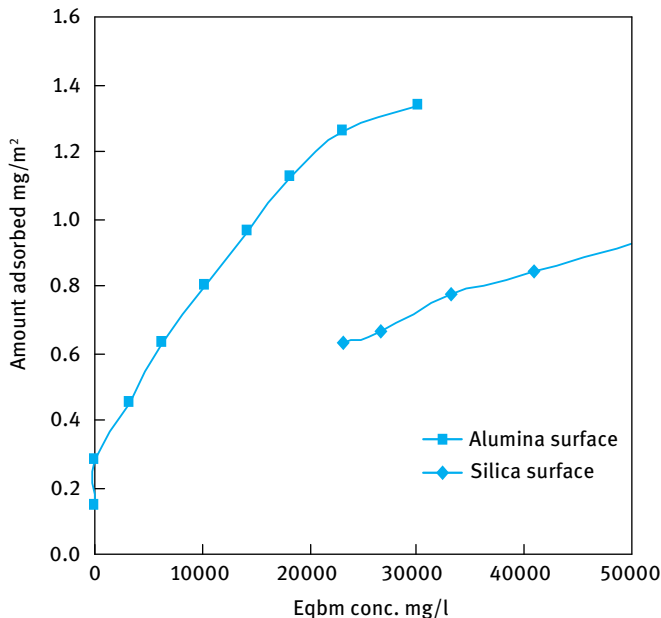


Fig. 11.10: Adsorption isotherms for PHS2500 on powder B (alumina surface) and powder C (silica surface).

The anchor of the chain to the surface (described qualitatively through χ^s) is very specific and this could be illustrated by silica-coated particles which showed lower adsorption of the PHS (Fig. 11.10).

In addition, when a quantity of emulsifier was added to an optimized dispersion of powder C (silica surface) the acid value of the equilibrium solution was seen to rise, indicating some displacement of the PHS2500 by the emulsifier.

The dispersant demand curves (Fig. 11.7 (a) and (b)) and solids loading curves (Fig. 11.9 (a) and (b)) show that one can reach a stable dispersion using PHS1000 or PHS2500 both in alkylbenzoate and in squalane. This can be understood in terms of the stabilization produced when using these polymeric dispersants. Addition of sufficient dispersant enables coverage of the surface and results in a steric barrier (Fig. 11.3) preventing aggregation due to van der Waals attraction. Both molecular weight oligomers were able to achieve stable dispersions. The much smaller molecular weight ‘monomer’, isostearic acid, is however insufficient to provide this steric barrier and dispersions were aggregated, leading to high viscosities, even at 30% solids. UV-vis curves confirm that these dispersions are not fully dispersed since their full UV potential is not realized (Fig. 11.8). Even at 20% isostearic acid the dispersions are seen to give a lower E_{\max} and increased scattering at visible wavelengths indicating a partially aggregated system.

The differences between alkylbenzoate and squalane observed in the optimum dispersant concentration required for maximum stability can be understood by examining the adsorption isotherms in Fig. 11.6 (a) and (b). The nature of the steric barrier depends on the solvency of the medium for the chain, and is characterized by the Flory–Huggins interaction parameter χ . Information on the value of χ for the two solvents can be obtained from solubility parameter calculations (equation (11.3)). The results of these calculations are given in Tab. 11.3 for PHS, alkylbenzoate and squalane.

Tab. 11.3: Hansen and Beerbower solubility parameters for the polymer and both solvents.

	δ_T	δ_d	δ_p	δ_h	$\Delta\delta_T$
PHS	19.00	18.13	0.86	5.60	
Alkyl benzoate	17.01	19.13	1.73	4.12	1.99
Squalane	12.9	15.88	0	0	6.1

It can be seen that both PHS and alkylbenzoate have polar and hydrogen bonding contributions to the solubility parameter δ_T . In contrast, squalane, which is nonpolar, has only a dispersion component to δ_T . The difference in the total solubility parameter $\Delta\delta_T$ value is much smaller for alkylbenzoate when compared with squalane. Thus one can expect that alkylbenzoate is a better solvent for PHS when compared with squalane. This explains the higher adsorption amounts of the dispersants in squalane when compared with alkyl benzoate (Fig. 11.6). The PHS finds adsorption at the particle surface energetically more favourable than remaining in solution. The adsorption values at the plateau for PHS in squalane ($> 2 \text{ mg m}^{-2}$ for PHS1000 and $> 2.5 \text{ mg m}^{-2}$ for PHS2500) is more than twice the value obtained in alkylbenzoate (1 mg m^{-2} for both PHS1000 and PHS2500).

It should be mentioned, however, that both alkylbenzoate and squalane will have χ values less than 0.5, i.e., good solvent conditions and a positive steric potential. This is consistent with the high dispersion stability produced in both solvents. However, the relative difference in solvency for PHS between alkylbenzoate and squalane is expected to have a significant effect on the conformation of the adsorbed layer. In squalane, a poorer solvent for PHS, the polymer chain is denser when compared with the polymer layer in alkylbenzoate. In the latter case a diffuse layer that is typical for polymers in good solvents is produced. This is illustrated in Fig. 11.11 (a), which shows a higher hydrodynamic layer thickness for the higher molecular weight PHS2500. A schematic representation of the adsorbed layers in squalane is shown in Fig. 11.11 (b), which also shows a higher thickness for the higher molecular weight PHS2500.

In squalane, the dispersant adopts a close packed conformation with little solvation and high amounts are required to reach full surface coverage ($\Gamma > 2 \text{ mg m}^{-2}$). It seems also that in squalane the amount of adsorption depends much more on the

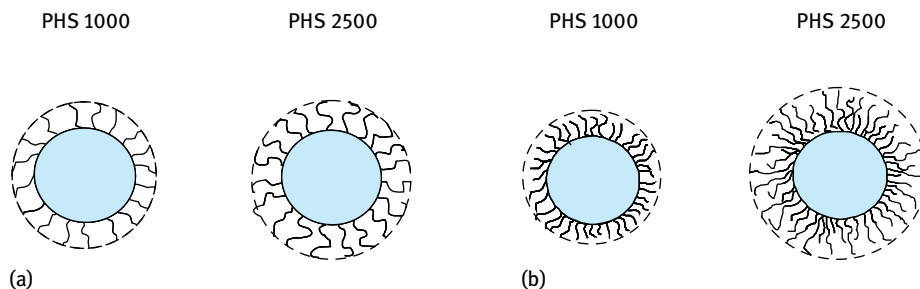


Fig. 11.11: (a) Well solvated polymer results in diffuse adsorbed layers (alkylbenzoate). (b) Polymers are not well solvated and form dense adsorbed layers (squalane).

molecular weight of PHS than in the case of alkylbenzoate. It is likely that with the high molecular weight PHS2500 in squalane the adsorbed layer thickness can reach higher values when compared with the results in alkylbenzoate. This larger layer thickness increases the effective volume fraction and this restricts the total solids that can be dispersed. This is clearly shown from the results of Fig. 11.9, which shows a rapid increase in zero shear viscosity at a solids loading $> 35\%$. With the lower molecular weight PHS1000, with smaller adsorbed layer thickness, the effective volume fraction is lower and high solids loading ($\approx 50\%$) can be reached. The solids loading that can be reached in alkylbenzoate when using PHS2500 is higher ($\approx 40\%$) than that obtained in squalane. This implies that the adsorbed layer thickness of PHS2500 is smaller in alkylbenzene when compared with the value in squalane as schematically shown in Fig. 11.11. The solids loading with PHS1000 in alkylbenzene is similar to that in squalane, indicating a similar adsorbed layer thickness in both cases.

The solids loading curves demonstrate that with an extended layer such as that obtained with the higher molecular weight (PHS2500) the maximum solids loading becomes severely limited as the effective volume fraction (equation (11.5)) is increased.

In squalane the monomeric dispersant, isostearic acid shows high affinity adsorption isotherm with a plateau adsorption of 1 mg m^{-2} but this provides an insufficient steric barrier (δ/R too small, Fig. 11.4) to ensure colloidal stability.

11.5 Competitive interactions in sunscreen formulations

Most sunscreen formulations consist of an oil-in-water (O/W) emulsion in which the particles are incorporated. These active particles can be in either the oil phase, or the water phase, or both as is illustrated in Fig. 11.12. For a sunscreen formulation based on a W/O emulsion, the added nonaqueous sunscreen dispersion mostly stays in the oil continuous phase.

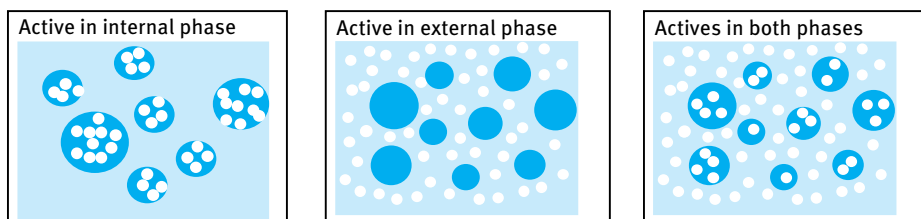


Fig. 11.12: Schematic representation of the location of active particles in sunscreen formulations.

On addition of the sunscreen dispersion to an emulsion to produce the final formulation, one has to consider the competitive adsorption of the dispersant/emulsifier system. In this case the strength of adsorption of the dispersant to the surface modified TiO_2 particles must be considered. As shown in Fig. 11.10 the silica coated particles (C) show lower PHS2500 adsorption compared to the alumina coated particles (B). However, the dispersant demand for the two powders to obtain a colloiddally stable dispersion was similar in both cases (12–14 % PHS2500). This appears at a first sight to indicate similar stabilities. However, when added to a water-in-oil emulsion prepared using an A–B–A block copolymer of PHS–PEO–PHS as emulsifier, the system based on the silica coated particles (C) became unstable, showing separation and coalescence of the water droplets. The SPF performance also dropped drastically from 29 to 11. In contrast, the system based on alumina coated particles (B) remained stable showing no separation as illustrated in Tab. 11.2. These results are consistent with the stronger adsorption (higher χ^s) of PHS2500 on the alumina coated particles. With the silica coated particles, it is likely that the PHS–PEO–PHS block copolymer becomes adsorbed on the particles thus depleting the emulsion interface from the polymeric emulsifier and this is the cause of coalescence. It is well known that molecules based on PEO can adsorb on silica surfaces [13]. By addition of more emulsifier (increasing its concentration from 2 to 3.5 %) the formulation remained stable as is illustrated in Tab. 11.2. This final set of results demonstrates how a change in surface coating can alter the adsorption strength which can have consequences for the final formulation. The same optimization process used for powder A enabled stable dispersions to be formed from powders B and C. Dispersant demand curves showed optimized dispersion rheology at similar added dispersant levels of 12–14 % PHS2500. To the dispersion scientist these appeared to be stable TiO_2 dispersions. However, when the optimized dispersions were formulated into the external phase of a water-in-oil emulsion differences were observed and alterations in formulation were required to ensure emulsion stability and performance.

References

- [1] Tadros T. Cosmetics. In: Tadros T, editor. Encyclopedia of colloid and interface science. Berlin: Springer; 2013.
- [2] Kessel LM, Naden BJ, Tooley IR, Tadros TF. Application of Colloid and Interface Science Principles for Optimisation of Sunscreen Dispersions. Tadros T, editor. Colloids in cosmetics and personal care. Weinheim: Wiley-VCH; 2008.
- [3] Robb JL, Simpson LA, Tunstall DF. Scattering and absorption of UV radiation by sunscreens containing fine particle and pigmentary titanium dioxide. Drug and Cosmetics Industry. 1994; March.
- [4] Herzog B. Models for the calculation of sun protection factor and parameters characterising the UVA protection ability of cosmetic sunscreens. Tadros T, editor. Colloids in cosmetics and personal care. Weinheim: Wiley-VCH; 2008.
- [5] Fleer GJ, Cohen-Stuart MA, Scheutjens JM, Cosgrove T, Vincent B. Polymers at interfaces. London: Chapman and Hall; 1993
- [6] Napper DH. Polymeric stabilization of Colloidal Dispersions. London: Academic Press; 1983.
- [7] Hildebrand JH. Solubility of Non-electrolytes. 2nd edition. New York: Reinhold; 1936.
- [8] Hansen CM. J Paint Technol. 1967;39:104–117, 505–514.
- [9] Hansen CM, Beerbower A. In: Barton AFM (Editor). Handbook of solubility parameters and other cohesive parameters. New York: CRC Press; 1983.
- [10] Tadros T, Izquierdo P, Esquena J, Solans C. Formation and stability of nanoemulsions. Advances in Colloid and Interface Science. 2004;108–109:303–318.
- [11] Kessel LM, Naden BJ, Tadros TF. Attractive and repulsive gels from inorganic sunscreen actives. Proceedings of the IFSCC 23rd Congress. Orlando, Florida; October 2004.
- [12] Diffey BL, Robson J. J Soc Cosmet Chem. 1989;40:127–133.
- [13] Shar JA, Obey TM, Cosgrove T. Colloids and Surfaces. 1999;A 150:15–23.

12 Colour cosmetics

12.1 Introduction

Pigments are the primary ingredient of any colour cosmetic and the way in which these particulate materials are distributed within the product will determine many aspects of product quality including functional activity (colour, opacity, UV protection) but also stability, rheology and skin feel [1, 2]. Several colour pigments are used in cosmetic formulations ranging from inorganic pigments (such as red iron oxide) to organic pigments of various types. The formulation of these pigments in colour cosmetics requires a great deal of skill since the pigment particles are dispersed in an emulsion (oil-in-water or water-in-oil). The pigment particles may be dispersed in the continuous medium in which case one should avoid flocculation with the oil or water droplets. In some cases, the pigment may be dispersed in an oil which is then emulsified in an aqueous medium. Several other ingredients are added such as humectants, thickeners, preservatives, etc. and the interaction between the various components can be very complex.

The particulate distribution depends on many factors such as particle size and shape, surface characteristics, processing and other formulation ingredients but ultimately is determined by the interparticle interactions. A thorough understanding of these interactions and how to modify them can help to speed up product design and solve formulation problems.

In this chapter, I will start with a section describing the fundamental principles of preparation of pigment dispersion. These consist of three main topics, namely wetting of the powder, its dispersion (or wet milling including comminution) and stabilization against aggregation. A schematic representation of this process is shown in Fig. 12.1 [3]. This will be followed by a section on the principles of dispersion stability for both aqueous and nonaqueous media. The use of rheology in assessing the performance of a dispersant will be included. The application of these fundamental principles for colour cosmetic formulation will be discussed. Finally, the interaction with other formulation ingredients when these particulates are incorporated in an emulsion (forming a suspoemulsion) will be discussed. Particular attention will be given to the process of competitive adsorption of the dispersant and emulsifier.

In this chapter I will try to demonstrate that optimization of colour cosmetics can be achieved through a fundamental understanding of colloid and interface science. I will show that the dispersion stability and rheology of particulate formulations depend on interparticle interactions which in turn depend on the adsorption and conformation of the dispersant at the solid/liquid interface. Dispersants offer the possibility of being able to control the interactions between particles such that consistency is improved. Unfortunately, it is not possible to design a universal dispersant due to specificity of anchor groups and solvent-steric interactions. Colour formulators

<https://doi.org/10.1515/9783110555257-013>

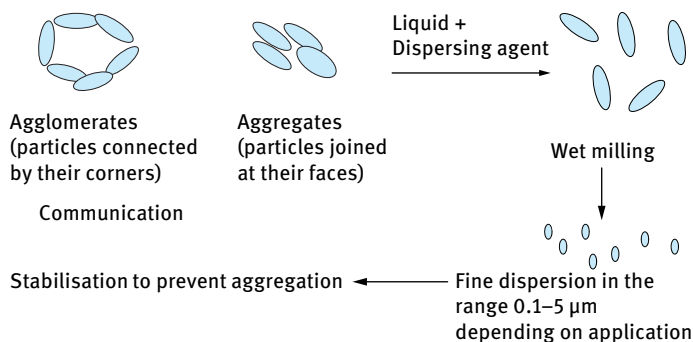


Fig. 12.1: Schematic representation of the dispersion process.

should be encouraged to understand the mechanism of stabilizing the pigment particles and how to improve that. In order to optimize performance of the final cosmetic colour formulation one must consider the interactions between particles, dispersant, emulsifiers and thickeners and strive to reduce the competitive interactions through proper choice of the modified surface as well as the dispersant to optimize adsorption strength.

12.2 Fundamental principles for preparation of a stable colour cosmetic dispersion

12.2.1 Powder wetting

Wetting of powders of colour cosmetics is an important prerequisite for dispersion of that powder in liquids (see Chapter 2, Vol. 2). It is essential to wet both the external and internal surfaces of the powder aggregates and agglomerates as schematically represented in Fig. 12.1. In all these processes one has to consider both the equilibrium and dynamic aspects of the wetting process [4]. The equilibrium aspects of wetting can be studied at a fundamental level using interfacial thermodynamics. Under equilibrium, a drop of a liquid on a substrate produces a contact angle θ , which is the angle formed between planes tangent to the surfaces of solid and liquid at the wetting perimeter. This is illustrated in Fig. 12.2, which shows the profile of a liquid drop on a flat solid substrate. An equilibrium between vapour, liquid and solid is established with a contact angle θ (that is smaller than 90°).

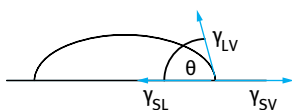


Fig. 12.2: Schematic representation of contact angle and wetting line.

The wetting perimeter is frequently referred to as the three-phase line (solid/liquid/vapour); the most common name is the wetting line. Most equilibrium wetting studies centre around measurements of the contact angle. The smaller the angle the better the liquid is said to wet the solid [4].

The dynamic process of wetting is usually described in terms of a moving wetting line which results in contact angles that change with the wetting velocity. The same name is sometimes given to contact angles that change with time [4].

Wetting of a porous substrate may also be considered a dynamic phenomenon. The liquid penetrates through the pores and gives different contact angles depending on the complexity of the porous structure. Studying the wetting of porous substrates is very difficult. The same applies to wetting of agglomerates and aggregates of powders. However, even measurements of apparent contact angles can be very useful for comparing one porous substrate with another and one powder with another [3].

The liquid drop takes the shape that minimizes the free energy of the system. Consider a simple system of a liquid drop (L) on a solid surface (S) in equilibrium with the vapour of the liquid (V) as was illustrated in Fig. 12.2. The sum ($\gamma_{SV}A_{SV} + \gamma_{SL}A_{SL} + \gamma_{LV}A_{LV}$) should be a minimum at equilibrium and this leads to Young's equation [4],

$$\gamma_{SV} = \gamma_{SL} + \gamma_{LV} \cos \theta. \quad (12.1)$$

In the above equation θ is the equilibrium contact angle. The angle which a drop assumes on a solid surface is the result of the balance between the cohesion force in the liquid and the adhesion force between the liquid and solid, i.e.

$$\gamma_{LV} \cos \theta = \gamma_{SV} - \gamma_{SL}, \quad (12.2)$$

or,

$$\cos \theta = \frac{\gamma_{SV} - \gamma_{SL}}{\gamma_{LV}}. \quad (12.3)$$

There is no direct way by which γ_{SV} or γ_{SL} can be measured. The difference between γ_{SV} and γ_{SL} can be obtained from contact angle measurements. This difference is referred to as the "wetting tension" or "adhesion tension" [3, 4],

$$\text{adhesion tension} = \gamma_{SV} - \gamma_{SL} = \gamma_{LV} \cos \theta. \quad (12.4)$$

Another useful parameter for describing wetting of liquids on solid substrates is the work of adhesion, W_a . Consider a liquid drop with surface tension γ_{LV} and a solid surface with surface tension γ_{SV} . When the liquid drop adheres to the solid surface it forms a surface tension γ_{SL} . This is schematically illustrated in Fig. 12.3. The work of adhesion is simply the difference between the surface tensions of the liquid/vapour and solid/vapour and that of the solid/liquid [3],

$$W_a = \gamma_{SV} + \gamma_{LV} - \gamma_{SL}. \quad (12.5)$$

Using Young's equation,

$$W_a = \gamma_{LV}(\cos \theta + 1). \quad (12.6)$$

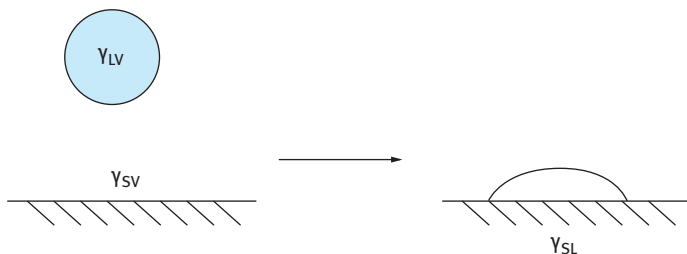


Fig. 12.3: Representation of adhesion of a drop on a solid substrate.

The work of cohesion W_c is the work of adhesion when the two phases are the same. Consider a liquid cylinder with unit cross-sectional area. When this liquid is subdivided into two cylinders, two new surfaces are formed. The two new areas will have a surface tension of $2\gamma_{LV}$ and the work of cohesion is simply,

$$W_c = 2\gamma_{LV}. \quad (12.7)$$

Thus, the work of cohesion is simply equal to twice the liquid surface tension. An important conclusion may be drawn if one considers the work of adhesion given by equation (12.6) and the work of cohesion given by equation (12.7): When $W_c = W_a$, $\theta = 0^\circ$. This is the condition for complete wetting. When $W_c = 2W_a$, $\theta = 90^\circ$ and the liquid forms a discrete drop on the substrate surface. Thus, the competition between the cohesion of the liquid to itself and its adhesion to a solid gives an angle of contact that is constant and specific to a given system at equilibrium [3]. This shows the importance of Young's equation in defining wetting.

The spreading of liquids on substrates is also an important industrial phenomenon. A useful concept introduced by Harkins [3, 4] is the spreading coefficient which is simply the work in destroying a unit area of solid/liquid and liquid/vapour interface to produce an area of solid/air interface. The spreading coefficient is simply determined from the contact angle θ and the liquid/vapour surface tension γ_{LV} ,

$$S = \gamma_{LV}(\cos \theta - 1). \quad (12.8)$$

For spontaneous spreading S has to be zero or positive. If S is negative only limited spreading is obtained.

The energy required to achieve dispersion wetting, W_d is given by the product of the external area of the powder, A , and the difference between γ_{SL} and γ_{SV} ,

$$W_d = A(\gamma_{SL} - \gamma_{SV}). \quad (12.9)$$

Using Young's equation,

$$W_d = -A\gamma_{LV} \cos \theta. \quad (12.10)$$

Thus wetting of the external surface of the powder depends on the liquid surface tension and contact angle [3]. If $\theta < 90^\circ$, $\cos \theta$ is positive and the work of dispersion is negative, i.e. wetting is spontaneous.

For agglomerates (represented in Fig. 12.4), which are found in all powders, wetting of the internal surface between the particles in the structure requires liquid penetration through the pores. Assuming the pores to behave as simple capillaries of radius r , the capillary pressure Δp is given by the following equation [3],

$$\Delta p = \frac{2\gamma_{LV} \cos \theta}{r}. \quad (12.11)$$

For liquid penetration to occur, Δp must be positive and hence θ should be less than 90° . The maximum capillary pressure is obtained when $\theta = 0$ and Δp is proportional to γ_{LV} which means that a high γ_{LV} is required. Thus to achieve wetting of the internal surface a compromise is needed since contact angle only decreases as γ_{LV} decreases. One needs to make θ as close to 0 as possible while not having too low a liquid surface tension [3].

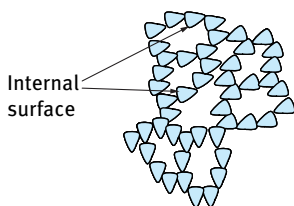


Fig. 12.4: Schematic representation of an agglomerate.

The most important parameter that determines wetting of the powder is the dynamic surface tension, γ_{dynamic} (i.e. the value at short times). γ_{dynamic} depends both on the diffusion coefficient of the surfactant molecule as well as its concentration [3]. Since wetting agents are added in sufficient amounts (γ_{dynamic} is lowered sufficiently) spontaneous wetting is the rule rather than the exception.

Wetting of the internal surface requires penetration of the liquid into channels between and inside the agglomerates. The process is similar to forcing a liquid through fine capillaries. To force a liquid through a capillary with radius r , a pressure Δp is required that was given by equation (12.11).

To assess the wettability of the internal surface, one must consider the rate of penetration of the liquid through the pores of the agglomerates [3]. Assuming the pores to be represented by horizontal capillaries with radius r , neglecting the effect of gravity, the depth of penetration l in time t is given by the Rideal–Washburn equation,

$$l = \left[\frac{rt\gamma_{LV} \cos \theta}{2\eta} \right]^{1/2}. \quad (12.12)$$

To enhance the rate of penetration, γ_{LV} has to be made as high as possible, θ as low as possible and η as low as possible. For a packed bed of particles, r may be replaced by r/k^2 , where r is the effective radius of the bed and k is the tortuosity factor, which takes into account the complex path formed by the channels between the particles [3],

i.e.,

$$l^2 = \left(\frac{r\gamma_{LV} \cos \theta}{2\eta k^2} \right) t. \quad (12.13)$$

Thus a plot of l^2 versus t gives a straight line and from the slope of the line one can obtain θ .

The Rideal–Washburn equation can be applied to obtain the contact angle of liquids (and surfactant solutions) in powder beds [3]. k should first be obtained using a liquid that produces zero contact angle.

12.2.2 Powder dispersion and milling (comminution)

The dispersion of the powder is achieved by using high speed stirrers such as the Ultra-Turrax or Silverson mixers. This results in dispersion of the wetted powder aggregate or agglomerate into single units [3]. The primary dispersion (sometimes referred to as the mill base) may then be subjected to a bead milling process to produce nanoparticles which are essential for some colour cosmetic applications. Subdivision of the primary particles into much smaller units in the nanosize range (10–100 nm) requires application of intense energy. In some cases high pressure homogenizers (such as the Microfluidizer, USA) may be sufficient to produce nanoparticles. This is particularly the case with many organic pigments. In some cases, the high pressure homogenizer is combined with application of ultrasound to produce the nanoparticles.

Milling or comminution (the generic term for size reduction) is a complex process and there is little fundamental information on its mechanism. For the breakdown of single crystals or particles into smaller units, mechanical energy is required. This energy in a bead mill is supplied by impaction of the glass or ceramic beads with the particles. As a result permanent deformation of the particles and crack initiation results. This will eventually lead to the fracture of particles into smaller units. Since the milling conditions are random, some particles receive impacts far in excess of those required for fracture whereas others receive impacts that are insufficient for the fracture process. This makes the milling operation grossly inefficient and only a small fraction of the applied energy is used in comminution. The rest of the energy is dissipated as heat, vibration, sound, inter-particulate friction, etc.

The role of surfactants and dispersants on the grinding efficiency is far from being understood. In most cases the choice of surfactants and dispersant is made by trial and error until a system is found that gives the maximum grinding efficiency [3]. Rehbinder and his collaborators investigated the role of surfactants in the grinding process [3]. As a result of surfactant adsorption at the solid/liquid interface, the surface energy at the boundary is reduced and this facilitates the process of deformation or destruction. The adsorption of surfactants at the solid/liquid interface in cracks facilitates their propagation. This mechanism is referred to as the Rehbinder effect.

12.2.3 Stabilization of the dispersion against aggregation

For stabilization of the dispersion against aggregation (flocculation) one needs to create a repulsive barrier that can overcome the van der Waals attraction [5, 6]. The process of stabilization of dispersions in cosmetics has been described in detail in Chapter 6, Vol. 1 and only a summary is given in this chapter. As discussed in Chapter 5, Vol. 1, all particles experience attractive forces on close approach. The strength of this van der Waals attraction $V_A(h)$ depends upon the distance h between particles of radius R and is characterized by the Hamaker constant, A . The Hamaker constant expresses the attraction between particles (in a vacuum). A depends upon the dielectric and physical properties of the material and for some materials such as TiO_2 , iron oxides and alumina this is exceptionally high so that (in nonaqueous media at least) despite their small size a dispersant is always needed to achieve colloidal stabilization. In order to achieve stability one must provide a balancing repulsive force to reduce interparticle attraction. This can be done in two main ways by electrostatic or steric repulsion as illustrated in Fig. 12.5 (a) and (b) (or a combination of the two, Fig. 12.5 (c)). A polyelectrolyte dispersant such as sodium polyacrylate is required to achieve high solids content. This produces a more uniform charge on the surface and some steric repulsion due to the high molecular weight of the dispersant. Under these conditions the dispersion becomes stable over a wider range of pH at moderate electrolyte concentration. This is electrosteric stabilization; Fig. 12.5 (c) shows a shallow minimum at long separation distances, a maximum (of the DLVO type) at intermediate h and a sharp increase in repulsion at shorter separation distances. This combination of electrostatic and steric repulsion can be very effective for stabilization of the suspension [3].

Electrostatic stabilization can be achieved if the particles contain ionizable groups on their surface such as inorganic oxides, which means that in aqueous media they can therefore develop a surface charge depending upon pH, which affords an elec-

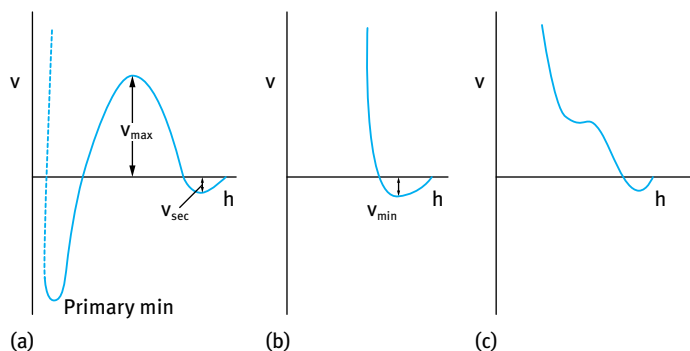


Fig. 12.5: Energy–distance curves for three stabilization mechanisms: (a) electrostatic; (b) steric; (c) electrosteric.

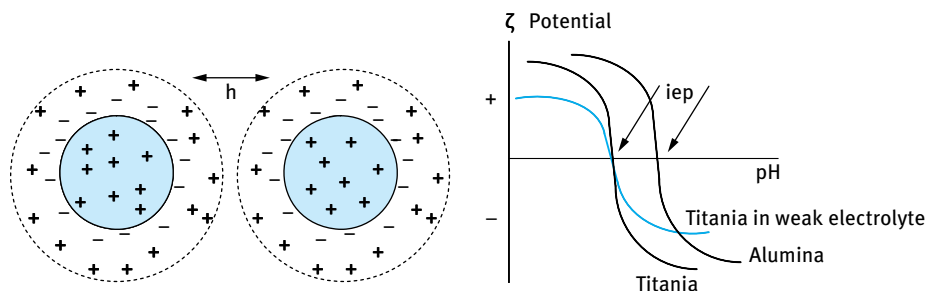


Fig. 12.6: Schematic representation of double layer repulsion (left) and variation of ζ potential with pH for titania and alumina (right).

trostatic stabilization to the dispersion. On close approach the particles experience a repulsive potential overcoming the van der Waals attraction which prevents aggregation [3]. This stabilization is due to the interaction between the electric double layers surrounding the particles as illustrated in Fig. 12.6.

Double layer repulsion depends upon the pH and electrolyte concentration and can be predicted from zeta potential measurements (Fig. 12.6). Surface charge can also be produced by adsorption of ionic surfactants. This balance of electrostatic repulsion with van der Waals attraction is described in the well-known theory of colloid stability by Deryaguin–Landau–Verwey–Overbeek (DLVO theory) [7, 8]. Fig. 12.5 (a) shows two attractive minima at long and short separation distances; V_{sec} that is shallow and of few kT units and V_{primary} that is deep and exceeds several $100kT$ units. These two minima are separated by an energy maximum V_{max} that can be greater than $25kT$ thus preventing flocculation of the particles into the deep primary minimum.

When the pH of the dispersion is well above or below the isoelectric point or the electrolyte concentration is less than $10^{-2} \text{ mol dm}^{-3}$ 1:1 electrolyte, electrostatic repulsion is often sufficient to produce a dispersion without the need for added dispersant. However, in practice this condition often cannot be reached since at high solids content the ionic concentration from the counter- and co-ions of the double layer is high and the surface charge is not uniform. Therefore a polyelectrolyte dispersant such as sodium polyacrylate is required to achieve this high solids content. This produces a more uniform charge on the surface and some steric repulsion due to the high molecular weight of the dispersant. Under these conditions the dispersion becomes stable over a wider range of pH at moderate electrolyte concentration. This is electrosteric stabilization. Fig. 12.5 (c) shows a shallow minimum at long separation distances, a maximum (of the DLVO type) at intermediate h and a sharp increase in repulsion at shorter separation distances. This combination of electrostatic and steric repulsion can be very effective for stabilization of the suspension.

Steric stabilization is usually obtained using adsorbed layers of polymers or surfactants. The most effective molecules are the A–B or A–B–A block or BA_n graft

polymeric surfactants [9] where B refers to the anchor chain. This anchor should be strongly adsorbed to the particle surface. For a hydrophilic particle this may be a carboxylic acid, an amine or phosphate group or other larger hydrogen bonding type block such as polyethylene oxide. The A chains are referred to as the stabilizing chains which should be highly soluble in the medium and strongly solvated by its molecules. A schematic representation of the adsorbed layers is shown in Fig. 12.7. When two particles with an adsorbed layer of hydrodynamic thickness δ approach to a separation distance h that is smaller than 2δ , repulsion occurs (Fig. 12.5 (b)) as a result of two main effects:

- (i) unfavourable mixing of the A chains when these are in good solvent condition;
- (ii) reduction in configurational entropy on significant overlap.

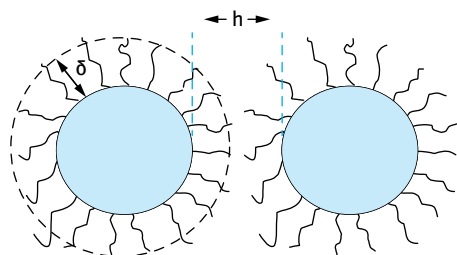


Fig. 12.7: Schematic representation of steric layers.

The efficiency of steric stabilization depends on both the architecture and the physical properties of the stabilizing molecule. Steric stabilizers should have an adsorbing anchor with a high affinity for the particles and/or insoluble in the medium. The stabilizer should be soluble in the medium and highly solvated by its molecules. For aqueous or highly polar oil systems the stabilizer block can be ionic or hydrophilic such as polyalkylene glycols and for oils it should resemble the oil in character. For silicone oils silicone stabilizers are best, other oils could use a long chain alkane, fatty ester or polymers such as poly(methylmethacrylate) (PMMA) or polypropylene oxide.

Various types of surface-anchor interactions are responsible for the adsorption of a dispersant to the particle surface: Ionic or acid/base interactions; sulphonic acid, carboxylic acid or phosphate with a basic surface e.g. alumina; amine or quat with acidic surface e.g. silica. H bonding; surface esters, ketones, ethers, hydroxyls; multiple anchors – polyamines and polyols (h-bond donor or acceptor) or polyethers (h-bond acceptor). Polarizing groups, e.g. polyurethanes can also provide sufficient adsorption energies and in nonspecific cases lyophobic bonding (van der Waals) driven by insolubility (e.g. PMMA). It is also possible to use chemical bonding e.g. by reactive silanes.

For relatively reactive surfaces, specific ion pairs may interact giving particularly good adsorption to a powder surface. An ion pair may even be formed in situ particularly if in low dielectric media. Some surfaces are actually heterogeneous and can

have both basic and acidic sites, especially near the IEP. Hydrogen bonding is weak but is particularly important for polymeric which can have multiple anchoring.

The adsorption strength is measured in terms of the segment/surface energy of adsorption χ^s . The total adsorption energy is given by the product of the number of attachment points n by χ^s . For polymers the total value of $n\chi^s$ can be sufficiently high for strong and irreversible adsorption even though the value of χ^s may be small (less than $1kT$, where k is the Boltzmann constant and T is the absolute temperature). However, this situation may not be adequate particularly in the presence of an appreciable concentration of wetter and/or in the presence of other surfactants used as adjuvants. If the χ^s of the individual wetter and/or other surfactant molecules is higher than the χ^s of one segment of the B chain of the dispersant, these small molecules can displace the polymeric dispersant particularly at high wetter and/or other surfactant molecules and this could result in flocculation of the suspension. It is, therefore, essential to make sure that the χ^s per segment of the B chain is higher than that of the wetter and/or surfactant adsorption and that the wetter concentration is not excessive.

In order to optimize steric repulsion one may consider the steric potential as expressed by Napper [9],

$$V(h) = 2\pi kT R\Gamma^2 N_A \left[\frac{V_p^2}{V_s} \right] [0.5 - \chi] \left(1 - \frac{h}{2\delta} \right)^2 + V_{\text{elastic}}, \quad (12.14)$$

where k is the Boltzmann constant, T is temperature, R is the particle radius, Γ is the adsorbed amount, N_A the Avogadro constant, V_p is the specific partial volume of the polymer, V_s the molar volume of the solvent, χ is the Flory–Huggins parameter and δ is the maximum extent of the adsorbed layer. V_{elastic} takes account of the compression of polymer chains on close approach.

It is instructive to examine the terms in equation (12.14):

- (i) The adsorbed amount Γ ; higher adsorbed amounts will result in more interaction/repulsion.
- (ii) Solvent conditions as determined by χ , the Flory–Huggins chain-solvent interaction parameter; two very distinct cases emerge. We see maximum interaction on overlap of the stabilizing layers when the chain is in good solvent conditions ($\chi < 0.5$). Osmotic forces cause solvent to move into the highly concentrated overlap zone forcing the particles apart. If $\chi = 0.5$, a theta solvent, the steric potential goes to zero and for poor solvent conditions ($\chi > 0.5$) the steric potential becomes negative and the chains will attract, enhancing flocculation. Thus, a poorly solvated dispersant can enhance flocculation/aggregation.
- (iii) Adsorbed layer thickness δ . The steric interaction starts at $h = 2\delta$ as the chains begin to overlap and increases as the square of the distance. Here it is not the size of the steric potential that is important but the distance h at which it begins.
- (iv) The final interaction potential is the superposition of the steric potential and the van der Waals attraction as shown in Fig. 12.5 (b).

For sterically stabilized dispersions, the resulting energy–distance curve often shows a shallow minimum V_{\min} at particle-particle separation distance h comparable to twice the adsorbed layer thickness δ . For a given material the depth of this minimum depends upon the particle size R , and adsorbed layer thickness δ . So V_{\min} decreases with increasing δ/R as is illustrated in Fig. 12.8. This is because as we increase the layer thickness the van der Waals attraction is weakening so the superposition of attraction and repulsion will have a smaller minimum. For very small steric layers V_{\min} may become deep enough to cause weak flocculation resulting in a weak attractive gel. So we can see how the interaction energies can also determine the dispersion rheology.

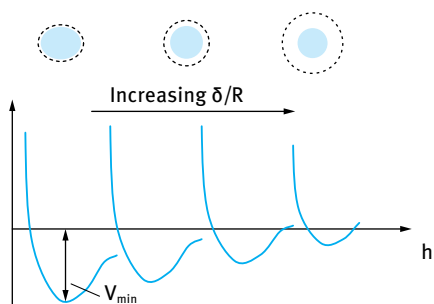


Fig. 12.8: Variation of V_{\min} with δ/R .

On the other hand if the layer thickness is too large, the viscosity is also increased due to repulsion. This is due to the much higher effective volume fraction ϕ_{eff} of the dispersion compared to the core volume fraction [2]. We can calculate the effective volume fraction of particles plus dispersant layer by geometry and we see it depends on the thickness of that adsorbed layer, as illustrated in Fig. 12.9. The effective volume fraction increases with relative increase of the dispersant layer thickness. Even at 10% volume fraction we can soon reach max packing ($\phi = 0.67$) with an adsorbed layer comparable to the particle radius. In this case overlap of the steric layers will result in significant viscosity increases. Such considerations help to explain why solids loading can be severely limited especially with small particles. In practice solids loading curves can be used to characterize the system and will take the form of those illustrated in Fig. 12.10.

Higher solids loading might be achieved with thinner adsorbed layers but may also result in interparticle attraction resulting in particle aggregation. Clearly a compromise is needed; choosing an appropriate steric stabilizer for the particle size of the pigment.

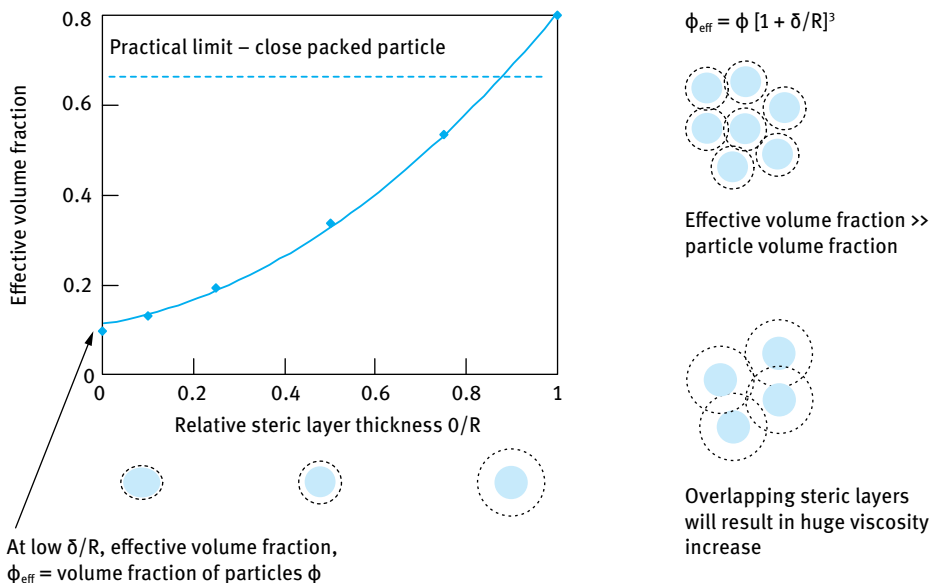


Fig. 12.9: Schematic representation of the effective volume fraction.

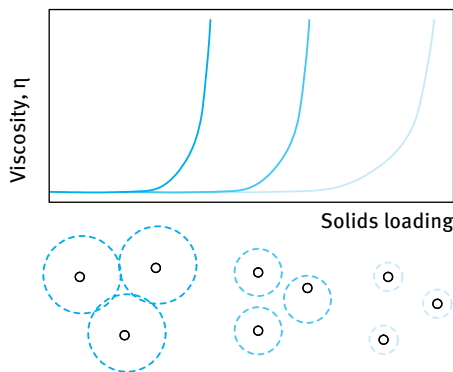


Fig. 12.10: Dependency of solids loading on adsorbed layer thickness.

12.3 Classes of dispersing agents

One of the most commonly used dispersants for aqueous media are nonionic surfactants. The most common nonionic surfactants are the alcohol ethoxylates $R-(\text{CH}_2-\text{CH}_2-\text{O})_n-\text{H}$, e.g. $\text{C}_{13/15}(\text{EO})_n$ with n being 7, 9, 11 or 20. These nonionic surfactants are not the most effective dispersants since the adsorption by the $\text{C}_{13/15}$ chain is not very strong. To enhance the adsorption on hydrophobic surfaces a polypropylene oxide (PPO) chain is introduced in the molecule giving $R-(\text{PPO})_m-(\text{PEO})_n-\text{H}$.

The above nonionic surfactants can also be used for stabilization of polar solids in nonaqueous media. In this case the PEO chain adsorbs on the particle surface leaving the alkyl chains in the nonaqueous solvent. Provided these alkyl chains are sufficiently long and strongly solvated by the molecules of the medium, they can provide sufficient steric repulsion to prevent flocculation.

A better dispersant for polar solids in nonaqueous media is poly(hydroxystearic acid) (PHS) with molecular weight in the region of 1000–2000 Daltons. The carboxylic group adsorbs strongly on the particle surface leaving the extended chain in the nonaqueous solvent. With most hydrocarbon solvents the PHS chain is strongly solvated by its molecules and an adsorbed layer thickness in the region of 5–10 nm can be produced. This layer thickness prevents any flocculation and the suspension can remain fluid up to high solids content [2].

The most effective dispersants are those of the A–B, A–B–A block and BA_n types. A schematic representation of the architecture of block and graft copolymers is shown in Fig. 12.11.

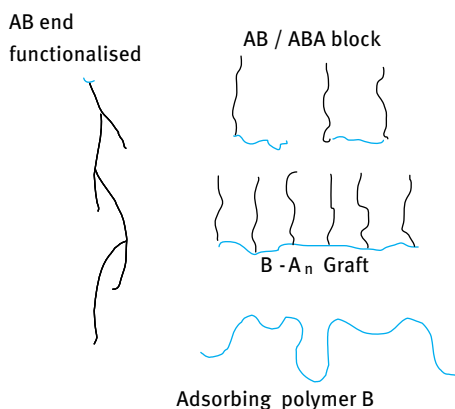


Fig. 12.11: Schematic representation of the architecture of block and graft copolymers.

B, the “anchor chain”(red), is chosen to be highly insoluble in the medium and has a strong affinity to the surface. Examples of B chains for hydrophobic solids are polystyrene (PS), polymethylmethacrylate (PMMA), poly(propylene oxide) (PPO) or alkyl chains provided these have several attachments to the surface. The A stabilizing (blue) chain has to be soluble in the medium and strongly solvated by its molecules. The A chain/solvent interaction should be strong giving a Flory–Huggins χ -parameter < 0.5 under all conditions. Examples of A chains for aqueous media are polyethylene oxide (PEO), polyvinyl alcohol (PVA) and polysaccharides (e.g. polyfructose). For nonaqueous media, the A chains can be polyhydroxystearic acid (PHS).

One of the most commonly used A–B–A block copolymers for aqueous dispersions are those based on PEO (A) and PPO (B). Several molecules of PEO–PPO–PEO are available with various proportions of PEO and PPO. The commercial name is followed by a

letter L (liquid), P (paste) and F (flake). This is followed by two numbers that represent the composition – the first digits represent the PPO molar mass and the last digit represents the % PEO. F68 (PPO molecular mass 1508–1800 + 80 % or 140 mol EO). L62 (PPO molecular mass 1508–1800 + 20 % or 15 mol EO). In many cases two molecules with high and low EO content are used together to enhance the dispersing power.

An example of a BA_n graft copolymer is based on polymethylmethacrylate (PMMA) backbone (with some polymethacrylic acid) on which several PEO chains (with average molecular weight of 750) are grafted. It is a very effective dispersant particularly for high solids content suspensions. The graft copolymer is strongly adsorbed on hydrophobic surfaces with several attachment points along the PMMA backbone and a strong steric barrier is obtained by the highly hydrated PEO chains in aqueous solutions.

Another effective graft copolymer is hydrophobically modified inulin, a linear polyfructose chain A (with degree of polymerization >23) on which several alkyl chains have been grafted. The polymeric surfactant adsorbs with multipoint attachment with several alkyl chains.

12.4 Assessment of dispersants

12.4.1 Adsorption isotherms

These are by far the most quantitative method for assessment and selection of a dispersant [3]. A good dispersant should give a high affinity isotherm as is illustrated in Fig. 12.12. The adsorbed amount Γ is recorded as a function of the equilibrium solution concentration, i.e. that left in solution after adsorption.

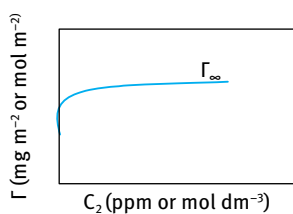


Fig. 12.12: High affinity isotherm.

In general, the value of Γ_∞ is reached at lower C_2 for polymeric surfactant adsorption when compared with small molecules. The high affinity isotherm obtained with polymeric surfactants implies that the first added molecules are virtually completely adsorbed and such a process is irreversible. The irreversibility of adsorption is checked by carrying out a desorption experiment. The suspension at the plateau value is centrifuged and the supernatant liquid is replaced by pure carrier medium. After redispersion, the suspension is centrifuged again and the concentration of the polymeric

surfactant in the supernatant liquid is analytically determined. For lack of desorption, this concentration will be very small indicating that the polymer remains on the particle surface.

12.4.2 Measurement of dispersion and particle size distribution

An effective dispersant should result in complete dispersion of the powder into single particles [3]. In addition, on wet milling (comminution) smaller particle distribution should be obtained (this could be assessed by light diffraction, e.g. using the Malvern Master Sizer). The efficiency of dispersion and reduction of particle size can be understood from the behaviour of the dispersant. Strong adsorption and an effective repulsive barrier prevent any aggregation during the dispersion process. It is necessary in this case to include the wetter (which should be kept at the optimum concentration). Adsorption of the dispersant at the solid/liquid interface results in lowering of γ_{SL} and this reduces the energy required for breaking the particles into smaller units. In addition by adsorption in crystal defects, crack propagation occurs (the Rehbinder effect) and this results in production of smaller particles [3].

12.4.3 Rheological measurements

Although “Brookfield” viscometers are still widely used in the industry they should be used with caution in the assessment of dispersion stability; high shear viscosity (as measured by “Brookfield”) can be misleading as a predictor of sedimentation velocity. Low or zero shear viscosity measured on a rheometer is the best indicator [10]. Fig. 12.13 demonstrates how at high shear, dispersion B has the highest viscosity and might be expected to give the best resistance to sedimentation. However, dispersion A has the highest low shear viscosity and will hence have the best sedimentation stability.

Concentrated dispersions are viscoelastic; that is they have both viscous and elastic characteristics. Oscillatory rheometry can therefore give us much more information about the interparticle interactions than viscometry [10]. For example, an elastic mod-

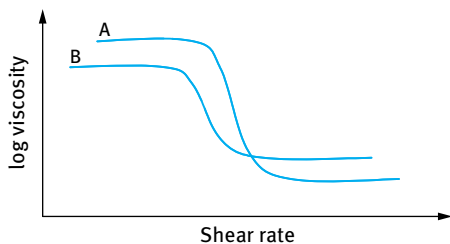


Fig. 12.13: Schematic flow curve for particulate dispersions.

ulus which dominates the shear sweep can confer significant stability to a formulation with dispersed solids.

Rheological techniques are often the most informative techniques for assessment and selection of a dispersant [3, 10]. The best procedure is to follow the variation of relative viscosity η_r with the volume fraction ϕ of the dispersion. For this purpose a concentrated suspension (say 50 % w/w) is prepared by milling using the optimum dispersant concentration. This suspension is further concentrated by centrifugation and the sedimented suspension is diluted with the supernatant liquid to obtain volume fractions ϕ in the range 0.1–0.7. The relative viscosity η_r is measured for each suspension using the flow curves. η_r is then plotted as a function of ϕ and the results are compared with the theoretical values calculated using the Dougherty–Krieger equation [11] as discussed below.

Dougherty and Krieger [11] derived an equation for the variation of the relative viscosity η_r with the volume fraction ϕ of suspensions assumed to behave like hard spheres,

$$\eta_r = \left[1 - \frac{\phi}{\phi_p} \right]^{-[\eta]\phi_p}, \quad (12.15)$$

where $[\eta]$ is the intrinsic viscosity that is equal to 2.5 for hard spheres and ϕ_p is the maximum packing fraction that is ≈ 0.6 –0.7. The maximum packing fraction ϕ_p is obtained by plotting $1/(\eta_r)^{1/2}$ versus ϕ and in most cases a straight line is obtained which is then extrapolated to $1/(\eta_r)^{1/2} = 0$ and this gives ϕ_p .

η_r – ϕ curves are established from the experimental data using the flow curves. The theoretical η_r – ϕ curves obtained from the Dougherty–Krieger equation are also established using a value of 2.5 for the intrinsic viscosity $[\eta]$ and ϕ_p calculated using the above extrapolation procedure. As an illustration Fig. 12.14 shows a schematic representation for results for an aqueous suspension of hydrophobic particles that are dispersed using a graft copolymer of polymethylmethacrylate (PMMA) backbone on which several polyethylene oxide (PEO) chains have been grafted [3].

Both the experimental and theoretical η_r – ϕ curves show an initial slow increase of η_r with increasing ϕ but at a critical ϕ value η_r shows a rapid increase with any further increase in ϕ . It can be seen from Fig. 12.14 that the experimental η_r values show a rapid increase above a high ϕ value (> 0.6). The theoretical η_r – ϕ curve (using equation

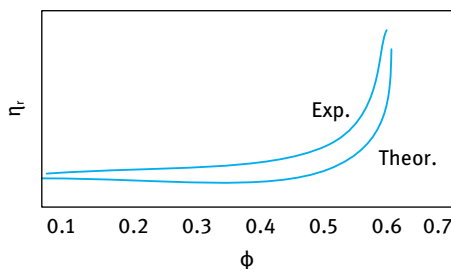


Fig. 12.14: Variation of η_r with ϕ for suspensions stabilized with a graft copolymer.

(12.15)) shows an increase in η_r at a ϕ value close to the experimental results [12]. This shows a highly deflocculated (sterically stabilized) suspension. Any flocculation will cause a shift in the η_r - ϕ curve to lower values of ϕ . These η_r - ϕ curves can be used for assessment and selection of dispersants. The higher the value of ϕ at which the viscosity shows a rapid increase, the more effective the dispersant is. Strong adsorption of the graft polymeric surfactant and the high hydration of the PEO chains ensure such high stability. In addition, such polymeric surfactant is not likely to be displaced by the wetter surfactant molecules provided these are not added at high concentrations. It is essential to use the minimum wetter concentration that is sufficient for complete wetting of the powder.

12.5 Application of the above fundamental principles to colour cosmetics

Pigments are in fact the primary ingredient of any modern colour cosmetic. Pigments need to be incorporated first into slurries and for most colour chemists the primary objective is to reduce the viscosity and improve ease of use of these slurries. It is important to remember that both attractive and repulsive interactions result in viscosity increase. The aim is thus to reduce particle-particle interactions. It is not just in the processing where optimization is required; the particle distribution in the final cosmetic formulation will determine its functional activity (colour, opacity, UV protection), stability, rheology and skin feel. The particle distribution depends upon a number of characteristics such as particle size and shape, surface characteristics, processing, compatibilities but is ultimately also determined by interparticle interactions.

There are two main consequences of instability in particulate dispersions; flocculation or agglomeration and sedimentation. For colour cosmetics, insufficient deagglomeration (all pigments are agglomerated as supplied) can manifest itself as poor colour consistency or streaking with colour being liable to change on application. Sedimentation effects can appear as colour flotation or plate-out. Sedimentation is determined by gravity and is not necessarily a sign of colloidal instability. It simply needs to be controlled. Sedimentation velocity tends to increase with particle size (thus aggregation is bad) but is reduced by increased fluid viscosity.

Dispersion stability may manifest itself in different ways and for the formulator one must have lower viscosity during manufacture. Fig. 12.15 demonstrates the potential benefits (for viscosity dependence on pigment concentration) when a suitable dispersant is added. This can be liberating in removing formulation restrictions and more practically in reducing processing times and cost. Higher pigment concentrations can be achieved giving increased functionality. The colour strength often improves with milling time but again can be stepped up by the incorporation of suitable dispersants. With improved product quality, one can expect improvements in stability, consistency and function.

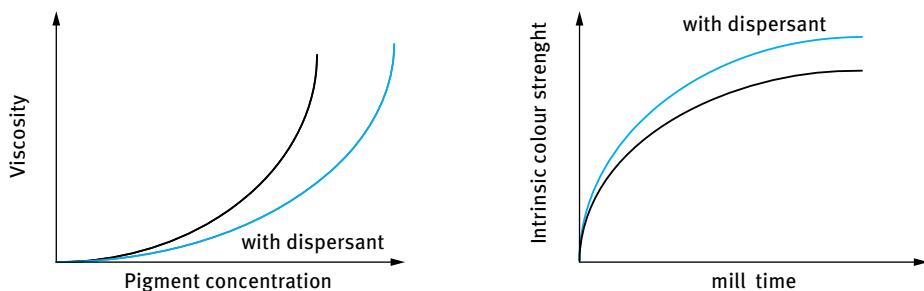


Fig. 12.15: Effect of dispersant on viscosity and intrinsic colour strength.

Product quality is the key to product differentiation in the market and it is highly desirable therefore to reduce flooding and floating caused by flocculation of differing pigments. The control and reproducibility of gloss/shine and brightness and the ability to control rheology and skin feel, particularly at high solids loadings, are all within reach here.

Finally, the optimization of functionality can often depend strongly on the state of dispersion. As mentioned in Chapter 6, opacity and UV attenuation of TiO_2 for example strongly depend on particle size [13] as illustrated in Fig. 12.16. A titanium dioxide pigment designed to provide opacity in a formulation will not realize its maximum hiding power unless it is dispersed and remains dispersed in its constituent particles of 200–300 nm. A UV attenuating grade of TiO_2 on the other hand must be dispersed down to its primary particle size of 50–100 nm in order to be optimally functional as a sunscreen agent. Both powders as supplied (in order to be handleable), however, have similar agglomerate sizes of several microns.

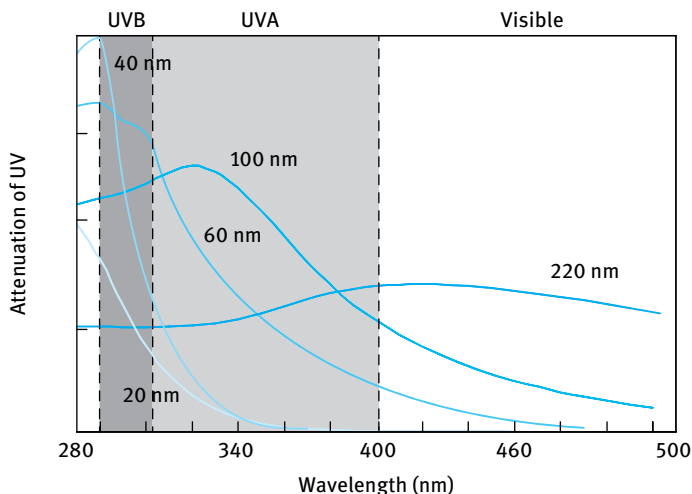


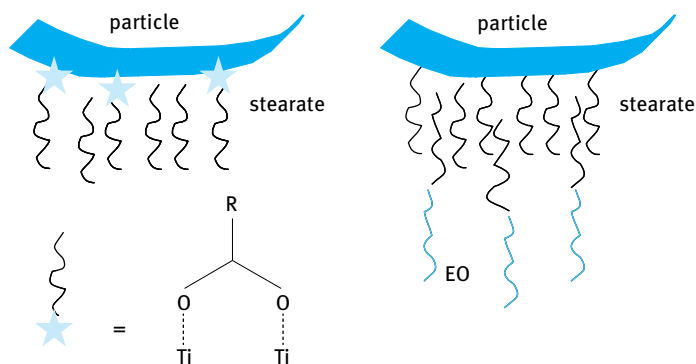
Fig. 12.16: Attenuation of UV versus wavelength for TiO_2 dispersion.

12.6 Principles of preparation of colour cosmetics

As mentioned above, the first task is to obtain complete wetting of the powder. Both external and internal surfaces of the agglomerates must be adequately wetted by using a suitable surfactant. For aqueous dispersions, the above mentioned wetting agents such as Aerosol OT or alcohol ethoxylates are generally efficient. For hydrophilic pigments in oil one can use coated particles (with hydrophobic coating) or sodium stearate which strongly binds to the hydroxyl surface. A schematic representation for binding of stearate to hydrophilic TiO_2 is shown in Fig. 12.17, thus rendering it easily wetted and dispersed in oils. This figure also shows the effect of addition of an alcohol ethoxylate to this coated TiO_2 which can then be dispersed in an aqueous medium.

This process is followed by complete dispersion and/or comminution and adequate stabilization of the resulting single particles, as illustrated in Fig. 12.18.

The next step is to control the process of dispersion and comminution. Simple mixing of inorganic powders can produce a fluid dispersion even at high solids. However this is not necessarily an indication of a “well dispersed” material and indeed a particle size analysis (and for UV attenuators, spectral analysis) demonstrates that particle dispersion is not optimized. Particulate powders are supplied in an aggre-



Eg specific attachment via carboxylate group to inorganic surface

Fig. 12.17: Schematic representation of specific interaction of stearate to TiO_2 (left) and effect of addition of alcohol ethoxylate (right).

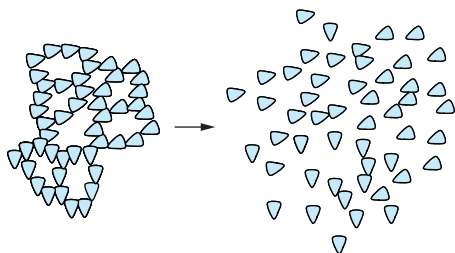


Fig. 12.18: Schematic representation of the dispersion process.

gated state. However, they must be milled down to their individual units in order to provide their designed function. This process must allow transport of the dispersant to the particle surface and adsorption there. Finally, the dispersion must remain stable to dilution or addition of further formulation components. The presence of a suitable dispersant/stabilizer at the right level can be critical in achieving a usable and stable dispersion and preventing re-aggregation on standing. In practice, the formulation chemist may use some simple laboratory tools to assess dispersion quality and arrive at an appropriate dispersion recipe. Having assessed wetting as previously described one will often plot a dispersant demand curve in order to establish the optimum dispersant loading. The pigment is processed (milling or grinding) in the presence of the carrier oil and wetting agent with varying levels of dispersant. The state of dispersion can be effectively monitored by rheology and/or some functional measurement (e.g. colour strength, UV attenuation). Fig. 12.19 shows the results for some fine particle TiO_2 in isopropyl isostearate as dispersing fluid and polyhydroxystearic acid as dispersant [14].

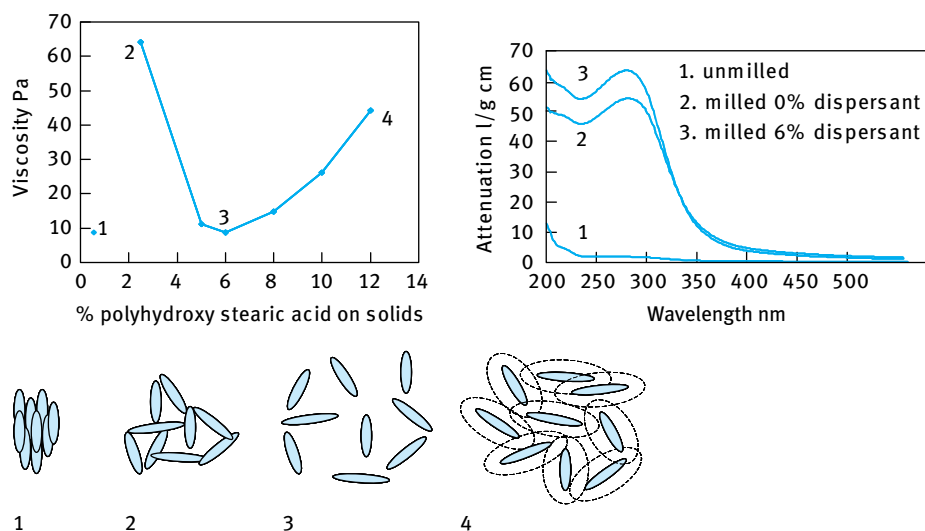


Fig. 12.19: Zero shear viscosity (dispersant demand curve), UV attenuation curves and a schematic of the milling process.

Dispersions were produced at 30 wt% solids so that they could be prepared on a bead mill at all dispersant loadings and their UV attenuation properties compared. Zero shear viscosities give an indication of interparticle interactions and were found to be at a minimum at around 5% dispersant. UV attenuation was used as an indicator of particle size.

The unmilled dispersions [2] appeared very fluid, but UV measurement revealed poor attenuation properties implying that the particles are still aggregated. The solid particles quickly settled out of suspension to form a sediment in the bottom of the beaker. An improvement of UV attenuation properties, along with an increase in viscosity, was observed upon milling. The aggregates are broken down into their constituent particles in the mill [2], but in the absence of dispersant they quickly reaggregate by van der Waals attraction in a more open structure. This caused the mill to block. Further improvements in UV properties were observed when the dispersion was milled in the presence of the dispersant [2] but viscosity was still high. Addition of sufficient dispersant allows the particles to disperse to single particulates [3] which are well stabilized and the viscosity drops. This is an optimized dispersion. UV properties are well developed. On addition of further dispersant the particles gain an extended stabilization layer [2], causing potential overlap of stabilization layers which is sufficient to produce a weak repulsive gel. The viscosity again rises and the dispersion has a measurable yield value. UV properties are still well developed but the solids loading becomes very limited.

The dispersant demand curves described in Chapter 12, particle size monitoring in addition to solids loading curves (Fig. 12.15) are very useful tools in optimizing a pigment dispersion in practice. Further examples were given in Chapter 12.

12.7 Competitive interactions in colour cosmetic formulations

The colour cosmetic pigments are added to oil-in-water (O/W) or water-in-oil (W/O) emulsions. The resulting system is referred to as a suspoemulsion [2]. The particles can be in the internal or external phases or both, as was illustrated in Fig. 7.12 of Chapter 6 for sunscreen formulations. An understanding of competitive interactions is important in optimizing formulation stability and performance. Several possible instabilities might arise in the final formulations:

- (i) Heteroflocculation from particles and droplets of differing charge sign.
- (ii) Electrolyte intolerance of electrostatically stabilized pigments.
- (iii) Competitive adsorption/desorption of a weakly anchored stabilizer which can lead to homoflocculation of the pigment particles and/or emulsion droplet coalescence.
- (iv) Interaction between thickeners and charge stabilized pigments.

Several steps can be taken to improve the stability of colour cosmetic formulations which are in fact very similar to those for optimal steric stabilization [2]:

- (i) Use of a strongly adsorbed (“anchored”) dispersant, e.g. by multipoint attachment of a block or graft copolymer.
- (ii) Use of a polymeric stabilizer for the emulsion (also with multipoint attachment).

- (iii) Preparation of the suspension and emulsion separately and allowing enough time for complete adsorption (equilibrium).
- (iv) Using low shear when mixing the suspension and emulsion.
- (v) Use of rheology modifiers that reduce the interaction between the pigment particles and emulsion droplets.
- (vi) Increasing dispersant and emulsifier concentrations to ensure that the lifetime of any bare patches produced during collision is very short.
- (vii) Use same polymeric surfactant molecule for emulsifier and dispersant.
- (viii) Reducing emulsion droplet size.

References

- [1] Tadros T. Cosmetics. In: Tadros T, editor. Encyclopedia of colloid and interface science. Berlin: Springer; 2013.
- [2] Kessel LM, Tadros T. Interparticle interactions in color cosmetics. In: Tadros T, editor. Colloids in cosmetics and personal care. Weinheim: Wiley-VCH; 2008.
- [3] Tadros T. Dispersions of powders in liquids and stabilisation of suspensions. Weinheim: Wiley-VCH; 2012.
- [4] Blake TB. Wetting. In: Tadros TF, editor. Surfactants. London: Academic Press; 1984.
- [5] Tadros T. Applied surfactants. Weinheim: Wiley-VCH; 2005.
- [6] Visser J. Advances Colloid Interface Sci. 1972;3:331.
- [7] Deryaguin BV, Landau L. Acta Physicochem USSR. 1941;14:633.
- [8] Verwey EJW, Overbeek JTG. Theory of stability of lyophobic colloids. Amsterdam: Elsevier; 1948.
- [9] Napper DH. Polymeric stabilisation of colloidal dispersions. London: Academic Press; 1983.
- [10] Tadros T. Rheology of dispersions. Weinheim: Wiley-VCH; 2010.
- [11] Krieger IM, Advances Colloid and Interface Sci. 1972;3:111.
- [12] Tadros TF. Advances Colloid and Interface Science. 2003;104:191.
- [13] Robb JL, Simpson LA, Tunstall DF. Scattering and absorption of UV radiation by sunscreens containing fine particle and pigimentary titanium dioxide. Drug and Cosmetics Industry. 1994; March.
- [14] Kessel LM, Naden BJ, Tadros TF. Attractive and repulsive gels from inorganic sunscreen actives. Proceedings of the IFSCC 23rd Congress. Orlando, Florida; October 2004.

Index

- absorbance
 - mechanism of 242
- adsorbed layer 9
- adsorbed layer thickness 82
- adsorption amount 8
- adsorption isotherm 7, 249, 253
- adsorption of polymer 7
- alkyl polyglucoside 106
- anionic polyelectrolyte
 - binding of cationic surfactant to 130
- association behaviour of polymer 31, 32
- aggregation 15
- associative thickeners 225–227

- Bancroft rule 168
- bile salt 36, 37
- biodegradable nanoparticle 77–79
- biological effect 44
- biological implication 39
- block copolymer 7, 28, 45, 58, 59, 73, 79, 81, 137, 138, 203

- capsule 65, 66, 70
- cholic acid 36, 37
- cleaning function 220
- coalescence
 - prevention of 138, 139
- colloidal nanoparticle 74
- colloidal properties 31, 36
- colour cosmetics 259
 - complex interaction in 279, 280
 - principles of preparation of 260, 277–279
- comminution 264
- constant stress measurement 156, 157, 207
- cosmetic emulsions 133
 - rheological properties of 153
- cosmetics 97
- creaming 12
- creep measurement 156, 157, 207
- critical aggregation concentration (CAC) 123, 124
- critical micelle concentration (cmc) 36, 79, 109–113
- critical packing parameter 5, 56, 112

- degree of dissociation 33
- diffusion coefficient 25, 40

- disperse systems 3
- dispersing agents 270–272
 - assessment of 272–274
- dispersion
 - efficiency of 18
 - process 260
 - stabilization of 4
- DLVO theory 5, 6
- double layer 4, 5
 - thickness of 5
- double layer repulsion 5
- drug absorption 40
- drug carriers 77
- drug delivery 73–80
- drug solubility 11
- drug targeting 74–80
- dynamic light scattering 25
- dynamic measurements 154–156, 208–210

- elastic interaction 9
- emulsification 20, 21
 - mechanism of 147, 148
- emulsifiers
 - selection of 139
- emulsion creaming/sedimentation
 - prevention of 136
- emulsion flocculation
 - reduction of 136, 137
- emulsion formation
 - breakdown processes of 135, 136
 - free energy of formation of 134
 - schematic representation of 134
 - thermodynamics of 133
- emulsion stability 140–143

- Flory–Huggins interaction parameter 9
- foam boosters 218, 221
- foam stability 221
- foam stabilization
 - by liquid crystalline phases 222
 - by micelles 222

- gels 65–69, 213
- Gibbs–Marangoni effect 152, 153, 167, 221
- graft copolymer 137

- hair
 - electrokinetic properties of 234
 - morphology of 228, 229
 - surface properties of 230–233
- hair conditioners 213, 214
 - role of surfactants and polymers in 234–239
- Hamaker constant 4, 244
- high pressure homogenizer 16, 17, 163, 169
- HLB number 135–140
- homopolymer 7
- hydrodynamic thickness 8
- hydrophilic-lipophilic-balance (HLB) 134–140
- hydrophobic effect 118
- hydrophobically modified polymer 127–129
- hydrotrope 45

- interaction between PEG layer and protein 83
- interaction energy 10
- interfacial dilational modulus 150, 166
- interfacial tension 23, 24, 146, 149
- interfacial tension gradients 151, 152, 166

- Kelvin equation 11
- Krafft temperature 113, 114

- laminar flow 164, 165
- Laplace pressure 20, 148, 163
- lipid nanoparticle 62
- lipids 37, 38, 50, 107
- liposomes 38, 43, 50
- liquid crystalline phases 59, 61, 114
- low energy emulsification 170–176

- Marangoni effect 151
- micelle formation 32
- micelle systems 35
- micelles 109, 111, 112
 - shapes of 113
- micellization 31, 109
 - driving force for 118
 - dynamic process of 115
 - enthalpy of 117
 - entropy of 117
 - free energy of 116
 - thermodynamics of 115
- microemulsions 24, 59, 60
 - stabilization of 57, 58
- microfluidization 17
- mills 15, 20

- multiple emulsions 193
 - breakdown processes of 194, 195
 - characterization of 205, 206
 - parameters affecting them 201, 202
 - preparation of 195–197
 - rheological testing of 206
 - schematic representation of 205
 - stability of 210, 211
 - type of 194
 - yield of 196
- nanodispersion 11, 12
- nanoemulsion 12, 25, 159, 160
 - based on polymeric surfactants 187–190
 - colloid stability of 160, 161
- nanoparticle 74, 75
- nanosuspension 13
 - preparation of 19

- oscillatory measurement 154–156, 208–210
- osmotic repulsion 9
- Ostwald ripening 27, 28, 137, 138, 161, 162
 - reduction of 27, 28, 161, 162

- packing parameter 222, 223
- personal care 97
- phase inversion 139, 199
- phase inversion composition (PIC) 21, 22, 172, 173
- phase inversion temperature (PIT) 22, 23, 145, 173–185
- PLA–PEG micelle 89, 90
 - blood circulation of 92
 - radio-labelled 91
- poloxamer 76
- poloxamine 76
- polylactic–polyglycolic (PLGA) nanoparticle 77, 80
 - aggregation number of 87, 88, 91
 - colloid stability of 83, 86
 - hydrodynamic diameter of 84
 - particle size of 90
 - zeta potential of 85
- polymer at interface 7
- polymer conformation 8
- polymer gels 65
- polymeric surfactant 7
- polymer layers 8
- polymer nanoparticle 73, 74

- polymer–surfactant interaction 122–127
- polystyrene latex 76, 78
- powder dispersion 264
- powder wetting 260–263
- power density 21
- preservatives 218
- pseudoplastic flow 154

- Rehbinder effect 18
- Reynold number 164
- Rideal–Washburn equation 14, 263
- rotor–stator mixer 16, 169

- scattering 242, 243
- shampoo 213
 - components of 217
 - properties of 216
 - rheology modifier for 224
 - role of components in 219, 220
 - silicone oil emulsions in 224
- silicone surfactant 108
- solid–liquid nanoparticle 65, 66
- solid–polymer nanoparticle 70–73
- solubilisation 44–49
 - factors affecting it 49–50
- solubilised systems 42, 44
- solubility parameter 244, 245, 254
- sorbitan esters 104, 142
- spreading coefficient 262
- stability ratio 6
- steady state measurements 153
- steric interaction 80
- sterically stabilized dispersions 246, 247
 - experimental results of 247–252
- steric repulsion 244
- steric stability 7
 - criteria of 10
- sunscreens 241, 242
 - complex interaction in 255, 256
- surface activity 31, 33
- surface force theory 222
- surface elasticity 221
- surface pressure 149, 166, 167
- surface viscosity 221
- surfactant classes 97–104
 - phase diagrams of 114, 115
- surfactant mixtures
 - interaction of 119–122

- topical administration 61, 62
- top-down process 13
- turbulent flow 164, 165

- van der Waals attraction 4, 244
- velocity gradient 165
- vesicles 33, 43, 50–57
 - aggregation number of 55
 - formation of 53, 54

- Weber number 165, 170
- well-dispersed particles 243
- wet milling 17, 18
- wetting 13
 - of internal surface 14
- wetting agents 15
- work of dispersion 13, 14

- Young's equation 14

